



# Thesis

**Nazariyah Binti Yahaya**

**Metabolic interactions between *Plasmodiophora brassicae* and  
*Arabidopsis thaliana* plant**

**PhD**

**June 2016**



**Metabolic interactions between *Plasmodiophora brassicae* and  
*Arabidopsis thaliana* plant**

**A thesis submitted by**

**Nazariyah Binti Yahaya**

**In partial fulfilment of the requirement for admittance to the degree of  
Doctor of Philosophy  
University of Sheffield**

**Department of Animal and Plant Sciences  
University of Sheffield  
Sheffield  
S10 2TN  
United Kingdom**



**June 2016**



## **Acknowledgements**

I would like to thank Stephen Rolfe for his supervision during my Ph. D and especially for his guidance, advice and patience during the preparation of this thesis. I would also like to thank Mike Burrell, Heather Walker and Pierre Petriacq for their help with the mass spectrometry work undertaken in this study.

I would also like to acknowledge the Ministry of High Education, Malaysia and Islamic Science University of Malaysia for financial support.

Thanks to Julia Van Campen and Luke A Cartwright for proof-reading parts of this thesis and giving grammar advice during the preparation of this thesis.

## **Nazariyah Binti Yahaya- Metabolic interactions between *Plasmodiophora brassicae* and *Arabidopsis thaliana***

### **Abstract**

Clubroot (*Plasmodiophora brassicae*) is a serious agricultural problem affecting Brassica crops. It also infects *Arabidopsis thaliana* plants. During infection, this biotrophic pathogen manipulates the development and metabolism of its host leading to the development of galls. In turn, its own development is strongly influenced by the host. The aim of this study was to understand the metabolic interaction between *A. thaliana* plants and *P. brassicae*. An initial non-targeted approach was used to obtain metabolic 'fingerprints', which were then combined with host transcriptomic data. In addition, a targeted approach was applied focusing on carbohydrate metabolism. Hypotheses were identified using transcriptomic data and tested using mutants of *A. thaliana* and analysis of reporter gene expression.

Changes in plant development occurring as a consequence of clubroot infection correlated with changes in metabolic status were investigated. Following *P. brassicae* infection, metabolite profiles altered at the beginning of cortical infection, although plant primary growth did not show clear differences between uninfected and infected tissue at this stage. This suggests that these changes in metabolites depended on responses of the plant to infection rather changes in plant development.

The accumulation of the amino acids glutamate, aspartate and alanine are likely to be related to pathogen nutrition. Metabolites such as proline protect plants from osmotic and oxidative stress. Meanwhile, compounds associated with plant defence such as cinnamic acid and phaseic acid accumulated at 16 DPI and decreased at 26 DPI. The accumulation of vitamin B6 precursor and compounds associated with folate biosynthesis were accompanied with increasing host gene expression associated with the synthesis of these metabolites. The accumulation of other metabolites such as thiosulfate was accompanied with the repression of genes associated with their degradation. This suggests that *P. brassicae* has the potential to suppress the expression of host metabolism genes to obtain nutrients from the host.

Transcriptomic analysis showed that sucrose synthase (*SUS*) and sugar permeases were induced during gall formation. The impact of inactivating these genes (and cytosolic invertase *CINV*) on gall formation was examined. In wildtype plants the hypocotyl width was not affected at 16 DPI, but increased by 26 DPI. Similar results were seen in *cinv1,2* and *sus1-,4* plants at 16 DPI. By 26 DPI, *cinv1,2* and *sus1-4* plants showed a smaller hypocotyl width than Col-0 plants when uninfected, but this difference was not evident in *sus1-4* plants when infected. Infected *cinv1,2* plants were smaller than Col-0 plants at 26 DPI, although plasmodia colonized host cells and pathogen development was similar to that in Col-0 plants. This indicates that *P. brassicae* itself makes the gall a sink. Meanwhile, *sweet11,12* mutants displayed slower *P. brassicae* development due to a change in carbohydrate partitioning. SWEET::GUS expression patterns support the hypothesis that sucrose was transported to plasmodia via these transporters.

## Abbreviations

DPI	days post inoculation
ROS	reactive oxygen species
SAR	systemic acquired resistance
CINV	cytosolic invertase
SUS	sucrose synthase
Col-0	Columbia ecotype ( <i>Arabidopsis</i> )
SE-CC	sieve element-companion cell complex
SUT/SUC	active sugar transporter protein
UDP	uridine-5'-diphosphate
CWINV	cell wall invertase
GUS	$\beta$ -glucuronidase

## Contents Page

Chapter 1. General Introduction	1
Chapter 2. Plant Metabolic Fingerprinting in <i>P. brassicae</i> -Infected <i>Arabidopsis thaliana</i>	35
Chapter 3. Investigating the Metabolism of Clubroot-Infected Plants by Integrating Metabolomic and Transcriptomic Approaches	88
Chapter 4. Carbohydrate Metabolism in <i>P. brassicae</i> -infected Plants	132
Chapter 5. General Discussion	175
References	189
Appendix	209

## **Chapter 1. General Introduction**

### **1.1 Introduction**

Plant pathogens such as necrotrophs, biotrophs and hemibiotrophs can be distinguished based on the survival of host tissues during nutrient acquirement by the pathogen and based on the mechanism of infection (Oliver and Ipcho, 2004). Necrotroph, biotroph and hemibiotroph pathogens manipulate their host to obtain nutrients. During the infection process, a necrotrophic pathogen secretes its effectors to suppress host defence, and degrades host macromolecules such as plant cell wall components to colonize host cells. This type of pathogen kills the host to obtain nutrients. Biotrophic pathogens on the other hand obtain nutrients from the living host. Biotrophic pathogens can also secrete effectors to suppress the host defence system, and alter host metabolism through the manipulation of host gene expression and transporters for nutrient uptake without killing their host. Hemibiotroph pathogens show elements of both biotrophic and necrotrophic lifestyles, including deriving nutrients from living host cells and requiring host cell death to grow and complete their life cycle (Muencha et al. 2008).

Successful colonization and growth of pathogens depends on the effectiveness with which pathogens obtain nutrients from their host. This is related to the adaptation and exploitation of the nutrient environment during host development and metabolism by the pathogen. For instance, some pathogens modify host development by inducing gall formation to optimize the production of nutrients for the pathogen whereas others form special feeding structures such as haustoria to absorb nutrients from the host (Voegelé et al., 2001, Divon and Fluhr, 2007). Penetration of pathogens inside the host could activate the plant defence. Moreover, during infection plant metabolism might be adjusted to enable pathogen nutrient acquisition.

### 1.1.2. How Do Pathogens Alter Host Development?

Many pathogens modify plant development as part of their infection strategy, but a broad spectrum of impacts exists from subtle manipulation of host metabolism through to extensive tumour formation (Figure 1.1). For instance, *Blumeria graminis* lives in the host epidermis and shows only the subtlest effects on plant. The obligate root pathogen *Spongospora subterranea* on the other hands establishes a long-term feeding relationship with the living cells of its host to complete its life cycle without killing the host. It causes powdery scab disease on potato crops, forms dark spots on potato tubers that contain a mass of powdery spores in the early stages, and develops tumours on plant roots at the later stages of infection. Meanwhile, the biotrophic smut fungus *Ustilago maydis* causes a strong effect on the development of its host. *U. maydis* infects and induces tumours on above ground tissues of crops (mostly grasses) such as maize, barley, wheat, and sugar cane. Moreover, *Agrobacterium* causes crown gall disease and the epiphyte pathogen *Rhodococcus fascians* causes leafy gall formation.

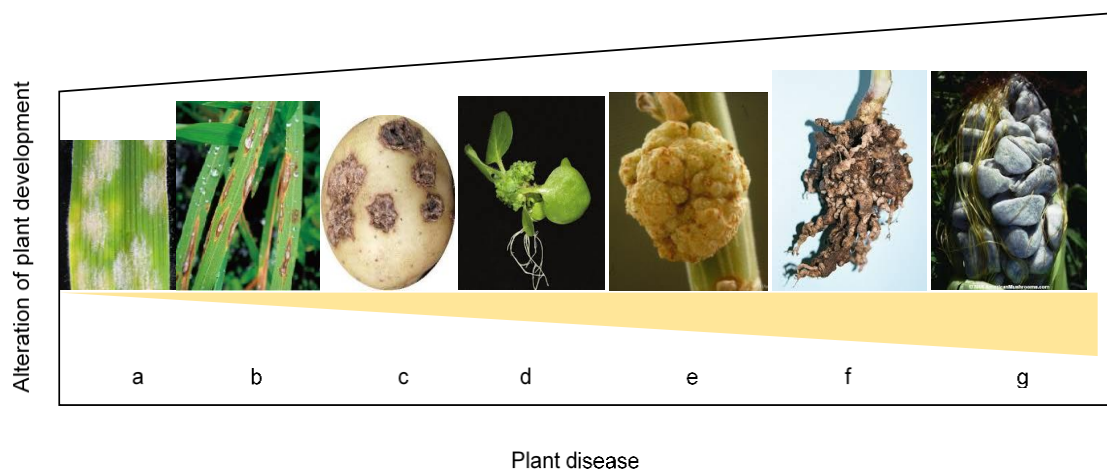


**Figure 1.1.** Spectrum of plant development alteration in response to specific plant diseases caused by the biotrophic pathogens a) Powdery mildew, b) rice blast fungus, c) Potato scab, d) Leafy galls, e) Crown galls, f) Clubroot, and g) Corn smut. Yellow line shows the severity of the impact of disease on plant development.

The ability of plant pathogens to induce tumours as they colonise habitats is dependent on their ability to reprogram different plant developmental states. For instance, crown galls only develop on host stems when *Agrobacterium* species *A. tumefaciens* successfully transfers and integrates T-DNA into the host genome

(Gohlke and Deeken, 2014, Chilton et al., 1977). During infection, *Agrobacterium* expresses multiple virulence genes and effector proteins that assist with the transport of T-DNA into host cells. The T-DNA integrates into the host genome and induces auxin and cytokinin biosynthesis to control plant response. This results in uncontrolled host cell proliferation and leads to the formation of crown galls (Gelvin 2010, 2012, Ward et al., 1988, Thompson et al., 1988).

In *R. fascians* infected plants, hyperplasia symptoms which lead to the development of leafy galls do not show as dramatic an impact on plant development as in plants infected with *Agrobacterium*. In this case, there is no evidence of DNA transfer from the *R. fascians* genome. Instead, the linear virulence plasmid of *R. fascians* consists of a *fas* operon that encodes cytokinins. *R. fascians* cytokinins, especially *cis*-zeatin and 2-methylthio-zeatin which are weak substrates for all host cytokinin oxidases, directly affect plant responses and development by continuously stimulating tissue proliferation (Stes et al., 2013, Pertry et al., 2009). In addition, cytokinins from *R. fascians* also stimulate the host to produce indole-3-acetic acid and the polyamine putrescine. Indole-3-acetic and putrescine function in activating meristem initiation and target the expression of a D3-type cyclin (Stes et al., 2012). This could initiate new meristem formation as well as reprogramming existing meristems to stimulate more cell division in host cortical cells by inducing them to re-enter the cell cycle (Goethals et al., 2001). As a result, adventitious meristems develop and differentiate into leafy gall on the upper part of the host plant. The leafy gall formed provides a special habitat niche for *R. fascians* to obtain energy from their host.

Some pathogens such as *Magnaporthe oryzae* and *U. maydis* form an appressorium, a specialized infection structure to penetrate the plant surface (Ryder et al., 2015, Perez-Nadales et al., 2014, Castanheira et al., 2014, Perez-Martin et al., 2006). However, the disease development differs between these pathogens. Rice blast fungus, which is caused by *M. oryzae*, exhibits disease lesions on the plant surface while corn smut fungus caused by *U. maydis* induces tumour formation on the plant cob (Figure 1.1). *M. oryzae* is a filamentous

ascomycete and uses a dome-shaped structure to break the plant cortical surface by mechanical force (Ryder et al., 2015, Perez-Nadales et al., 2014). Hyphae are formed on the plant plasma membrane and disease lesions are formed on the plant surface (Perez-Nadales et al., 2014). The disease lesion consists of conidiophores that produce conidia to infect a new plant (Perez-Nadales et al., 2014). In contrast, *U. maydis*, which is a basidiomycete fungus, uses a filament in which the cell cycle is arrested to grow on the plant surface (Castanheira et al., 2014, Perez-Martin et al., 2006). Filaments stop growing in response to unidentified plant signals and form an appressorium structure that is differentiated into a haustoria, which is used to penetrate plant surface. Cell cycle arrest in the pathogen filament is important in infection. Once the filament of *U. maydis* enters the plant, cell cycle arrest is released (Castanheira et al., 2014). *U. maydis* releases its several effectors into the specific plant tissue to induce tumours (Djamei and Kahmann, 2012). One of the effector is See1 (seedling efficient effector1), which functions to reactivation of plant DNA synthesis for *de novo* tumour formation in leaf cells. This effector function in an organ-specific manner, which does not affect tumour formation in immature tassel floral tissues, the organ that contains highly proliferating tissue (Redkar et al., 2015). In floral tissue, specifically in the anther, tumour is formed from redirecting host cell division and cell expansion into tumour pathways by delayed cell-fate specification (Gao et al., 2013).

### **1.1.3. How Do Pathogens Avoid Plant Defence Responses?**

The plant defence system consists of defence against unwanted visitors. Plants activate their basal resistance which is a first line of plant defence against entire groups of pathogens. Plant basal resistance is triggered when pattern recognition receptors (PRRs) located in the plant surface, detect pathogen-associated molecular patterns (PAMPs). PAMPs could be specific proteins, lipopolysaccharides and cell wall components. PRRs activate PAMP-triggered immunity (PTI). PAMPs of plants detect cell wall damage and trigger plant defence through the activation of ROS and the secretion of antimicrobial compounds such as glucosinolate. In response to plant PTI, the pathogen

secretes its virulence factors, also called 'effectors', inside the host cytoplasm. If the pathogen successfully delivers its effectors to suppress plant PTI, it is able to obtain nutrients from the host and spread (Jones and Dangl, 2006).

The second layer of plant defence is the activation of effector-triggered immunity (ETI), which occurs after nucleotide binding/leucine-rich repeat (NLR) receptors recognize pathogen effectors. In the plant ETI system, plants trigger a hypersensitive response, leading to programmed cell death at the infected site and surrounding cells to restrict spreading of the pathogen. Necrosis of cells, which is a result of the hypersensitive response, occurs often in plants attacked by necrotrophic pathogens. The combination of PTI and ETI responses can enhance the accumulation of the phytohormone salicylic acid (SA) and induce systemic acquired resistance (SAR), which leads to the suppression of the jasmonate (JA)/ethylene (ET) defense pathway, cell wall remodelling and biosynthesis of secondary metabolites (Witteck et al., 2015, Gruner et al., 2013). SAR produces long-distance signals that can travel from the root tissue to the leaves of infected plants and induces the expression of pathogenesis-related (PR) proteins systemically (Gruner et al., 2013, Lovelock et al., 2013). Successful colonization indicates that pathogens can avoid host defence responses in multiple ways. Pathogens may subsequently release new effectors which manage to suppress plant ETI and enable them to colonize host tissues. Figure 1.2 shows a 'ZigZag' model that illustrates the plant immune system in response to pathogen infection.

Some pathogens such as *Venturia inaequalis*, which is the causal agent of apple disease scab, proliferate in the subcuticular tissue above the epidermal host cells and remain undetected by the plant defence response (Bowen et al., 2011). During powdery mildew fungus infection, the host senses the presence of the extrahaustorial membrane of *Golovinomyces orontiihaustoria* by expressing the plant resistance protein RPW8.2 (Micali et al., 2011). In response to such plant resistance proteins, pathogens secrete various types of effectors. These effectors function in multiple ways, including manipulating and reprogramming host

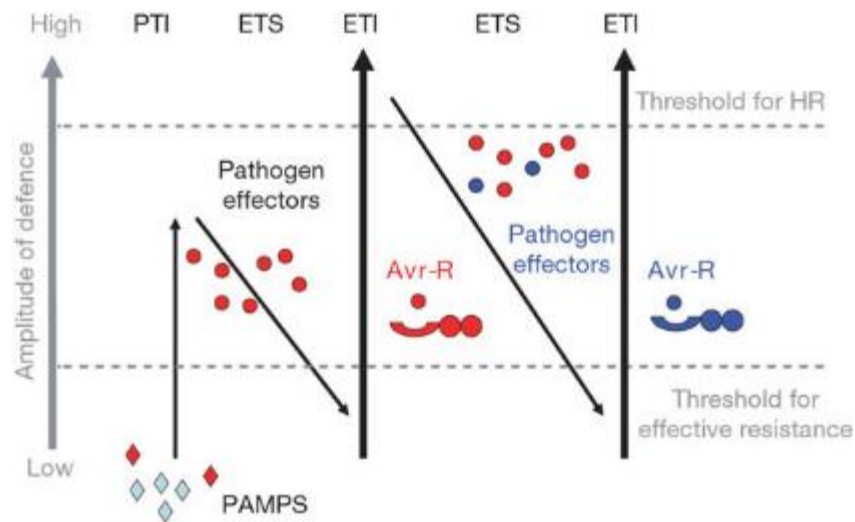


**Figure 1.2.** A 'ZigZag' model that illustrates the plant immune system in response to the pathogen infection. Figure is taken from Jones and Dangl (2006).

metabolism and targeting host immune response pathways. The biotrophic smut fungus *U. maydis*, which uses haustoria to penetrate inside host tissues, secretes lytic enzymes after it recognizes and responds to plants signals (Lanver et al., 2014). Before penetration occurs, *U. maydis* secretes the effector chorismate mutase (CMU1) into the host plant to suppress plant defence. CMU1 re-channels choristamate, a precursor of SA, to reduce SA biosynthesis (Djamei and Kahmann, 2012).

Furthermore, nutrient compounds, which are important to plant and pathogen growth, can be used to suppress plant defence or to increase plant resistance against pathogens. For instance, *Uromyces fabae* takes up glucose and fructose from the host and converts these compounds into mannitol by expressing its mannitol dehydrogenases genes in haustoria, and stores the mannitol inside its spores (Voegelé et al., 2001, 2005). Mannitol is present in both spores extracts and apoplastic fluid of infected leaves (Voegelé et al., 2005). The presence of mannitol in the apoplast of plant cells can suppress plant ROS signalling, which is induced by the plant defence in response to pathogen infection. Besides the mannitol in spores functions as a carbohydrate storage compound (Voegelé et al., 2005).

### **1.1.3. How Does The Pathogen Manipulate Host Metabolism to Obtain Nutrients?**

Plant development is accompanied by source-sink transitions. Source tissues, where photosynthesis is active, export carbohydrate to sink tissues such as roots and developing leaves, where photosynthesis is less active or inactive. Long-distance sugar transport from source to sink tissue is facilitated by phloem loading and unloading processes through the sieve element-companion cells (SE-CC) complex. The allocation of carbon and regulation of source-sink transitions are dependent on sink strength. An increase in carbohydrate utilisation in sink tissues can increase sugar import and change sink strength through the regulation of the source-sink transitions (Roitsch et al., 1999). For instance, competition for common sugars occurs when the sink strength of each plant organ changes because of pathogen infection or due to the development of various sink organs, such as developing leaves and galls. Pathogen infection in sink tissues can increase the export of carbon from source tissues by increasing the phloem loading process. In contrast, pathogen infection in source tissues may alter the host photosynthetic process, decrease the export of carbon and decrease phloem loading to reduce the carbon allocation to uninfected tissues. The phloem loading and unloading processes in source and sink tissues respectively are accompanied by the activities of sugar transport and hydrolysis (Doidy et al., 2012).

However, the alteration of host metabolism and source-sink transition during pathogen infection are dependent on the infection phase, type of pathogen and mode of pathogen nutrition. For example, in infected tissues, the absorption of nutrients from the host by the pathogen is dependent on the phase of infection. During the penetration process, the pathogen is in a state of starvation. It is dependent on nutrients derived from internal stores of the spore. Spores store valuable nutrient sources such as trehalose, glycogen, polyols, mannitol, and lipids (Divon and Fluhr, 2007). Once pathogens enter the host, their internal energy sources are exhausted. In order to absorb nutrients from the host, pathogens need to establish themselves rapidly by preparing a mechanism that

enables nutrient uptake from the host. Some pathogens such as *U. maydis* develop a haustorium structure to absorb nutrients from the host, while some pathogens develop mechanisms to manipulate host metabolism to establish a new sink tissue such as a gall.

For instance, during plant interaction with the root knot nematode (*Meloidogyne* spp) and the cyst nematode (*Heterodera schachtii*), both parasitic animals, the pathogens form a haustoria structure and gall-like organs on their infected host, without destroying the infected plants. Root knot nematodes change the development of host phloem and xylem through the formation of giant cells in the central cylinder. This results in the formation of galls on plant roots (Bartlem et al., 2013, Fester et al., 2008). Feeding cells of root knot nematodes contain high levels of proteins, glucose, glucose-6-phosphate, and ATP. Nematode-induced giant cells, which act as sinks for photosynthesis, express highly a sucrose transporter (SUC1) (Hammes et al., 2005). Similarly, cyst nematodes induce the formation of syncytia in the root vascular cambium of infected plants. Syncytia act as a strong sink, to which sucrose is unloaded via the apoplastic route using the SUC2 transporter to unload sucrose into the apoplastic space between sieve elements and companion cells (Juergensen et al., 2003). The formation of phloem containing SE-CC complexes increases in nematode-infected *Arabidopsis* tissues, indicating an increase in phloem unloading processes (Hoth et al., 2005). Nutrients in companion cells are absorbed by nematode-induced syncytia through symplastic pathways (Hoth et al., 2005), which results in the accumulation of soluble sugars and starch (Hofmann and Grundler, 2008). Starch synthesis and degradation genes are highly expressed in nematode-induced syncytia, suggesting that starch serves as a long and short-term carbohydrate source to the nematode (Hofmann et al., 2008). Nematode feeding activity in syncytia increases the mobilization of sucrose from the shoot to infected tissues, as this results in the formation of a new sink tissue (Hofmann and Grundler, 2008).

Some pathogens such as *Agrobacterium* transfer their metabolite biosynthesis genes into the host genome to synthesise nutrients. Crown gall tumours produce nutrients called opines, induced by *Agrobacterium* T-DNA that is integrated into the host genome and expressed in the plant nuclei. Opines provide a source of carbon, nitrogen, phosphorous and sulfur to *Agrobacterium* in plant tumours (Dessaux et al., 1993, Flores-Mireless et al., 2012). Each strain of *Agrobacterium* transfers more than one opine biosynthetic gene and different *Agrobacterium* strains transfer diverse types of opine biosynthetic genes (Flores-Mireless et al., 2012). For instance, *Agrobacterium* derived opine synthase (Ocs) uses S-methylmethionine and pyruvate as a substrate to produce opines (Flores-Mireless et al., 2012). The *Agrobacterium* T-DNA, which is integrated into the host genome, also encodes other opine metabolism genes including those encoding permeases, enzymes which convert opines to digestible compounds, and regulatory proteins. These genes are important to control the transport of opines from plant tumour to *Agrobacterium*, and increase the efficiency of the uptake process (Vladimirov et al., 2015, Lang et al., 2014).

Some pathogens are capable of altering carbohydrate metabolism and photosynthetic processes in infected leaves of the host. For instance, white blister rust disease, which is caused by the biotrophic oomycete *Albugo candida*, results in the appearance of white or creamy raised pustules scattered on the abaxial surface of the leaves. Pustule development and opening are regulated by enzymatic digestion of the host epidermal cell wall (Heller and Thines, 2009). The pustule releases white sporangia on the adaxial surface of *A. candida*-infected leaves, and infected leaves become yellow during disease progression (Verma and Petrie, 1980). The *A. candida* genome lacks enzymes that are required for nitrate and sulfur assimilation (Links et al., 2011). The development of the fungal mycelium of *A. candida* is associated with a reduction in photosynthetic rate and the accumulation of soluble carbohydrates in the infected regions of leaves (Chou et al., 2000). The accumulation of soluble carbohydrate in leaves is closely related to the repression of photosynthetic genes. In addition, during *A. candida* infection, this accumulation of soluble carbohydrate in leaves induces cell wall

invertase activity. Cell wall invertase is involved in the hydrolysis of sucrose to hexose sugars. The increase in cell wall invertase activity in the infected leaf causes a reduction of sucrose export to the other parts of the plant, and increases phloem unloading to the infected leaf (Chou et al., 2000) through alteration of the source-sink transition. Furthermore, *Xanthomonas campestris*, which infects pepper (*Capsicum annuum*) leaves, suppresses the host cell wall invertase to prevent sugar-mediated defence signalling (Sonnewald et al., 2012). This indicates that plant pathogens can change host metabolite flow in order to compete with the host for carbon sources or to avoid plant defence responses. In contrast with *A. candida*, *Puccinia striiformis* f. sp. *triticia*, an agent of stripe rust disease on wheat, induces the expression of the host genes related to photosynthesis to promote photosynthetic rate and increase the production of sucrose in infected leaves for its own benefit (Chang et al., 2013).

Biotrophic plant pathogens obtain nutrients from the host using specific mechanisms to avoid a host defence response. For example, *U. maydis* expresses a plasma membrane-localized sucrose transporter for transporting disaccharide sugars (SRT1) that competes with host sucrose transporters (Djamei and Kahmann, 2012). Similarly, *U. fabae* expresses the *HXT1* gene, which is required on the haustoria plasma membrane to take up D-glucose and D-fructose from the host (Voegelé et al., 2001). Moreover, in hemibiotrophic pathogens, the transition from the biotrophic to the necrotrophic phase is related to plant carbon source availability. For instance, witches broom disease, which exhibits a long biotrophic phase, disrupts the carbon cycle in the apoplast of infected cacao plants by increasing the activity of host cell wall invertase to maintain hexose levels by breaking down sucrose. Carbon depletion in the apoplastic space at the end of the biotrophic phase is sensed by the pathogen. Fungal necrotrophic effectors then stimulate senescence and plant necrosis, which results in a decrease in photosynthetic rate and eventually death of infected plants (Barau et al., 2015). Necrosis, which is stimulated in the necrotrophic phase in senescence-infected tissues, is required to avoid carbon remobilization to the other parts of the plant. Necrotrophic pathogens access the nutrients from

the dead cells that remain in the infected plants and infect the active growing tissues nearby to repeat the biotrophic phase (Barau et al., 2015).

During plant infection with the necrotrophic pathogen *Botrytis cinerea*, the pathogen induces phytotoxic metabolites, oxidative burst, oxalic acid and host-selective toxins (HST) to cause host cell death (Van Kan 2006). The accumulation of reactive oxygen species (ROS) and the presence of virulence factors of *B. cinerea* in grapevine (*Vitis vinifera*) plants induce the expression of *VvSWEET4*, a glucose transporter that is localised on the host plasma membrane (Chong et al., 2014). The expression of *VvSWEET4* during *B. cinerea* infection in host plants enhances sugar efflux into the apoplast, which subsequently causes an accumulation of hexose sugars in the apoplast of plant cells. This suggests that sugar in the apoplast is taken up by a fungal sugar transporter which induces the susceptibility of host plants in response to *B. cinerea* (Chong et al., 2014). After *B. cinerea* takes up sugar from the host, extensive plant cell death is seen in infected plants. This indicates that sugar acquisition from plant cells by the pathogen occurs during pathogen-induced cell death. Besides, the process of sugar uptake by *B. cinerea* from plant cells does not occur in senescent leaves, which are present as a consequence of programmed cell death in plants (Chong et al., 2014). Moreover, plants that are colonized by *B. cinerea* have a high pectin content in their cell wall (Van Kan 2006). Methylated pectin of the host, which can be demethylated by pectin methylesterases and depolymerised by endopolygalacturonase of *B. cinerea*, is a carbon source for fungal growth (Van Kan 2006). Endopolygalacturonase is a type of pectinase, which is involved in fungal penetration into host epidermal cells.

## **1.2. *Plasmodiophora brassicae* Causes Clubroot Disease**

*Plasmodiophora brassicae* is a soil obligate biotrophic pathogen and causes clubroot disease, which is a serious disease affecting the plant family *Brassicaceae* (Howard et al., 2010) including the model plant system *Arabidopsis thaliana* (Mithen and Magrath, 1992). The pathogen causes economically significant problems in humid and temperate areas including the United Kingdom

(UK) and in particular, Scotland (Dixon 2009). Elsewhere it causes major problems in North America, Australia and New Zealand (Dixon 2009). Clubroot disease mostly infects vegetable crops, including those which provide an essential source of vegetable oils (Canola oils, *Brassica napus*), that are used in human foodstuffs and potentially in biofuels. In Britain, Brassica crops are the most valuable fresh vegetables, which are grown in South West Kent, East Anglia, South Wales, Yorkshire, Lancashire, the Lothians and Fife (Dixon 2009). Formation of galls on the roots of clubroot infected plants is the main symptom associated with the development of the disease. The developing gall acts as a strong sink for carbohydrate and other nutrients. This may result in dwarfing of the aerial parts of plants, for example in Chinese cabbage (Ludwig-Muller and Schuller, 2008) and loss of oil content as in canola plants (Dixon 2009).

*P. brassicae* is classified as a Phytomyxea supergroup of Rhizaria based on its ribosomal RNA gene sequence (Figure 1.3). The groups in Rhizaria are composed of unicellular eukaryotic species that are difficult to maintain in laboratory culture. *S. subterranea* is a parasite of the plant genera *Solanum* and it is in the same group as *P. brassicae* (Burki et al., 2010). The Phytomyxea group is a monophyletic group of eukaryotes composed of obligate biotrophic parasites of green plants. Under suitable environmental conditions, pathogens that are categorized in this group can induce physiological changes in their host, avoid host defence responses and require a specific host to complete their life cycle (Neuhauser et al., 2011).

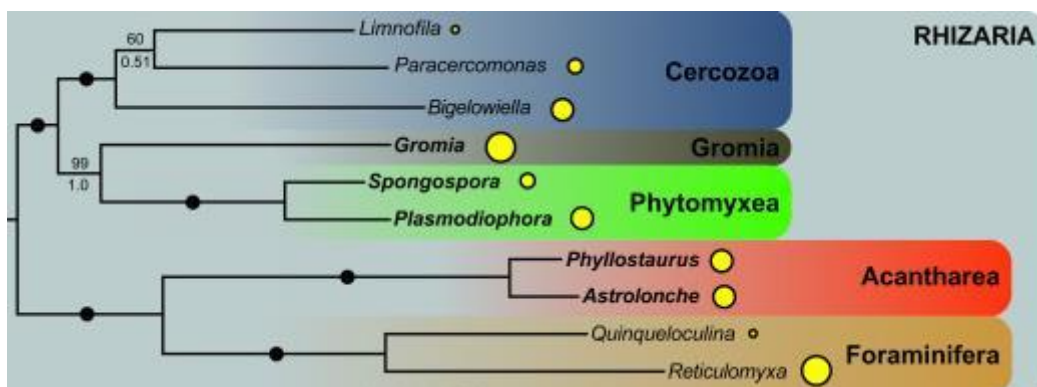


**Figure 1.3:** Phylogeny of Rhizaria super group. A figure taken from Burki et al., (2010).

### 1.2.1 The Life Cycle of *P. brassicae*

The life cycle of *P. brassicae* is composed of two generations and three stages: survival in the soil, root hair infection and cortical infection (Figure 1.4, Kageyama and Asano, 2009). The first stage in *P. brassicae* life cycle is survival in the soil as a resting spore. Resting spores contain 25% chitin in their cell wall (Thornton et al., 1991) and this composition of their cell wall allows them to survive in the soil for several years or even decades depending on the environment of the soil (Kageyama and Asano, 2009).

Haploid resting spores germinate to primary zoospores in the presence of a compatible or a non-compatible host, and other germination factors such as a soil temperature of 15 °C and a soil pH of 6.0 – 6.4 assist in triggering the expression of pathogen serine protease protein (Feng et al., 2010, Webster and Dixon, 1991). The expression of serine protease stimulates the secretion of root exudates from plant root hairs and acts as an initial signal for *P. brassicae* resting spore germination (Feng et al., 2010). Primary zoospores can only survive for a limited time in the absence of a compatible or non-compatible host (Suzuki et al., 1992, Takahashi, 1994).

The second stage of the *P. brassicae* life cycle is root hair infection, also known as primary infection. At this stage, motile primary zoospores attach to the root hair surface and form cysts to produce tubular structures, which consist of a projectile-like structure to assist in the penetration of host cell walls (Ludwig-Muller and Schuller, 2008). *P. brassicae* injects a small spherical amoeba from their cell contents into the host root hairs. This amoeba enlarges, propagates and develops to a primary multinucleate plasmodium inside the host root hair. The primary multinucleate plasmodium cleaves to form zoosporangia in a membranous envelope and releases secondary zoospores into the soil to re-infect plant root hairs and either repeat the zoosporangia stage or continue to cortical infection in the main root tissues (Naiki et al., 1984, Kageyama and Asano, 2009). Re-infection of root hairs by secondary zoospores causes the

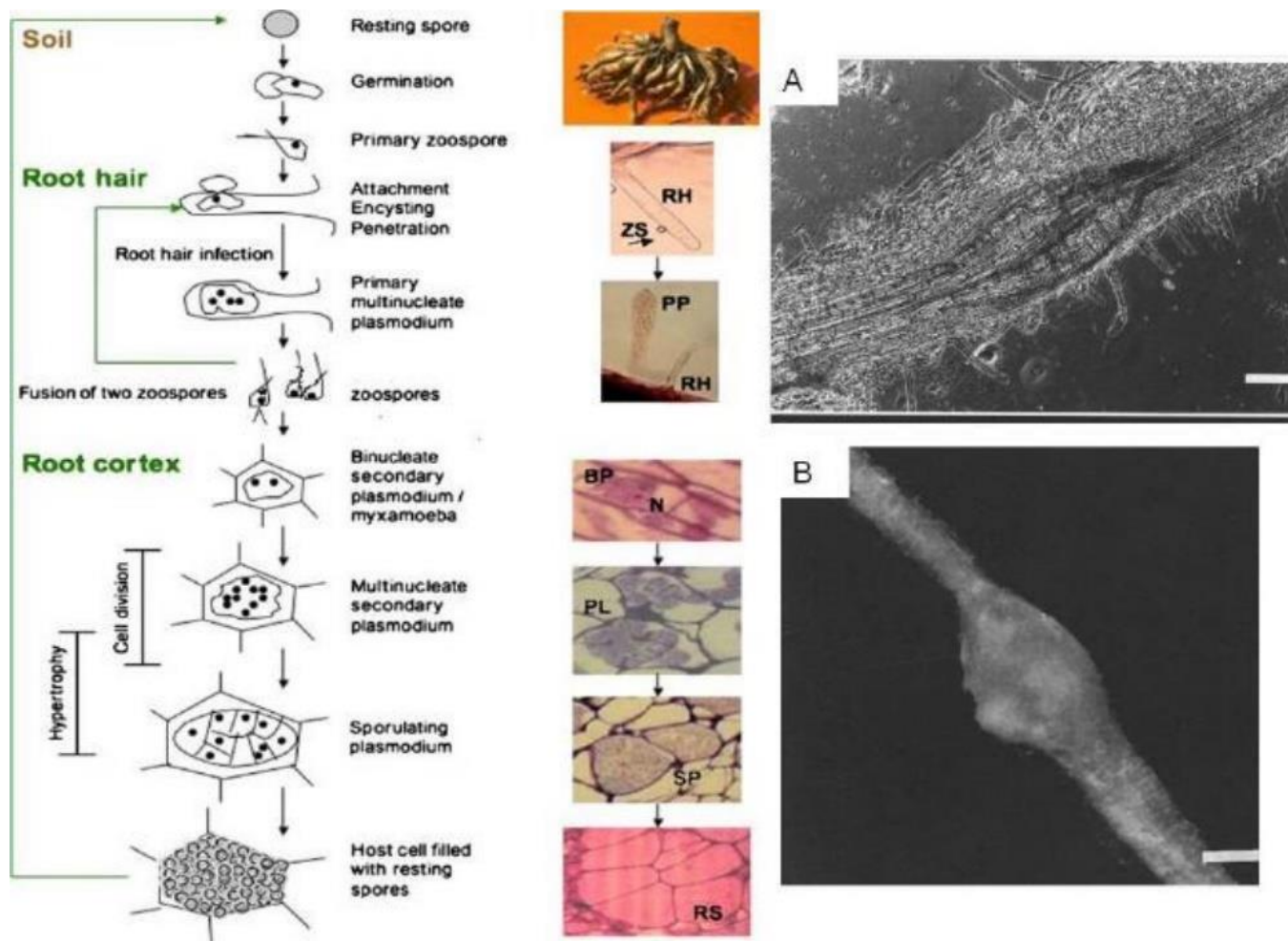


**Figure 1.4** Life cycle of *Plasmodiophora brassicae*. Root hairs (RH), zoospores (ZS), primary plasmodium (PP), binucleate plasmodium (BP), multinucleate secondary plasmodium (PL), sporulating plasmodium (SP) and resting spores (RS). Figure taken from Ludwig-Muller and Schuller (2008). **A**, Primary infection in hairy root of *Brassica napus* plants. **B**, Small gall formation in root of *B. napus* plants. Figure taken from Graveland et al., (1992).

presence of various developmental stages of *P. brassicae* afterwards. Secondary zoospores can also move from root hairs to the main root and hypocotyl tissues through the xylem and continue to cortical infection.

In the cortical infection stage, *P. brassicae* infection either by diploid or haploid secondary zoospores, lead to gall formation. A diploid secondary zoospore is formed by the fusion of two haploid secondary zoospores (Tommerup and Ingram 1971; Ludwig-Muller and Schuller, 2008). However, there is a lack of evidence on the existence of diploid secondary zoospores. Most evidence shows that all the secondary zoospores with a size between 9.6 to 14.4  $\mu\text{M}$  are present in a uninucleate form during cortical infection (McDonald et al., 2014, Schwelm et al., 2015). In this stage, secondary zoospores infect host cortical tissues, develop into a binucleate secondary plasmodium and spread within the host cortical tissues by mitosis (Tommerup and Ingram, 1971). Then plasmodia develop into a new generation of resting spores (Kageyama and Asano, 2009).

Disintegration of clubroot galls releases a second generation of resting spores into the soil to complete the pathogen's life cycle (Tommerup and Ingram, 1971, Kageyama and Asano, 2009). Populations of long-lived spores are increased when the host is repeatedly grown in the infected soil and this may increase disease severity in host crops (Faggian and Strelkov, 2009).

### **1.2.2 How does *P. brassicae* Alter Host Development?**

Similarly to *R. fascians*, *P. brassicae* reprograms host cortical cell division of existing meristems which leads to the formation of clubroot galls (Malinowski et al., 2012). This contrasts with the findings of Devos et al. (2006), who suggest that gall formation occurs through *de novo* meristem formation. Besides, the reprogramming of existing host meristems infected by *P. brassicae* is similar to that seen in plants infected with root-knot nematodes and cyst nematodes. Both pathogens manipulate the host vascular cambium by increasing the number of phloem cells in order to obtain nutrients from the host.

During primary infection, primary zoospores attach to root hairs of *B. rapa* or to the root epidermal cell wall 18 hours after inoculation (Tommerup and Ingram, 1971). Then, primary zoospores penetrate the cell walls and develop to primary plasmodia inside the host cytoplasm. Six days post inoculation (DPI), plasmodia enlarge and the number of nuclei increase inside numerous root hairs. At 8 DPI, a new generation of resting spores are released during sporogenesis (Tommerup and Ingram, 1971). The secondary stage of infection is associated with the development of gall formation. During cortical infection, infected roots of *B. napus* show some swelling and disruption of the two layers of cells between the root cortex and stele at 21 DPI. The breakdown of the root cortex and cellular division and cell expansion within the root stele occur in sections of *B. napus* root tissue infected with *P. brassicae* at 28 DPI. After 35 DPI, infected roots of *B. napus* show the development of small galls with extensive thickening (Graveland et al., 1992). Extensive cell division, but little cell expansion occurs at several places within the galls. Meanwhile, extensive cell division within the stele and the breakdown of cortical cells are seen in sections of thickened roots of *B. napus* infected with *P. brassicae*, suggesting that *P. brassicae* moves from the epidermal cells to the stele (Graveland et al., 1992).

In *A. thaliana* plants, primary infection occurs in a similar manner to other *Brassica* plants (Mithen and Magrath, 1992). Primary infection occurs in primary and secondary roots of *A. thaliana* at 10 DPI. At this stage, sections of *A. thaliana* roots containing plasmodia show the presence of cell wall breakage due to the movement of plasmodia between cells (Mithen and Magrath, 1992). During cortical infection, galls develop on primary, secondary and lateral roots, but most predominantly in hypocotyl tissue at 21 DPI (Mithen and Magrath, 1992). At this stage, hypocotyl sections show extensive cell division and disorganization of cell structure within infected tissues (Mithen and Magrath, 1992). In uninfected *A. thaliana* plants, cell division is stimulated at the onset of secondary hypocotyl thickening in the continuous ring of vascular cambium. However, in infected plants, the continuous ring of vascular cambium is disrupted through the presence of swollen host cells (Malinowski et al., 2012). Swollen host cells

contain secondary plasmodia and a new generation of resting spores at late stages of infection. Extensive cell division occurs in the discontinuous vascular cambium in infected tissue and outside the vascular cambium, especially in phloem parenchyma cells (Malinowski et al., 2012). The extensive cell division and cell expansion lead to the development of galls in infected hypocotyl tissues of *A. thaliana* plants (Mithen and Magrath, 1992).

During secondary hypocotyl thickening in uninfected plants, the expression of *AINTEGUMENTA* (*ANT*), which is used as a marker for meristematic activity, is reduced in the proliferating area of vascular cambium cells that are ready to stop dividing. The reduction of meristematic activity triggers vascular differentiation. Cells which are located on the inner side of the continuous ring of vascular cambium differentiate into xylem parenchyma and mature xylem cells. Vascular cambium cells, which are located on the opposite side of the xylem, differentiate into phloem parenchyma and phloem bundles. Following *P. brassicae* infection, *ANT* promoter activity is extended into the proliferating area of vascular cambium and phloem parenchyma to inhibit those cells from exiting the cell cycle (Malinowski et al., 2012). As a consequence, in *P. brassicae*-infected plants, the vascular differentiation process is disturbed due to pathogen colonization. Infected hypocotyl tissues show a reduction in the formation of xylem cells. The development of gall formation is associated with the reduction of xylogenesis in vascular differentiation cells. However, the formation of immature xylem cells or xylem parenchyma cells is similar between uninfected and infected hypocotyl tissues. In contrast, the formation of phloem parenchyma cells and phloem bundles is increased. Besides, the expression of genes associated with phloem development and of the sucrose H<sup>+</sup> symporter, which are specifically expressed in phloem cells, is increased at the onset of gall formation and at the late gall formation stage in infected tissue (Malinowski et al., 2012).

The alteration of plant development by *P. brassicae* seems to be associated with their strategy to absorb nutrients from the host's living cells. The increase in phloem parenchyma and phloem bundles may increase sink strength during

clubroot gall formation. Figure 1.5 shows a cellular model of changes in vascular system differentiation in hypocotyl tissues of *A. thaliana* plants in response to *P. brassicae* infection. In uninfected plants, proliferated vascular cambium cells differentiate to form phloem and matured xylem. However, in infected plants, the number of proliferated vascular cambium cells is increased. In addition, the number of phloem cells is increased, but the number of mature xylem cells is reduced (Figure 1.5).

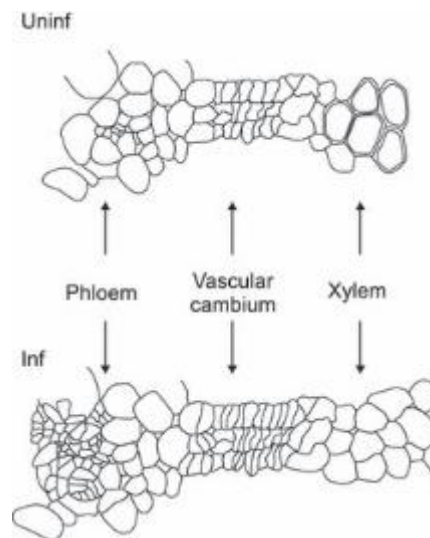


**Figure 1.5.** A cellular model of plant development alterations in response to *P. brassicae* infection. Figure taken from Malinowski et al., (2012).

### 1.2.3 The Role of Plant Growth Regulators in *P. brassicae*-infected Plants

The development of disease symptoms in infected plants is closely related to alterations in hormone metabolism, such as cytokinin, auxin, and brassinosteroid metabolism. There are various types of cytokinins in plants that are classified by the configuration of their N<sup>6</sup>-side chain, either as isoprenoid or aromatic (Mok and Mok, 2001). Isoprenoid cytokinins are N<sub>6</sub>-( $\Delta^2$ -isopentenyl)-adenine (iP), *trans*-zeatin (tZ), *cis*-zeatin (cZ) and dihydrozeatin (DZ). Figure 1.6 shows a model of cytokinin biosynthesis in plants to synthesise active cytokinins forms iP, tZ, DZ and cZ.

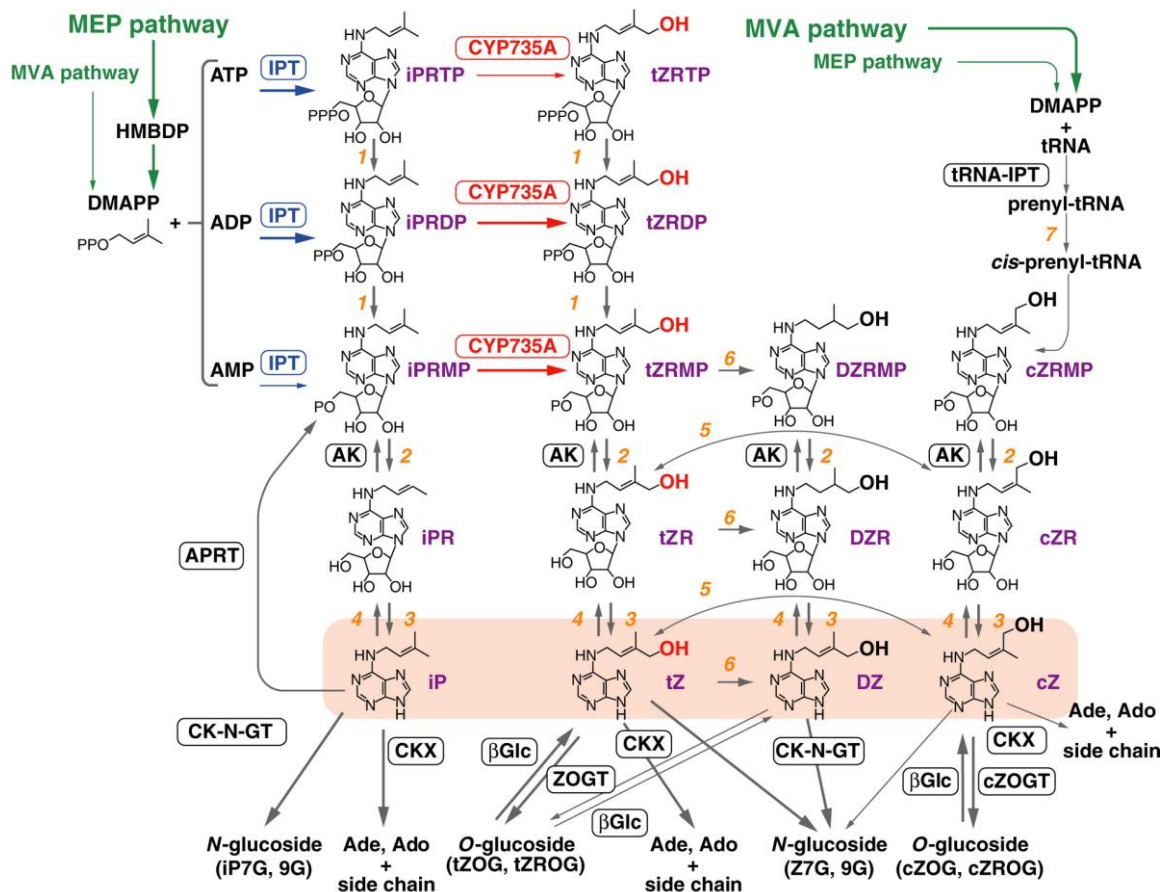


**Figure 1.6.** A model for cytokinin biosynthesis in plants. In this model, active cytokinins isopentenyladenine (iP) is directly synthesised through DMAPP and trans-zeatin is synthesised through HMBDP substrate with AMP or ATP/AMP as an additional substrate. Cis-zeatin is derived from DMAPP and tRNA. Figure taken from Sakakibara (2006).

In cytokinin biosynthesis, isoprenoid side chains of iP and tZ are derived from the methylerythritol phosphate (MEP) pathway, while the cZ isoprenoid side chain originates from the mevalonate (MVA) pathway (Sakakibara 2006). Synthesis of iP and tZ starts when the isopentenyl group of dimethylallyl diphosphate (DMAPP) or hydroxymethylbutenyl diphosphate (HMBDP) is transferred to the N<sup>6</sup> of AMP, ADP or ATP through the activity of adenosine-phosphate isopentenyltransferase (*IPT*). Meanwhile, the synthesis of cZ is derived from the reaction of *IPT* activity with DMAPP and tRNA. The occurrence of cZ or tZ in plants depends upon the substrate specificities of *IPT* genes and is species specific. The major active cytokinins present in *Arabidopsis* plant are tZ and iP with very low amounts of cZ (Sakakibara 2006). Meanwhile cZ is reported to be present in chickpea (*Cicer arietinum* L. cultivar *kaniva*) (Emery et al., 1998) and maize (*Zea mays*)

(Yonekura-Sakakibara et al., 2004). In *A. thaliana* plants, cytokinin biosynthesis occurs as a result of the activity of IPT1, 3, 4-8 which are ATP/ADP *IPTs* as well as IPT2 and IPT 9 which are tRNA *IPTs* (Miyawaki et al. 2006).

Several studies demonstrate the accumulation of cytokinins in root tissues of *P. brassicae*-infected plants (Dekhuijzen and Overeem, 1971, Dekhuijzen 1981, Devos et al. 2005) . This is said to induce local abnormal cell division in *P. brassicae*-infected tissues, which leads to the gall formation. Extracts of clubroot-infected turnips species contain cytokinins at three times the concentration of healthy turnips. The cytokinin in this tissue extract is believed to be involved in controlling cell division of both host and pathogen (Dekhuijzen and Overeem, 1971, Dekhuijzen 1981). It has been suggested that young plasmodia can directly synthesise low amounts of *trans*-zeatin (Muller and Hilgenberg, 1986). Muller and Hilgenberg (1986) demonstrate the uptake of labelled adenine and the conversion of adenine to *trans*-zeatin by plasmodia. Zeatin, which is the predominant active cytokinin in Chinese cabbage plants species, is decreased in infected tissues at 6, 13 and 21 DPI (Devos et al. 2005). The occurrence of zeatin in Chinese cabbage plants was not distinguished by Devos et al. (2005), and could be present as either *cis* or *trans* isomers. In addition, zeatin riboside (ZR) is decreased at those times (Devos et al. 2005). In *Arabidopsis*, iP adenine concentration is two times higher in *P. brassicae*-infected tissue compared with uninfected tissue. The occurrence of isopentenyl adenosine (iPA) which could not be detected in uninfected tissues, occurred in measureable amounts in infected plants at 4 DPI (Devos et al. 2006). This is an unusual concentration for what would normally be relatively abundant compounds in *Arabidopsis* plants. Beside the concentration of zeatin, which is not distinguished between *cis* and *trans*-isomers, is not significantly different between uninfected and infected plants at the very early stages of *P. brassicae* infection (4 DPI). Therefore, improved microanalytical techniques are required to obtain precise quantification of cytokinins in milligram amount of tissue (Malinowski et al., 2016). Devos et al. (2006) suggests the increase of iP and iPA in infected root tissue at very early stages of infection correlates with the increase of cell division which results in *de*

*de novo* biosynthesis of new meristem that leading to gall formation. It has been assumed that iP and iPA are originated from *P. brassicae*.

It has been shown that cytokinins are necessary for vascular cambium formation since deletion *IPT1,3,5,7* genes stops the secondary thickening process in hypocotyl of *A. thaliana* plants (Miyawaki et al., 2006). In infected *A. thaliana* plants, gall formation occurs as a result of a reprogramming of the meristem, and not via *de novo* meristem formation. Blocking host vascular cambium activity through expression of the cell cycle inhibitor ICK1/KRP1 during secondary thickening leading to reduce gall size does not stop the development of *P. brassicae* (Malinowski et al. 2012). Inactivation of host iP and tZ biosynthesis in *ipt1,3,5,7* mutant abolish vascular cambium development in uninfected plants. When infected, no additional cell division occurs but cell expansion and lack of differentiation is still evident. Also plasmodia development is slowed. It is likely *P. brassicae* development is dependent on host cytokinins. Cytokinins iP and tZ are significantly lower in infected *A. thaliana* plants compared with uninfected plants at 16 DPI when the gall is initiated and 26 DPI when a large gall has developed in the hypocotyl and upper roots of infected plants. The reduction of iP and tZ concentration in infected tissue is consistent with the down regulation of host gene expression associated with cytokinin biosynthesis at 16 and 26 DPI (Malinowski et al., 2016).

It has been reported that the isopentenyl-transferase (IPTs) genes are present in the *P. brassicae* genome (Schwelm et al., 2015). However, the substrate and the product of *P. brassicae* *IPT* genes remains unclear and needs to be explored (Malinowski et al., 2016). Malinowski et al. (2016) reported that *P. brassicae* has the biosynthetic pathways for synthesis of isopentenyl pyrophosphate from acetyl CoA via MVA pathway and the conversion of this compound to DMAPP through isopentenyl diphosphate-delta-isomerase. Genes involved in this biosynthetic process are expressed during gall formation. In the *A. thaliana* quadruple mutant *ipt 1,3,5,7*, deficient in host cytokinin biosynthesis, the expression of cytokinin-responsive genes *ARR4*, *ARR5*, *ARR6* and *ARR7* is elevated in response to *P.*

*brassicae* infection. This suggests that expression of these genes occurs as a cytokinin response resulting from the occurrence of a small amount of *P. brassicae*-derived cytokinin. However, cytokinin originated from *P. brassicae* is not enough to trigger the formation of the vascular cambium in host plants (Malinowski et al. 2016).

In cytokinin signal transduction, three cytokinin receptor proteins have been identified in *A. thaliana* plants including AHK2, AHK3 and AHK4 (Heyl and Schmulling, 2003). These receptor proteins transduce signals to activate *Arabidopsis* response regulator (ARR) proteins to activate plant defence responses and regulate source/sink relations, and are correlated in various plant developmental processes including cell division (Heyl and Schmulling 2003, Choi et al., 2011, Roitsch and Ehness, 2000). The expression of the ARR5 gene is closely correlated with cytokinin content. Siemens et al., (2006) reported that the expression of *GUS* under the ARR5 promoter is increased in infected roots. Devos et al. (2006) reported an increase of ARR5::*GUS* expression at very early infection stages consistent with the occurrence of iP and IPA which suggested that these originated from *P. brassicae*. Malinowski et al. (2016) on the other hands reported that ARR5::*GFP* expression in infected tissue is  $\leq$  that observed in uninfected tissue at the onset and during late gall formation, when the secondary thickening process occurs and is consistent with the transcriptomic data in that study. It has been suggested that repression of ARR5 reflects the repression of genes associated with cytokinin metabolism. In uninfected plants, ARR5::*GFP* is expressed in growing primary root tips and tissues undergoing secondary thickening. Cross sections of hypocotyl tissue specifically shows that this gene is localised in phloem bundles exterior the continuous ring of vascular cambium. Expression of ARR5 gene is closely associated with phloem development as phloem is a rich source of transported cytokinin. This gene is repressed when gall formation is initiated at 16 DPI (Malinowski et al., 2016).

Metabolic regulation of cytokinins content occurs through irreversible cleavage of the N<sup>6</sup> side chain of isoprenoid cytokinins including *cis*-zeatin, cytokinin 9-

glucoside, through cytokinin oxidase (*CKX*) activity (Spichal 2012). Following *P. brassicae* infection, the *A. thaliana* genes *CKX1* and *CKX6* are down-regulated in infected roots before clubroot symptoms become apparent and in the presence of gall formation (Siemens et al., 2006), specifically in cells containing large plasmodia (Schuller et al., 2014). *GUS* under the *CKX1* promoter is expressed in specific root tissues. The expression of *GUS* under *CKX1* promoter activity is reduced during early infection, but not observed at late infection especially at branching points of root tissue (Siemens et al., 2006). Meanwhile, *GUS* under *CKX6* promoter activity, which is predominantly expressed in the whole root-vascular cylinder of uninfected plants, is reduced in infected root tissue at early stages of infection and the stained cells are irregular at late stages of infection (Siemens et al., 2006). The overexpression of host *CKX* genes in *P. brassicae*-infected *A. thaliana* plants is correlated with reduced cytokinins content, increased disease tolerance, with the formation of tiny clubroot galls observed, possibly due to the degradation of pathogen cytokinins (Siemens et al., 2006). The down-regulation of *CKX1* and *CKX6* genes are consistent with those reported by Malinowski et al. (2016). However, they suggest that cytokinin oxidase reducing cytokinin content in infected tissue which leads to a reduction in vascular cambium development and small galls. Therefore, manipulation of host cytokinins metabolism slows *P. brassicae* development whereas other changes to vascular cambium activity would not be effective to slow the *P. brassicae* development (Malinowski et al., 2012, 2016).

Generally Chinese cabbage plants contain higher levels of free indole-3-acetic acid (IAA) in response to *P. brassicae* infection when compared with uninfected plants (Ludwig-Muller et al., 1993, Raa 1971). It has been suggested that the increase in the level of IAA within infected cells is most likely due to a change in the balance between synthesis and degradation in clubroot galls (Raa 1971). The accumulation of auxin in *P. brassicae*-infected tissue is demonstrated by the up-regulation of the auxin related gene nitrilase I (*NTI1*) during the colonization process and the upregulation of *NTI2* during the maturation of pathogen spores (Siemens et al., 2006). A lack of *NIT1* gene in infected plants contributes to a

smaller gall formation (Grsic-Raush et al., 2000). This suggests that loss of *NIT* gene which is important at early *P. brassicae* infection could reduce the size of gall formation. Meanwhile, *NTI2* and another auxin biosynthesis gene, *CYP79B2* are up-regulated in infected cells containing large plasmodia (Schuller et al., 2014). The up regulation of *NIT2* is found in infected cells containing sporulating plasmodia (Grsic-Rausch et al., 2000), which indicates that auxin is involved in the cell enlargement required to develop a gall at the late stages of *P. brassicae* infection. In addition, GUS coupled to the synthetic DR5 auxin response element in transgenic *A. thaliana* plants clearly shows a high signal along the cell layers of the hypocotyl tissue, especially near gall formation (Devos et al., 2006). In uninfected plants, DR5: GUS is expressed in the plant meristematic area and in vascular tissues (Devos et al., 2006). GUS under control of the DR5 auxin response element is predominantly expressed in the epidermis cells of infected roots. Auxin resistant mutant *alh1*, which defects at the site of auxin transport, shows three times lower infection ratio than wild type in response to *P. brassicae* infection indicating IAA from the host not able to extend to the site of infection (Devos et al., 2006). However, clubroot symptom progression in *alh1* mutants is similar to wild types with the evident hypocotyl size two times larger than uninfected mutant plants.

*P. brassicae* genomic analysis reveals the presence of the auxin-responsive Gretchen Hagen 3 (GH3) protein, which helps to maintain hormonal balance in biological systems by binding plant hormones to amino acids (Schwelm et al., 2015). Meanwhile, host genes that encode GH3 proteins are predominantly up-regulated in *P. brassicae*-infected tissue (Siemens et al., 2006). It seems like both pathogen and host are responding to auxin accumulation and competing between each other with different aims. Pathogens respond to auxin by inducing abnormal host cell division and cell expansion to enable colonization, while hosts respond to auxin to activate their defence systems. However, the mechanism of how auxin plays a role in plant defence during clubroot infection is not fully understood and requires further exploration.

The plant hormone Brassinosteroid (BR) has been reported to be involved in the alteration of plant development during *P. brassicae* infection (Schuller et al., 2014). Most genes associate with BR biosynthesis and signalling pathways are up-regulated in root tissues of *P. brassicae*-infected *A. thaliana* plants, which indicates that these genes play a role in clubroot development (Schuller et al., 2014). It has been demonstrated that inhibiting the BR synthesis pathway using the inhibitor propiconazole reduces the size of galls in *P. brassicae*-infected plants, which increases disease tolerance towards *P. brassicae* infection (Schuller et al., 2014). Besides, *br1-6* mutant plants, which have a deletion in a BR signalling component, show a lower disease severity with a reduction of gall size compared to wild type plants. Upon infection, genes involved in brassinosteroid metabolism and degradation are either down-regulated or not regulated at all, except *BAS1* which is strongly up-regulated in infected root tissues. *BAS1* degrades brassinolide, a brassinosteroid active compound (Schuller et al., 2014).

It has been suggested that BR is involved in xylem formation through the BR-related transcription factors VND6 and VND7 (Schuller et al., 2014). Both genes are down-regulated in *P. brassicae*-infected plants, which indicates the reduction of xylogenesis during gall development (Schuller et al., 2014, Malinowski et al., 2012). Malinowski et al., (2012) demonstrated that disrupting meristematic activity in the vascular cambium during gall development can reduce the gall size in *P. brassicae*-infected plants. Moreover, BR is suggested to be involved in abnormal cell expansion, which leads to clubroot gall formation, together with auxin (Schuller et al., 2014). BR induces the transcription factor ARF, which is involved in the activation of auxin-responsive genes. It has been suggested that PP2A, which is a BR signalling regulator, triggers the inactivation of the ARF2 repressor resulting in auxin-dependent gene expression via the positive regulator ARF. The ARF2 repressor inhibits auxin-dependent gene expression by binding to auxin-response elements in the promoter of BR/auxin related genes (Schuller et al., 2014).

#### 1.2.4. How Does the Host Respond to *P. brassicae* Infection?

Plants have a complex and multi-layered defence system. Successful colonization indicates that *P. brassicae* can avoid host defence responses in multiple ways. During primary infection, the host starts to recognize *P. brassicae* as an unwanted visitor and induces its chemical and molecular defences (McDonald et al., 2014, Ludwig-Muller et al., 2015). In incompatible interactions between *A. thaliana* plants and *P. brassicae* infection, host cells necrosis occurs which results in small nodules and tiny swelling in infected plants (Kobelt et al. 2000). The resistant *A. thaliana* plants to *P. brassicae* restrict the pathogen growth (Kobelt et al., 2000). In compatible interactions on the other hand, *P. brassicae* can induce its effector proteins to suppress the host defence response (McDonald et al., 2014). It has been predicted that the *P. brassicae* genome contains 553 secreted proteins, expressed at different stages of development (Schwelm et al., 2015). These secreted proteins could potentially be effectors to suppress host defence responses. For instances, Ludwig-Muller et al. (2014) discovered *P. brassicae* secretes the methyltransferase (PbBSMT) enzyme to modify host salicylate acid (SA), which is involved in plant defence.

The ability of *P. brassicae* to enter and colonize host tissues is also dependent on their strategy to avoid plant defence systems and re-channel plant metabolites for their requirements. Putrescine, spermidine and spermine polyamines are increased in the infected regions of *B. rapa* roots and in susceptible *A. thaliana* Col-0 plants (Walters and Shuttleton, 1985, Jubault et al., 2008). It has been suggested that *P. brassicae* induces the synthesis of these polyamines in susceptible plants as part of their strategy for colonization (Jubault et al., 2008). During cortical infection, *P. brassicae* re-channels the catabolism of the amino acid arginine by increasing the production of polyamines, increasing the metabolic flux from the degradation of arginine to ornithine, glutamate and proline, and inhibits the synthesis of nitrogen oxide in order to inactivate host mediated host defence (Jubault et al., 2008, Wagner et al., 2012). In contrast, root tissues of partially resistant *A. thaliana* Bur-0 plants, which show slow disease development upon *P. brassicae* infection, contain less of the amino acid

proline, accompanied by low arginase activity, and contain a high accumulation of agmatine. Agmatine is decarboxylated arginine as well as an initial compound in the synthesis of polyamines (Jubault et al., 2008). It seems that proline may be a source of nitrogen for secondary development of *P. brassicae* while arginine may be a compound which increases resistance in plants to *P. brassicae* infection.

During gall formation, a plant triggers its plant defence systems in response to *P. brassicae* cortical infection. Several studies have demonstrated changes in metabolites that are involved in plant defence in infected plants. Pedras et al. (2008) showed that phytoalexins and phytoanticipins, which are involved in antimicrobial and constitutive defence, are changed in roots of oilseed rape (*Brassica napus*) infected with *P. brassicae*. For instance, the phytoanticipin indolyl-3-acetonitrilase is increased in infected plants at the early stage of cortical infection, while indolyl glucosinolate is decreased at the late stage. The phytoalexins brassicanal and brassilexin are produced at later stages of infection in oilseed canola infected with *P. brassicae* (Pedras et al., 2008). However, there is a lack of information on how these metabolites are involved in plant defence during *P. brassicae* infection. Defence metabolites might be produced in uninfected cells of infected tissues to prevent the spreading of the pathogen, or they may be transported out of uninfected cells to infected cells.

Camalexin, which is a primary phytoalexin that is involved in *A. thaliana* plant defence, is increased in infected *A. thaliana* Bur-0 plants indicating that this compound is correlated to disease development upon *P. brassicae* infection (Lemarie et al., 2015). It has been suggested that camalexin biosynthesis is involved in the second layer of defence and could be a potential resistance factor in plants upon *P. brassicae* infection. Moreover, in *P. brassicae* susceptible *A. thaliana* plants, camalexin is decreased upon infection (Lemarie et al., 2015). It seems like *P. brassicae* suppresses this plant defence reaction during the infection interaction, but how this happens is not yet fully understood. In contrast, Siemens et al., (2008) reported that camalexin is increased in *A. thaliana* root

galls which suggests that camalexin does not influence the development of clubroot disease in *A. thaliana* plants (Siemens et al., 2008).

Indole glucosinolates are also suggested to be involved in plant defence. Chinese cabbage and *A. thaliana* plants that are susceptible to *P. brassicae* infection contain high concentrations of indole glucosinolates in their infected tissues (Ludwig-Muller et al., 1993, 1999b). However, it has also been suggested that cruciferous plants are suitable hosts to *P. brassicae* due to the presence of large quantities of indole glucosinolates in their vacuoles. *P. brassicae* infection causes cell damage and subsequently triggers the release of indole glucosinolates from the vacuole into the cytoplasm (Ludwig-Muller et al., 1999a). However, it has been reported that indole glucosinolate does not influence the development of clubroot disease in *A. thaliana* plants (Siemens et al., 2008).

Flavonoids such as naringenin, quercetin and kaempferol are also accumulated in root galls of *P. brassicae*-infected *A. thaliana* plants (Paesold et al., 2010). In addition, genes associated with flavonoids biosynthesis are up-regulated before and after the presence of clubroot galls. Flavonoid compounds are not involved in plant defence, since the deletion of flavonoid biosynthesis genes causes tolerance, with the formation of smaller galls in mutant plants observed (Paesold et al., 2010). Application of prehexadane-calcium (PRoCa), an inhibitor of flavonoid synthesis, can reduce the abundance of the flavonols quercetin and kaempferol in clubroot infected plants (Paesold and Ludwig-Muller, 2013). *P. brassicae*-infected plants with PRoCa treatment develop better root systems, although galls are still visible (Paesold and Ludwig-Muller, 2013).

However, flavonoids are not involved directly in clubroot development. It has been suggested that the role of flavonoids in *P. brassicae* infection is related to the distribution of auxin in the root system. Flavonoids inhibit auxin transport by modifying auxin efflux carriers (Paesold et al., 2010). Mutant lines with deletions in flavonoid synthesis genes including *tt4*, *tt5* and *tt6* have a similar auxin concentration to wild type plants. It has been demonstrated using *IAA:GUS* transgenic plants that application of flavonoids can cause an accumulation of

auxin in the infected cells containing plasmodia (Paesold et al., 2010). However, in the absence of flavonoids, auxin is distributed to the whole root system which subsequently reduces the size of gall formation in *P. brassicae*-infected root tissues (Paesold et al., 2010).

### **1.2.5 The Role of Plant Hormones in Defence against *P. brassicae* Infection**

Several studies also demonstrate the alteration of the metabolism of salicylic acid (SA) during *P. brassicae* infection. SA is reported to be involved in promoting the expression of pathogenesis related genes *PR-1* and *PR-2* during the host acquired resistance (SAR) response. It accumulates in the root and leaves of *P. brassicae*-infected *A. thaliana* plants, particularly at the late stages of infection. At this stage, *P. brassicae*-infected plants exhibit stunted phenotypes (Ludwig-Muller et al., 2015). Application of exogenous SA to root tissues of *P. brassicae*-infected *B. oleracea* plants results in reduced gall size (Lovelock et al., 2013). This suggests that SA is a phytohormone that can potentially enhance plant resistance to *P. brassicae* infection (Lovelock et al., 2013). In contrast, the activity of SA in root tissues of *P. brassicae*-infected plants might be suppressed by the production of methylated SA (MeSA) by *P. brassicae* (Ludwig-Muller et al., 2015). Host deficiency in the production of MeSA (inactive SA) does not alter the development of gall formation. Ludwig-Muller et al. (2015) discovered that *P. brassicae* can modify SA through secreting its methyltransferase (PbBSMT) enzyme. PbBSMT modifies host SA into MeSA in root tissues. MeSA in root tissues is transported to leaves of infected plants and converted back to active SA by host MeSA esterase to trigger the SAR response.

Although ethylene (ET) does not appear to have a direct role in defence responses to *P. brassicae* infection, alteration in ET signalling have been implicated in disease development. The role of ET in plants during *P. brassicae* infection can be explored using ET biosynthesis pathway, ET signalling and ET response genes. During *P. brassicae* infection, the ET precursor aminocyclopropane-1-carboxylic acid (ACC) is decreased due to the upregulation of ACC oxidase to release ET, both when the gall is not present and when the

gall is present (Knaust and Ludwig-Muller, 2013). This suggests that ET is accumulated in infected plants due to the high expression of ACC oxidase. Genes associated with ET signalling are clearly down-regulated in the presence of gall formation. In the ET signalling pathway, deletion of *ETO2* genes causes overexpression of ET biosynthesis genes which reduces the size of galls but does not increase the tolerance against *P. brassicae* infection because the galls are present in the whole root tissue, despite the fact that they are smaller (Knaust and Ludwig-Muller, 2013). Meanwhile, deletions in ET receptors (*etr1* and *ein4*) or positive regulators of ET response genes (*ein2* and *ein3*) increase the susceptibility of *A. thaliana* plants towards *P. brassicae* infection with the presence of more pathogen structures within the root than in wild type plant, with various sizes of galls observed. This suggests that ET signalling is required to restrict gall growth in hosts susceptible to *P. brassicae* infection (Knaust and Ludwig-Muller, 2013).

The ET signaling pathway is more related to plant development by promoting radial growth in *Arabidopsis* (Etchells et al. 2012). Overproducing ET in *eto1* mutant shows an early onset of secondary growth in vascular cambium cell division through high expression of ET responsive genes ERF109 and ERF108 (ET response factor), which results in larger vascular bundles when compared with wild type plants. ET responsive genes ERF109 and ERF108 act in promoting cell division in vascular bundles during primary and secondary plant growth (Etchells et al. 2012). This is not in agreement with the involvement of ET pathways in reduction of gall size in *P. brassicae*-infected *eto1* mutants.

The *ein2* mutant which has a complete loss of ET signalling, does not show a reduction in vascular cell number which indicates that ET signaling and ET responsive genes act differently in vascular tissue (Etchells et al., 2012). EIN2 has been demonstrated to enhance cell division in mutants with defects in the receptor kinase PXY (Phloem Intercalated with Xylem), which acts to repress the ET/ERF pathway by binding to peptide derived from ESR-like, CLE41 and CLE44. CLE41 promotes cell division in vascular cambium. However, *pxy*

mutants show no evidence of an increase in vascular cells, but rather shows a small reduction in vascular cell number. The *pxy, ein2* double mutant shows evidence of a reduction in vascular cell numbers compared with the single mutants. However, *pxy* and *ein2* single mutants are similar to wild types, indicating that EIN2 maintains vascular tissue in the *pxy* mutant (Etchells et al., 2012). This suggests that ET/ERF signaling could be an alternative of PXY/CLE41 pathway to promote cell division in vascular cambium of *A. thaliana* plants.

EIN5 on the other hand, is involved in mRNA decay. Vascular cell division in the *ein5* mutant is similar to wild type. The *pxy ein5* double mutant shows a reduction in vascular cell division similar to *pxy erf109* and *pxy erf108* double mutants (Etchells et al., 2012). The *ein5* mutant shows a reduction in EIN3 accumulation and results in accumulation of EBF1 and EBF 2. This suggests that EIN5 destabilizes EIN3 family transcription factors in wild type plants to inhibit EIN3 degradation and induce ET responsive genes. The *ein5* mutant shows a tolerance response following *P. brassicae* infection with a small gall size compared with wild type plants (Akhtar 2014). This may suggest that the activity of cell division in vascular cambium of *P. brassicae*-infected plants which leads to gall formation is reduced in *ein5* mutants. Figure 1.7 shows a model for the regulation of ET and PXY signalling act in aligned pathway in vascular development. These two signalling pathways are associated with regulation of ERF transcription factors which is involved in controlling the number of vascular cell divisions (Figure 1.7).

### **1.2.6 How does *P. brassicae* Manipulate Host Metabolism?**

As a biotrophic pathogen, *P. brassicae* is dependent on the host for its nutrients. However, during the germination and penetration phase, *P. brassicae* survives using nutrients that are stored in their resting spores, such as trehalose and lipids. Trehalose is hydrolysed into glucose by germinated spores of *P. brassicae*, and used as an energy source to support the germination process (Schwelm et al., 2015).

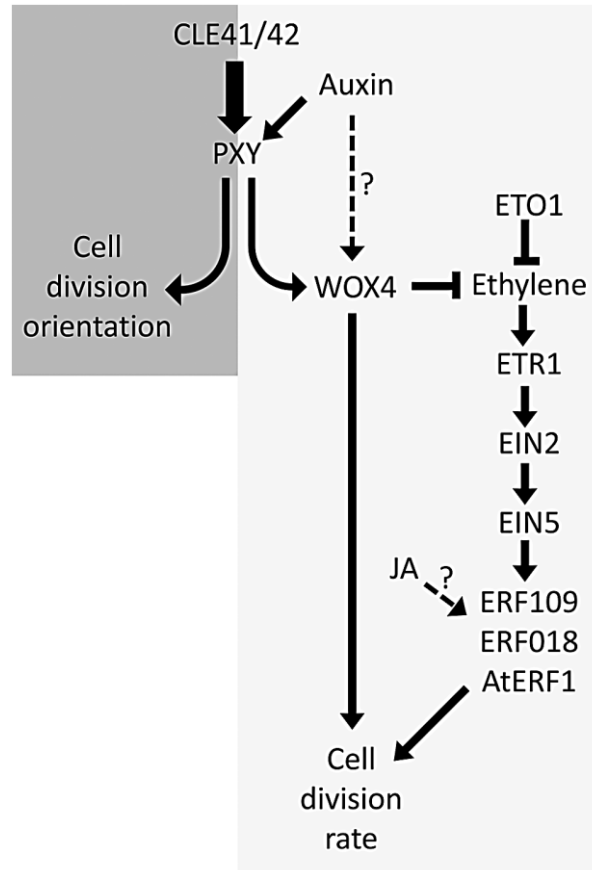


**Figure 1.7.** A model of ethylene and PXY signalling act in aligned pathway in vascular development Figure taken from Etchells et al. (2012).

In addition, genes involved in converting lipids to energy are highly expressed in germinating spores (Schwelm et al., 2015). Moreover, the development of *P. brassicae* inside host tissues causes an accumulation of lipids, amino acids, sugar and starch, and these metabolites are strongly associated with the enlargement of clubroot galls (Williams et al., 1968). The concentration of starch in gall tissues is associated with the activity of host enzymes involved in the synthesis and degradation of starch (Keen and Williams, 1969). During vegetative growth of *P. brassicae*, the activity of starch synthetic enzymes is increased, followed by the accumulation of starch in the hypocotyl tissues. A high specific activity of alpha-amylase occurs in isolated plasmodia (Keen and Williams, 1969). This indicates that a high metabolic activity is present in infected root tissues. This activity increases the mobilization of energy sources from shoot to root, which results in newly formed sink tissue. Besides, in clubroot-infected

plants, there are massive transport flows of sucrose through the phloem to sink tissues (Keen and Williams, 1968). Meanwhile, rates of photosynthesis in leaves of *P. brassicae*-infected plants are not different to those of uninfected plants, but carbohydrate content is low due to the export of carbohydrate from the leaves to the developing gall (Evans and Scholes, 1996).

During sporogenesis, starch synthetic enzymes are down regulated and starch degradation enzymes are up regulated. During sporogenesis, starch and sugar concentrations decrease at late gall formation, specifically in host cell cytoplasm that contains a new generation of *P. brassicae* resting spores (Williams et al., 1968). This indicates that starch and sugars are taken up by the pathogen directly or indirectly, which subsequently causes a lower concentration of these metabolites during sporogenesis and a higher accumulation of trehalose in *P. brassicae* spores (Keen and Williams, 1969). Besides, during sporogenesis, amino acid levels continue to increase in late gall formation, also specifically in host cell cytoplasm that contained a new generation *P. brassicae* resting spores (Williams et al., 1968). Specifically, the amino acids that increase in abundance in infected *B. napus* plants are aspartate, asparagines and glutamine (Wagner et al., 2012).

### **1.3 Hypotheses, Aims and Objectives of the Project**

The work presented in this thesis was carried out to understand the metabolic interaction between *A. thaliana* and *P. brassicae*. It is hypothesised that *P. brassicae* hijacks normal plant development and causes the accumulation of metabolites that are involved in metabolism and signalling. Previously, it had been shown that *P. brassicae* hijacks the vascular cambium by increasing cell division, reducing the number of xylem and increasing the number of phloem produced in cell differentiation during secondary thickening (Mallinowski et al., 2012). The response to infection of Col-0 in terms of plant development, specifically of hypocotyl cellular structures was therefore examined. Further to this, it was investigated whether the changes in plant development in response to clubroot infection were correlated with a change in metabolic status. In this

study, the metabolites that change in response to infection were identified, and the relevant metabolic pathways and the expression of genes involved were examined. Finally, a targeted approach was applied by focusing on carbohydrate metabolism in *A. thaliana* during clubroot infection. Specific hypotheses were identified by using transcriptomic analysis data and tested by using *A. thaliana* mutant plants and reporter genes.

**The aims of this thesis:**

1. Understand the metabolic interaction between *A. thaliana* plants and *P. brassicae* using an indirect approach to obtain metabolic 'fingerprinting'.
2. Verify metabolomics data by combining this data with host transcriptomic data obtained from a previous study
3. Understand carbohydrate metabolism in *A. thaliana* plants during *P. brassicae* infection by testing specific hypotheses.

**The project objectives were:**

1. To identify when metabolic changes occur and to identify metabolic pathways that change in response to *P. brassicae* infection in *A. thaliana* Col-0 plants.
2. To identify the metabolites that respond to *P. brassicae* infection, and determine how the intensity of these metabolites changes over the duration of the experiment.
3. To analyse the gene expression patterns that are responsible for the alteration of metabolites in response to *P. brassicae* infection.
4. To test specific hypotheses that were produced from transcriptomic data, focusing on carbohydrate metabolism.

## **Chapter 2: Plant Metabolic Fingerprinting in *P. brassicae*-Infected *Arabidopsis thaliana***

### **2.1 Introduction**

During clubroot infection, *P. brassicae* obtains carbon and other compounds such as organic nitrogen, vitamins, and minerals by manipulating host development and metabolism. In turn, its own development is strongly influenced by the host. These changes in host and pathogen development are brought about by changes in host and pathogen gene expression. The metabolism is at the interface between the two. The metabolome is a set of all of the metabolites of an organism. Its composition represents the activity of protein functions and substrates with multiple regulatory loops. However, the metabolites in *P. brassicae* infected plants do not originate from one organism alone; they also result from metabolite exchange between host and pathogen. This chapter looked to use a non-targeted approach to explore global changes in metabolites that occurs when *P. brassicae* infects its host *A. thaliana* plants.

#### **2.1.1. Metabolomics Technology**

Metabolic analyses allow the measurement of thousands of metabolites per sample in minutes. There are two major approaches used in metabolic studies; targeted metabolomics and untargeted metabolomics. Targeted metabolomics analyses specific groups of compounds to test a specific biological hypothesis about particular compounds with the further aim to understand those compounds in depth and their activities under specific physiological conditions (Roberts et al., 2012). For instance, targeted metabolomics is suited to the study of plant immunity against pathogen infection since many classes and types of metabolites involved in plant defence are known (Heuberger et al., 2014). Untargeted metabolomics deals with all the measurable compounds in a sample, including unknown chemicals. This approach could potentially be used for discovering novel targets in a particular experimental system (Roberts et al., 2012). In addition, this approach is suited to discovering unknown secondary metabolites involved in plant defence. Moreover, it is a very useful approach to explore the

pathogen of interest (Heuberger et al., 2014). The untargeted metabolomic approach used here was metabolic fingerprinting with mass spectrometry (MS). The compounds detected using this approach are not readily identifiable. As such it is suitable for identifying unique patterns in a particular tissue. There are multiple techniques available in MS applications, with samples injected directly or following separation by chromatographic methods (liquid, gas or electrophoretic). The method used here employed direct injection MS (DI-MS) with a time of flight (TOF) mass analyser system to provide a very rapid technique to analyse a large number of metabolites with greater mass to charge ( $m/z$ ) accuracies (Shulaev 2006; Sumner et al., 2003). This method loses the compounds that have low ionization efficiencies at the mass spectrometer interface (Shulaev 2006, Shulaev et al., 2008).

Briefly, metabolite extracts are obtained using a chloroform/methanol/water mix to separate polar and non-polar metabolites. Samples from uninfected and infected plants are injected into the mass spectrometer individually and the compounds in each sample are ionised using the electrospray ionisation method, in either positive or negative ion mode. In positive ion mode, metabolites often receive additional  $H^+$ ,  $Na^+$ , or  $K^+$  adducts. After ions are formed in the source, they are accelerated into the mass analyser (TOF-MS) and separated in a vacuum according to their mass to charge ratio ( $m/z$ ). The ions then pass to the ion detector, producing an electrical current that is amplified and detected to generate an image current in Total Ion Chromatograms (TIC). Figure 2.1 shows the basic components of the mass spectrometer, including an ion source, a mass analyser and an ion detector.

### **2.1.2 Combination of MarVis Filter and MetaboAnalyst to Analyse MS Data**

Mass spectra consist of several thousand peaks. From these spectra, MS data from each experimental condition and replicate need to be aligned before further analysis. The aligned sample data contains more variables than detected peaks. This is because detected peaks in each spectrum are slightly different between each technical and biological replicate. For better comparison between

treatments in statistical analysis, it is important to reduce the number of variables by filtering the data based on variance using specialized methods (Shulaev et al., 2008, Hackstadt and Hess, 2009). The MarVis filter software provides a complete pipeline for processing MS data, including statistical ranking, filtering, adduct detection, isotope correction, and molecular formula calculation (Kaeffer et al., 2012).

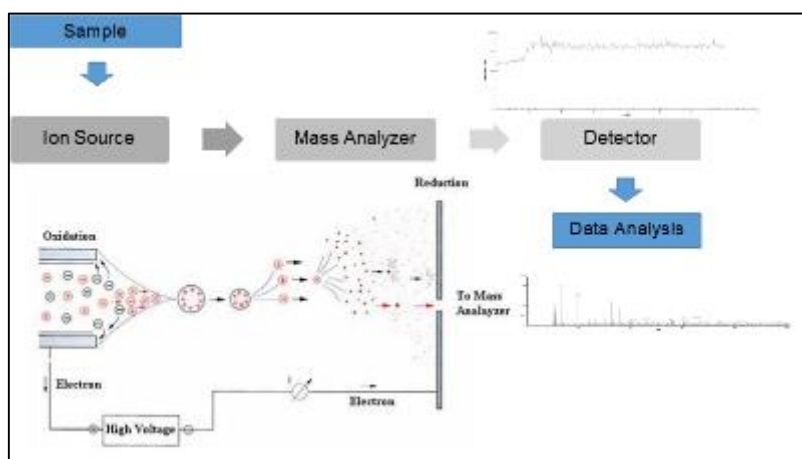


**Figure 2.1.** Basic components in Mass Spectrometry.

Metabolic fingerprinting data from direct MS requires a classification tool to identify metabolic signature patterns associated with different experimental treatments. It can be obtained using multivariate statistical analysis from unsupervised or supervised algorithms (Sumner et al., 2003). MetaboAnalyst software provides univariate and multivariate analysis (Xia et al., 2012, 2015). Univariate analysis explores each variable from two data sets separately, while multivariate analysis explores multiple variables from two data sets at a time. In addition, MetaboAnalyst can be used to visualize metabolic signature patterns and the most significantly different variables between treatments, using univariate analysis to produce fold-change plots or hierarchical clustering heat maps. MetaboAnalyst can also be used for multivariate analysis including Principle Component Analysis (PCA) and Partial Least Square – Discriminant Analysis (PLS-DA).

### 2.1.3 Accumulation of Metabolites in *P. brassicae*-Infected Plants

Accumulation of metabolites in infected tissues strongly influences host development and correlates with the enlargement of clubroot galls (Williams et al., 1968). Cell enlargement and cell proliferation in clubroot galls are influenced by the plant growth regulators cytokinin and auxin, which subsequently establish galls as sink tissue for photosynthetic products (Ludwig-Muller et al., 2009). Zeatin and zeatin riboside, which are responsible for increased cell division in infected tissues, accumulate 10-100 times higher in infected *Brassicae napus* (turnip) tissue than in uninfected tissue (Dekhuijzen and Overeem 1971). Dekhuijzen and Overeem (1971) suggested that these cytokinins are derived from the host. However, further study discovered that zeatin and zeatin riboside synthesised from plants and clubroot galls are potentially different, which indicate that these compounds in infected *P. brassicae* tissue are derived from plasmodia (Dekhuijzen 1981). Besides, the *P. brassicae* genome contains isopentenyl-transferase (IPTs) genes involved in cytokinin biosynthesis as well as PbGH3, a gene that can modify auxin (Schwelm et al., 2015). In addition, the reprogramming of existing meristematic activity during the secondary thickening of infected tissues could also influence the development of gall formation (Malinowski et al., 2012).

The development of *P. brassicae* inside host tissues also influences the type and the concentration of metabolites. Early work using metabolite analyses on hypocotyls of cabbage infected with clubroot showed that concentrations of DNA, RNA, lipids, amino acids, sugar, and starch increase during spore germination until the vegetative growth stage of plasmodia, and changes in the concentrations of these metabolites are strongly associated with the enlargement of clubroot galls (Williams et al., 1968). Lipids which increase during spore germination remain constant in abundance until sporogenesis indicating plasmodia are lipid-rich throughout infection (Williams et al., 1968). In sporogenesis which occurs during late gall formation, starch, sugars, RNA, and DNA concentrations decrease and amino acid levels continue to increase specifically in host cell cytoplasm that contains *P. brassicae* resting spores (Williams et al., 1968). The

fluctuation of starch and sugar concentration in the host during *P. brassicae* infection may indicate that starch and sugars are taken up by the pathogen directly, or indirectly through host enzyme activity leading to the synthesis and degradation of starch (Keen and Williams, 1969). During vegetative growth of *P. brassicae*, the activity of starch synthetic enzymes is increased, followed by an accumulation of starch in the hypocotyl tissues. During sporogenesis, starch synthetic enzymes are down-regulated and starch degradation enzymes are up-regulated. A high specific activity of alpha-amylase occurs in isolated plasmodia (Keen and Williams, 1969). This results in a lower concentration of starch during sporogenesis and could potentially cause an accumulation of trehalose in *P. brassicae* spores (Keen and Williams, 1969, Brodmann et al., 2002).

*P. brassicae* requires certain metabolites from the host in order to complete its life cycle. The *P. brassicae* genome lacks genes that function in sulfur and nitrogen uptake and in the biosynthesis of several amino acids, such as histidine, tryptophan, threonine, arginine, lysine, and thiamine (Schwelm et al., 2015). Studies in rapeseed also show that the accumulation of several amino acids such as serine, glutamine, aspartate, histidine, asparagine, glutamate and arginine could increase host disease susceptibility (Wagner et al., 2012).

#### **2.1.4 Aims and Objectives**

This chapter has an in-depth microscopic analysis of the infection process at 7, 9, 11, 14, 18, 21, 23, 25 and 28 DPI in *A. thaliana* Col-0 plants and contrasts this with uninfected Col-0 plants, defining the changes in primary and secondary growth of cellular structures that occur throughout infection. The second part of the chapter describes the direct injection ESI-MS approach used to obtain metabolic signatures in response to clubroot infection at 7 to 28 DPI. Peak picking and sample alignment, data filtering, quality checking and normalization are described. Univariate and multivariate analysis were then performed in order to select the most significantly different variables between treatments, fold-change analysis was used to classify and discriminate the biological replicate samples based on treatments, and hierarchical clustering analysis, PCA and PSL-DA were

carried out. The last part of this chapter covers the identification of predicted metabolites with coefficient scores between 100-80 as generated by PLS-DA, to identify novel metabolites and known metabolites that change at each stage of clubroot infection for further analysis in the future.

**Aims:**

1. To examine the cellular structure of *A. thaliana* hypocotyl tissues in response to *P. brassicae* infection.
2. To identify the metabolite patterns in each stage of *P. brassicae* infection.
3. To identify the putative metabolites that change upon *P. brassicae* infection.

**Objectives:**

1. To establish the cellular structure of hypocotyl tissue in uninfected Col-0 plants and in infected Col-0 plants as the infection progresses.
2. To conduct a metabolic analysis by using direct injection electrospray ionization mass spectrometry (ESI-MS).
3. To examine metabolite changes in Col-0 plants during infection by using the 'MALDIquant' R Package, MarVis Filter, and MetaboAnalyst 3.0.
4. To identify the metabolite compounds that change during infection.

## **2.2 Materials and Methods**

### **2.2.1 Preparation of *P. brassicae* Resting Spore Inoculum**

Resting spores of *P. brassicae* were originally isolated from clubroot-infected roots of *Brassicae oleracea* obtained from Penyrheol, South Wales, according to Mithen and Magrath (1992). This isolate is defined as European Clubroot Definition set 16/2/12 (Devos et al., 2005). To maintain stock *P. brassicae* inoculum, *Brassica rapa* var Wong Bok seeds (Chiltern Seeds, Ulverston, UK) were sown on moist M3 compost (Levington) and placed into a growth chamber with a temperature of 20°C, a photoperiod of 16 hours and irradiance of 100  $\mu\text{mol m}^{-2} \text{sec}^{-1}$ . Plants were watered from the bottom three times per weeks to avoid the compost drying out. Seven days after germination seedlings were transplanted individually into moist M3 compost in pots and returned to the growth chamber. Fourteen days after germination plants were inoculated with *P. brassicae* spores by pipetting 5 ml of spore suspension with a concentration  $2 \times 10^6$  spores  $\text{ml}^{-1}$  onto the soil around the base of the plant. The large galls, which developed within 6-8 weeks, were harvested, rinsed, and stored at -20°C until required.

Galls from *B. rapa* (Chinese cabbage) were placed in a blender (KENWOOD) and homogenised with 300ml of distilled H<sub>2</sub>O until no large pieces of tissue remained. The homogenate was passed through three layers of muslin and the resulting filtrate was centrifuged at 7500 *g* for 30 minutes at 4°C. The supernatant was discarded and starch, lipids, and other plant material were removed from the pellet using a spatula. The remaining layer of spores was re-suspended in 40 ml distilled H<sub>2</sub>O. Then, the spore solution was re-centrifuged and processed as described above. Spores were re-suspended in 40 ml distilled H<sub>2</sub>O and stored at 4°C. Spore concentration was calculated using the method described in the next section.

### **2.2.2 Counting *P. brassicae* Active Resting Spores**

A fluorescent staining technique was used to determine spore concentration and pathogenicity, according to Donald et al., (2002). Following this technique, the

spore suspension was stained with equal volumes of 50 µg/ml ethidium bromide (EB) and 100 µg/ml calcofluor white (CFW, disodium salt of 4, 4'-bis-(4-anilino-bis-diethylamino-S-triazin-2-ylamino)-2,2'-stilbene-disulphonic acid) (Fluorescent brightener, Sigma). Stained spores were pipetted onto a haemocytometer and counted under a fluorescent microscope (BX51; Olympus). The light source was a mercury lamp (HBO 200 W/2), and the filter consisted of an exciter filter U-MWIBA2 (460-490 nm). Images in bright field and fluorescent light were captured using a CCD camera (DP71; Olympus, [www.microscopy.olympus.eu](http://www.microscopy.olympus.eu)).

### **2.2.3 Plant Growth Conditions and Inoculation with *P. brassicae* Spores**

All experiments were carried out at a growth irradiance of 100 µmol m<sup>-2</sup> sec<sup>-1</sup>, with a 10 h photoperiod and day/night temperatures of 22°C/20°C.

Seeds of plants were stratified at 4°C in the dark for 4 days to break dormancy and transferred to the above growth chamber conditions afterwards. Seven days after germination, seedlings were transferred into pots containing a mix of moistened M3 compost and perlite at a 3:1 ratio. They were infected 14 days after germination using 2 ml of spore suspension with spore concentration of 2 X 10<sup>6</sup> spores ml<sup>-1</sup>.

### **2.2.4 Technovit Sectioning of Hypocotyl Samples**

Three hypocotyl samples of approximately 5 mm in length were harvested and excised from uninfected and infected plants at the 10 time points (7, 9, 11, 14, 16, 18, 21, 23, 25, and 28 DPI). Samples were placed in 100% ethanol for at least 30 minutes. Ethanol was removed and replaced with fresh ethanol for another 30 minutes. Samples were pre-infiltrated with Technovit 1 solution (1g Hardener 1 powder/100 ml of base liquid from a Technovit 7100 kit, TAAB, Bershire, UK) and 100% Ethanol at a 1:1 ratio for at least 1 hour. Then, the samples were infiltrated with 100% Technovit 1 for at least 15 minutes. Technovit 1 was removed and replaced with fresh 100% Technovit 1 for at least three days.

In the sample embedding process, hypocotyls with a length of 5 mm were placed vertically in 1.5 ml Eppendorf lids in a solution of Hardener 2 and Technovit 1 in a 1:15 ratio according to kit instructions and left at least overnight to allow the resin to set. The embedded samples were removed from tube lids and mounted onto 'Histobloc' mounting blocks (TAAB with order no. T395, Berkshire, UK) using Technovit 3040 (Yellow powder: 3040 in a ratio 3:1).

Mounted material was sectioned using a Leica RM2145 (Leica Instruments GmbH, [www.leicamicrosystems.com](http://www.leicamicrosystems.com)) microtome for 7  $\mu$ m (Technovit) sections. After mounting Technovit sections in DePeX (R) (GURR) mounting medium, images were captured using a CCD camera (DP71; Olympus, [www.microscopy.olympus.eu](http://www.microscopy.olympus.eu)) mounted on a light microscope (BX51; Olympus). Three representative plants from each time point were selected and 30 sections per plant were stained with a drop of 0.1% (w/v) toluidine blue in 100 mM buffer at pH7 (Sigma-Aldrich, Dorset, UK).

### **2.2.5 Metabolite Extraction**

Hypocotyl and root tissue samples with a length of approximately 5 mm were excised for each tissue, weighted, placed individually into a grinder tube, and immediately frozen in liquid nitrogen. The frozen samples were stored at -80°C before proceeding to the metabolite extraction method.

In metabolite extraction procedures, the frozen sample in a grinder tube was homogenized under liquid nitrogen with a micro-pestle. Pre-chilled single-phase solvent A (Methanol: Chloroform: H<sub>2</sub>O ratio 5:2:2) was added to homogenized samples with a ratio of 100mg fresh weight sample to 1 ml solvent. The mixture was vortexed for 10 seconds and left on ice for five minutes, and this step was repeated once more. The samples were vortexed and centrifuged at 17000 *g* for 2 minutes at 4 °C. The supernatant was transferred to a pre-chilled Eppendorf tube and the pellet re-extracted with solvent B (Methanol: Chloroform ratio 1:1), using half the volume of Solvent A. The mixture was vortexed for 10 seconds and left on ice for 10 minutes. The samples were vortexed and centrifuged at

17000 *g* for 2 minutes at 4 °C. Supernatant from solvent B was transferred to the tube containing supernatant from solvent A. Metabolites in methanol and chloroform were separated by adding H<sub>2</sub>O to half the volume of Solvent B. The samples were vortexed and centrifuged at 17000 *g* for 2 minutes at 4 °C. The methanol phase (at the top) and the chloroform phase (at the bottom) were placed in separate tubes. The metabolites in methanol and chloroform were stored at -80°C, before proceeding to the next procedure. A summary of the metabolite extraction used in this thesis is shown in Figure 2.2.

### **2.2.6 Direct Injection Mass Spectrometry**

Samples in methanol/H<sub>2</sub>O were diluted at a ratio of 1:100 in 50% methanol, 50% H<sub>2</sub>O and 0.1% formic acid and 0.1 mg/ml of phenylalanine (SIGMA) as a standard. Ten µL of diluted samples or standard were loaded into a syringe. The sample running method was set up in Analyst software (<http://sciex.com/>). Samples in the syringe were injected into the spraying nozzle of a Qstar mass spectrometer with a running speed of 6 µL/hour. The spraying nozzle was kept at positive potential (Positive ion mode) and samples were run into the machine for seven minutes for each sample. Molecular ions were accelerated into the mass analyser (Time of Flight, +TOF-MS) and separated in a vacuum according to their mass-to-charge ratio (*m/z*). Masses with a mass range between 50 and 1000 were detected in positive ion mode, and a total ion current chromatogram (TIC) was generated. The TIC was selected after three minutes running time to generate three mass spectra. Each mass spectrum represents a one-minute region of the TIC chromatogram. Data from each mass spectrum with *m/z* value and intensity was saved in a .txt file.

### **2.2.7 Binning Data**

Data in .txt files was transferred to a single csv file, containing *m/z* value and intensity from 10 time points, with a maximum of 12 biological replicates for each treatment and three technical replicates for each biological sample. Two .csv files, of which one file contained *m/z* values and intensities and the second file contained a total ion current (TIC) value for each data set, were imported into the

Homogenized hypocotyl (100 mg fresh weight) under liquid nitrogen



Added 1 ml of Solvent A (Methanol: Chloroform: H<sub>2</sub>O ratio 5:2:2)



Vortexed for 10 seconds and left on ice for 5 minutes, repeated 2 times

Centrifuged at 17000 g for 2 minutes at 4°C



Transferred supernatant into pre-chilled Eppendorf tube



Re-extracted the pellet with 0.5ml Solvent B (Methanol: Chloroform ratio 1:1)



Vortexed for 10 seconds, left on ice for 10 minutes

Centrifuged at 17000 g for 2 minutes at 4°C



Transferred supernatant from extraction in Solvent B into tube containing supernatant from extraction in Solvent A



Added 0.25 ml of H<sub>2</sub>O to the supernatant Solvent A and B mixture



Vortexed and centrifuged at 17000 g for 2 minutes at 4°C



Placed methanol phase (at the top) and chloroform phase (at the bottom) in separate tubes



Stored tubes at -80°C

**Figure 2.2.** Flow chart summarising the steps in metabolite extraction of plant tissues.

R program (<https://www.r-project.org/>). The binning process was carried out using a script written in the 'MALDIquant' package (Gibb and Strimmer 2012). Each run was normalized according to the TIC value obtained from the absolute intensities of three regions of the chromatogram. This was allowed to minimize the ionization efficiency variation that occurs between runs. A summary of the workflow used in the 'MALDIquant' package is shown in Figure 2.3. Data was exported to a binned .csv file. The average of all technical replicates for each sample was then calculated. Data from each infection stage was saved into a separate .csv file for further analysis.

### **2.2.8 Data Filtering Using MarVis-Suite 2.0**

Each infection stage dataset in .csv format was imported separately into MarVis Filter from the Marvis-Suite 2.0 package (<http://marvis.gobics.de/>). Ion features from each dataset were sorted and ranked according to the p-values of ANOVA. Adduct and isotope correction were performed on full datasets using predicted sets of adduct rules for the positive ionization mode and a mass tolerance 0.05 Da. After correction, the data sets were filtered for a p-value of 0.05. Data sets with p-values  $\leq 0.05$  were firstly exported to a .csv files for data processing, normalization and statistical analysis. The same dataset was used for annotation of known metabolites from public biological databases (described below).

### **2.2.9 Data Processing and Statistical Analysis Using MetaboAnalyst3.0 Web-Based Package**

The imported file from MarVis Filter was uploaded into MetaboAnalyst3.0 (<http://www.metaboanalyst.ca/>). The uploaded data were read and a data integrity check was performed during data processing. The intensity of variables with zero values was either excluded from the downstream analysis or replaced with a small value (half of the minimum positive value in the original data). No data filtering process was applied using this package. Processed data were normalised to median intensity and using automatic scaling (mean-centred and divided by the standard deviation of each variable) to generate a normal

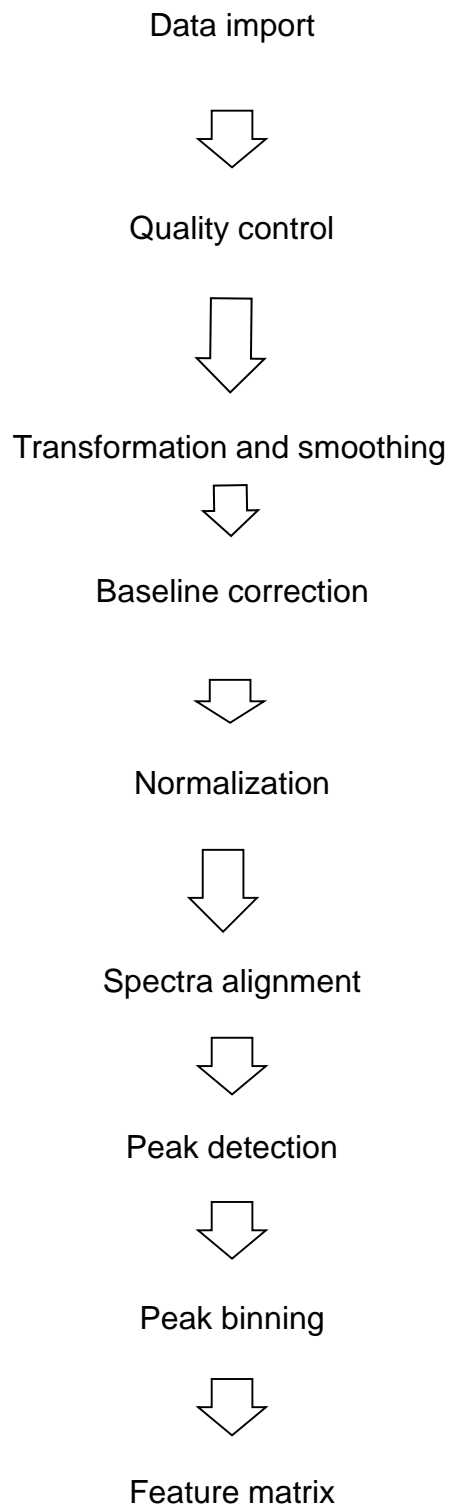


**Figure 2.3** A summary of workflow written in 'MALDIquant' package according to Gibb and Strimmer (2012).

distribution data before submitting to univariate and multivariate statistical analysis.

#### **2.2.10 Identification of Metabolites Using MarVis Filter for Ion Correction and MarVis Pathways**

Data sets with  $p$ -value  $\leq 0.05$ , which were obtained from section 2.2.8, were imported to MarVis pathways for identification of metabolites using *A. thaliana*-specific pathways from the Kyoto Encyclopedia of Genes and Genomes (KEGG) with a tolerance 0.05 Da. A summary of data filtering, processing, statistical analysis and data annotation is shown in Figure 2.4.

Binned data was imported to MarVis Filter provided in MarVis-Suite 2.0 package



Ion features from each dataset was sorted and ranked according to the p-value of ANOVA



Adduct and isotope correction according to adduct rules for the positive ionization mode and mass tolerance 0.05



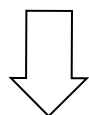
The data set was filtered according to a significance level for p-value of  $\leq 0.05$



The data set was exported to csv. file



Csv. file was uploaded into MetaboAnalysis 3.0



The uploaded data was checked for data quality during data processing

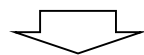


Normalization



Univariate and multivariate analysis

The data set was exported to MarVis pathways



The data set was annotated according to KEGG database

**Figure 2.4.** A summary of work flow for data filtering, data processing, statistical analysis and metabolite identification

## 2.3 Results

### 2.3.1 Quantification of *P. brassicae* Resting Spores

*P. brassicae* resting spores were quantified using fluorescent staining. This technique was used to examine the viability of the inoculum directly as well as distinguishing between starch grains and pathogen spores in the *P. brassicae* spore suspension (Figure 2.5). The spore suspension was stained with equal volumes of ethidium bromide and calcofluor white (see section 2.2.2). According to Takahashi and Yamaguchi (1988), the walls of all spores exhibit intense blue fluorescence due to calcofluor white binding to chitin. The cytoplasm of active spores exhibited a pale blue fluorescence but inactive spores exhibited red fluorescence as they were unable to exclude ethidium bromide which then bound to the spore DNA (Figure 2.5 B).

### 2.3.2 Primary Growth in *P. brassicae*-Infected *A. thaliana* Col-0 Plants

Transverse sections of the hypocotyls of uninfected and infected wild type *A. thaliana* (Col-0) plants were taken at 7, 9 and 11 DPI, in order to record the changes in the cellular structure that occurred during clubroot infection when the host was in the primary phase of growth. Toluidine blue was used to stain the cross section with all cell types stained purple except xylem cells, which stained a light blue. Figure 2.6 shows the primary growth of cellular structures in hypocotyls of *A. thaliana* plants infected with *P. brassicae*. The tissue of the hypocotyl consists of epidermis, endodermis, cortex, and stele. The stele includes all the tissue inside the cortex. An epidermis, which is one cell thick, surrounds the hypocotyl. No obvious difference in cellular organization was observed between uninfected and infected Col-0 plants at 7, 9 and 11 DPI (Figure 2.6 A).

Figure 2.6 (B) shows stele tissue, which consists of the pericycle and vascular tissues. The pericycle is the meristematic layer inside the cortex. Inside the pericycle is the hypocotyl vascular tissue. The vascular tissue consists of primary phloem bundles, primary xylem, and procambium during primary root growth. At this stage, the vascular cambium is not yet formed.

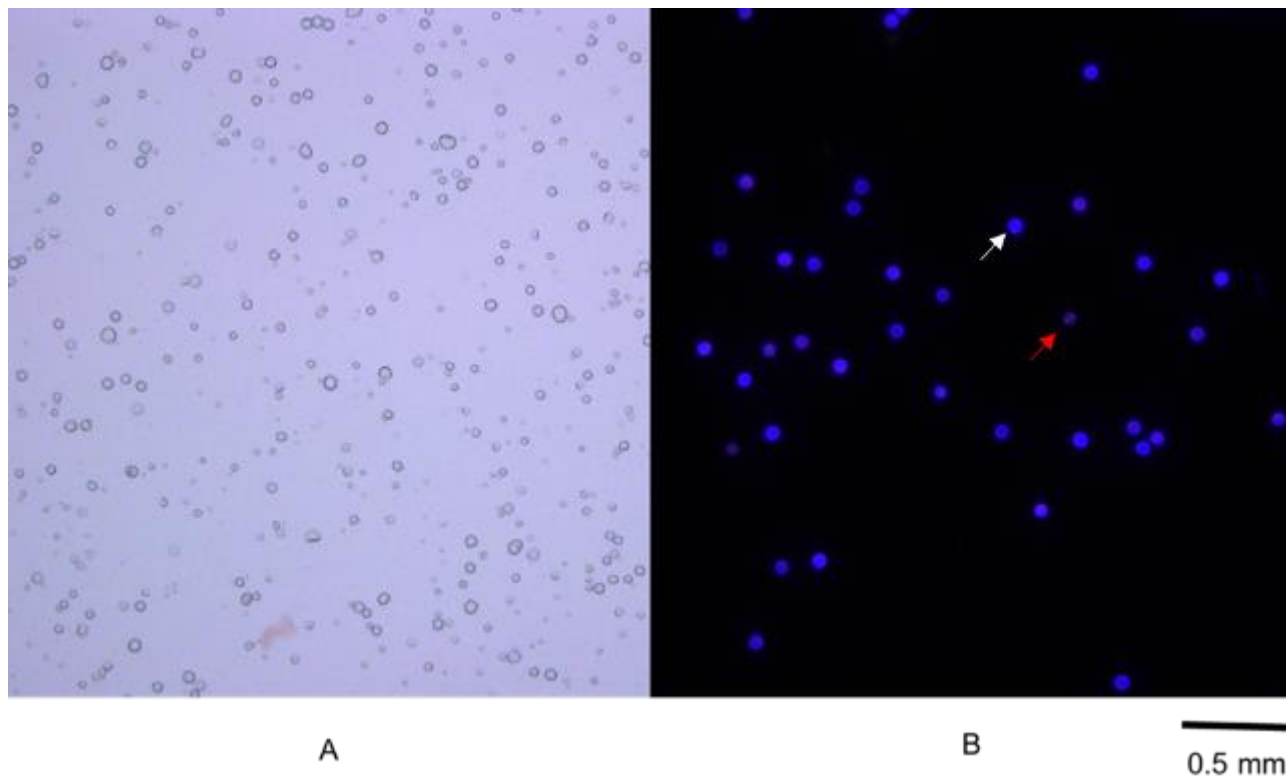


**Figure 2.5.** (A) Bright field (B) Active spore with pale blue fluorescence (White arrow) and inactive spore with red fluorescence in cytoplasm (Red arrow).



### **2.3.3 Secondary Growth in *P. brassicae*-Infected *A. thaliana* Col-0 Plants**

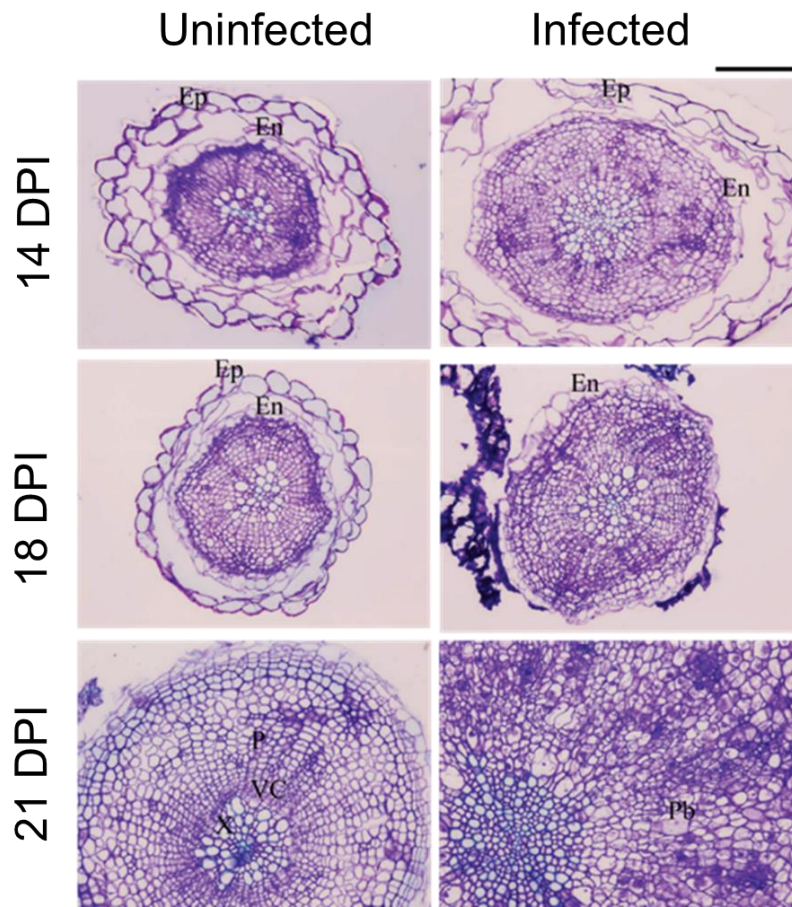
Transverse sections of the hypocotyl of uninfected and infected wild type *A. thaliana* (Col-0) plants were taken at 14, 18, 21, 23, 25 and 28 DPI (Figure 2.7), in order to record the changes in cellular structure and secondary growth that occur during clubroot infection.

As shown in Figure 2.7, hypocotyls underwent secondary thickening. This resulted in the gradual disintegration of the epidermis and endodermis cell layers (Gendreau et al., 1997). The hypocotyls of *P. brassicae*-infected plants were larger than those of uninfected plants (Figure 2.7 A, C). Infected hypocotyl tissue showed the presence of plasmodia inside host cells (Figure 2.7 B). Several infected cells containing plasmodia were approximately 10 times larger than the equivalent uninfected cells (Figure 2.7). Consequently, infected hypocotyls became swollen and distorted, leading to the development of a gall. In Figure 2.7 (C), xylem formation was disrupted in infected plants at 23 DPI, while phloem cell numbers were increased in infected plants at 28 DPI.

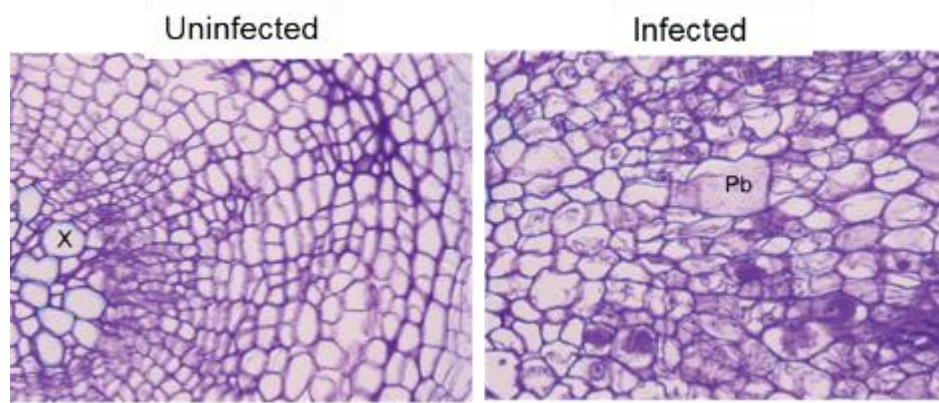
### **2.3.4 The Use of Electrospray Ionisation-Mass Spectrometry (ESI-MS) in Non-Targeted Metabolomics during Clubroot Infection**

Electrospray ionisation-mass spectrometry (ESI-MS) was used to obtain metabolite fingerprints of uninfected and *P. brassicae*-infected hypocotyl tissues at different stages of infection. In this study, hypocotyl tissues of uninfected and *P. brassicae*-infected plants were extracted using chloroform/methanol/water, separating polar metabolites and non-polar metabolites. Methanol/water soluble metabolites were used for further analysis using direct injection ESI-MS. In ESI-MS, intact molecular ions were produced via protonation when the spraying nozzle was kept at a positive potential (Positive ion mode). Molecular ions were accelerated into the mass analyser (Time of Flight, +TOF-MS) and separated in a vacuum according to their mass-to-charge ratio ( $m/z$ ). Ions passed to the ion detector produced an electrical current that was amplified, detected, and displayed as a Total Ion Chromatogram (TIC) for seven minutes for each biological sample (Figure 2.8).

A) 14, 18 and 21 DPI



B) 21 DPI



C) 23, 25 and 28 DPI

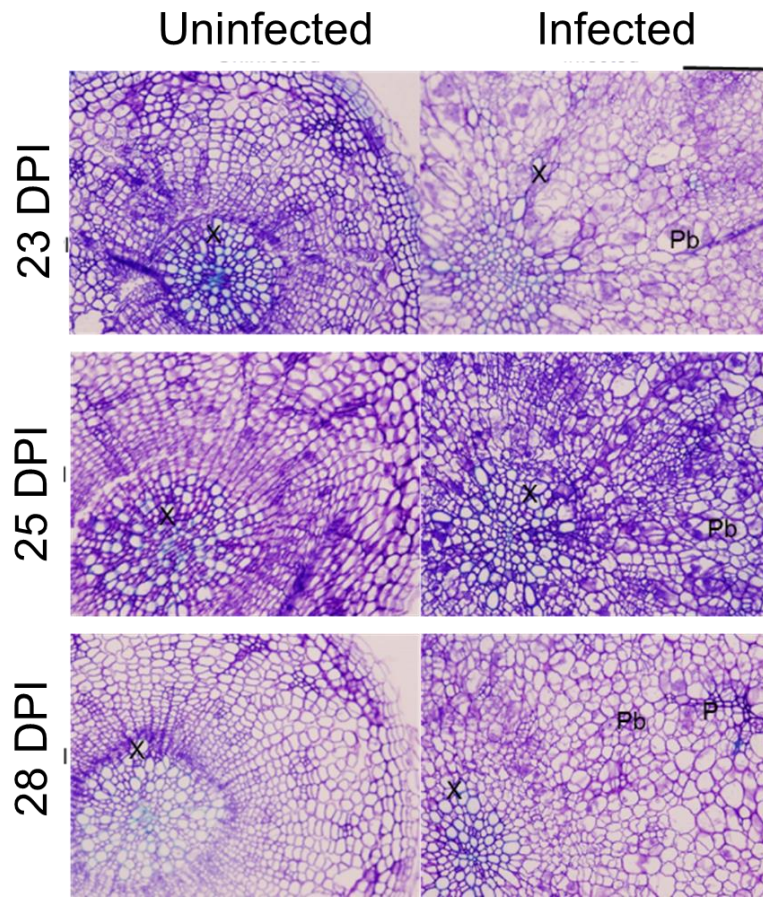


**Figure 2.7** A time course study of the hypocotyl of uninfected and clubroot-infected *A. thaliana* (Col-0) plants A) at 14, 18 and 21 DPI B) at 21 DPI in close-up image and C) 23, 25 and 28 DPI. En, endodermis; X, xylem; Ep, epidermis; P, phloem; Pp, phloem parenchyma; Xp, xylem parenchyma. Scale bar= 1mm.

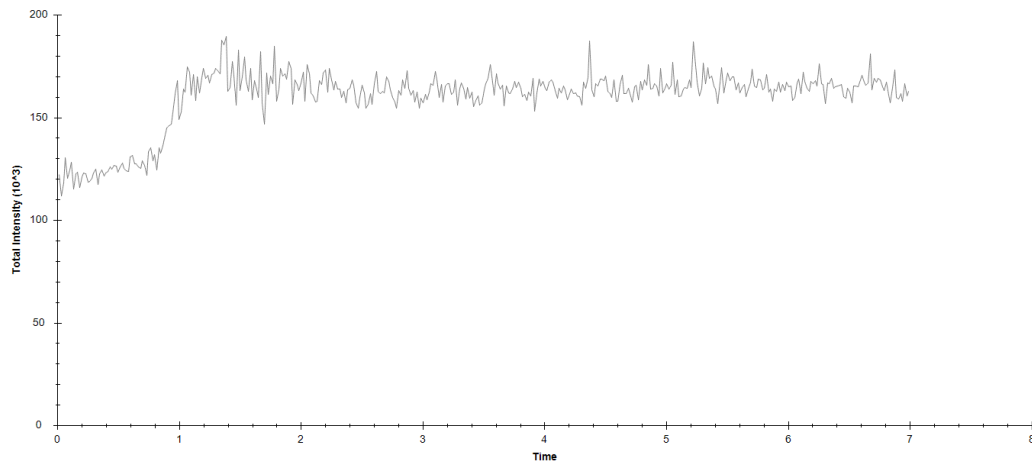


**Figure 2.8** A typical Total Ion Chromatogram (TIC) of *P. brassicae*-infected hypocotyl tissue at 7 DPI

The TIC was selected after three minutes running time to generate an ESI-Mass spectrum. The three ESI-Mass spectra produced from each biological replicate represented three technical replicates and the output files were saved in comma separated value (. csv) format for further analysis. Generally, ESI-Mass spectra for uninfected and *P. brassicae*-infected hypocotyl tissues showed the presence of similar  $m/z$  peaks (Figure 2.9). ESI-Mass spectra were analysed statistically to identify differences between treatments at each time point.

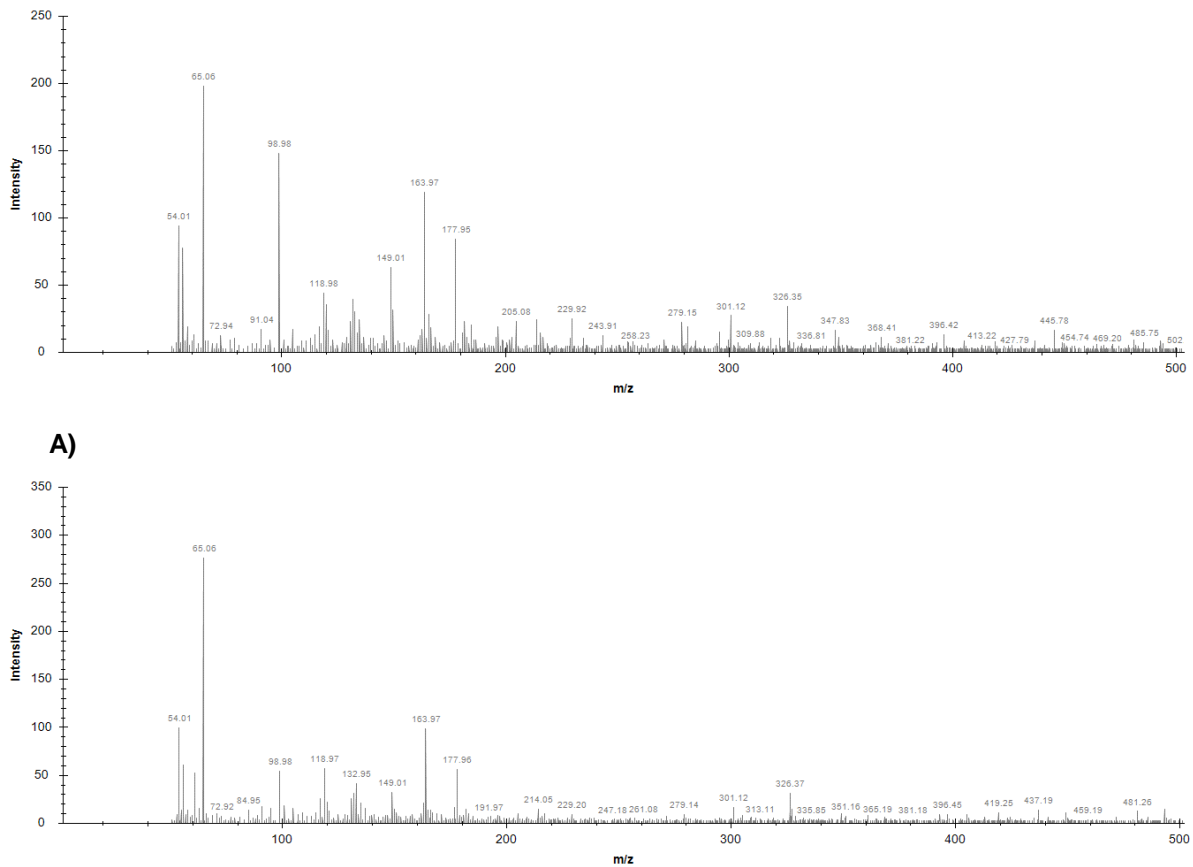


**Figure 2.9** Typical ESI-Mass spectra of A) Uninfected B) Infected hypocotyl at 18 DPI

A binning step was performed since the peaks of each ESI-Mass spectrum showed some variation in technical and biological replicates. In this study, the 'MALDIquant' package was used for the binning process. As described in Gibb and Strimmer (2012), the 'MALDIquant' package provides a complete analysis tool for MALDI-TOF data, but it can also be used for other mass spectrometry

data including direct injection ESI+TOF-MS. Before binning, the input data contained between 4399 to 6000 peaks. The output data after the binning process contained 34254 variables.

### **2.3.5 Data Processing and Normalization**

The binned spectral data from direct injection mass spectrometry represented 10 infection stages and two experimental conditions with each condition containing 12 biological replicate samples from hypocotyl tissue. Each infection stage dataset in .csv format was imported separately into MarVis Filter. Each dataset contains 12 biological replicate samples from uninfected and *P. brassicae*-infected plants and 34254 variables.

Ion features from each dataset were sorted and ranked according to the p-values resulting from an ANOVA test on uninfected and infected samples. The data sets were filtered according to a significance level for p-values of 0.05. The filtered data was saved in .csv files and uploaded to MetaboAnalyst 3.0. The uploaded data was read and a data integrity check was performed during data processing. There were no missing values found in any data set. Table 2.1 shows a summary of the data processing I carried out in order to improve the results of downstream analysis.

Then, the processed metabolite data were normalised to their mean intensity and by automatic scaling (data were mean-centred and divided by the standard deviation of each variable). This was used to generate a normal distribution plot of density versus normalized intensity for each infection stage (Figure 2.10). Normalisation was performed to minimize and standardise non-biological variation in order allow comparisons between uninfected and *P. brassicae*-infected samples.

**Table 2.1** Summary of data processing data using ‘MALDIquant’ package for binning, MarVis Filter for filtering and MetaboAnalyst 3.0 for checking the data quality. Total peaks in binned spectra=34254.

Time point (DPI)	Total peaks in mass spectrum	Total metabolites with p-value $\leq$ 0.05	Total processed metabolites
7	4811	1050	368
9	5998	825	519
11	5094	980	498
14	6051	697	388
16	4366	817	427
18	2658	517	371
21	5740	2550	1993
23	5684	896	608
25	5743	2960	2661
28	2158	941	752

### 2.3.6. Univariate Analysis and Fold-Changes

Univariate analysis provided in MetaboAnalyst 3.0 was used to identify differential accumulation of metabolites in *P. brassicae*-infected plants. The analysis allows pairs of treatments to be contrasted and allows a top table of differential accumulation of metabolites for each contrast, including the log Fold-change (FC) in metabolite intensity. In FC analysis, the algorithm first counted the total number of pairs with a FC that was consistently above or below the specified FC for each metabolite. A metabolite above the FC threshold 2 was defined as significant based on statistical analysis between two means of infected samples and uninfected samples. Figure 2.11 shows log<sub>2</sub>FC of intensity per spectra bins at 7 to 28 DPI. Metabolite with FCs above 1 and below -1 on were defined as increased and decreased respectively in infected samples. Table 2.2 shows the total number of metabolites that increased or decreased in abundance at each stage of infection. The total number of significant metabolites increased in late gall formation compared to either early infection or the onset of gall formation (Figure 2.11, Table 2.2).

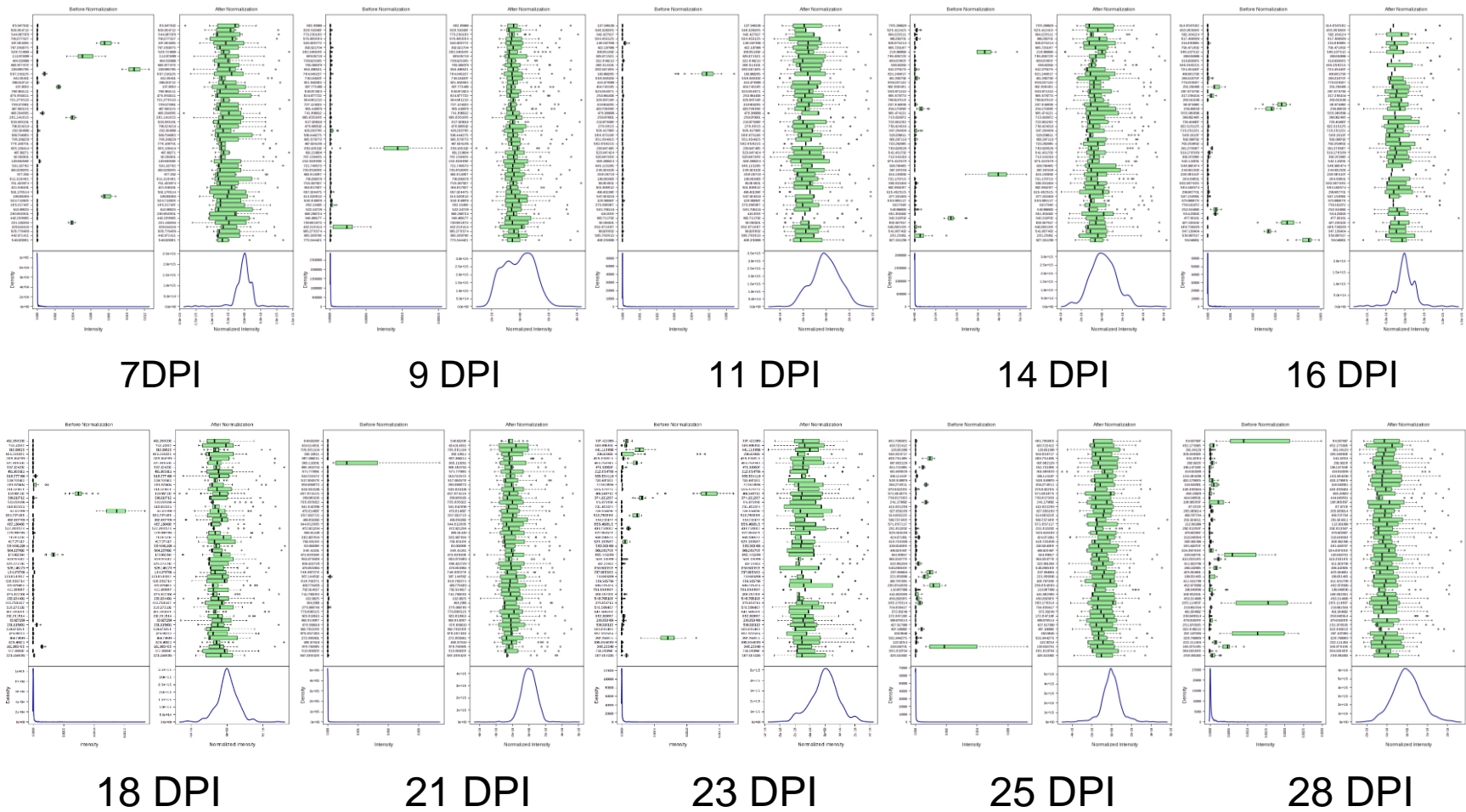


**Figure 2.10** Box plots and kernel density plot before and after normalization to sample median and auto scaling of samples at 7, 9, 11, 14, 16, 18, 21, 23, 25 and 28 DPI.

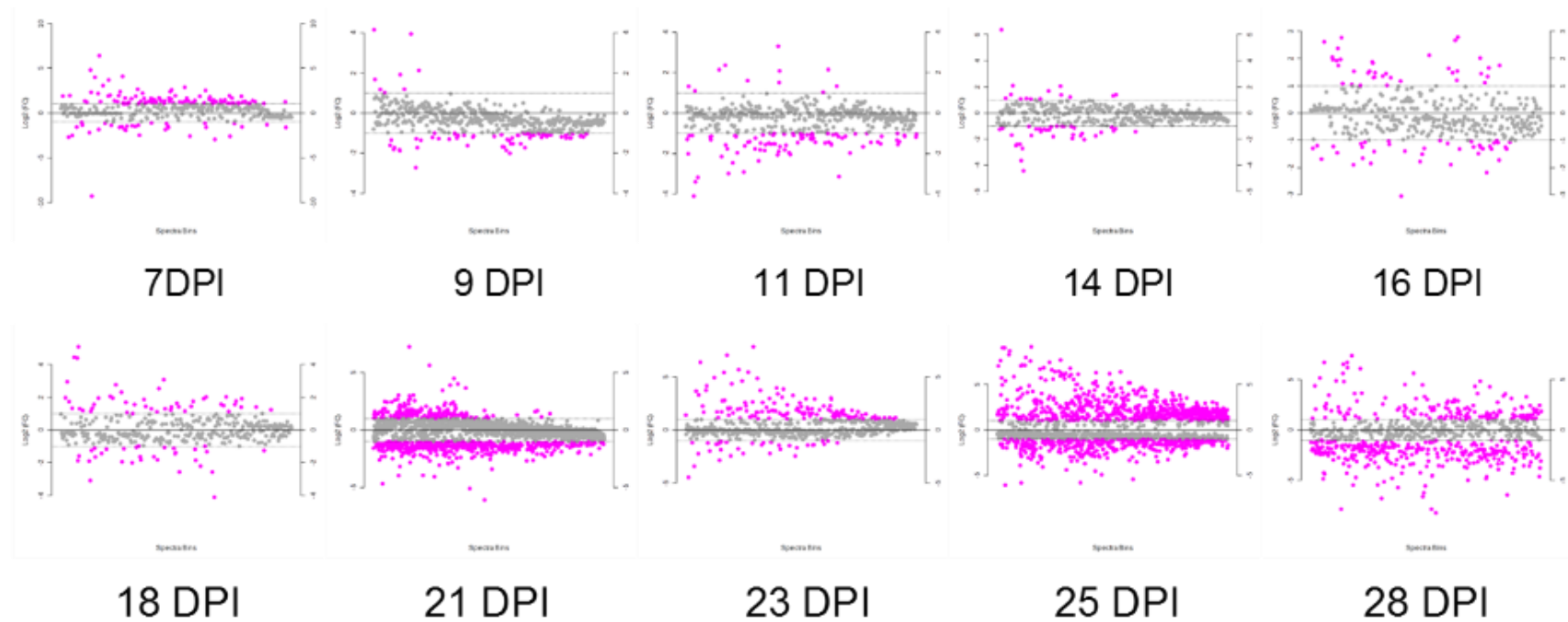


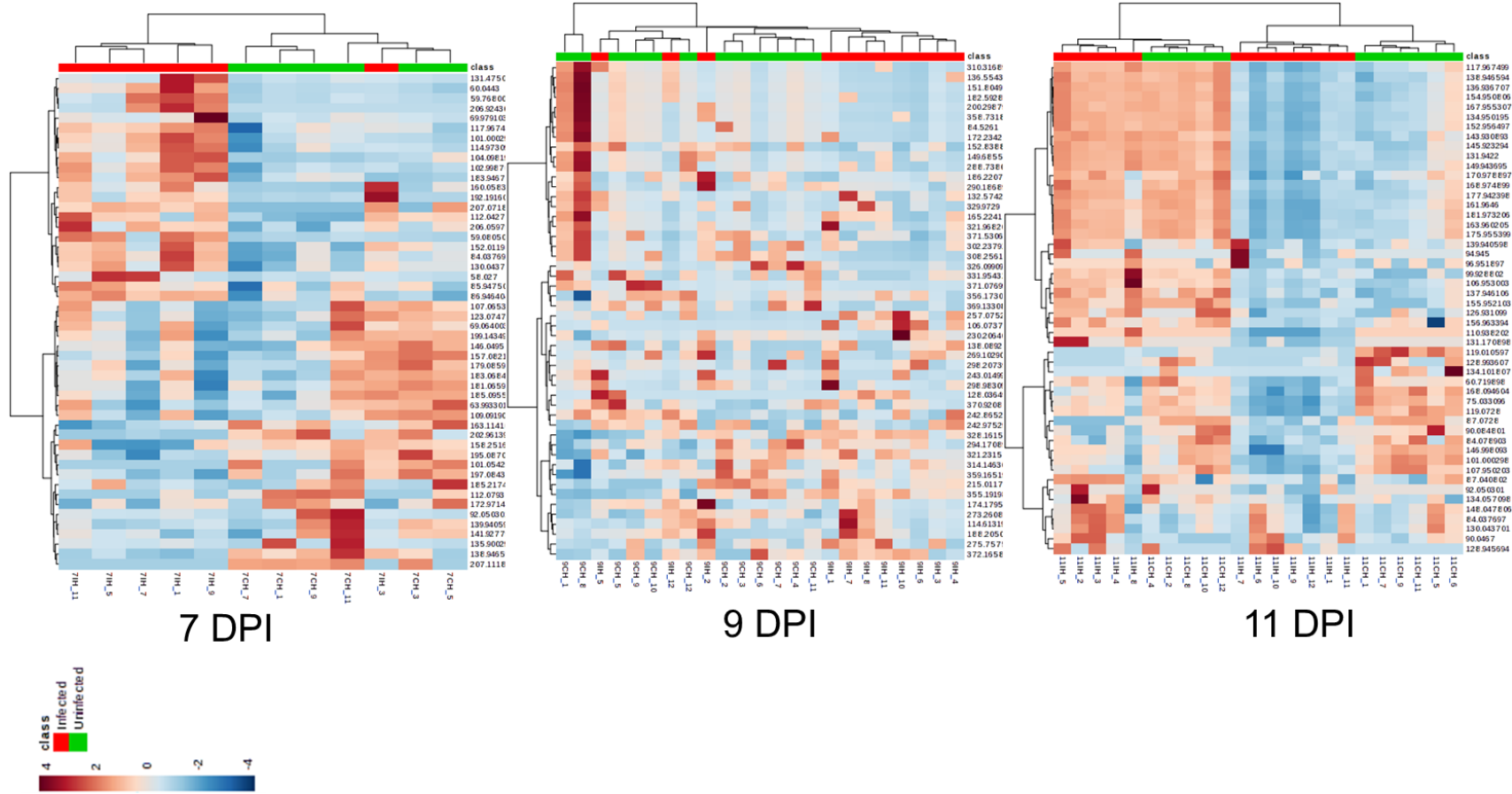
**Figure 2.11** Fold-changes of samples at 7, 9, 11, 14, 16, 18, 21, 23, 25 and 28 DPI. The red circles represent metabolite features above the threshold FC of 2. A value above the threshold FC of 2 on the log scale represents metabolite features that were up-regulated in infected samples, while values below threshold -2 on the log scale represent metabolite features that were down-regulated in infected samples.

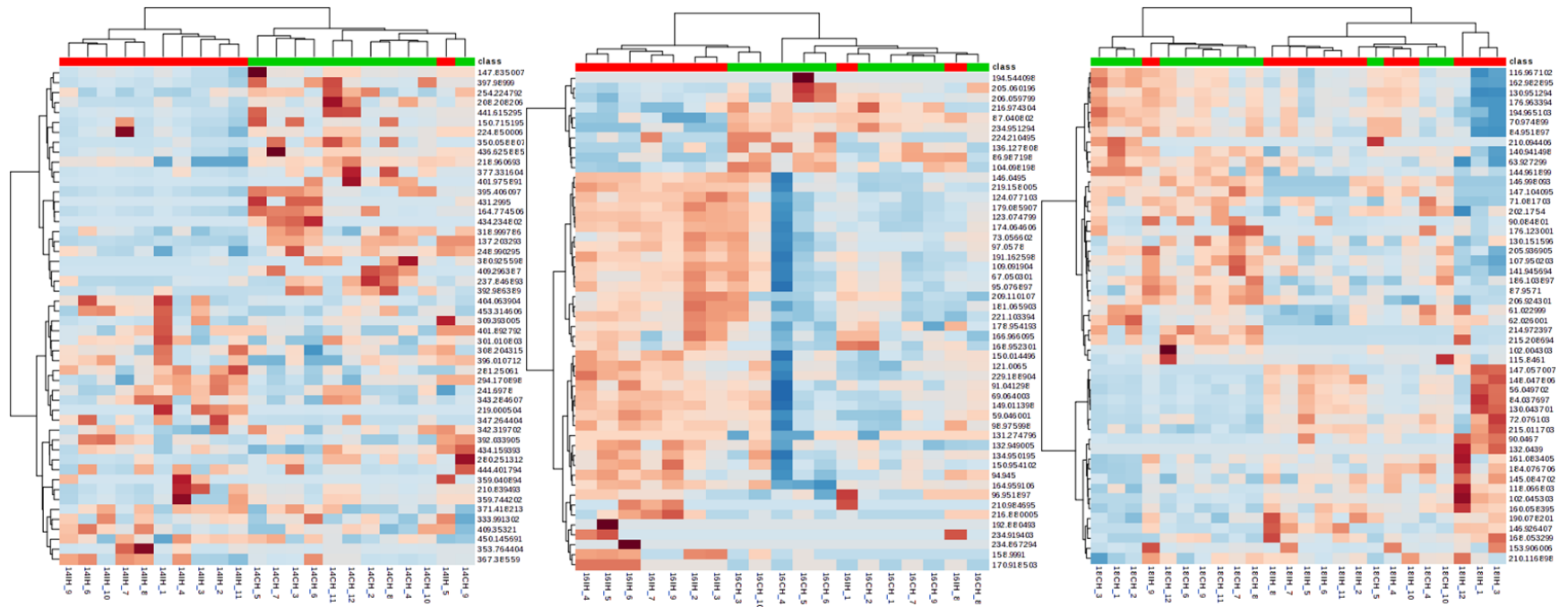
**Table 2.2:** Total of metabolite features that increased and decreased in infected samples at each stage of infection from 7 to 28 DPI.

Time point (DPI)	Total metabolites decreased	Total metabolites increased
7	33	84
9	64	9
11	88	12
14	35	15
16	39	38
18	31	48
21	440	177
23	34	128
25	407	568
28	305	151

### 2.3.7. Clustering Analysis of Uninfected and *P. brassicae*-Infected *A. thaliana* Col-0 Plants

Next, the metabolite features that responded to *P. brassicae* at every stage of infection were clustered using hierarchical clustering and visualized in a heat map. The analysis began when each sample formed a separate cluster and the algorithm proceeds to combine them until all samples belong to one cluster as visualized in the heat map (Figure 2.12). Along the side of the heat map is a dendrogram showing how the variables and the samples are independently clustered. Rows represent m/z variables, while the columns represent biological replicates of each treatment. M/z variables were colour coded by a gradient depending on the Log<sub>10</sub> of the intensity value - those variables that had high intensity are dark brown and those that had low intensity are dark blue. The heat map represents the top 50 m/z variables according to the most significant p-values when uninfected and infected samples are compared using a t-test (Figure 2.12). As mentioned in section 2.2.9, data sets that uploaded into Metaboanalyst for univariate and multivariate statistical analysis were filtered according to a significant p-value of  $\leq 0.05$ .

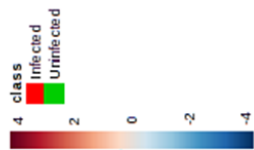




14 DPI

16 DPI

18 DPI





Comparisons between different biological replicates of samples at each stage of *P. brassicae* infection were made, which indicated that the metabolite intensities in the heat maps were different between treatments and similar in biological replicates. The metabolite pattern of uninfected and infected samples began to differ at 7 DPI and the difference continued until 28 DPI. At 7 DPI, uninfected and infected samples, which were clustered in two different clusters, showed that a first group of metabolites were increased in infected samples and decreased in uninfected samples and *vice versa* for a second group of metabolites (Figure 2.12). Although some infected samples in each stage of infection showed a similar metabolite pattern to uninfected samples especially at 11 DPI, almost half of all biological replicates showed a similar response to *P. brassicae* infection.

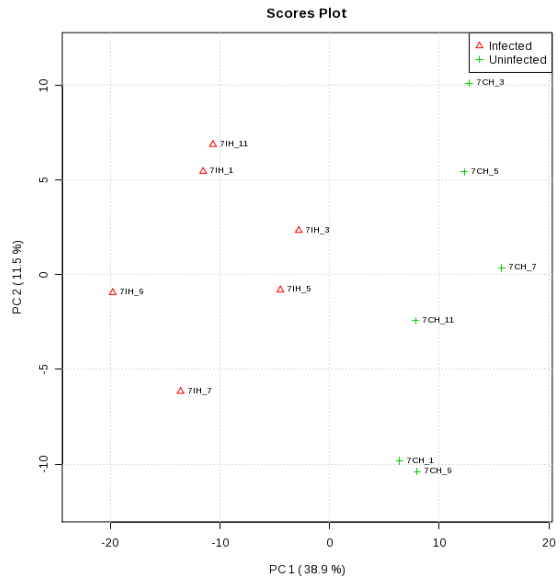
### **2.3.8 Multivariate Analyses of Metabolite Responses to Clubroot Infection in Uninfected and *P-brassicae*-Infected Col-0 *A. thaliana* Plants**

Multivariate analysis of metabolic data from the uninfected and infected tissues was performed using Principle Component Analysis (PCA) and Partial Least Square – Discriminant Analysis (PLS-DA). The two dimensions of the PCA score plot used the two most informative components based on the variance of individual components, respectively, of the total variance. Figure 2.13 shows Principal component (PC) 2 plotted against PC1 in a PCA from the data set at 7 to 28 DPI. In the PCA model, the highest accumulated variance between any two PCs could clearly discriminate uninfected samples from infected samples. PC1 distinguished infected samples from uninfected samples at 7, 14, 18, 25 and 28 DPI, while PC2 distinguished infected samples from uninfected samples at 9, 11, 21 and 23 DPI (Figure 2.13). At 16 DPI, infected and uninfected samples were distinguished by both PCs, indicating variables in both PC are changed in response to *P. brassicae* infection at the onset of gall formation.

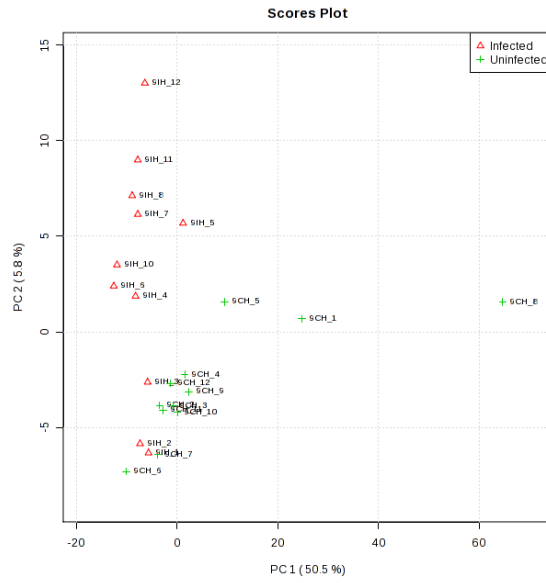
PLS-DA distinguished uninfected and *P. brassicae*-infected samples at each stage of infection using supervised methods in contrast with PCA, which used an unsupervised method. Supervised methods are used to build models that discriminate between labelled data. In this study, PSL-DA identifies the

parameters that are significant for each cluster and uses the most important parameters to discriminate between uninfected and infected samples. In the PLS-DA model, the highest pairwise explained variance between two components could clearly discriminate uninfected samples from infected samples. Besides, the PLS-DA plot visualized the relationship between sample groups; any samples that were difficult to discriminate will group very closely in the plot and can be considered to be very similar, whereas samples that do not group closely can be considered to be more different. Figure 2.14 shows Component 2 plotted against Component 1 in PLS-DA from the data set at 7 to 28 DPI. Component 1 separated infected samples from uninfected samples at 7, 11, 14, 16, 18, 25 and 28 DPI, while Component 2 separated both different treatments at 21 DPI (Figure 2.14). This indicates that variables in Component 1 changed in response to *P. brassicae* earlier in infection, at the onset of gall formation and during late gall formation.

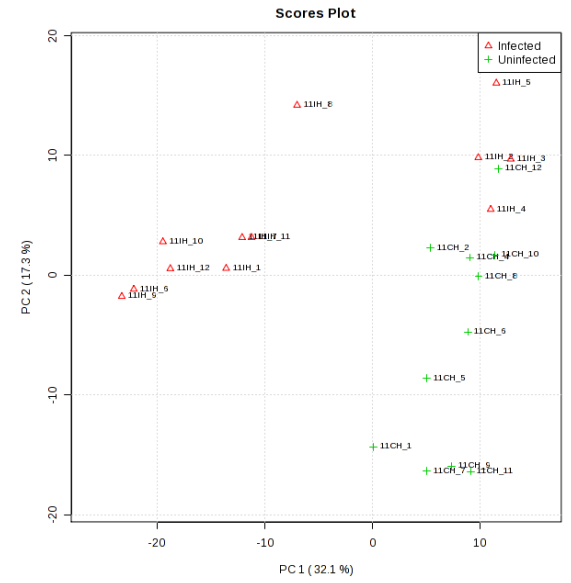
Following this, PLS-DA coefficients with a score range between 80 and 100 for uninfected and infected tissues were investigated. The coefficient score is a weighted sum of absolute measurements between the mean value of a variable in infected tissues and the corresponding mean value of the variable in uninfected tissue. At each stage of infection, variables with a similar coefficient score range were selected in order to identify the variables that were most important in response to *P. brassicae* infection at particular stages. The infection stage at 14 DPI showed the greatest total number of variables with a coefficient score range between 80 and 100, while the infection stage at 18 DPI showed the fewest number of variables in this range (Figure 2.15). This indicates that infected plants at 14 DPI exhibited strong responses to infection by altering the concentration of more compounds when compared with other infection stages. At 7 DPI, 26 variables with a coefficient score range between 80 and 100 were increased in concentration in infected plants, which is similar to the 14 variables at 23 DPI and contrasts with the number of variables at 14 DPI (Figure 2.15). This indicates that the concentration of specific metabolites was altered at specific infection stages.



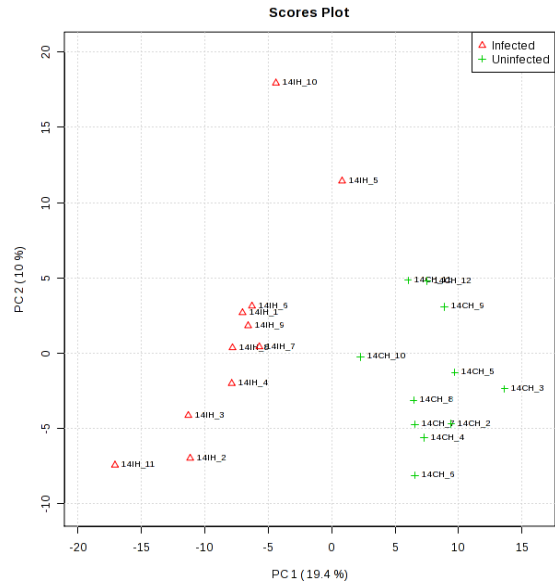
7 DPI



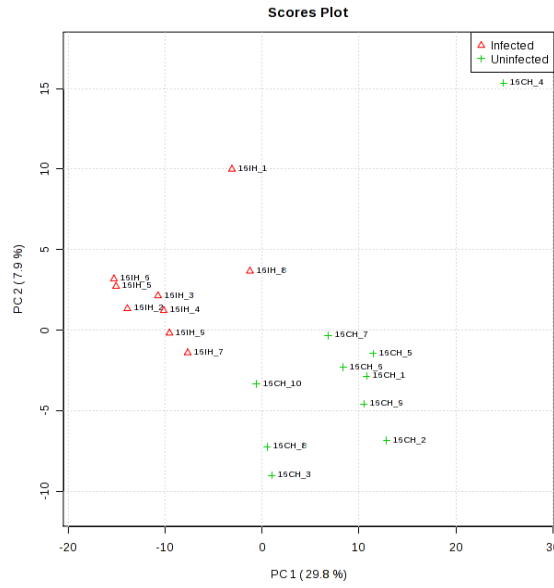
9 DPI



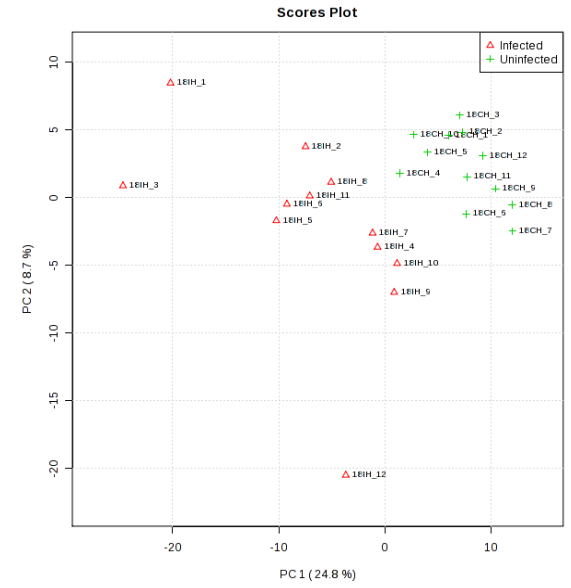
11 DPI



14 DPI

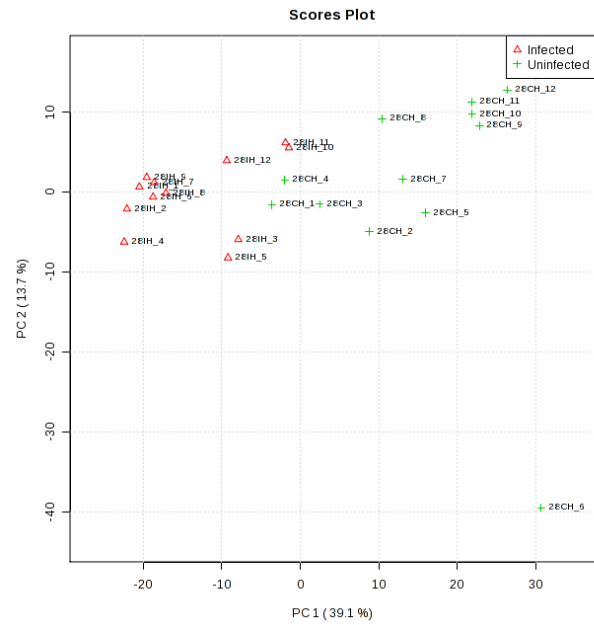


16 DPI



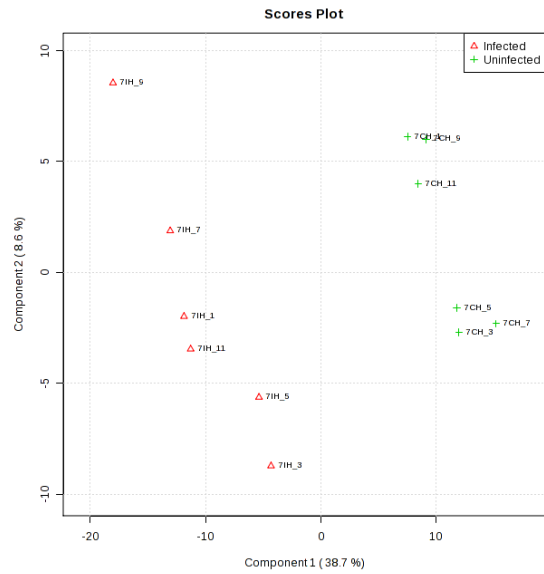
18 DPI



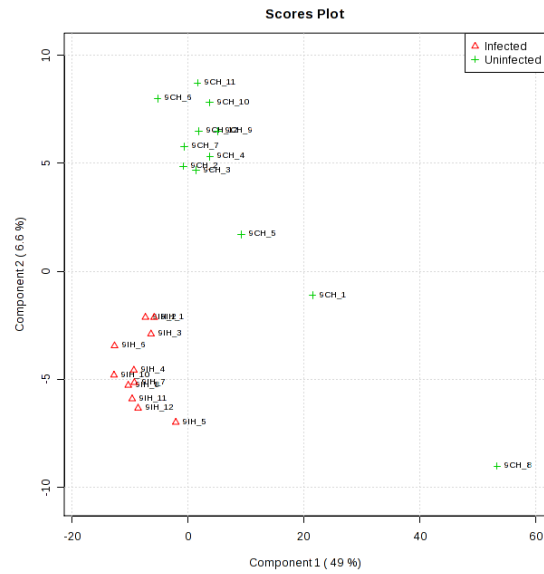


## 28 DPI

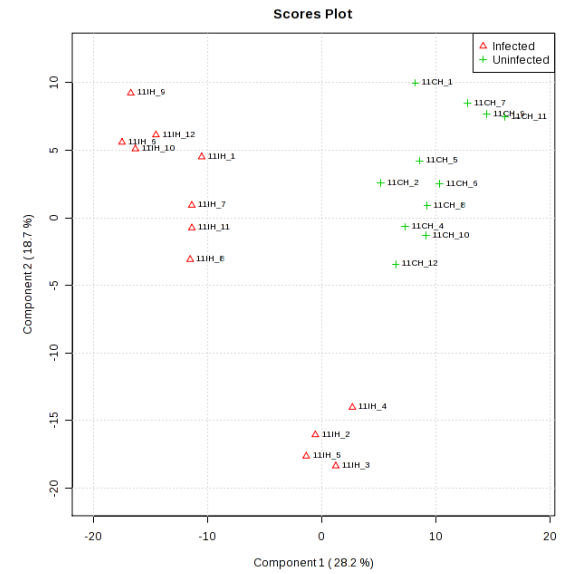
**Figure 2.13** Principle component (PC) 1 and 2 with individual variance components at 7, 9, 11, 14, 16, 18, 21, 23, 25 and 28 DPI. Samples were uninfected hypocotyl (CH) and infected hypocotyl (IH) of *A. thaliana* Col-0 plants, with a number of total biological replicates between 7 and 12.



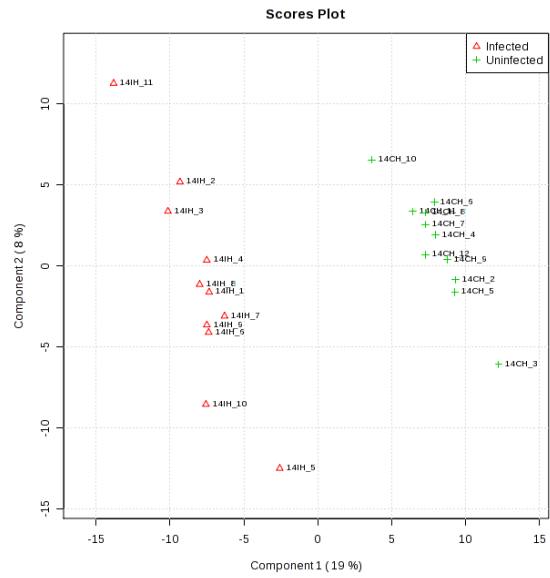
7DPI



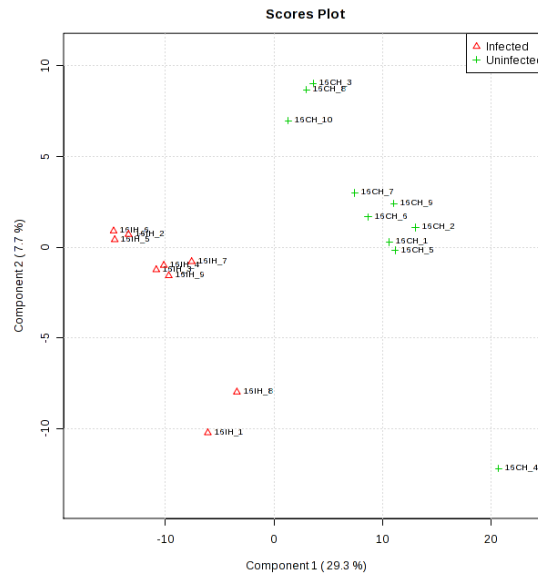
9 DPI



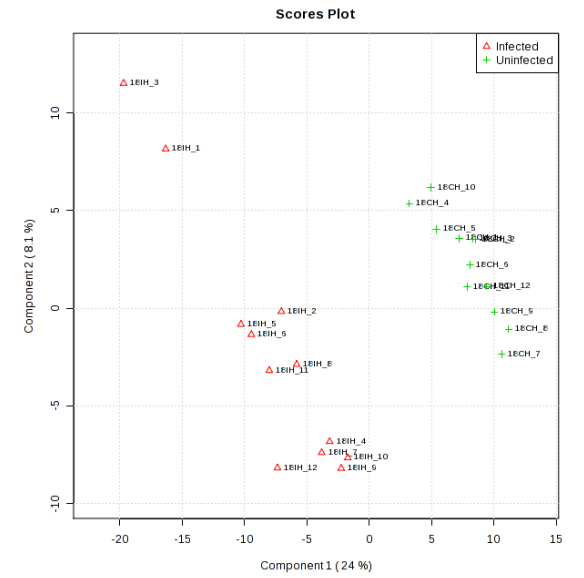
11 DPI



14 DPI

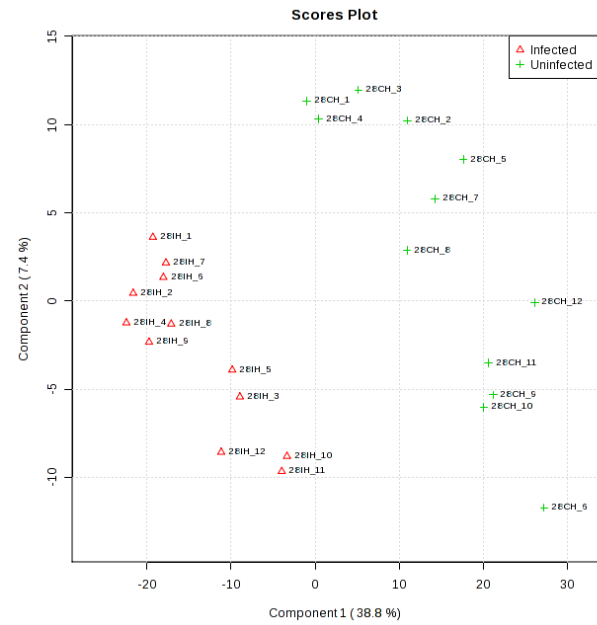


16 DPI



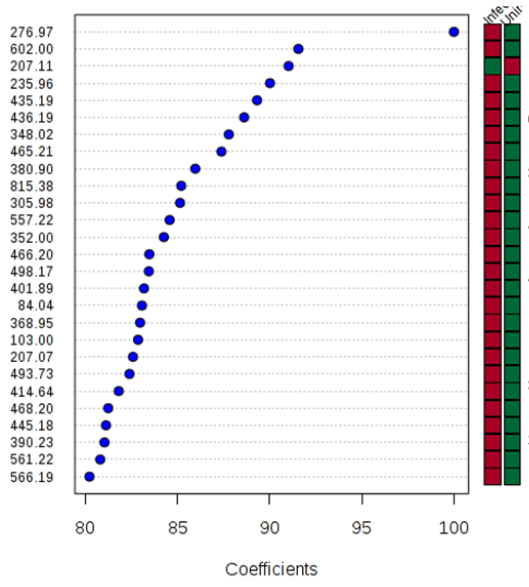
18 DPI



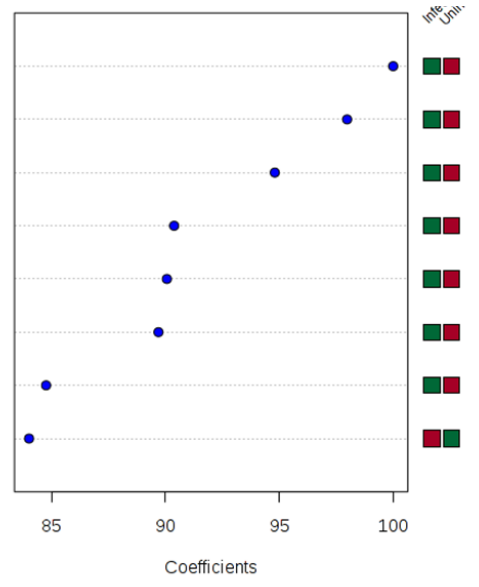


## 28 DPI

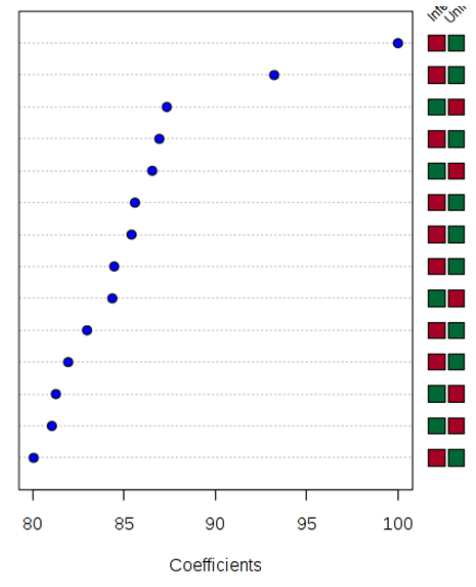
**Figure 2.14** PSL-DA analysis at 7, 9 and 11, 14, 16, 18, 21, 23, 25 and 28 DPI. Samples were uninfected hypocotyl (CH) and infected hypocotyl (IH) of *A. thaliana* Col-0 plants, with a number of total biological replicates between 7 and 12.



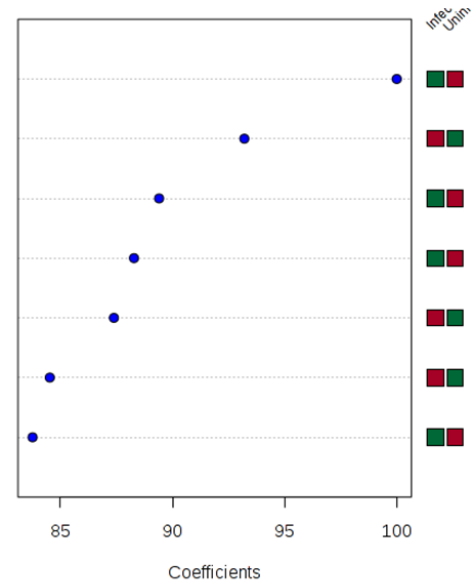
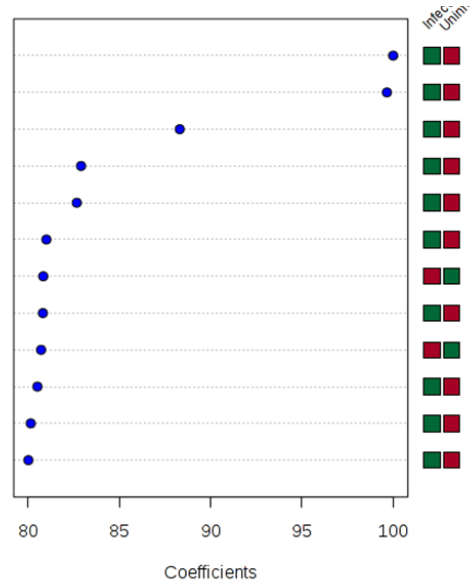
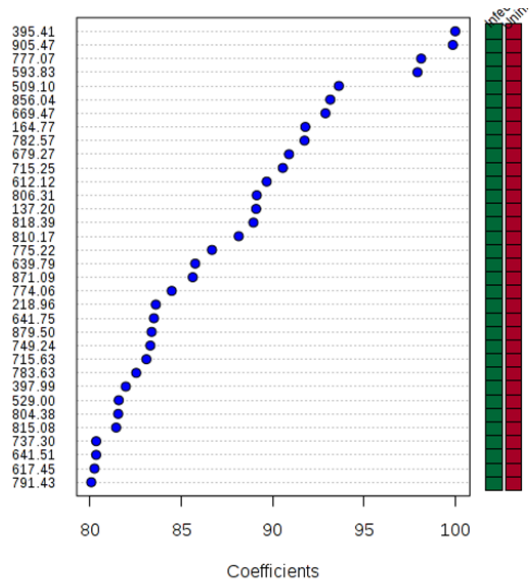
7 DPI



9 DPI



11 DPI



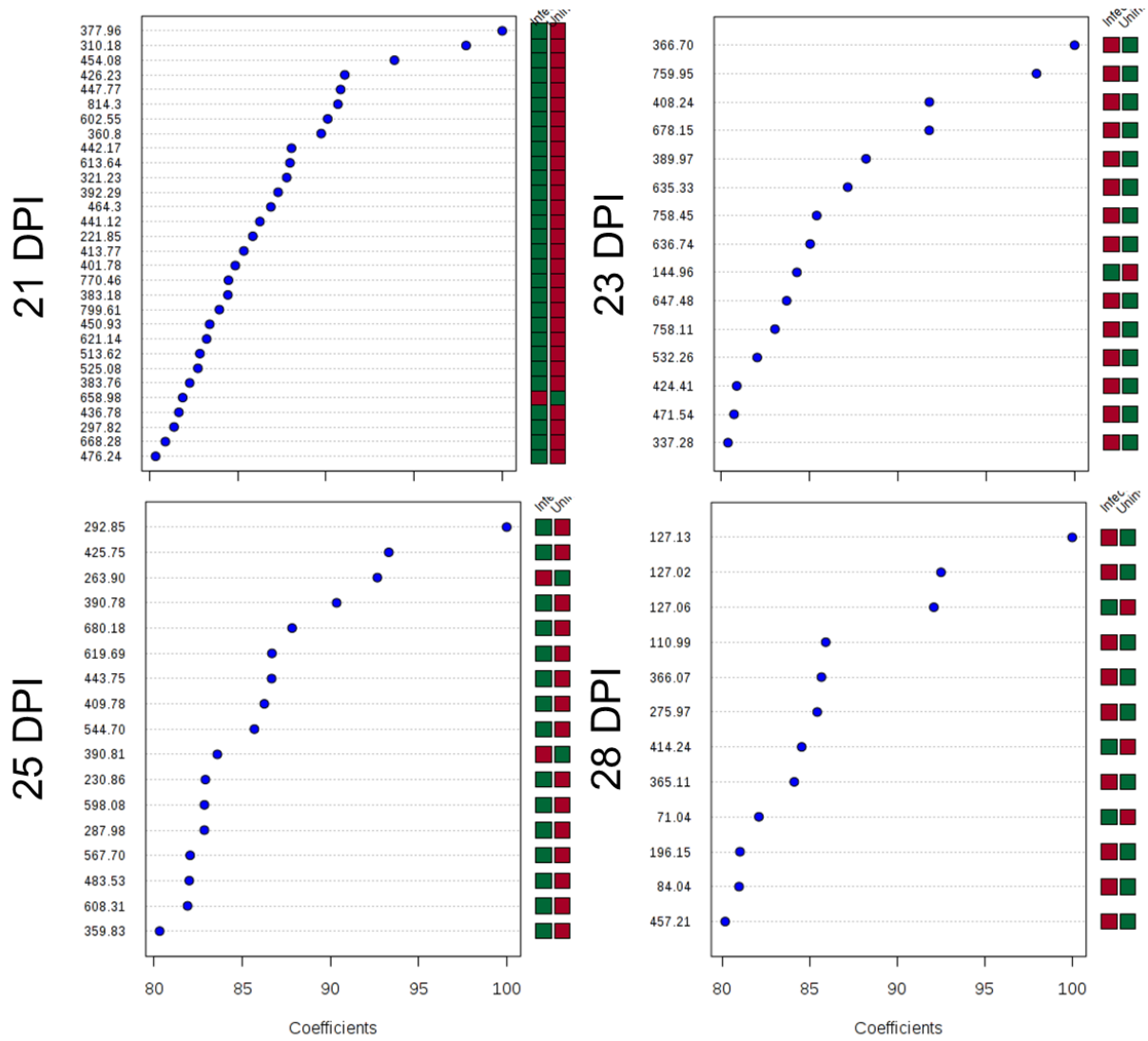


**Figure 2.15** Variables with coefficient scores between 100-80 % identified by PLS-DA. The coloured boxes on the right indicate the relative intensity of the corresponding metabolites between uninfected (box at the right) and *P. brassicae*-infected (box at the left) samples at each stage of infection.

### 2.3.9 Putative Metabolites that Changed in Response to *P. brassicae* Infection

MarVis pathways were used to annotate selected variables according to a particular coefficient score range (Figure 2.15). Selected variables were annotated according to known metabolites from the Kyoto Encyclopedia of Genes and Genomes (KEGG). Identified putative metabolites could be divided into two groups at each stage of infection (Table 2.3). The first group of metabolites contained compounds that accumulated in response to *P. brassicae* infection and the second group of metabolites contained those decreased in abundance upon exposure to infection. At 7 DPI, the putative metabolites increased in infected tissues included adenosine 5'-monophosphate involved in zeatin and purine metabolism, and 6, 7-dimethoxycoumarin, an enzyme of coumarin biosynthesis involved in plant secondary metabolism. Putative metabolites involved in glucosinolate metabolism decreased at 9 and 16 DPI and increased at 11 DPI in infected tissue. Moreover, putative metabolites associated with amino acid metabolism including L-serine increased at 9 DPI, whereas 3-iodo-L-tyrosine, D-glutamine and 3-aminopropionitrile decreased at 16, 18 and 28 respectively. Besides, putative metabolites associated with cofactor and vitamin metabolism including porphyrin and chlorophyll metabolism increased at 7 DPI and folate biosynthesis decreased at 14 DPI in infected tissue. Full lists of putative compound annotations are given in Table 2.3. Selected variables with a coefficient score range between 80 and 100 that are not shown in Table 2.3 were either classified as unknown chemical compounds, originated from bacteria or known as synthetic drugs including antibiotics, pesticides, insecticides and fungicides.

**Table 2.3.** Putative metabolites with corrected mass (Mz), and m+H adducts, detected mass per charge by mass analyser (FormerY), exact mass according to KEGG and the pathways they are involved in. A red line refers to a high intensity signal of metabolites and a green line refers to a low intensity signal in infected tissue at 7 to 28 DPI. Listed metabolites are those variables which have a PLS-DA coefficient score with a range between 80 and 100.

Mz	FormerY	Exact mass	Pathway	Putative compound
7 DPI				
434.18	435.19	434.23	Glutathione metabolism	Glutathionylspermidine
347.02	348.02	347.06	Zeatin biosynthesis	Adenosine 5'-monophosphate
556.21	557.22	556.23	Porphyrin and chlorophyll metabolism	3-Vinylbacteriochlorophyllide d
83.03	84.04	83.05	Purine metabolism	5-Aminoimidazole
206.06	207	206.06	Coumarins biosynthesis	6, 7-dimethoxycoumarin
9 DPI				
368.13	369.13	368.10	Glucosinolate biosynthesis from tryptophan	indolylmethyl-desulfoglucosinolate
479.12	480.13	480.16	Glucosinolate biosynthesis from tryptophan	indole-3-acetohydroximoyl-glutathione
325.09	326.1	325.10	Amino sugar and nucleotide sugar metabolism	N-Glycoloyl-neuraminate
391.07	392.07	391.06	Glucosinolate biosynthesis from dihomomethionine	$\beta$ -D-glucopyranose
105.07	106.07	105.0426	Cysteine and methionine metabolism	L-Serine
11 DPI				
578.15	579.15	579.17	Anthocyanin biosynthesis	Pelargonidin 3-O-rutinoside
481.03	482.03	481.07	Glucosinolate biosynthesis from homomethionine	3-benzoyloxypropyl-glucosinolate
240.17	241.18	240.12	Arginine and proline metabolism	Homocarnosine
14 DPI				
809.16	810.17	809.13	Glycolysis / Gluconeogenesis	Acetyl-CoA
774.21	775.22	774.25	Folate biosynthesis	7;8-Dihydromethanopterin
878.49	879.5	878.44	Porphyrin and chlorophyll metabolism	Hydrogenobyrrinate diamide
396.98	397.99	395.01	Folate biosynthesis	Molybdopterin

16 DPI				
379.20	380.20	379.53	Glucosinolate biosynthesis from hexahomomethionine	9-methylthiononylhydroximoyl-cysteinyglycine
541.10	542.11	541.06	Calcium signaling pathway	Cyclic ADP-ribose
306.98	307.99	306.97	Tyrosine metabolism	3-Iodo-L-tyrosine
18 DPI				
372.16	373.16	372.14	Phenylpropanoid biosynthesis	Syringin
146.1	147.1	146.07	D-Glutamine and D-glutamate metabolism	D-Glutamine
21 DPI				
382.17	383.18	382.13	Carotenoid biosynthesis	trans,trans-Farnesyl diphosphate
620.13	621.14	621.11	Anthocyanin biosynthesis	Cyanidin 3-O-3",6"-O-dimalonylglucoside
28 DPI				
126.01	127.02	126.04	Pyrimidine metabolism	Thymine
364.1	365.11	364.39	Gibberellin inactivation	Gibberellin A8
195.14	196.15	195.14	Biosynthesis of alkaloids derived from histidine and purine	Dolichotheline
83.03	84.038	83.07	Tropane, piperidine and pyridine alkaloid biosynthesis	Piperideine
456.2	457.21	456.24	Ubiquinone and other terpenoid-quinone biosynthesis	Phytyl diphosphate
70.036	71.044	70.05	beta-Alanine metabolism	3-Aminopropionitrile

## **2.4 Discussion**

The first aim of this chapter was to establish the structure of hypocotyl tissue in uninfected and infected Col-0 plants as the infection progresses. I have established that *P. brassicae* causes developmental impacts on the host during infection. Microscopic analysis of the cellular structure of plant hypocotyl tissues was performed to visualize changes before a gall becomes apparent, at the onset of gall formation, and during late gall formation. During plant primary growth, no obvious impact of clubroot infection was observed in the development of infected hypocotyl tissue (Figure 2.6). At 14 DPI, uninfected tissue underwent secondary hypocotyl thickening, but secondary hypocotyl thickening of infected tissue, specifically in the vascular cambium, was hijacked by *P. brassicae* (Figure 2.4a). The number of xylem cells (Figure 2.7 c, 23 DPI) was reduced, as reported by Malinowski et al., (2012) and shown in the results presented here. In addition, the host cells became distorted and swollen. Swollen host cells contained plasmodia. Meristematic activity within the vascular cambium was altered with a reduction in xylogenesis and an increase in phloem parenchyma. Malinowski et al (2012) demonstrated that cell division increases and becomes more widespread across the hypocotyl leading to the development of a gall.

### **2.4.1 How Does Infection Influence Host Metabolite Patterns in Plants?**

Does a change in plant cellular structure lead to a change in the plant metabolome? As clubroot disease is caused by a biotrophic pathogen, it was not surprising that this pathogen causes accumulation of metabolites and alters plant signals and hormones. The pathogen manipulates host metabolism to counteract defence responses. The pathogen may be able to induce favourable nutritional conditions after successfully colonizing host cells. The second aim of this chapter was to identify the metabolite patterns at each stage of *P. brassicae* infection. To meet this aim, metabolic fingerprinting using DI-MS was performed. The un-targeted metabolite analysis performed allows the comparative analysis of metabolite levels in different samples at different stages of infection. The method which was used in this study,

was selective, repeatable, reproducible, sensitive, and high-throughput, with output data that is compatible with other platforms, and that allows reliable identification of metabolites (Maag et al., 2015).

In this study, metabolites detected using DI-MS were selectively measured, and some were not measured. This was because only polar metabolites in methanol/water extracted from hypocotyl tissues of *P. brassicae*-infected and uninfected *A. thaliana* plants at 7 to 28 DPI were used in the metabolomic analysis. In addition, metabolites, which are detected by the TOF mass analyser system, strongly depend on the positive ionization conditions. The TOF mass analyser system provides a very rapid technique to analyse a large number of metabolites with great mass to charge ratio ( $m/z$ ) accuracies (Shulaev 2006; Sumner et al., 2003). Moreover, a large dataset containing between 2158 and 6051 detected peaks in each spectrum was obtained in this study. These data were subjected to binning using Maldiquant (Gibb and Strimmer, 2012). Binned data contained 34254 variables, which were subjected to filtering using MarVis and statistical analysis using MetaboAnalyst 3.0 (Xia et al., 2015).

Statistical analysis was used to create an observation that gives a general comparison between uninfected and infected samples. As uninfected and *P. brassicae*-infected *A. thaliana* Col-0 plants share similar genotypes, the only factor that influenced the difference between uninfected and *P. brassicae*-infected plants was the response to infection. It was not surprising that metabolome pattern between uninfected and infected plants were very similar; infected plants showed subtle metabolite responses to the infection. Heat maps show that between plant variation occurred between biological replicates (Figure 2.12). The data obtained is repeatable and reproducible since half of the biological replicates showed similar response to *P. brassicae* infection. The comparison between uninfected and infected tissue as visualized using a heat map indicated that the differences between the two treatments was initiated at early stages of cortical infection (7 DPI) and

continued until late gall formation. In addition, multivariate analysis using PCA indicated that variables in one or both PCs distinguished between biological replicates of uninfected and infected samples, although some variables overlapped. However, more than half of the biological replicates of each treatment grouped together. Similar results were observed in the PLS-DA plot, which indicated that metabolite levels in infected samples were different from those in uninfected samples at the very beginning of cortical infection in hypocotyl tissues, until the end of the experiment.

Previously, a targeted metabolomics analysis based on a combination of ultra-performance liquid chromatography tandem mass-spectrometry (UPLC-MS/MS) and GC-MS identified metabolite profiles in susceptible and resistant genotypes of *Brassica napus* following *P. brassicae* infection (Wagner et al., 2012). It has been reported that the accumulation of several amino acids is positively correlated with disease susceptibility (Wagner et al., 2012). Besides, susceptible genotypes of *B. napus* alter their metabolic activity earlier than resistant genotypes (Wagner et al., 2012).

In another study of a plant-pathogen interaction, non-targeted metabolomics has been applied to identifying resistance related (RR) metabolites based on liquid chromatography-high resolution mass spectrometry (LC-HRMS) in susceptible and resistant genotypes of diploid potato against late blight (Yogendra et al., 2015). It has been suggested that resistance to late blight is mainly associated with cell wall thickening, after RR metabolites were discovered to include hydroxycinnamic acid amides, which are involved in phenylpropanoid, flavonoids and alkaloids biosynthesis (Yogendra et al., 2015). RR metabolites were mapped onto metabolic pathways and potato and other genomics databases were searched to identify the candidate RR genes (Yogendra et al., 2015). The candidate RR genes, which are further confirmed using transcriptomic analysis, show an increase in transcript expression in resistant genotypes when compared with susceptible genotypes,

indicating the role of these genes in resistance against late blight (Yogendra et al., 2015).

Furthermore, a different study found that following rice blast infection, changes in metabolite patterns, which are obtained using flow injection electrospray mass spectrometry (FIE-MS), are similar among host plants including barley, rice and *Brachypodium distachyon* (Parker et al., 2009). Targeted metabolite profiling by GC-TOF-MS was used to further confirm that host metabolic re-programming occurred in response to rice blast infection (Parker et al., 2009). It has been revealed that *Magnaporthe grisea*, the agent of rice blast disease, suppresses the host hypersensitive reaction through manipulation of host phenylpropanoid metabolism, which allows the pathogen to enter inside the host (Parker et al., 2009). During plant colonization and rapid proliferation of *M. grisea*, metabolites associated with nutrient metabolism are increased, which indicates that those metabolites are required for the pathogen (Parker et al., 2009).

#### **2.4.2 What are the Potential Metabolites that Change in Response to *P. brassicae* Infection?**

The third aim of this chapter was to identify putative metabolites that change upon *P. brassicae* infection. To meet this aim, we focused on metabolite changes during early stages of cortical infection until late gall formation, specifically in hypocotyl tissue. A small number of variables with a coefficient score range between 80 and 100 were identified and annotated using MarVis according to the KEGG database (Table 2.3). These potential putative metabolites then need to be validated either by integration with other 'omics' data (e.g. Yogendra et al., 2015) or by combining this initial identification with other MS separation methods such as gas chromatography-MS, liquid chromatography-MS or MS-MS (Heuberger et al., 2014).

At early stages of cortical infection at 7, 9 and 11 DPI, no obvious impact of *P. brassicae* infection was observed on plant growth or on the development of infected

hypocotyl tissues (Figure 2.6). However, statistical analysis of metabolite patterns showed that some metabolites were altered in response to *P. brassicae* infection at early stages. This indicates that the plant metabolism of *P. brassicae* infected plants did not have an impact on plant primary growth or *vice versa*. Potential metabolites that could be induced during early infection stages may be involved in plant recognition of secondary zoospores. This could subsequently induce plant defence, increased energy production and plant metabolism. Those metabolites that are important to supporting plant development include those involved in synthesis of the plant cell wall, which leads to protection of the plant against *P. brassicae* during early infection stages. Some of the putative metabolites that increased in infected tissue at early infection stages are associated with amino acid metabolism. This includes L-serine, homocarnosine, metabolites involved in purine metabolism such as 5-aminoimidazole, and adenosine 5'-monophosphate which is involved in zeatin biosynthesis (Table 2.3). However, when a precursor of metabolites synthesis such as adenosine 5'-monophosphate is increased, it does not indicate that the product also increases- alternatively precursors in a biosynthetic pathway may accumulate if downstream steps are reduced. Meanwhile, some secondary metabolites, include glutathionyl spermidine, which is part of glutathione metabolism, 6,7-dimethoxycoumarin, which is part of coumarin biosynthesis, and 3-benzoyloxypropyl-glucosinolate, were increased in infected tissue during early infection.

Moreover, at the onset of gall formation (14, 16, 18 DPI), putative metabolites that are changed in abundance at this stage may be involved in plant defence, which is associated with oxidative stress, and a signal such as methyl salicylate to trigger systemic acquired resistance (SAR) (Ludwig-Muller et al., 2015). In this study, almost all metabolites with a coefficient score of 80-100 in our PLS-DA decreased in infected tissue at the onset of gall formation. These metabolites are involved in folate biosynthesis and glucosinolate and phenylpropanoid biosynthesis (Table 2.3). This suggests that metabolites involved in plant defence could potentially be suppressed

by plasmodia. In addition, I speculate that metabolites which are potentially associated with plant development, for example those involved in cell expansion and cell division, could be altered to initiate gall formation.

Finally, at late gall formation, the cellular structure of infected tissue contained swollen and distorted cells. The cytoplasm of infected cells contained secondary plasmodia and a new generation of spores. At this stage, it has been suggested that large plasmodia that colonize infected cells have acquired a high metabolic activity compared with small plasmodia (Schuller et al., 2014), which are mostly present during onset gall formation. This suggests that most of the metabolites that change at late gall formation are important to the pathogen. Identified metabolites with a coefficient score of 80-100 in our PLS-DA which are involved in carotenoid and anthocyanin biosynthesis decreased in infected tissue at late gall formation. In contrast, putative metabolites associated with pyrimidine metabolism, gibberellin inactivation, and the biosynthesis of alkaloids and piperidine increased at 28 DPI, when a large gall was visible (Table 2.3).

Previous studies reported that gene expression and protein levels in infected and uninfected samples are different at early stages of primary infection and late stages of cortical infection (Agarwal et al., 2011, Cao et al., 2008, Siemens et al., 2006). However, these studies reported that the response of infected plants to *P. brassicae* occurs in the root tissue, but not in the hypocotyl tissue where the cortical infection is present. Moreover, Schuller et al., (2014) reported that the expression of genes associated with plant metabolism in infected cells is different between cells containing small and large plasmodia. This finding supports our result that different stages of infection acquired or dispersed different types of metabolites.

Details of specific putative compounds, and their pathways and function during *P. brassicae* infection are discussed in Chapter 3 of this thesis. Only a few metabolites with a coefficient score with range between 80 and 100 in our PLS-DA were identified

after annotation using MarVis. For this reason, in the next chapter, metabolites with a significant p-value of 0.05 are annotated using MarVis. Then, those metabolites that are altered in response to infection are integrated with transcriptomic data that was obtained from a previous study to better understand the changes in metabolism of infected tissue (Malinowski et al., *unpublished*).

## **2.5 Conclusion**

Non-targeted metabolomics was a useful approach to study the global changes in plant metabolism in response to *P. brassicae* infection. Following *P. brassicae* infection, an alteration of metabolites occurred at the very beginning of cortical infection, although the plant primary growth did not show clear differences between uninfected and infected hypocotyl tissue at this stage. This suggests that this change in metabolites depended on responses of the plant to *P. brassicae* infection, rather than on an alteration of plant development.

## Chapter 3: Investigating the Metabolism of Clubroot-Infected Plants by Integrating Metabolomic and Transcriptomic Approaches

### 3.1. Introduction

Data presented in the previous chapter showed that when *A. thaliana* was infected with *P. brassicae*, an alteration of plant metabolism occurred between 7 and 28 DPI. It indicates that metabolic changes occurred before host cell expansion and cell division altered. These findings were consistent with data from previous studies on Chinese cabbage and rapeseed showing an alteration in metabolites in gall tissue (Williams et al., 1968, Keen and Williams, 1969, Wagner et al., 2012). Previous studies also reported that gene expression and protein levels in infected and uninfected tissues of *A. thaliana* plants are different at early stages of primary infection and late stages of cortical infection (Agarwal et al., 2011, Siemens et al., 2006, Devos et al., 2006).

Agarwal et al. (2011) have reported the use of microarrays to examine gene expression following inoculation of susceptible *A. thaliana* with *P. brassicae* at 4, 7 and 10 days after inoculation (DAI). These time points are within the primary infection stages, which take place in the root. The 4 DAI is the first time point the pathogen can be detected using quantitative real-time PCR (qPCR) in plant root tissue, while 7 and 10 DAI represent different pathogen stages of the primary phases of the *P. brassicae* lifecycle (Agarwal et al., 2011). Meanwhile, Devos et al. (2006) reported the use of a proteomic approach to examine protein expression following inoculation of susceptible *A. thaliana* with *P. brassicae* at 4 DAI. Siemens et al. (2006) used microarray analysis to examine gene expression following inoculation of susceptible *A. thaliana* with *P. brassicae* at 10 and 23 DAI, specifically in root tissue. These time points are within the cortical infection stages, which take place in the root and hypocotyl. The 10 DAI time point represents the growth stages of pathogen as young vegetative plasmodia, where no visible galls have developed, while 23 DAI represents the growth stages of the pathogen where secondary plasmodia,

sporangia and resting spores exist, and galls are visible in the root tissue. Schuller et al. (2014) reported *A. thaliana* transcriptional changes in cells containing specific developmental stages of *P. brassicae* by using laser microdissection and pressure catapulting (LMPC) to isolate individual cells.

### **3.1.1 Alteration of Plant Metabolism Correlates with Plant Development during *P. brassicae* Infection**

The development of disease symptoms in infected plants is closely related to alterations in the metabolism of hormones such as cytokinin, auxin and brassinosteroids (BR). Several studies have demonstrated the accumulation of cytokinins in root tissues of *P. brassicae*-infected plants. These are said to induce abnormal cell division in local *P. brassicae*-infected tissues leading to the gall formation (Dekhuijzen and Overeem, 1971, Dekhuijzen 1981, Muller and Hilgenberg, 1986, Devos et al., 2005, 2006, Siemens et al., 2006). Cytokinins being necessary for vascular cambium formation (Miyawaki et al., 2006). In infected *A. thaliana* plants, gall formation occurs as a result of a reprogramming of the meristem, and not via *de novo* meristem formation. Blocking host vascular cambium activity through expression of the cell cycle inhibitor ICK1/KRP1 during secondary thickening leading to reduced gall size does not stop the development of *P. brassicae* (Malinowski et al. 2012). Inactivation of host iP and tZ biosynthesis in *ipt1,3,5,7* mutant abolishes vascular cambium development in uninfected plants. When infected, no additional cell division occurs but cell expansion and lack of differentiation is still evident. Also plasmodia development is slowed (Malinowski et al., 2016).

The accumulation of auxin in *P. brassicae*-infected tissue demonstrates that auxin is involved in cell enlargement to develop a gall at later stages of *P. brassicae* infection (Ludwig-Muller et al., 1993, Raa 1971, Schuller et al., 2014, Grsic-Rausch et al., 2000, Devos et al., 2005, 2006). Most genes associated with BR biosynthesis and signalling pathways are up-regulated in root tissues of *P. brassicae*-infected *A.*

*thaliana* plants, which indicates that these genes play a role in clubroot development (Schuller et al., 2014). BR is involved in xylem formation through BR-related transcription factors VND6 and VND7 during gall development (Schuller et al., 2014, Malinowski et al., 2012).

Cell expansion in infected tissues changes the plant cells' turgor, causing cell distortion and destruction of plant primary cell walls. Agarwal et al. (2011) have reported that the expression of genes associated with cell wall modification and cell growth such as pectinesterase and expansin are up-regulated at 4 DAI. Expression of genes encoding enzymes that synthesise components of plant cell walls are down-regulated at 4 DAI. For instance down-regulated genes at 4 DAI include those involved in lignin biosynthesis such as 4-coumarate-CoA ligase, cinnamyl coenzyme A reductase and cinnamyl alcohol dehydrogenase and genes involved in the synthesis of glycoprotein and arabinogalactan. It has been suggested that cell wall lignification, callose deposition and cell wall thickening which are important for early plant defence during pathogen attack has been suppressed in compatible interaction of *A. thaliana* plants and *P. brassicae* to allow the pathogen to spread in plant tissue. In addition, Devos et al. (2006) identified proteins involved in cell architecture are down-regulated in infected tissue at 4 DAI. Those proteins are tubulin  $\beta$ 4, tubulin  $\alpha$ , tubulin  $\beta$ -1,4 and tubulin  $\beta$ -2/ $\beta$ -3. The down-regulation of these proteins is suggested to be associated with the loss of cell structure during the compatible interaction between *A. thaliana* plants and *P. brassicae*. In addition pectin methylesterase which is up-regulated in infected tissue, is involved in cell degradation and is associated with alterations in the cell wall to facilitate infection (Devos et al., 2006).

Expression of genes associated with growth and cell cycle control are strongly induced at 10 DAI including several genes encoding cyclins. This suggests that cell division which leads to gall formation is stimulated at the very beginning of *P. brassicae* cortical infection in root tissue. At 23 DAI, expression of genes associated with cell expansion and elongation in gall development are mostly up-regulated in

infected tissue of *A. thaliana* plants (Siemens et al., 2006). In addition, genes associated with cell wall metabolism are down-regulated in large hypertrophied cells indicating those cells are losing cell structure (Schuller et al., 2014).

### **3.1.2 The Host Facilitates Nutrient Acquisition during *P. brassicae* Infection**

Compatible plant pathogens are able to avoid or suppress host immunity, making plants more susceptible to infection. Plants play an active role in supporting disease progression. Once pathogens are able to enter inside hosts, the plant provides a suitable environment and facilitates nutrient provision, especially for biotrophic pathogens like *P. brassicae*. The accommodation of *P. brassicae* inside the host involves the development of a gall as a new sink tissue, which is important for nutrition uptake. In biotrophic interactions, the plant provides carbon, sulfur, nitrogen and other nutrients to infecting pathogens. The demand for carbon in infected tissue requires that there is compensation by carbon allocation from uninfected tissues, in particular photosynthetically active tissue and the developing inflorescence tissue. Flowering in *P. brassicae*-infected plants is therefore delayed due to the effect of competing carbon sinks between developing galls and inflorescence tissue (Mithen and Magrath, 1992, Koch et al., 1991, Dixon 2009). Besides, in *P. brassicae*-infected plants, rates of photosynthesis in leaves are no different to those in uninfected plants, but carbohydrate content is low due to the export of carbohydrate from leaves to the developing gall (Evans and Scholes, 1996). The *P. brassicae* infected tissue becomes an important sink so that nutrients, including amino and nucleotide sugars, amino acids, nucleotides, sulfur, vitamins, cofactors and secondary metabolites, are accumulated there.

Generally, at 4 DAI, differentially expressed genes in response to *P. brassicae* infection are involved in biosynthesis degradation, utilisation and assimilation of amino acid, cofactors, plant secondary metabolites, aromatic compounds, nucleoside and nucleotides, plant hormone, cell structures, fatty acid and lipids as well as photosynthesis. Expression of genes associated with metabolism such as

phenylpropanoids, lipid and carbohydrate are up-regulated at 4 DAI. At 7 and 10 DAI, differential genes expression in response to *P. brassicae* infection include those involved in biosynthesis, degradation, utilisation and assimilation of amino acid, plant hormones, cell structure, sugars and polysaccharides. In addition, genes associated with plant basal resistance including pathogen recognition and signal transduction are expressed differently following *P. brassicae* infection at 4 DAI. (Agarwal et al., 2011). This indicates that the accommodation of *P. brassicae* inside the host during primary infection stages could alter plant metabolism in order to induce plant defence or facilitate nutrient provision. At 23 DAI, differentially expressed genes include those involved in photosynthesis, starch, lipid and secondary metabolism such as flavonoid metabolism. Genes associated with several transport process including sugar, lipid, ion and nutrient containing nitrogen, sulfur and phosphate compounds are not altered as much at 10 DAI compared with 23 DAI. This indicates that the infected tissue becomes a sink for favorable nutrients for the pathogen at 23 DAI (Siemens et al., 2006).

It has been reported that genes associated with major metabolic pathways are differentially expressed including carbohydrate synthesis, tricarboxylic acid (TCA) cycle and lipid metabolism. Cells containing small plasmodia and large plasmodia show major differential gene expression compared with the expression of genes between time points. This indicates that different growth stages of *P. brassicae* development manipulate different host metabolic activity (Schuller et al., 2014). Cells in the inner cortex layer containing small plasmodia at 14 and 21 DAI show up-regulation of genes associated with tetrapyrrole, light reaction, nitrogen and sulfur metabolism, glycolysis, TCA cycle and fermentation. Cells located at the outer cortex layer that contain large plasmodia show down-regulation of genes expression associated with terpenoid biosynthesis and up-regulation of genes expression associated with mevalonate pathway (Schuller et al., 2014). The mevalonate pathway is involved in multiple cellular process by synthesizing sterol isoprenoids. Isoprenoids such as isopentenyl tRNA, is used in cytokinin biosynthesis. However,

this is not a major route of cytokinin biosynthesis in *A. thaliana* plants (Sakakibara 2006). In addition, genes associated with the shikimate pathway and flavonoid synthesis are up-regulated in cells containing large plasmodia at 14 and 21 DAI (Schuller et al., 2014).

### 3.1.3 Aims and Objectives

Chapter 2 described the effect of an early event of cortical infection on the hypocotyl tissue of *P. brassicae*-infected *A. thaliana* plants until successful *P. brassicae* colonization inside host cells. In addition, the changes in global metabolites were analysed during these events. This chapter focuses on the identification of the metabolites in hypocotyl tissue of *A. thaliana* plants with a significant p-value of  $\leq 0.05$  in response to *P. brassicae* infection, and are annotated using MarVis. Metabolites are grouped according to their pathways and function. Then, the concentration of metabolites that change are visualised using heat maps, with the identification of putative metabolites included in the appendix. The metabolome is an interface between the plant and the pathogen and is influenced by transcribed genes from both. Therefore the metabolites of specific pathways that change in response to *P. brassicae* infection were integrated with plant transcriptomic data in hypocotyl tissue at 16 and 26 DPI. This approach was taken in order to validate the non-targeted metabolomic approach. The pathogen genome of Schwelm et al., (2015) has been referred to in order to understand pathogen influences.

#### Aims:

1. To understand how the metabolites change over time and how compounds in particular biosynthetic pathways alter.
2. To understand how gene expression in particular biosynthetic pathways change.

**Objectives:**

1. To identify metabolite changes during infection using MarVis Pathway and Kyoto Encyclopedia of Genes and Genomes (KEGG).
2. To examine the concentration of metabolites during *P. brassicae* infection based on specific pathways and functions.
3. To integrate host gene expression with metabolite concentration during *P. brassicae* infection.

## 3.2 Materials and Methods

### 3.2.1 Metabolomic Analysis

Metabolomic data used in this Chapter is obtained from the processed data of Chapter 2 (Refer to sections 2.2.8 and 2.2.10, Figure 2.4). Identified putative metabolites, with their intensity signal, among biological replicates of uninfected and infected plants at 7 to 28 DPI based on their potential functions and pathways were visualised using heat maps (<http://www.metaboanalyst.ca/>, refer to section 2.2.9).

### 3.2.2 Microarray Analysis

Malinowski et al. (*unpublished*) uses microarray technology to examine *A. thaliana* gene expression in clubroot infected plants at the onset 16 days post inoculation (DPI) and 26 DPI stages of gall formation in the hypocotyls and upper roots of clubroot-infected plants. Each biological treatment has three biological replicates and one technical replicate. Each biological sample contains a pool of RNA samples from multiple plants (8 plants). Pooling samples from multiple plants in each biological replicates can reduce the biological component of variation, but it can reduce the variability due to sample handling or measurement error.

RNA from these biological samples is extracted. RNA mixtures resulting from this extraction contain messenger RNA (mRNA), transfer RNA (tRNA), ribosomal RNA (rRNA) and small ribosomal RNA (srRNA). Random primers are used in order to synthesis cDNA from mRNA, together with mixture of biotin-labelled nucleotides and reverse transcriptase enzyme. Malinowski et al. (*unpublished*) uses the Affymetrix Ara Gene-1-1.ST Exon chip based on the TAIR10 annotation of the *Arabidopsis* genome.

GeneChip (Affymetrix) uses oligonucleotides as a probe. Each oligonucleotide is around 20-25 bases long and there is a median of 25 probes across the full length of the gene which provides up to 26 unique probes per transcript. Those multiple probes per gene are synthesized *in situ* in Affymetrix before hybridization to labelled

cDNA. Samples which are not hybridized on the array are removed during washing step. A fluorescent dye, phycoerythrin bound to streptavidin is added to the array which stains the bound cDNA by binding the biotin. After that, a fluorescent scanner is used to measure the signal intensity per probe and produces an expression value for each probe which correlates to gene expression. The Raw data set is produced in CEL files, one file per microarray.

The raw data output is normalized by using R package 'oligo' with the RMA (Robust multi-array average) option. R package 'oligo' identified the CEL file which is imported into the R session. The raw data can be visualised as a pseudo-image, smoothed histogram to compare the distribution of intensities across samples, box plot which assesses data distribution and MA plot to assess the dependency of log-ratios on the average log-intensity of the data (Carvalho and Irizarry, 2010). Then, the raw data is preprocessed using RMA option. The RMA algorithm is used in *ExpressionFeatureSet* object to adjust the background of the data, normalized the data to identify and remove the source of variation other than differential expression, as well as transformed the data into log-transformed (Irizarry et al., 2003).

Statistical analysis is performed by using the linear model ('limma') package. In this step, differential gene expression for selected comparisons either for each probe or for each gene is measured by using this equation:

#### Equation 1

$$\Delta \text{Expression value} = \Delta \text{ biological treatment} + \Delta \text{ biological variation} + \Delta \text{ technical variation} + \text{noise.}$$

The output of these analyses is differential gene expression that can be log-intensities value between selected samples, a probability (corrected for false discovery using Benjamin-Hochberg method) that the expression values are truly

different according to an adjusted p-value, and an average value for expression in the samples analysed as measured using the equation 1.

### **3.2.3 Integration of Metabolomic and Transcriptomic Analysis**

Transcriptomic data at 16 and 26 DPI in root and hypocotyl tissue was obtained from previous work (Malinowski et al., *unpublished*). The expression of gene with  $\log_2 FC \geq 1$  and  $\leq -1$ , p-value  $\leq 0.05$  in particular KEGG pathways was visualised using the KEGG mapper ([http://www.genome.jp/kegg/tool/map\\_pathway2.html](http://www.genome.jp/kegg/tool/map_pathway2.html)). Metabolites that differently changed was coloured brown (increase) and blue (decrease) in KEGG pathways with the alteration of genes expression.

### **3.3 Results and Discussion**

#### **3.3.1 Identification of Putative Metabolites that Respond to *P. brassicae* Infection**

As described in Section 2.2.8, metabolites with a p-value of  $\leq 0.05$  in differences between uninfected and infected samples were annotated according to known metabolites from Kyoto Encyclopedia of Genes and Genomes (KEGG) database. The metabolites identified as changing during *P. brassicae* infection were grouped according to their potential functions and pathways (Figure 3.1). As shown in Figure 3.1, the total number of metabolites that changed in response to *P. brassicae* infection increased during the later stages of gall formation (25 and 28 DPI) compared with earlier in the infection (7 to 11 DPI) or at the onset of gall formation (14-18 DPI). Most of the metabolites that changed in response to *P. brassicae* infection were terpenoids, polyketides and other secondary metabolites (Figure 3.1).

#### **3.3.2 Alteration of Metabolites Involved in Carbohydrate Metabolism of *P. brassicae*-infected Plants**

Carbohydrate metabolism maintains the pools of hexoses, pentose and triose sugars in plant cells. These metabolites provide an energy source and form structural elements in living cells such as the cell wall. A comparison of the signal intensities of metabolites associated with carbohydrate metabolism is shown as a heat map (Figure S1). The patterns in the heat map figure indicates the similarity or differences among biological replicates at 7, 16 and 25 DPI. Specific putative metabolites whose concentration altered at 7, 16 and 25 DPI in response to *P. brassicae* infection are shown in Table S1 of the Appendix. Overall, metabolites associated with changes in carbohydrate metabolism were also associated with amino sugar and nucleotide sugar metabolism.

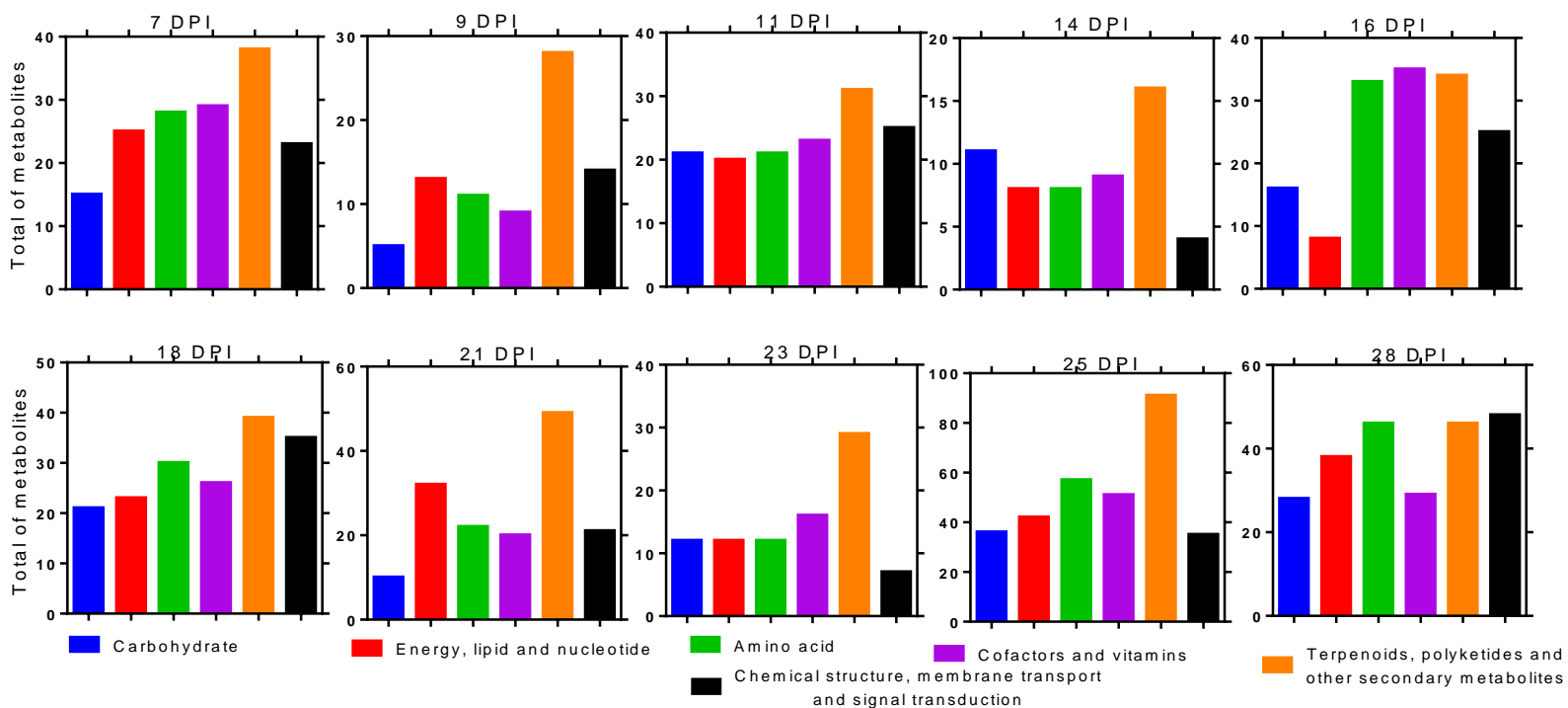


**Figure 3.1.** Total numbers of metabolites that were altered in carbohydrate, energy, lipid, nucleotides, amino acids, cofactors, vitamins, chemical structure, membrane transport and signal transduction during *P. brassicae* infection, at 7 to 28 DPI.

To better understand the changes in metabolism occurring within the infected hypocotyl, the alterations in metabolite concentrations found in this study were integrated with transcriptomic data at 16 and 26 DPI obtained from a previous study (Malinowski et al., *unpublished*). At 16 DPI, compounds with an exact mass 607.08, which were predicted to be UDP-N-acetylglucosamine (UDP-GlcNAc), UDP-N-Acetyl-D-mannosamine (UDP-ManNAc) or UDP-N-Acetyl-D-galactosamine (UDP-GalNAc), accumulated in infected tissue. These three putative compounds share similar mass and cannot be distinguished in this study. The accumulation of these putative compounds of amino sugar and nucleotide sugar metabolism in infected tissue was accompanied by the down-regulation of the host gene UDP-N-acetylglucosamine diphosphorylase (2.7.7.23) and an up-regulation of chitinase (3.2.1.14, AT2G43610) that hydrolyses chitin to N-Acetyl-D-glucosamine (GlcNAc) (Figure 3.2).

Plant chitinase is involved in plant defence against oomycete plant pathogens (Lee et al., 2000, Kim and Hwang, 1994), fungi (Yokotani et al., 2014, Hong and Hwang, 2002, Hietala et al., 2004) and bacteria (Ott et al., 2006, Kim et al., 2015). The chitinase gene is not only activated by chitin, an important structural component of the fungal cell wall, but also by pathogen protein effectors (Ott et al., 2006). Recently, it has been reported that in pepper plants, chitinase and receptor-like cytoplasmic protein kinase form a complex to activate plant cell death and plant defence. This complex is formed after plant responses to the ROS and nitrite oxidase burst that is triggered by *Xanthomonas campestris* (*Xcv*) infection (Kim et al., 2015). Furthermore, the up-regulation of the chitinase gene is positively correlated with the accumulation of salicylic acid (SA) which subsequently induces resistance against avirulent pathogens (Ahmad et al., 2014). On the other hand, chitinase, which acts as a positive regulator of early basal resistance in response to pathogen infection, is suppressed by virulent pathogens (Ott et al., 2006). The up-regulation of chitinase after the establishment of infection is considered to be too late to reduce and prevent pathogen colonization, however (Hietala et al., 2004).

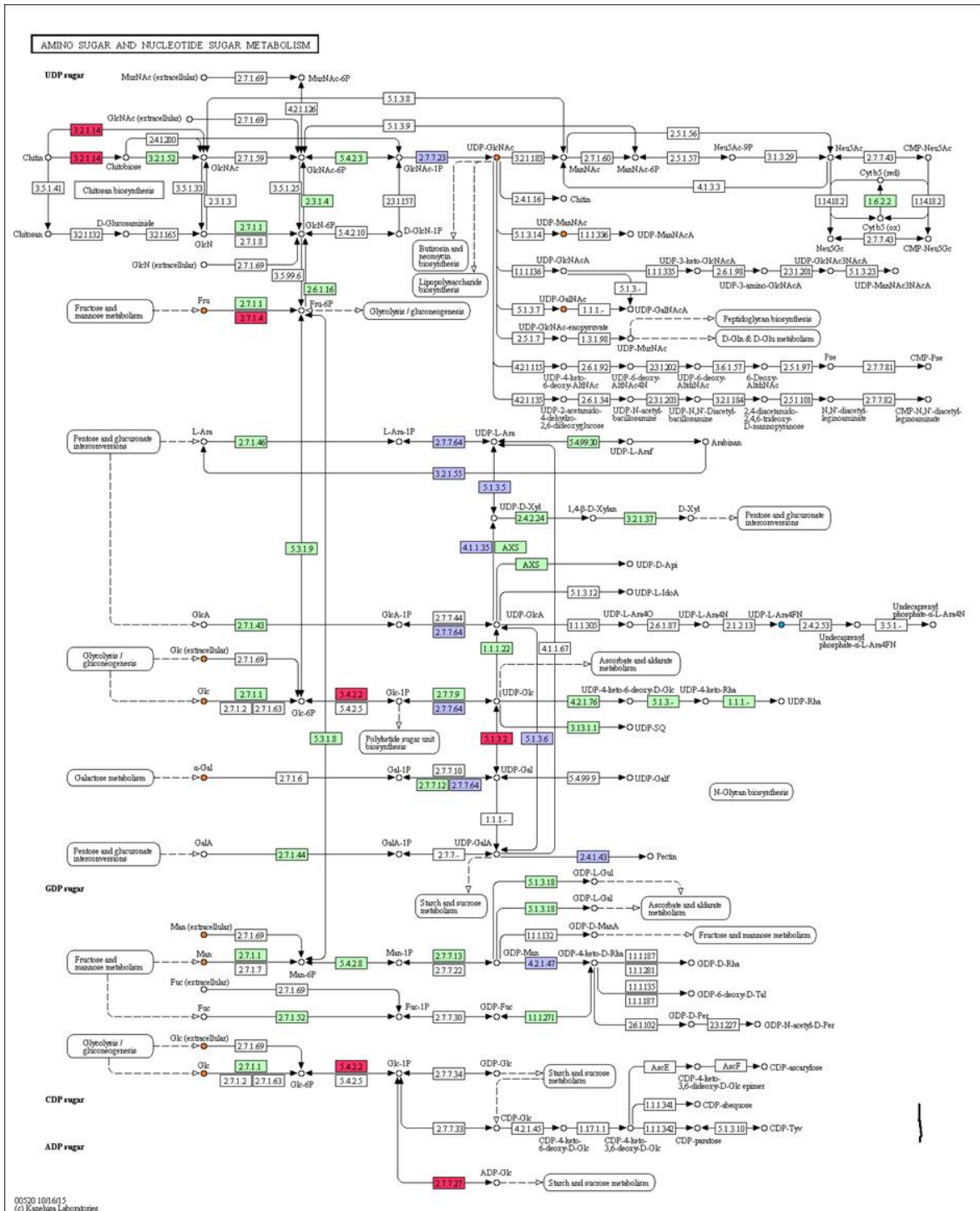


**Figure 3.2.** The expression of genes involved in amino sugar and nucleotide sugar metabolism in *P. brassicae*-infected tissue at 16 DPI. Light blue boxes show down-regulated gene expression ( $\log_2$  fold-change  $\leq -1$ ,  $p \leq 0.05$ ), red boxes show up-regulated gene expression ( $\log_2$  FC  $\geq 1$ ,  $p \leq 0.05$ ), green boxes show genes that do not show a significant change in expression between uninfected and infected tissue. White boxes show genes that have not been identified in *A. thaliana*. Blue circles show metabolites that potentially decreased and orange circles show metabolites that potentially increased in *P. brassicae*-infected tissue ( $p$ -value  $\leq 0.05$ ) at 16 DPI.

The *P. brassicae* genome contains chitin-related Carbohydrate-Active enZymes (CAZymes) domain protein models that belong to GH18 chitinase, CE4 and CBM18 groups. Pd1-chitinase genes which belong to GH18 chitinase group, are expressed during spore formation and germination. This suggests that these genes are important in resting spore cell wall modification and degradation. Meanwhile, CBM18 domains which bind to chitin presumably function to protect the pathogen from breakdown by chitinase. The CE4 domain protein converts chitin into chitosan which is a weaker inducer of plant immune system. Besides *P. brassicae* could release a LysM effector to avoid their chitin compound being recognized by the host immune system (Schwelm et al., 2015).

It has been observed that, at late stages of *P. brassicae* infection, large galls are present in infected plants (Mithen and Magrath, 1992). This is since cell expansion in plant tissue reduces the pressure of water pushing the plasma membrane against the cell wall (Hamann et al., 2009) and as a result *P. brassicae*-infected cells became distorted (Chapter 2, result section). The presence of galls therefore indicates that the primary cell wall has been compromised. At late stages of the infection, the concentration level of Beta-L-arabinose 1-phosphate (L-Ara-1P), glucuronate-1P (GlcA-1P) and galacturonate (GalA-1P) increased in infected tissue (Figure 3.3, 3.4). L-Ara-1P is derived either from free arabinose via a salvage pathway or through *de novo* synthesis involving epimerisation of UDP-D-xylose by UDP-xylose-4-epimerase. Since the *A. thaliana* gene encoding UDP-xylose-4-epimerase (5.1.35) was down-regulated in infected hypocotyl tissue at 26 DPI (Figure 3.3), this suggests that L-Ara-1P was derived from free arabinose of the pentose and glucuronate interconversion pathway. Moreover, the *A. thaliana* gene encoding UDP-arabinopyranose mutase (5.4.99.30) was up-regulated, leading to the production of UDP-L-arabinofuranose (UDP-L-Araf).

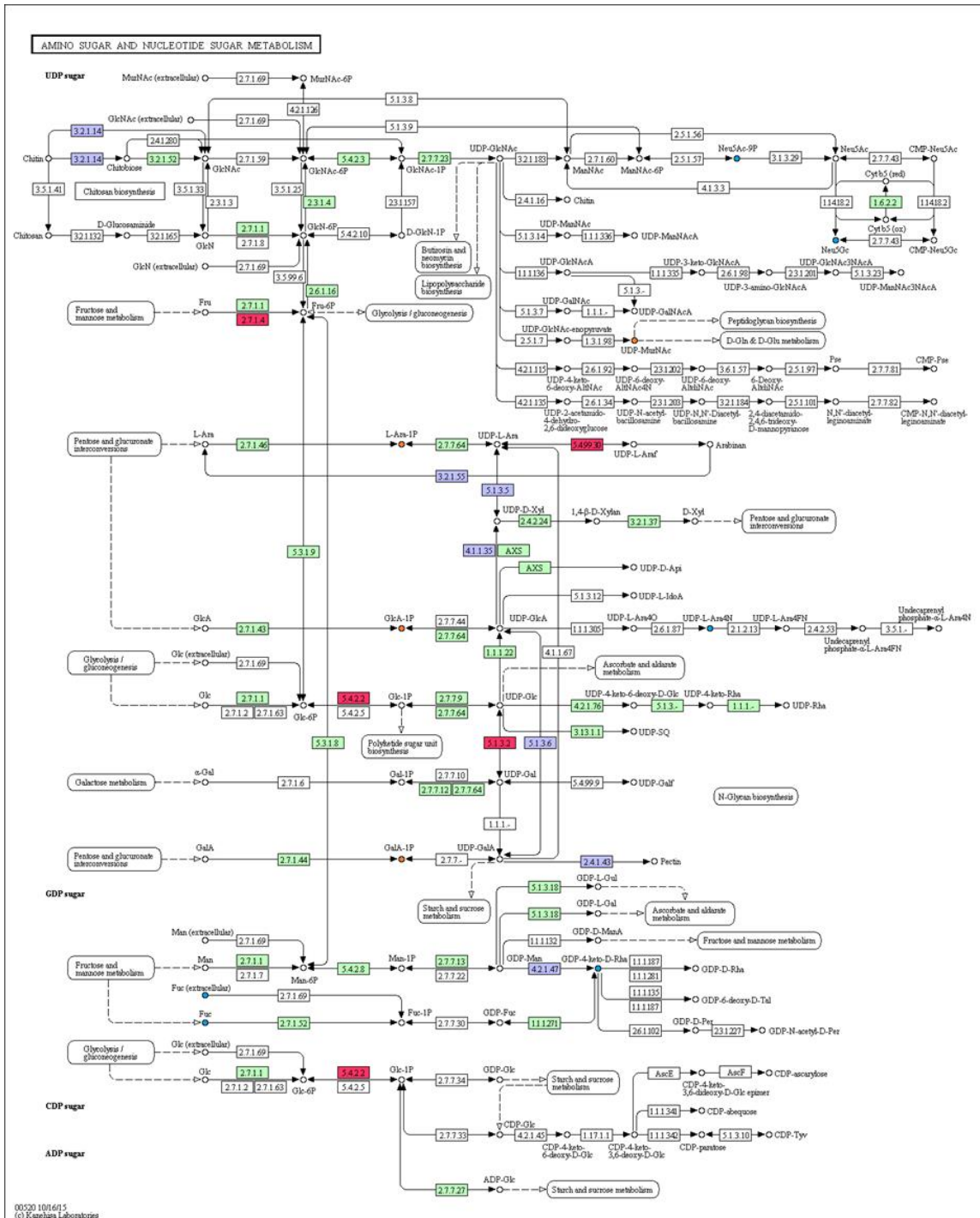


**Figure 3.3.** The expression of genes involved in amino sugar and nucleotide sugar metabolism in *P. brassicae*-infected tissue at 26 DPI. Light blue boxes show down-regulated gene expression ( $\log_2$  fold-change  $\leq -1$ ,  $p \leq 0.05$ ), red boxes show up-regulated gene expression ( $\log_2$  FC  $\geq 1$ ,  $p \leq 0.05$ ), green boxes show genes that do not show a significant change in expression between uninfected and infected tissue. White boxes show genes that have not been identified in *A. thaliana*. Blue circles shows metabolites that potentially decreased and orange circles show metabolites that potentially increased in *P. brassicae*-infected tissue ( $p$ -value  $\leq 0.05$ ) at 25 DPI.

Plant primary cell walls consist of cellulose, hemicellulose and pectin. Pectin is composed of various components including glucuronate, galacturonate, arabinose and galactose (Loewus and Loewus, 1983, Harholt et al., 2010).

Following *P. brassicae* infection, *A. thaliana* genes encoding UDP-glucuronate 4-epimerase (5.1.3.6) and alpha-1,4-galacturonosyltransferase (2.4.1.43) leading to pectin synthesis, were down-regulated at 26 DPI (Figure 3.3). This suggests that the plant primary cell wall lost its strength due to a decrease in pectin synthesis which subsequently resulted in an abundance of free L-Ara-1P, GlcA-1P and GalA-1P. Pectin polysaccharide which is a large polymer in the middle lamella, plays a role in cell adhesion. When a plant mother cell divides into two daughter cells, adhesion between the daughter plant cells is maintained. As plant cells expand, adherent walls between two daughter cells remained fused along the line of the middle lamella. However, abnormal cell adhesion in reinforcing zones could cause cell separation (Jarvis et al., 2003) letting a single cell expand. This may lead to disorganisation of cell structure in *P. brassicae*-infected tissues.

During infection, necrotrophic fungi such as *Botrytis cinerea* enter the host cell by secreting enzymes such as polygalacturonase to depolymerize pectin structure in order to decrease the strength of plant cell walls (Ferrari et al., 2003). As a result of this depolymerisation, oligogalacturonides are released from pectin and could act as a carbon source for the pathogen (Ridley et al., 2001, D'Ovidio et al., 2004). In response to *B. cinerea* polygalacturonase and accumulation of oligogalacturonidase, the plant up-regulates the expression of polygalacturonase-inhibiting proteins (*PGIPs*) that could serve to limit the pathogen colonization (D'Ovidio et al., 2004, Ferrari et al., 2003). Compared to other pathogens such as the oomycetes, *Bigeloviella natans* and *Reticulomyxa filose*, however, the *P. brassicae* genome lacks the domain of the plant cell wall degrading carbohydrate-active enzymes (CAZymes) that are involved in pectin degradation (Schwelm et al., 2015). At 16 DPI, the expression of the *PGIP1* gene was increased in hypocotyl and root tissues of *P.*

*brassicae*-infected *A. thaliana* plants, while at 16 and 26 DPI, *PGIP2* was strongly decreased in both tissues (Table 3.1). This result contrasts with necrotrophic pathogens. In response to *P. brassicae* infection, the expression of *PGIP1* was induced at 16 DPI, but not at 26 DPI, when plasmodia had successfully colonized host cells. This indicates that *P. brassicae* does not enter host cells via degradation of pectin localized in the plant primary cell walls, corroborating the previous suggestion that secondary plasmodia inside cortical cells are distributed by host cytoplasmic movement and host cell division, but not through degradation of the plant cell wall itself (Kageyama and Asano, 2009).

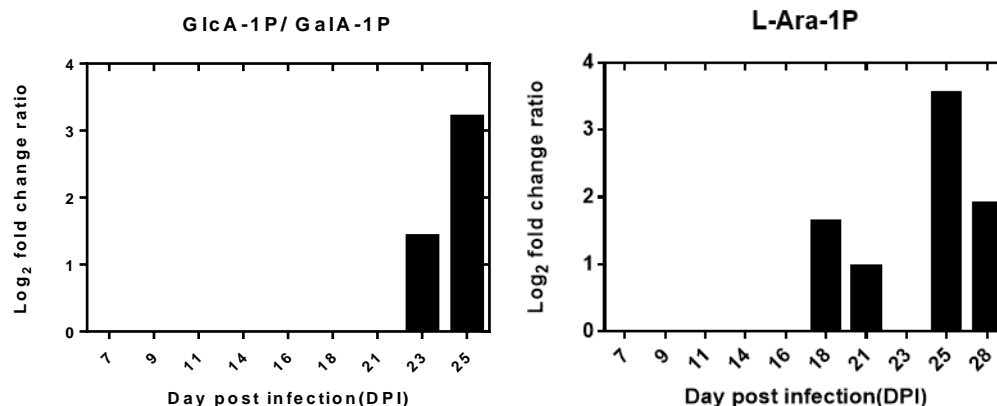


**Figure 3.4.** Fold-change of differential intensity of glcA-1P or GalA-1P and L-ara-1P during *P. brassicae* infection at 18 to 28 DPI (*P*-value  $\leq 0.05$ ).

**Table 3.1** Expression of genes encoded polygalacturonase inhibiting protein in clubroot-infected plants at 16 and 26 dpi in hypocotyl and root tissues. Expression values are log<sub>2</sub>-fold change in infected plants relative to uninfected plants at a significance of p-value  $\leq 0.05$ .

Polygalacturonase inhibiting protein	AGI	Hypocotyl		Root		Average Expression
		16 dpi	26 dpi	16 dpi	26 dpi	
<i>PGIP1</i>	AT5G06860	0.92	n.s	1.43	n.s	6.24
<i>PGIP2</i>	AT5G06870	-1.75	-3.22	n.s	-3.01	5.44

n.s.=not significant.

Average value= average of log-intensities value between uninfected and infected samples. Genes with average value  $\leq 3$  are not showing in this table.

Biological replicates= three plants in each treatment.

Expression value scale:



### 3.3.3 Alteration of Metabolites Involved in Energy and Nucleotide Metabolism of *P. brassicae*-infected Plants

A comparison of the signal intensities of metabolites associated with energy, lipid and nucleotide metabolism is shown as a heat map (Figure S2). The metabolites associated with changes in energy metabolism were also associated with sulfur metabolism, whilst the changes of nucleotide metabolism occurred in those also associated with purine and pyrimidine metabolism (Table S2).

In infected *A. thaliana* plants, the regulation of the sulfur metabolism pathway was altered by *P. brassicae* presumably to prevent plants activating their defence mechanism. The sulfur metabolism pathway involves thiosulfate as the electron donor and sulfate as the electron acceptor. In *A. thaliana* plants, thiosulfate is synthesised from mercaptopyruvate by 3-mercaptopyruvate sulfurtransferase activity which is a part of the cysteine and methionine metabolism pathway. Electron transfer from thiosulfate to sulfate is regulated by a sulfur-oxidation reaction through the cytochrome C-1 (SOX) gene. Thiosulfate can also be converted to sulfite through the regulation of thiosulfate sulfur transferase. Then, sulfite is converted to sulfate by sulfite oxidase. Sulfite can also be converted into sulfide by sulfite reductase. The reaction from sulfite and O-acetyl-serine substrate through cysteine synthase A/O-acetylserine (Thio) lyase releases the amino acid L-cysteine. In this context, following *P. brassicae* infection, pathogen colonization at 25 DPI caused an accumulation of thiosulfate and O-Acetyl-L-Serine (Figure 3.5). Sulfite and amino acid L-cysteine, however, decreased in infected tissue at 25 DPI (Figure 3.5).

The changes found here in sulfur metabolism occurring within the infected hypocotyl, together with the alterations in thiosulfate, sulfite, O-Acetyl-L-Serine and L-cysteine concentrations were integrated with transcriptomic data at 16 and 26 DPI obtained from a previous study (Malinowski et al., *unpublished*). This showed that the expression of the *A. thaliana* 3-mercaptopyruvate sulfurtransferase gene to synthesise thiosulfate and pyruvate from 3-mercaptopyruvate was not significantly

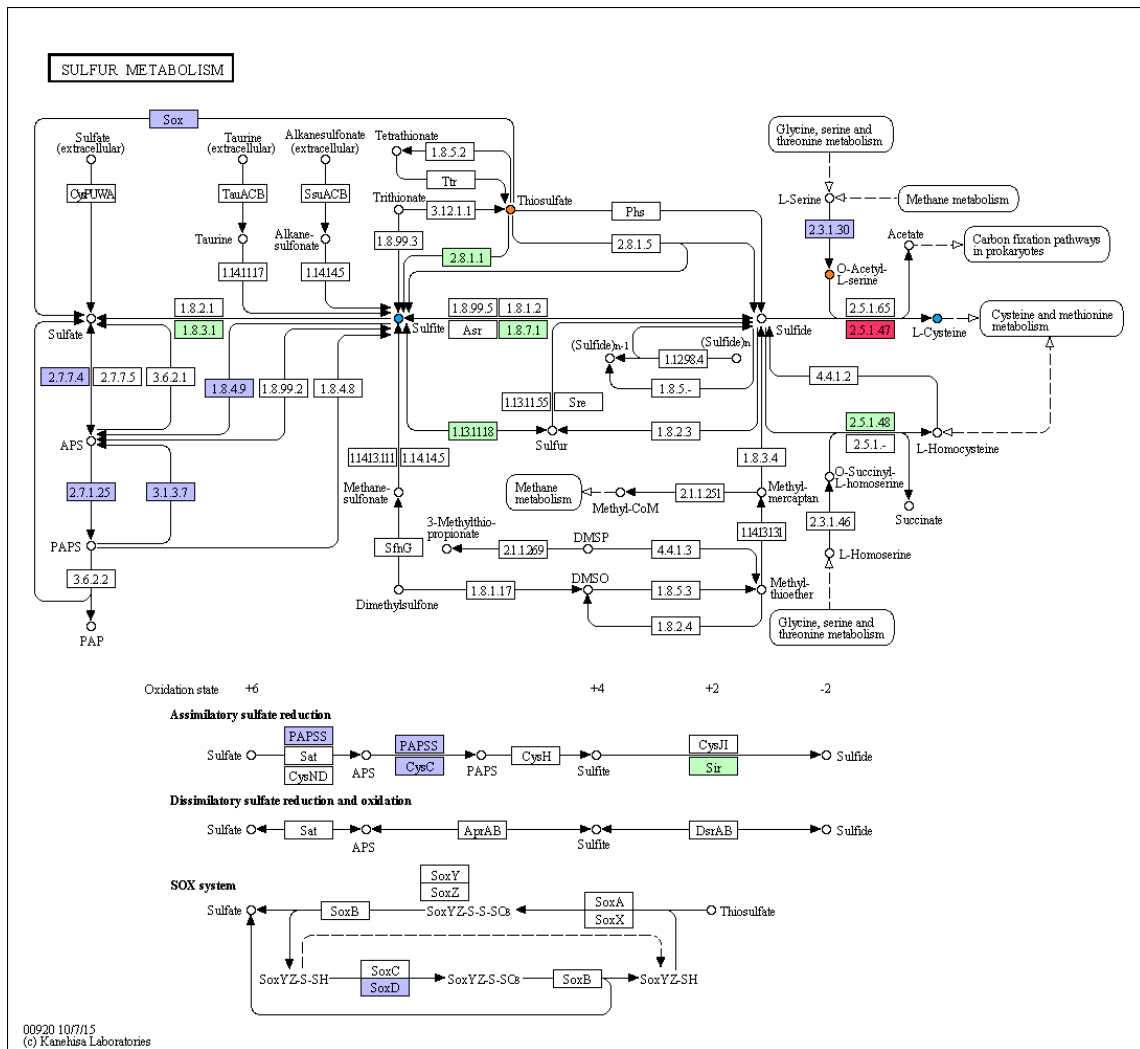


**Figure 3.5.** The expression of genes involved in sulfur metabolism in *P. brassicae*-infected tissue at 26 DPI. Light blue boxes show down-regulated gene expression ( $\log_2$  fold-change  $\leq -1$ ,  $p \leq 0.05$ ), red boxes show up-regulated gene expression ( $\log_2$  FC  $\geq 1$ ,  $p \leq 0.05$ ), green boxes show genes that do not show a significant change in expression between uninfected and infected tissue. White boxes show genes that have not been identified in *A. thaliana*. Blue circles show metabolites that potentially decreased and orange circles show metabolites that potentially increased in *P. brassicae*-infected tissue ( $p$ -value  $\leq 0.05$ ).

different between infected and infected tissue (data not shown). The expression of the *A. thaliana* SOX gene, which converts thiosulfate to sulfate, was down-regulated in infected hypocotyl tissue at 16 DPI (data not shown) and 26 DPI (Figure 3.5). Furthermore, expression of thiosulfate sulfur transferase (2.8.1.1) and sulfite oxidase (1.8.3.1), which convert thiosulfate to sulfite and sulfite to sulfate, respectively, appeared not to be significantly different between infected and uninfected tissues at

16 DPI (data not shown) and 26 DPI (Figure 3.5). On the other hand, genes encoding cysteine synthase A/O-acetylserine (Thio) lyase (2.5.1.47), which convert the substrates O-Acetyl-L-serine and sulfide to L-cysteine were up-regulated at 16 and 26 DPI (Figure 3.5).

Thiosulfate is a compound that could potentially supply sulfur molecules to *P. brassicae*. Given that results in this study show that thiosulfate increased in hypocotyl tissue of *P. brassicae*-infected plants at 7, 21, 25 and 28 DPI (Figure 3.5 and 3.6), The down-regulation of the host's SOX gene in infected tissue at 16 and 26 DPI is hypothesised caused the accumulation of thiosulfate. The *P. brassicae* genome on the other hands, contains the SOX gene, which could oxidize thiosulfate and is also the gene encoding thiosulfate sulfur transferase (Schwelm et al., 2015), which converts thiosulfate to sulfite. Probably, *P. brassicae* regulates the sulfur cycle to increase the production of thiosulfate as its sulfur source and suppress the host's sulfur metabolism genes.

The sulfur metabolism pathway correlates with plant defence through sulfite. Sulfite can act as a plant defence response when it is oxidized by sulfite oxidase to release sulfate and H<sub>2</sub>O<sub>2</sub> (Bloem et al., 2015, Riemenschneider et al., 2005a). However, the expression of the host's sulfite oxidase (1.8.3.1) was found not to be significantly different between infected and uninfected tissues at 16 DPI (data not shown) and 26 DPI (Figure 3.5). Meanwhile, the *P. brassicae* genome contains a gene encoding persulfide dioxygenase (Schwelm et al., 2015). Persulfide dioxygenase serves to oxidize sulfur/S-sulfanylglutathione and release glutathione, sulfite, H<sup>+</sup> and S-sulfino-glutathione, acting in plant defence. The expression of *A. thaliana* persulfide dioxygenase (1.13.11.18) was not shown to be significantly different in infected and uninfected tissues (Figure 3.5), however, and I therefore hypothesise that *P. brassicae* induced the accumulation of thiosulfate by repressing host SOX gene. Therefore, *P. brassicae* converts thiosulfate to glutathione as a sulfur transport compound so as to avoid the plant activating its own defence response through

expression of the sulfite oxidase gene, and thus finally causing a low accumulation of sulfite. Besides, it has been reported that glutathione accumulates in root tissue of *P. brassicae*-infected *Brassica napus* plants (Wagner et al., 2012). The role of glutathione in clubroot infection remains unclear, however, in respect to whether it is involved in plant defence or is required for the development of the pathogen (Wagner et al., 2012). If plasmodia potentially produce glutathione, this compound is probably beneficial for their growth. Transcriptomic data from Malinowski et al. (*unpublished*) shows up-regulation of genes encoding Glutathione-S-transferase which plays a role in detoxification (data not shown).

Furthermore, the O-Acetyl-L-Serine component of sulfur metabolism increased at 25 DPI in infected tissue (Figure 3.5). It has been reported that the exogenous supply of O-Acetyl-L-Serine could increase thiol content and restrict the synthesis of cysteine (Neuenschwander et al., 1991, Smith et al., 1997). In this study, this accumulation of O-Acetyl-L-Serine was accompanied by the up-regulation of genes encoding cysteine synthase A/O-acetylserine (Thio) lyase (2.5.1.47) at 16 and 26 DPI (Figure 3.5). The desulphydrase activity of O-acetylserine (thio) lyase could trigger plant defence mechanisms through the production of sulfite as a plant defence compound (Riemenschneider et al., 2005b). The fact that this compound decreased in infected tissue in this study suggests that plant defence responses were repressed by *P. brassicae* infection. Moreover, in this study, it showed that the expression of genes encoding sulfur transporters in hypocotyl and root tissues of *P. brassicae*-infected plants were generally down-regulated except for *SULTR3*; which was up-regulated (Table 3.2). I suggest that plasmodia obtain sulfur from the sulfur metabolism of the host which subsequently reduces the distribution of sulfur from root to the shoot.

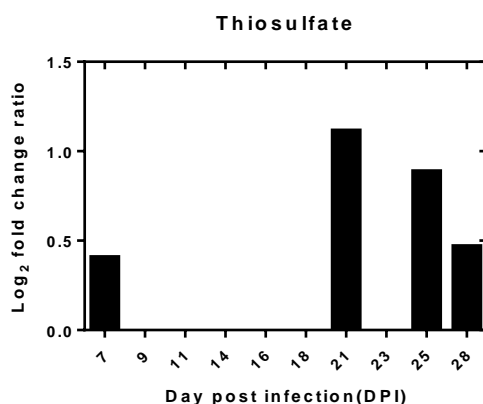


**Figure 3.6.** Fold-change of differential thiosulfate intensity during *P. brassicae* infection at 7, 21, 25 and 28 DPI (p-value  $\leq 0.05$ ).

**Table 3.2.** Expression of genes encoding sulfur transporters in clubroot-infected plants at 16 and 26 DPI in hypocotyl and root tissues. Expression values are log<sub>2</sub>-fold change in infected plants relative to uninfected plants at a significance of p-value  $\leq 0.05$ .

		Hypocotyl		Root		Average Expression
Sulfur transporter	AGI	16 dpi	26 dpi	16 dpi	26 dpi	
<i>SULTR3;3</i>	AT1G23090	1.90	2.96	1.11	2.54	4.83
<i>SULTR2;2</i>	AT1G77990	-2.13	0.99	-1.98	-0.69	5.36
<i>SULTR1;2</i>	AT1G78000	-1.29	0.76	-0.59	n.s	7.78
<i>SULTR4;2</i>	AT3G12520	-2.00	n.s	-1.86	n.s	7.35
<i>SULTR3;4</i>	AT3G15990	n.s	n.s	n.s	-1.26	8.33
<i>SULTR3;1</i>	AT3G51895	n.s	n.s	0.67	n.s	8.11
<i>SULTR3;2</i>	AT4G02700	n.s	0.86	n.s	1.87	4.35
<i>SULTR1;1</i>	AT4G08620	-1.29	n.s	n.s	-1.97	4.70
<i>SULTR2;1</i>	AT5G10180	-1.43	-1.41	n.s	-1.47	8.62
<i>SULTR4;1</i>	AT5G13550	-0.77	n.s	-0.86	n.s	7.60
<i>SULTR3;5</i>	AT5G19600	-5.29	-6.41	-2.24	-6.07	7.43

n.s=not significant.

Average value= average of log-intensities value between uninfected and infected samples. Genes

with average value  $\leq 3$  are not showing in this table.

Biological replicates= three plants in each treatment.

Expression value scale:



Following infection of *A. thaliana* by *P. brassicae*, potential metabolites involved in purine and pyrimidine metabolism, changed at 7, 16 and 25 DPI (Table S2 in appendix section). Purine and pyrimidine nucleotides are essential precursors for

DNA and RNA synthesis, both for the plant and pathogen. In addition, purine and pyrimidine metabolism can be energy sources and precursors for the synthesis of products such as sucrose, polysaccharides and phospholipids.

At 16 DPI, inosine monophosphate (IMP) of purine metabolism increased in infected tissue (Figure 3.7). IMP is synthesised through *de novo* purine nucleotide biosynthesis from 5-phosphoribosyl-1-pyrophosphate (PRPP). At 25 DPI, D-Ribose 5'-phosphate, 1-(5'-Phosphoribosyl)-5-amino-4-imidazolecarboxamide (AICAR) and 1-(5'-Phosphoribosyl)-5-amino-4-(N-succinocarboxamide)-imidazole (SICAR), increased in infected tissue at 25 DPI (Figure 3.8). The transcriptomic data showed that expression of *A. thaliana* genes associated with *de novo* purine biosynthesis did not differ significantly between uninfected and infected plants at 26 DPI (Figure 3.8).

In pyrimidine metabolism, *de novo* biosynthesis of pyrimidine nucleotides starts from carbamoyl phosphate and glutamine to produce Uridine monophosphate (UMP) via orotate compound (Stasolla et al., 2003, Garavito et al., 2015). Following infection of *A. thaliana* by *P. brassicae*, orotate, UDP, dUMP and UMP were found to have accumulated in infected tissue at 25 DPI (Figure 3.9). Since the *A. thaliana* gene encoding apyrase (3.6.1.5) that hydrolyses UDP to UMP was down-regulated and uridylate kinase (2.7.4.22) that phosphorylates UMP to UDP was up-regulated in infected tissue at 26 DPI, this indicates that plant RNA synthesis also increased in response to *P. brassicae* infection (Figure 3.9). This suggests that UMP, which is a precursor of other pyrimidine nucleotides (Garavito et al., 2015), was also important in the pyrimidine metabolism of *P. brassicae*-infected plants. This further indicates that *de novo* biosynthesis of pyrimidine nucleotides increased in the late gall formation, which consists of actively dividing cells. The number of actively dividing is increased in hypocotyl of *A. thaliana* plants upon *P. brassicae* infection at 16 until 26 DPI, but abruptly stops at 32 DPI (Malinowski et al., 2012).

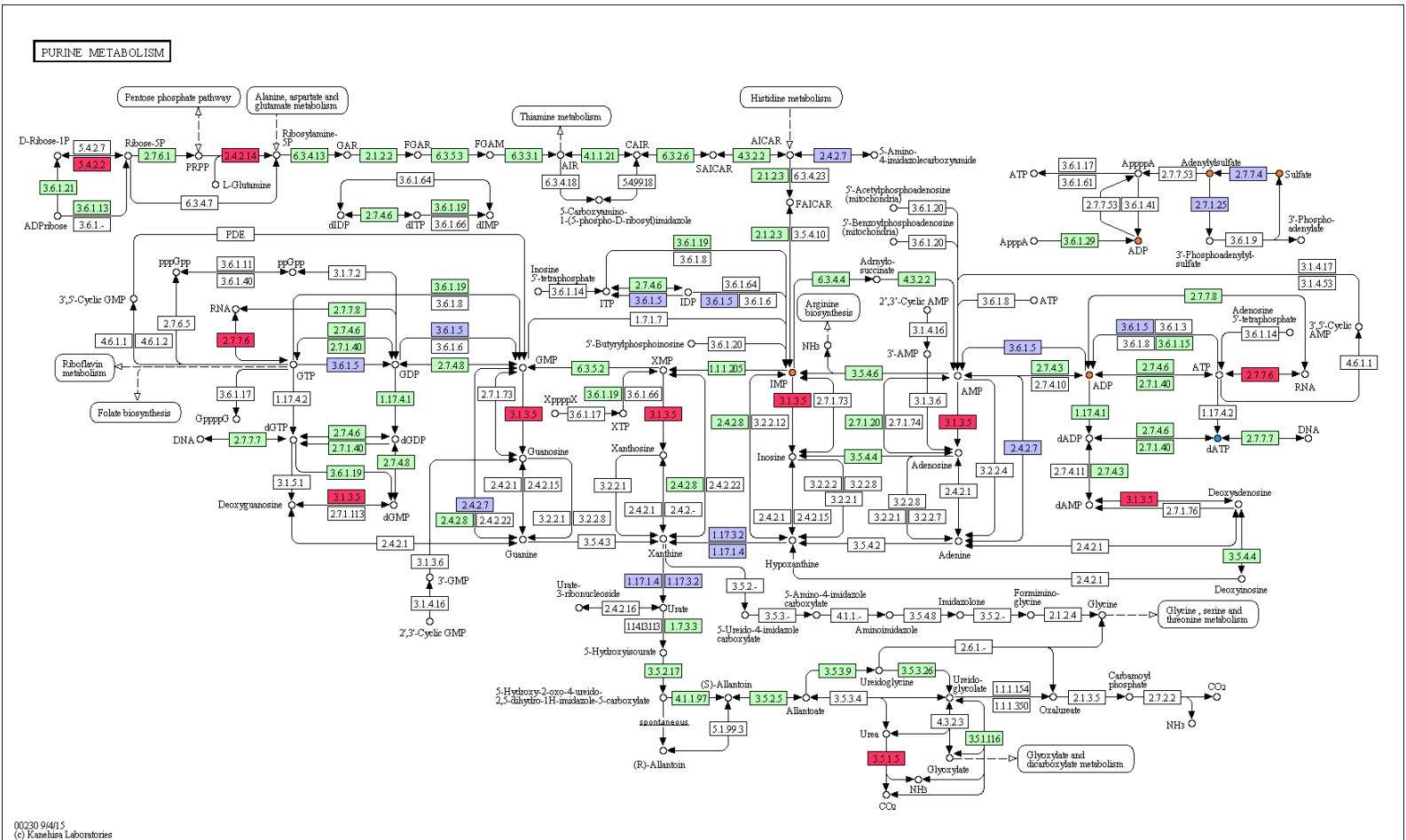


**Figure 3.7.** The expression of genes involved in purine metabolism in *P. brassicae*-infected tissue at 16 DPI. Light blue boxes show down-regulated gene expression ( $\log_2$  fold-change  $\leq -1$ ,  $p \leq 0.05$ ), red boxes show up-regulated gene expression ( $\log_2$  FC  $\geq 1$ ,  $p \leq 0.05$ ), green boxes show genes do not show a significant change in expression between uninfected and infected tissue. White boxes show genes that have not been identified in *A. thaliana*. Blue circles show metabolites that are potentially decreased and orange circles show metabolites that are potentially increased in *P. brassicae*-infected tissue ( $p$ -value  $\leq 0.05$ ).

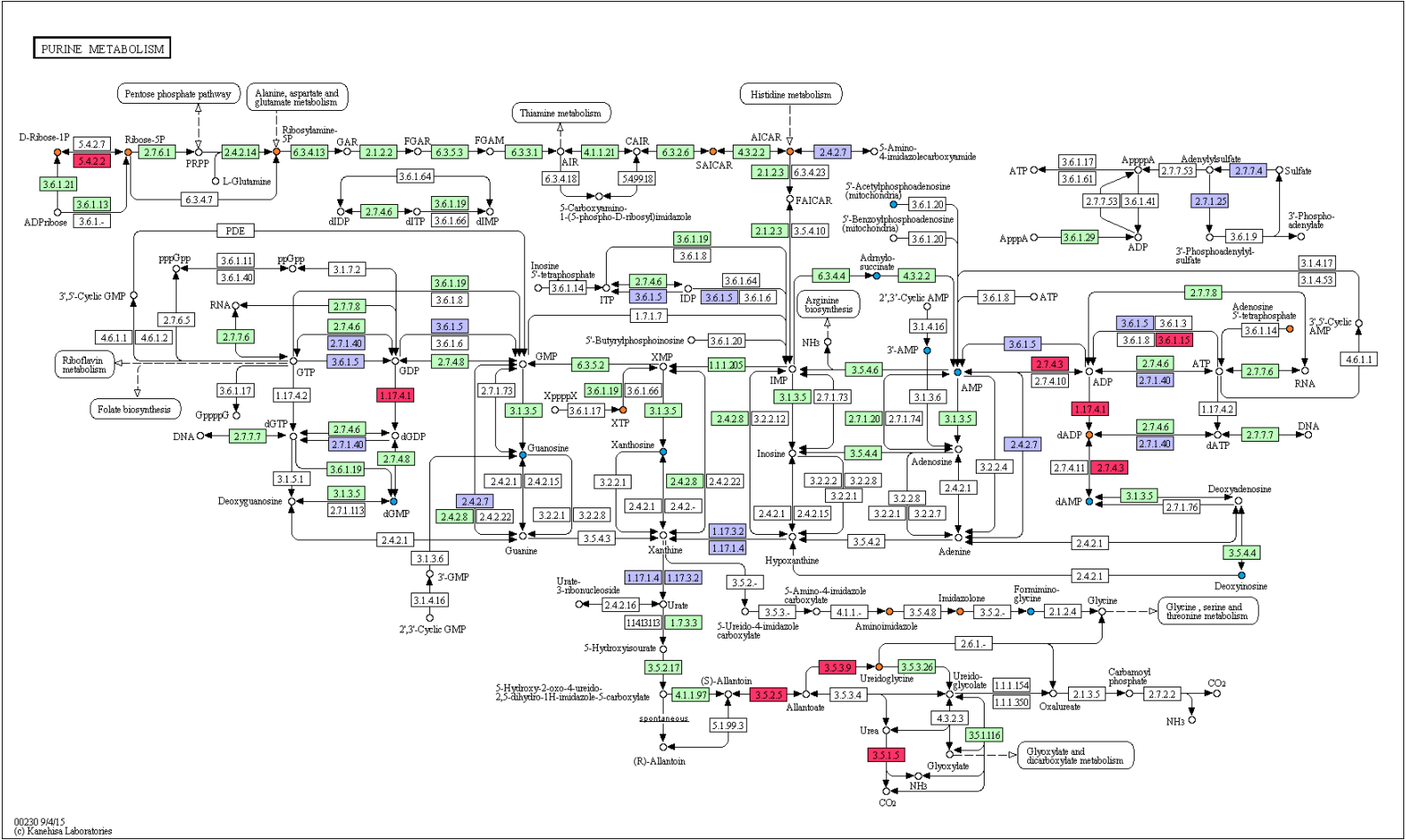


**Figure 3.8.** The expression of genes involved in purine metabolism in *P. brassicae*-infected tissue at 26 DPI. Light blue boxes show down-regulated gene expression ( $\log_2$  fold-change  $\leq -1$ ,  $p \leq 0.05$ ), red boxes show up-regulated gene expression ( $\log_2$  FC  $\geq 1$ ,  $p \leq 0.05$ ), green boxes show genes do not show a significant change in expression between uninfected and infected tissue. White boxes show genes that have not been identified in *A. thaliana*. Blue circles shows metabolites that are potentially decreased and orange circles show metabolites that are potentially increased in *P. brassicae*-infected tissue ( $p$ -value  $\leq 0.05$ ).

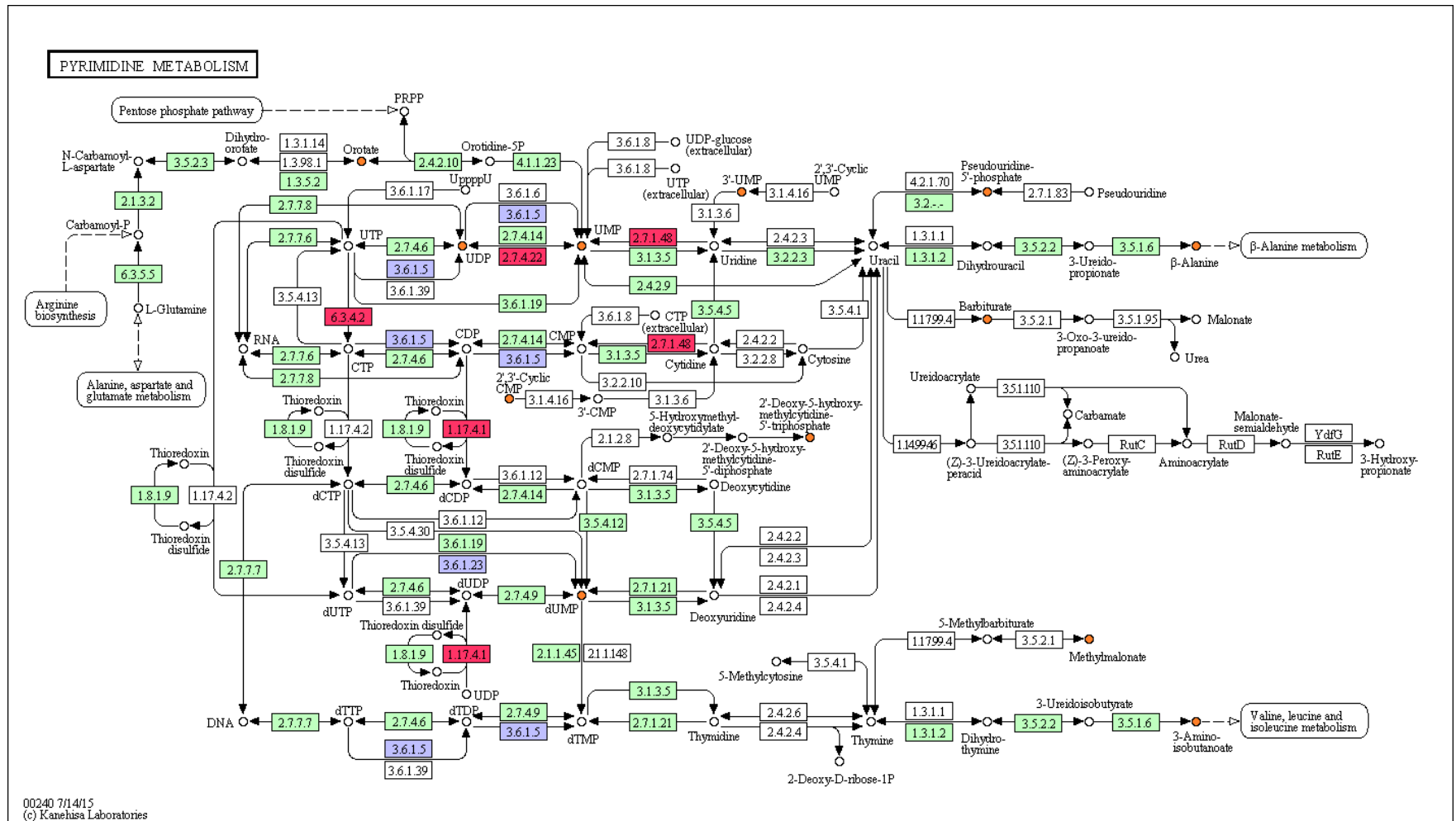


**Figure 3.9.** The expression of genes involved in pyrimidine metabolism in *P. brassicae*-infected tissue at 26 DPI. Light blue boxes show down-regulated gene expression ( $\log_2$  fold-change  $\leq -1$ ,  $p \leq 0.05$ ), red boxes show up-regulated gene expression ( $\log_2$  FC  $\geq 1$ ,  $p \leq 0.05$ ), green boxes show genes that do not show a significant change in expression between uninfected and infected tissue. White boxes show genes that have not been identified in *A. thaliana*. Blue circles show potentially decreased metabolites and orange circles show potentially increased metabolites in *P. brassicae*-infected tissue ( $p$ -value  $\leq 0.05$ ).

Catabolism of pyrimidine nucleotides is an important pathway to maintain pyrimidine homeostasis and the recycling of nitrogen from pyrimidine to nitrogen metabolism (Zrenner et al., 2009).  $\beta$ -alanine, methylmalonate and 3-aminoisobutyric acid following catabolism of pyrimidine nucleotides accumulated in infected tissue at 25 DPI (Figure 3.9). Methylmalonate is a secondary product of oxidized thymine and  $\beta$ -alanine which is a precursor of pantothenic acid, is derived from uracil (Garavito et al., 2015, Katahira and Ashihara, 2006).

The transcriptomic data showed that *A. thaliana* gene expression associated with the synthesis of  $\beta$ -alanine, methylmalonate and 3-aminoisobutyric acid were not significantly different between uninfected and infected tissue at 26 DPI (Figure 3.9). Although it has been reported that pyrimidine catabolism recycles pyrimidine nitrogen to nitrogen metabolism when the cell is under nitrogen limitation (Zrenner et al., 2009), this study reveals no evidence of any *A. thaliana* gene expression associated with the catabolism of pyrimidine in response to *P. brassicae* infection. The accumulation of compounds associated with pyrimidine catabolism occurs under the control of plasmodia therefore has been assumed in this study. It is possible that the plasmodia use these compounds as a carbon or nitrogen source.

#### **3.3.4 Alteration of Metabolites Involved in Amino Acid Metabolism of *P. brassicae*-infected Plants**

A comparison of the signal intensities of metabolites associated with amino acid metabolism is shown as a heat map (Figure S3). Specific putative metabolites associated with amino acid metabolism, whose concentration altered in response to *P. brassicae* infection at 7, 16 and 25 DPI are shown in Table S3 of the Appendix.

Following *P. brassicae* infection, amino acid glutamate, aspartate, alanine and proline all increased in infected tissue, while tryptophan and cysteine decreased (Figure 3.10). Glutamate was found to have increased at 11, 18, 25 and 28 DPI in infected tissue (Figure 3.10). The accumulation of glutamate was accompanied

by the up-regulation of gene encoding glutamine synthetase at 16 DPI (data not shown) and 26 DPI (Figure 3.11). It has been reported that glutamate accumulates in root tissue of *P. brassicae*-infected *Brassica napus* plants (Wagner et al., 2012). This may suggest that glutamate is required for the development of *P. brassicae* inside a susceptible host (Wagner et al., 2012). Besides, glutamate can be catabolized with the production of energy.

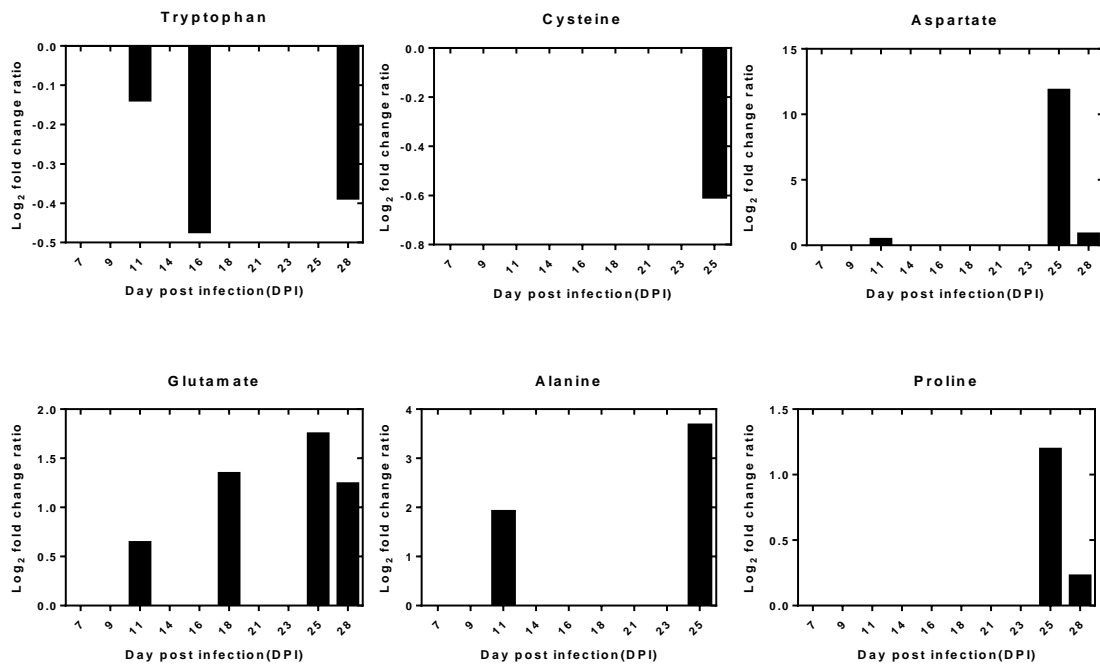


**Figure 3.10.** Fold-change of differential intensities of tryptophan, cysteine, aspartate, glutamate, alanine and proline during *P. brassicae* infection at 7 to 28 DPI ( $p$ -value  $\leq 0.05$ ).

Aspartate accumulated in response to infection at 25 DPI, but the *A. thaliana* gene encoding aspartate aminotransferase and aspartate kinase at 16 DPI (data not shown) and 26 DPI were down regulated in infected tissue (Figure 3.11). Aspartate aminotransferase transfers the nitrogenous group of glutamate to the carboxyl group of oxaloacetate and releases 2-oxoglutarate and aspartate, whilst aspartate kinase transfers the phosphorus group to the carboxyl group of aspartate and releases 4-phospho-L-aspartate. The *P. brassicae* genome contains a gene encoding aspartate kinase (Schwelm et al., 2015). In addition, the gene encoding homoserine O-succinyltransferase is present in *P. brassicae* genome, but is not present in the *A. thaliana* genome. This gene synthesises O-

Succinylhomoserine and releases coenzyme A (CoA). Consequently, it seems as if the accumulation of aspartate in infected tissue was regulated by the plasmodia. Aspartate can be catabolized with the production of energy.

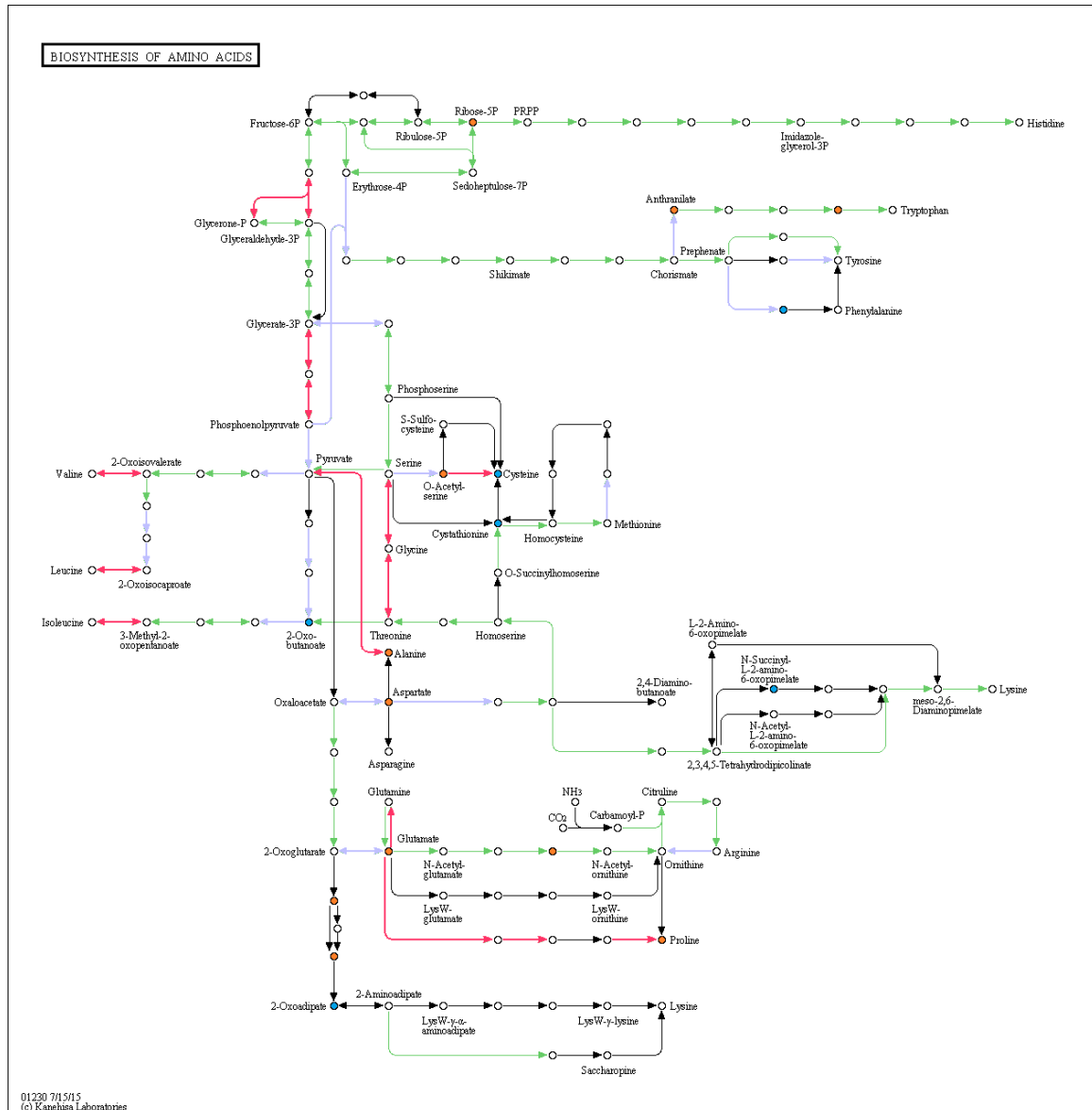


**Figure 3.11.** The expression of genes involved in the biosynthesis of amino acid in *P. brassicae*-infected tissue at 26 DPI. Light blue arrows show down-regulated gene expression ( $\log_2$  fold-change  $\leq -1$ ,  $p \leq 0.05$ ), red arrows show up-regulated gene expression ( $\log_2$  FC  $\geq 1$ ,  $p \leq 0.05$ ), green arrows show genes that do not show a significant change in expression between uninfected and infected tissue and black arrows show genes that have not been identified in *A. thaliana*. Blue circles show potentially decreased metabolites and orange circles show potentially increased metabolites in *P. brassicae*-infected tissue ( $p$ -value  $\leq 0.05$ ).

Moreover, alanine aminotransferase activity transfers the nitrogenous group of glutamate to the methyl group of pyruvate and releases 2-oxoglutarate and

alanine. Alanine was also found to be accumulated in infected tissue at 11 and 25 DPI (Figure 3.10), and the gene encoding alanine aminotransferase was up-regulated in response to *P. brassicae* infection at 16 (data not shown) and 26 DPI (Figure 3.11). This result also corroborates the accumulation of alanine in root tissue of *B. napus* plants in response to *P. brassicae* infection (Wagner et al., 2012), indicating that plasmodia requires the amino acid alanine.

Furthermore, proline accumulated in infected tissue at 25 and 28 DPI (Figure 3.10). Since proline is synthesised from glutamate, its synthesis can be initiated after the carboxyl group of glutamate receives the phosphorous-containing group from glutamate 5-kinase to form glutamate 5-phosphate. The glutamate 5-phosphate is dehydrogenated by glutamate semialdehyde dehydrogenase to become glutamate semialdehyde. Genes encoding both of the enzymes were down-regulated at 16 DPI (data not shown), whilst at 26 DPI they were up-regulated in infected tissue (Figure 3.11). Glutamate semialdehyde is cyclized spontaneously to form delta-pyrroline-5-carboxylate and becomes proline by the activity of pyrroline-5-carboxylate reductase. The gene encoding the latter enzyme was also found to be up-regulated in infected tissue at 26 DPI (Figure 3.11). It has been reported that proline accumulates only at the later stages of infection of *P. brassicae*-infected *B. napus* plants, when the concentration of *P. brassicae* DNA is relatively high compared to the early stage of infection (Wagner et al., 2012). In addition, accumulation of proline in plants that are partially resistant to *P. brassicae* infection is delayed when compared with clubroot-susceptible plants (Jubault et al., 2008). This indicates that proline is not involved in the plant defence response since partially resistant plants show a stronger induction of plant defence at the very beginning of *P. brassicae* infection (Jubault et al., 2013).

It has been suggested that since proline could act as an osmotic protectant, it could possibly accumulate inside plasmodia, either for their growth or to protect them from the osmotic and oxidative stress of the host environment (Jubault et al., 2008). Proline is a compatible solute associated with host stress including

drought. The reduction of xylem formation in infected plants could have limited water transport to the whole plants, mimicking drought conditions. The accumulation of proline in infected tissue with *P. brassicae* might protect plants from the osmotic stress. The role of proline to protect plants from oxidative stress on the other hand, is associated with the production of reactive oxygen species (ROS) by the plant in order to kill pathogens. ROS could kill pathogens directly by causing oxidative damage to macromolecules, or indirectly by activating plant systemic acquired resistance (SAR) (Wittek et al., 2015). This indicates that during *P. brassicae* infection, surrounding host cells are in a condition of oxidative stress leading to macromolecular damage. Following *P. brassicae* infection, proteins associated with ROS detoxification are decreased after 12 hours' infection and increased after 24-72 hours' infection (Cao et al., 2008, Devos et al., 2006). The ROS detoxification process is required so as to avoid macromolecular damage inside host tissue by the dismutation of superoxide into oxygen and hydrogen peroxide. Proline, which acts as a stress protector, could potentially scavenge ROS in cells as well as its functions as a protein and membrane stabilizer (Takagi 2008).

### **3.3.5 Alteration of Metabolites Involved in Cofactor and Vitamin Metabolism of *P. brassicae*-Infected Plants**

A comparison of the signal intensities of metabolites associated with cofactor and vitamin metabolism is shown as a heat map (Figure S4). Specific putative metabolites associated with cofactor and vitamin metabolism whose concentrations altered at 7, 16, and 25 DPI in response to *P. brassicae* infection are shown in Table S4 of the Appendix. The metabolites associated with changes in vitamin metabolism were those associated with vitamin B6 and folate metabolism. Specifically, metabolites related to vitamin metabolism including pyridoxal 5'-phosphate for vitamin B6 metabolism fluctuated in response to *P. brassicae* infection, whilst 4-aminobenzoate for folate biosynthesis increased during late gall formation (Figure 3.12).

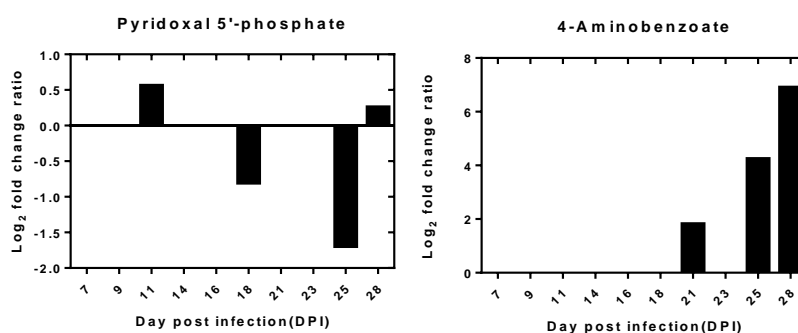


**Figure 3.12.** Fold-change of the differential intensity of pyridoxal 5'-phosphate for vitamin B<sub>6</sub> metabolism and 4-aminobenzoate for folate biosynthesis during *P. brassicae* infection at 7 to 28 DPI (p-value  $\leq$  0.05).

Most of the vitamins that are synthesised in plants, including Vitamin B6 and folate, possess antioxidant activity and are important in the scavenging of Reactive Oxygen Species (ROS) that cause damage to plant macromolecules. In plants, vitamin B6 is present in various forms including pyridoxine, pyridoxamine, pyridoxal and their phosphorylated derivatives. In *A. thaliana* plants, vitamin B6 is synthesised from Ribulose 5-phosphate by the enzyme pyridoxal 5'-phosphate synthase (Tambasco-Studart et al., 2005). Following *P. brassicae* infection, D-Ribulose 5-phosphate, a precursor of pyridoxal 5'-phosphate was found to have increased in infected tissue (Figure 3.13).

As D-Ribulose 5-phosphate accumulated, the *A. thaliana* gene encoding pyridoxal 5'-phosphate synthase (4.3.3.6), synthesising pyridoxal 5'-phosphate by hydrolysing glutamine to release glutamate, was up-regulated in response to *P. brassicae* infection at 26 DPI (Figure 3.17). This indicates that *de novo* biosynthesis of vitamin B6 was increased in infected tissue. The concentration of pyridoxamine phosphate for vitamin B6 metabolism decreased in infected tissue at 7 DPI (Table S4 of Appendix), whilst pyridoxal 5'-phosphate increased at 11 DPI, decreased at 18 and 25 DPI and slightly increased at 28 DPI (Figure 3.12). The accumulation of pyridoxine phosphate at 25 DPI (Figure 3.13) indicates that antioxidant compounds were present in infected tissue. Among vitamin B6 forms, pyridoxal shows the strongest antioxidant activity in respect to maintaining tissue integrity and viability (Denslow et al., 2005).

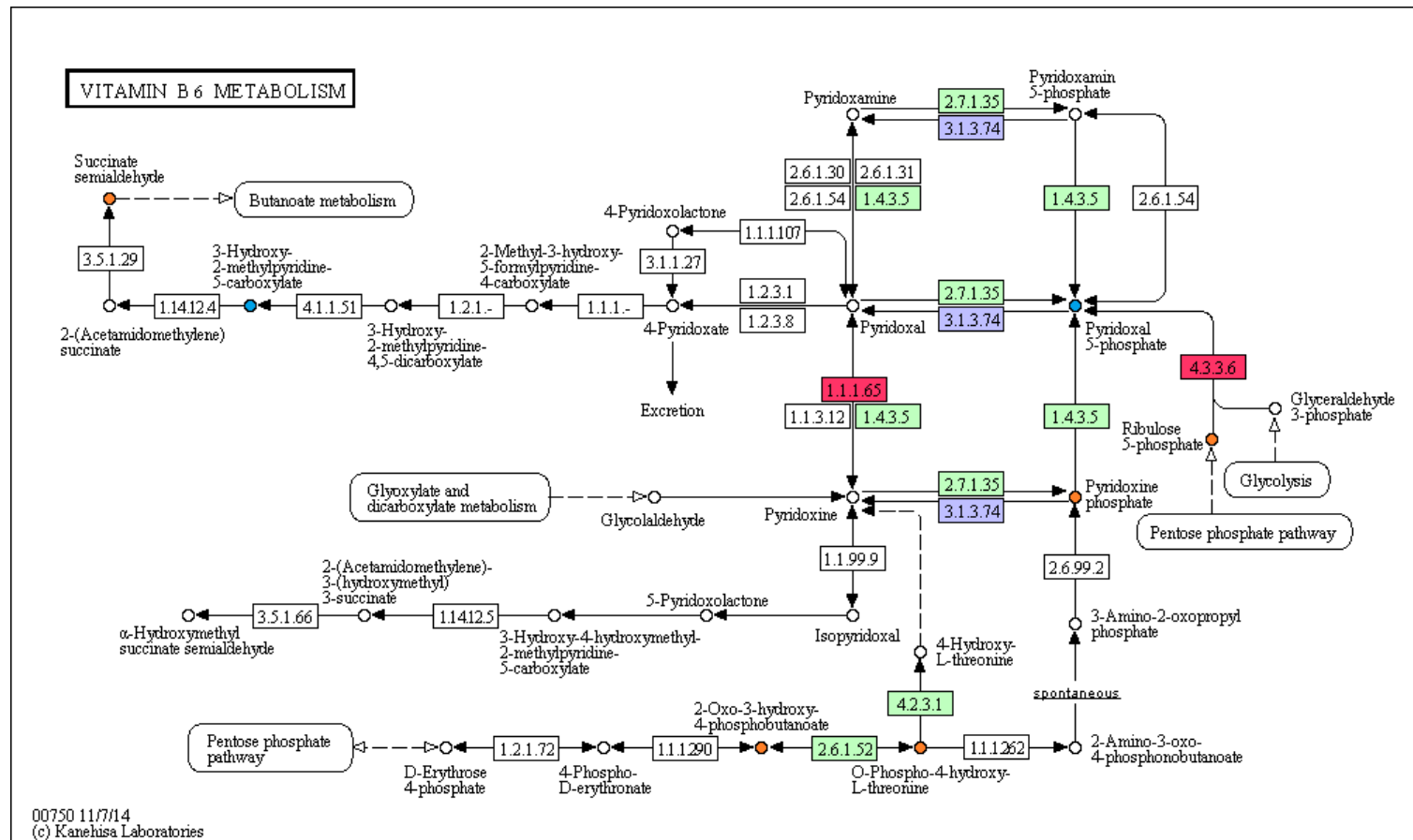


**Figure 3.13.** The expression of genes involved in vitamin B6 metabolism in *P. brassicae*-infected tissue at 26 DPI. Light blue boxes show down-regulated gene expression ( $\log_2$  fold-change  $\leq -1$ ,  $p \leq 0.05$ ), red boxes show up-regulated gene expression ( $\log_2$  FC  $\geq 1$ ,  $p \leq 0.05$ ), green boxes show genes that do not show a significant change in expression between uninfected and infected tissue. White boxes show genes that have not been identified in *A. thaliana*. Blue circles shows potentially decreased metabolites and orange circles show potentially increased metabolites in *P. brassicae*-infected tissue ( $p$ -value  $\leq 0.05$ ).

Pyridoxal is synthesised through the activities of two genes. First, it is synthesized from pyridoxine by the *A. thaliana* gene encoding pyridoxine 4-dehydrogenase (1.1.1.65) and this gene was up-regulated at 26 DPI in infected tissue (Figure 3.13). Secondly, the *A. thaliana* gene encoding pyridoxal phosphate phosphatase (3.1.3.74) dephosphorylates pyridoxal 5'-phosphate to pyridoxal and this gene was down-regulated in infected tissue at 16 DPI (data not shown) and 26 DPI (Figure 3.13). Moreover, the gene encoding pyridoxal kinase (2.7.1.35), and associated with the salvage pathway of vitamin B6, was not found to be significantly different between uninfected and infected tissue (Figure 3.13).

The *P. brassicae* genome lacks of genes associated with thiamine biosynthesis. It has been suggested that *P. brassicae* depends on its host for this vitamin (Schwelm et al., 2015). Other biotrophic pathogens such as oomycete white rust pathogens have lost most of the genes associated with cofactor and vitamin biosynthetic pathway including thiamine and molybdopterin (Kemen et al., 2011, Garnica et al., 2013). Meanwhile, this pathogen genome contains cofactor transporter genes such as nicotinic acid transporter which indicates that pathogen obtains this essential cofactor from the host (Garnica et al., 2013). The loss of genes associated with the cofactor and vitamin biosynthetic pathway is a signature of the biotrophic lifestyle (Kemen et al., 2011, Schwelm et al., 2015). It has been suggested that biotrophic pathogens have evolved to synthesise from less energy-consuming source of metabolites such as nitrogen and sulfate rather than vitamins which is more energy-consuming (Kemen et al., 2011).

In addition, I assume that vitamin B6 is also required to protect the plant cell, including plasmodia, from molecular damage caused by ROS that were stimulated by the plant defence response. This contrasts with the activity of antioxidants in cells infected by *Pseudomonas syringae* and *Botrytis cinerea* (Denslow et al., 2005, Zhang et al., 2014). In those cases, antioxidant activity decreases in infected cells subsequently causes cell death, indicating that the presence of ROS is required in

plant cells to ward off *P. syringae* (Denslow et al., 2005). At the same time, antioxidant activity is required in the region not affected by the pathogen in order to keep ROS at a low level and subsequently reduce the macromolecular damage (Denslow et al., 2005). In addition, the gene involved in vitamin B6 biosynthesis has been shown to be induced in tomato leaves infected with *B. cinerea*. Deleting this gene causes an increase in disease severity. This indicates that antioxidant activity is required in plant defence against *B. cinerea* (Zhang et al., 2014).

Tetrahydrofolates (THF) for folate biosynthesis play a role as a cofactor in one-carbon reactions. The structure of THF consists of a pterin branch, *p*-aminobenzoate branch and an amino acid glutamate (Basset et al., 2005). The pterin branch is derived from Guanosine 5'-triphosphate through five steps of GTP cyclohydrolase (3.5.4.16) activity to release 7,8-Dihydroneopterin 3'-triphosphate. Following *P. brassicae* infection, formamidopyrimidine nucleoside triphosphate, an intermediate compound in the synthesis of 7,8-Dihydroneopterin 3'-triphosphate, decreased at 16 DPI. 7,8-Dihydroneopterin, however, a compound derived from 7,8-dihydroneopterin 3'-triphosphate, was found to have increased in infected tissue at 16 DPI (Figure 3.14). Although formamidopyrimidine nucleoside triphosphate increased, the other intermediate compounds needed to synthesise 7,8-Dihydroneopterin 3'-triphosphate decreased in infected tissue at 25 DPI (Figure 3.15). Expression of the *A. thaliana* gene encoding GTP cyclohydrolase (3.5.4.16) was down regulated at 26 DPI in infected hypocotyl tissue (Figure 3.15), indicating that the synthesis of the pterin branch for THF component was reduced. A second step in the synthesis of THF was the formation of a *p*-aminobenzoate branch, derived from chorismate. Following *P. brassicae* infection, 4-aminobenzoate increased at 21, 25, and 28 DPI in infected tissue (Figure 3.12, 3.15), indicating that the production of the second THF branch was increased.

The last step in the synthesis of THF is to couple the pterin branch and *p*-aminobenzoate branch by dihydrofolate synthase and folylpolyglutamate synthase



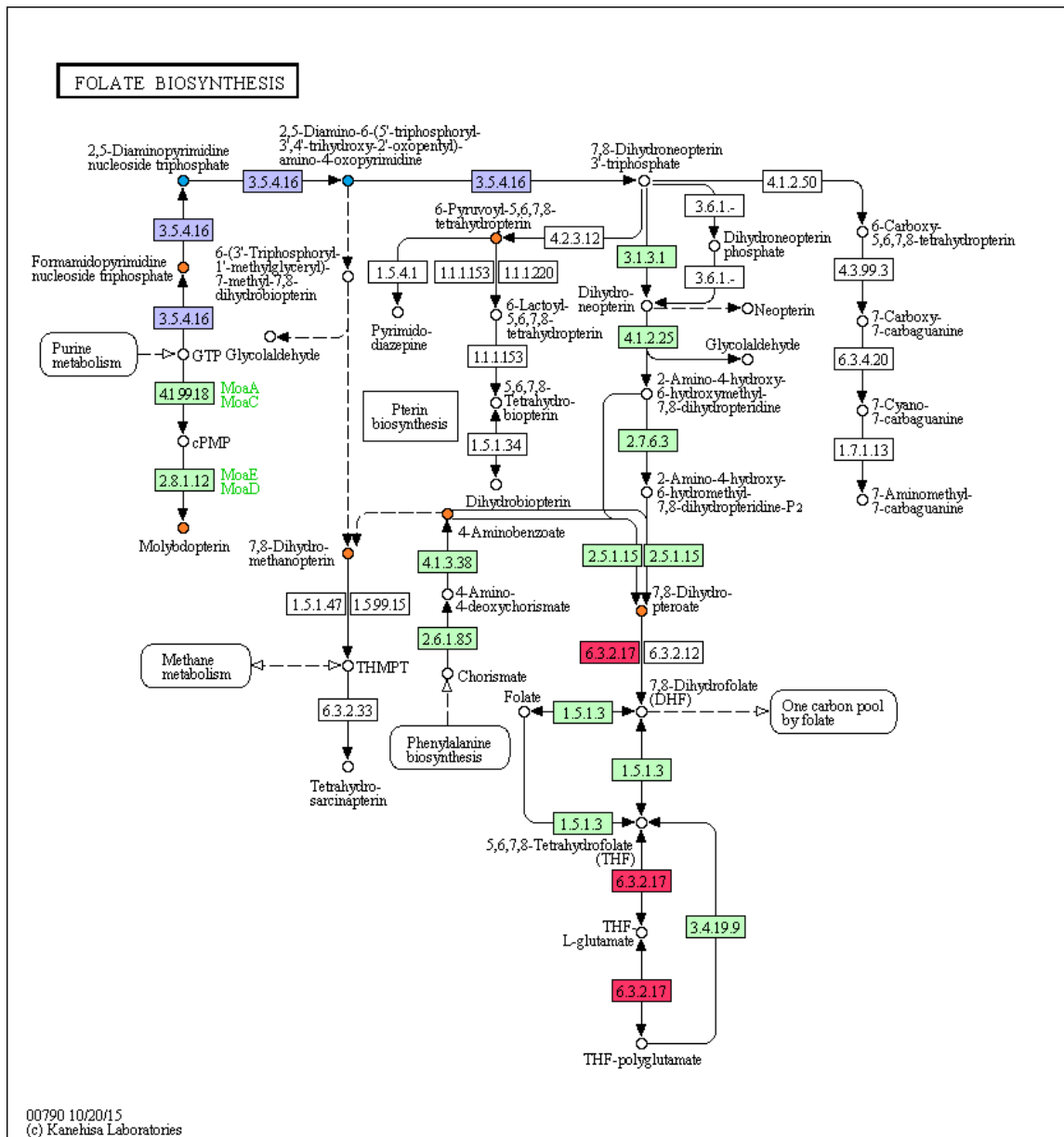


**Figure 3.15.** The expression of genes involved in folate biosynthesis in *P. brassicae*-infected tissue at 26 DPI. Light blue boxes show down-regulated gene expression ( $\log_2$  fold-change  $\leq -1$ ,  $p \leq 0.05$ ), red boxes show up-regulated gene expression ( $\log_2$  FC  $\geq 1$ ,  $p \leq 0.05$ ), green boxes show genes that do not show a significant change in expression between uninfected and infected tissue. White boxes show genes that have not been identified in *A. thaliana*. Blue circles show potentially decreased metabolites and orange circles show potentially increased metabolites in *P. brassicae*-infected tissue ( $p$ -value  $\leq 0.05$ ).

(Basset et al., 2005). Following *P. brassicae* infection, the expression of the *A. thaliana* gene encoding polypolyglutamate synthase (6.3.2.17) was up-regulated at 16 (Figure 3.14) and 26 DPI, which is accompanied by an accumulation of 7, 8-Dihydropteroate at 25 DPI in infected tissue (Figure 3.15). It has been reported that the folate precursor, 7,8-dihydropterate, increased in *A. thaliana* plants in response to the effector protein of *P. syringae* (Wittek et al., 2015). It has also been shown that the application of 7,8-dihydroneopterin to *A. thaliana* plants could increase plant resistance against *P. syringae* through activation of a gene associated with salicylic acid (SA). In contrast, 7,8-dihydroneopterin served to increase the susceptibility of *A. thaliana* against the necrotrophic fungus *Alternaria brassicicola* through suppression of Jasmonic acid-mediated response (Wittek et al., 2015).

Following *P. brassicae* infection, SA, which is synthesised in infected plants, is suppressed by *P. brassicae* methyltransferase (PbBSMT) (Ludwig-Muller et al., 2015). This gene methylates host SA to suppress plant defence response (Lovelock et al., 2013, Ludwig-Muller et al., 2015). Moreover, it was shown that, application of *p*-aminobenzoate on pepper plants could induce plant defence against *Cucumber mosaic virus* and *Xanthomonas axonopodis* through the synthesis of THF (Song et al., 2013). This indicates that, although accumulation of 7, 8-Dihydropteroate and 4-aminobenzoate compounds at late stages of infection are related to activating the plant's defence response, it is not sufficiently effective to stop *P. brassicae* colonization.

### **3.3.6 Alteration of Terpenoids, Polyketides and other Secondary Metabolites in *P. brassicae*-Infected Plants**

A comparison of the signal intensities associated with terpenoids, polyketides and other secondary metabolites is shown as a heat map (Figure S5). Specific putative metabolites associated with this category whose concentration altered at 7, 16, and 25 DPI in response to *P. brassicae* infection are shown in Table S5 of the Appendix. The changes in terpenoids, polyketides and other secondary metabolites with a

combination of gene expression at 16 and 26 DPI in infected tissue occurs via biosynthesis of carotenoids, glucosinolates, phenylpropanoid and zeatin. Whilst, the changes in gene expression associated with brassinosteroid biosynthesis only occur at 26 DPI in infected tissue.

The plant surface is equipped with pattern recognition receptors (PRRs) to perform the plant's first layer of defence. PRRs probably detect pathogen-associated molecular patterns (PAMPs) and could potentially activate PAMP-triggered immunity (PTI). Plant PAMPs detect cell wall damage and trigger plant defence through activation of ROS and secretion of antimicrobial compounds such as glucosinolate and cinnamic acid. Specifically, cinnamic acid for biosynthesis of phenylpropanoids increased at the onset of gall formation and decreased during late gall formation (Figure 3.16). Cinnamic acid is derived from amino acid phenylalanine by the activity of phenylalanine ammonia-lyase (*PAL*), which removes the nitrogenous group of phenylalanine. As cinnamic acid accumulated at 16 DPI, *A. thaliana PAL* gene (4.3.1.24) expression was up-regulated (S6 of the Appendix). As cinnamic acid decreased in infected tissue at 25 DPI, meanwhile, the *A. thaliana PAL* gene was down-regulated at 26 DPI (Figure S7 of the Appendix).

Cinnamic acid has antimicrobial activity, which suggests that *A. thaliana* plants activate its defence response at 16 DPI, when this compound accumulates in infected tissue. Accumulation of cinnamic acid has been reported in pea plants, acting against the soft rot pathogen *Sclerotinia sclerotiorum*, and *Musa acuminata* roots infected with *Fusarium oxysporum*, in each case positively correlated with the up-regulation of the *PAL* gene (Jain et al., 2012, 2015, De Ascensao and Dubery, 2003). The high accumulation of the phenylpropanoid compounds and its derivatives, including cinnamic acid and *p*-coumaric acid, which have antimicrobial and antioxidant activities resulted in infected plants that exhibited fewer or no disease symptoms (Jain et al., 2015, Dixon and Paiva, 1995). These reports are

consistent with my finding that cinnamic acid decreased in infected tissue, which may correlate with the formation of galls in *P. brassicae*-infected plants.

Moreover, phaseic acid for carotenoid biosynthesis, derived from the degradation of abscisic acid (ABA), increased at the onset of gall formation and decreased during late gall formation (Figure 3.16). As phaseic acid increased, the *A. thaliana* gene that encodes ABA-beta-D-glucosidase (3.2.1.175) to hydrolyse Abscisic acid glucose ester to form ABA, was up-regulated at 16 DPI (Figure S8 of the Appendix section). As phaseic acid decreased, however, this gene (3.2.1.175) was down-regulated in gall tissue (Figure S9, of the Appendix section). It has been reported that ABA plays a major role in the susceptibility of tomato against *Botrytis cinerea* through repression of *PAL* activity, which subsequently reduced SA-defence pathways (Audenaert et al., 2002). As previously mentioned, the expression of the *PAL* gene was up-regulated at 16 DPI, which is associated with the accumulation of cinnamic acid and phaseic acid. From this result, firstly I assume that the accumulation of phaseic acids at 16 DPI is correlated with the inactivation of ABA in *P. brassicae*-infected plants to increase the expression of the *PAL* gene, which subsequently triggers SA-dependent pathways. Maybe this was achieved by ABA being actively converted to unstable 8'-hydroxy-ABA, which subsequently rearranges to phaseic acid. In the meantime, SA could be suppressed by *P. brassicae* effector PbBSMT to inactive to the role of SA in plant defence (Ludwig-Muller et al., 2015). However, it has been reported that ABA content was four times higher in *P. brassicae*-infected root of Chinese cabbage plants than uninfected plants at 21 DPI (Devos et al., 2005). It was not correlated with the down-regulation of *PAL* gene at 26 DPI which found in the transcriptomic data of this study.

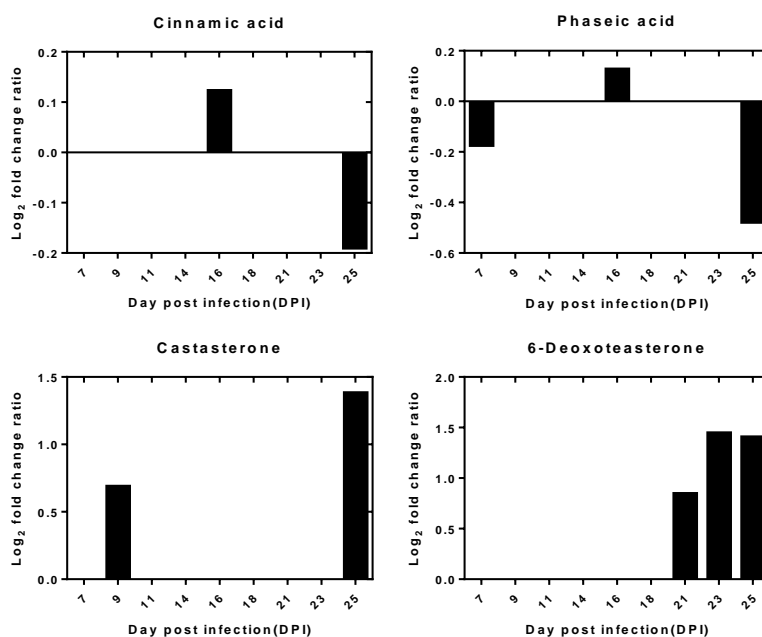


**Figure 3.16.** Fold-change of the differential intensity of cinnamic acid for phenylpropanoids biosynthesis, phaseic acid for carotenoid biosynthesis, castasterone and 6-deoxoteasterone for brassinosteroid biosynthesis during *P. brassicae* infection at 7 to 28 DPI (p-value  $\leq 0.05$ ).

Furthermore, castasterone and 6-deoxoteasterone for brassinosteroid biosynthesis increased in infected tissue (Figure 3.16). The accumulation of these compounds at 25 DPI was integrated with the expression of *A. thaliana* genes at 26 DPI in infected tissue (Figure 3.17). Generally, most of the genes associated with brassinosteroid biosynthesis lead to the synthesis of brassinolide, the most biologically active brassinosteroid, which were up-regulated in infected tissue at 26 DPI (Figure 3.17). The brassinolide was synthesised from steroid biosynthesis through campestanol to castasterone. The accumulation of castasterone and 6-deoxotesterone is in line with the up-regulation of the expression of *A. thaliana* genes associated with this pathway, indicating biologically active brassinosteroid is required in *P. brassicae*-infected plants. This result agrees with the previous finding of transcriptomic analysis in a cell type-specific manner that showed gene expression associated with brassinosteroid synthesis was up-regulated in hypertrophied cells containing large plasmodia (Schuller et al., 2014). This was supported by the observation that the



as proline protect the plant from osmotic and oxidative stress. Meanwhile, compounds associate with plant defence such as cinnamic acid and phaseic acid accumulated at 16 DPI and decreased at 26 DPI indicating the suppression of plant defence when pathogen colonization was successful. The accumulation of vitamin B6 precursor and compounds associated with folate biosynthesis were accompanied with an increase in host gene expression associated with the synthesis of these metabolites. However, the accumulation of certain metabolites such as thiosulfate was accompanied with a decrease of genes expression associated with the degradation of this compound. This suggests that *P. brassicae* has potential to suppress the expression of host metabolism genes in order to obtain favourable nutrient from the hosts.

## Chapter 4. Carbohydrate Metabolism in *P. brassicae*-infected Plants

### 4.1 Introduction

The main symptom of clubroot disease is the formation of galls on the roots and hypocotyls of infected plants (Mithen and Magrath, 1992). In *P. brassicae*-infected plants, both systemic and local effects occur at different points during the infection cycle. Although the precise timing within different species, generally, the pattern of infection is similar. Infection by *P. brassicae* of host plants consists of three phases; an early stage before symptoms are visible; the onset of gall formation (which in *Arabidopsis* normally starts at 14 days after inoculation (DPI)); and gall development at late stages of infection occurring at 26 or 28 DPI, when spores are formed (Mithen and Magrath, 1992).

In Chinese cabbage plants, leaf growth and lateral root development increase during early infection up to 9 DPI, indicating growth stimulation in response to *P. brassicae* infection (Devos et al., 2005, Macfarlane and Last, 1959). By 14 DAI, galls are apparent as a swelling in the upper root system of Chinese cabbage plants (Devos et al., 2005). By 20 DPI, galls form in the infected root of Chinese cabbage plants (Devos et al., 2005). In *A. thaliana*, lateral root formation is decreased at onset and later stages (Siemens et al., 2011). Galls only form in the hypocotyl of *A. thaliana* plants. Elsewhere, galls are restricted to the upper part of the root system (Siemens et al., 2006). At the onset of gall formation, infected plants show an inhibition of xylogenesis and stimulation of cell division and cell expansion in the vascular cambium of infected tissues (Malinowski et al., 2012). At later stages, when spores are formed, a large gall develops through massive cell expansion in hypocotyl tissues. Gall development causes the disruption of water relations due to the repression of xylogenesis, which leads to wilting and stunting on the upper part of *A. thaliana* plants and eventually death (Malinowski et al., 2012). In addition, small extra leaves develop around the hypocotyl region (Devos et al., 2006, Evans and Scholes, 1996). A reduction in lateral root formation and delayed flowering (Siemens et al.,

2011, Dixon, 2009, Mithen and Magrath, 1992) have a major impact on infected plants through altering sink-source relationships. Through the development of a strong sink, the gall influences the development of other sinks within the plant.

Following *P. brassicae* infection, the gall becomes a strong sink for carbohydrate (Evans and Scholes, 1996, Williams et al., 1968, Keen and Williams, 1969). The sink strength of the gall is dependent on alterations in both host and pathogen metabolism. The pathogen, which acts as a sink, takes up carbohydrates and metabolizes these compounds. It may also modify the expression of host genes to increase sink strength, which subsequently reduces the plant growth above ground.

#### **4.1.1 Carbohydrate Metabolism in Plasmodia and Host**

Resting spores of *P. brassicae* contain trehalose (Schwelm et al., 2015). During germination the pathogen expresses trehalase to degrade trehalose providing glucose for growth (Schwelm et al., 2015). Plasmodia synthesise trehalose during gall formation (Brodmann et al., 2002). This provides the energy source for spores but the host generates a concentration gradient of carbohydrate into the plasmodia. However, there is a lack of knowledge about how carbohydrates enter the pathogen.

Trehalose is synthesised through two enzyme reactions. First, UDP-glucose and glucose-6 phosphate is converted into trehalose-6-phosphate by trehalose phosphate synthase (TPS). Then, trehalose-6-phosphate is converted into trehalose by trehalose phosphate phosphatase (TPP) activity (Fernandez et al., 2010). Normally, the trehalose concentration in *Arabidopsis* is extremely low. Besides, the *P. brassicae* genome contains the trehalose biosynthesis genes TPS, TPP and trehalase, which indicates that in clubroot-infected plants, trehalose is synthesized by plasmodia (Brodmann et al., 2002, Schwelm et al., 2015). In the root and hypocotyl of clubroot-infected plants, the host trehalase activity is induced before the accumulation of trehalose (Brodmann et al., 2002, Keen and Williams, 1969). It is thought that the induction of host trehalase is regulated by auxin as part of plant

defence and it is not induced by its substrate (Brodmann et al., 2002). The accumulation of trehalose by the pathogen could interfere with the regulation of carbon metabolism inside the host by converting carbon sources from the host into trehalose and creating a carbon sink. Besides, trehalose biosynthesis could interfere with the sugar sensing system of the plant through the accumulation of trehalose-6-phosphate (Schluepmann et al., 2003, Schluepmann et al., 2004). Trehalose-6-phosphate acts as a signal molecule for plant growth and development. For instance, the accumulation of trehalose in plant tissues inhibits TPP activity, which leads to the accumulation of trehalose-6-phosphate that reduces the growth of *A. thaliana* seedlings (Schluepmann et al., 2003, Schluepmann et al., 2004). This suggests that pathogen derived trehalose inhibits host TPP leading to accumulation of host derived trehalose-6-phosphate and affects the growth. Maybe induction of host trehalose by over-expressing TPP would be less affected than in response to *P. brassicae* infection. This would have been interesting to test.

In clubroot infected plants, soluble sugar and starch accumulate in the root and hypocotyl tissues (Williams et al., 1968, Keen and Williams, 1969, Evans and Scholes, 1996, Wagner et al., 2012). Accumulation of sugars in developing galls induces a hypoxia response and consequently triggers anaerobic respiration (Jubault et al., 2013). In addition, the bulk density of gall formation, which limits the oxygen uptake by root systems, also causes hypoxia and anaerobic respiration. In *A. thaliana* plants susceptible to *P. brassicae* infection, the expression of genes associated with anaerobic respiration, which leads to ethanol fermentation, increases with gall formation (Jubault et al., 2013).

#### **4.1.2. Sucrolytic Enzymes in Host Plants**

Carbohydrate metabolism is a complex process, which involves multiple enzymes in source and sink tissues. The utilisation of sucrose requires the presence of sucrolytic enzymes and transporters that facilitate the movement of sucrose or hexose sugars (Roitsch, 1999). In host plants, sucrolytic enzymes are located in different subcellular

compartments. Invertases are located in the cell wall (CWINV), vacuole (VINV) and cytoplasm (CINV) whilst sucrose synthase (SUS) is located in the cytoplasm. Previously, clubroot disease studies are focused on the role of CWINV as a requirement for the apoplastic unloading of sucrose into the developing galls. Whilst CWINV is known to be important in apoplastic loading of sucrose into some sink tissue (e.g. maize seed filling, (Li et al., 2013)), its role in gall formation remains unclear. Expression of a cell wall invertase inhibitor driven by a root-specific promoter reduces gall formation in the roots of *P. brassicae* infected plants (Siemens et al., 2011) although gall development in infected hypocotyls does not change, presumably due to the use of a root specific promoter. Quilliam (Thesis, 2006) reported that the majority of CWINV activity in *Arabidopsis* results from *CWINV1* expression. This gene is responsible for all stress-induced invertase activity. Nonetheless, inactivation of *CWINV1* does not affect gall development and the expression of *CWINV1* is reduced at the late stage of clubroot infection in this study, contrasting with the data reported by Siemens et al., (2011).

The other sucrolytic enzyme is sucrose synthase. Sucrose synthase catalyses a reversible reaction depending on substrate concentration. In the presence of a high concentration of sucrose, SUS acts as a sucrolytic enzyme to hydrolyse sucrose into UDP-glucose and fructose. *A. thaliana* contains six SUS isoforms, which have similar kinetic properties, but different spatial and temporal expression patterns (Baud et al., 2004, Barratt et al., 2009, Bieniawska et al., 2007). SUS1-4 proteins are found in soluble and membrane fractions of *A. thaliana* plants (Bieniawska et al., 2007), while SUS5 and SUS6 proteins are found mainly in cell wall (insoluble) material from the root, hypocotyl and stems, and are thought to be involved in callose synthesis (Barratt et al., 2009). A knockout of a single isoform of the *SUS* gene (*SUS1*, *SUS2*, *SUS3*, or *SUS4*) did not show obvious growth phenotypes in terms of starch, sugar, cellulose, seed weight and seed composition when compared with wild type (Bieniawska et al., 2007). It is reported that, *sus1,4* double mutants and *sus1,2,3,4* quadruple mutants show similar phenotypes to wild type plants when root tissues of

the plant undergo aerobic respiration, although the growth of these mutants is retarded when root tissues under hypoxia (Barratt et al., 2009, Bieniawska et al., 2007). Sugar accumulates in the leaves of *sus1, 4* double and *sus1,2,3,4* quadruple mutants due to the increase of neutral invertase activity (Bieniawska et al., 2007). This indicates that plant root tissues growing under hypoxic conditions require specific SUS activity. CINV might replace SUS activity in *sus1,2,3,4* quadruple mutants.

#### **4.1.3. Sucrose Transporters in Host Plants**

There are two types of sucrose transporter in plants: active and passive transporters. Active sucrose transporters (SUTs) transport sucrose against a concentration gradient, which requires energy. SUTs transport sucrose during phloem loading in leaves and phloem unloading in other parts of the plant including root tissue (Doidy et al., 2012). Passive transporters (SWEETs) transport sugar down a concentration gradient (Chen et al., 2010). Rates of photosynthesis in leaves of *P. brassicae*-infected plants are not different to those in uninfected plants, but carbohydrate content is low due to the export of carbohydrate from the leaves to the developing gall (Evans and Scholes, 1996).

During phloem loading, sucrose in mesophyll cells is transported through plasmodesmata into parenchyma cells and further to sieve element-companion cell (SE-CC) complexes (Doidy et al., 2012). Sucrose concentration in mesophyll cells is between 1 and 2 mM, while sucrose concentration in the SE-CC complex is 0.2 M, which is 100 times higher than in source tissue. Presumably, sucrose in parenchyma cells is transported into the apoplastic space between parenchyma cells and companion cells by SWEET transporters. The SWEET transporters, which are located on the plasma membrane of parenchyma cells, transport out sucrose to apoplastic space along a concentration gradient (Chen et al., 2010, Doidy et al., 2012). Active SUT transporters transport sucrose from the apoplastic space against the concentration gradient into the SE-CC complex.

In clubroot-infected plants, there is a large mass flow of sucrose in transport phloem towards sink tissues (Keen and Williams, 1969). In sink tissues, sucrose is transported out usually through plasmodesmata to the cytoplasm of sink cells along a concentration gradient. In some cases, for instance when sugar in sink tissue is in high demand, sucrose can also be transported out using SUT transporters against a concentration gradient to the apoplastic space between SE and CC (Juergensen et al., 2003). Sucrose in the apoplastic space is hydrolysed by CWINV or transported into the plant's cytosol by SWEET transporters (sugar permease) and hydrolysed by either SUS or CINV. Then, hydrolysed sugars are eventually taken up by plasmodesma inside host cells. Figure 4.1 shows the transporters that are involved in the mass flow of sucrose from source to sink tissues via phloem transport.

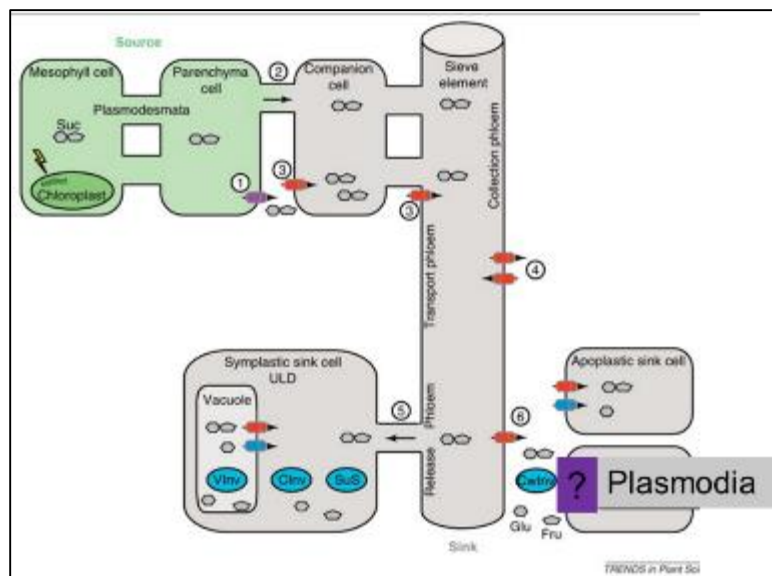


**Figure 4.1** Sugar is transported via the phloem from source to sink organs in plants. Sucrose is synthesized in mesophyll cells of leaves. It is transported to sink tissue by different transporters. 1) SWEET transporter, 2) plasmodesmata, 3) Suc/H<sup>+</sup> symporter, 4) Load and reuptake of sucrose in stems, 5) plasmodesmata to symplastic space and 6) SUT/SUC to apoplastic space. A figure taken from Doidy et al., (2012).

There are 16 members of the SWEET gene family in *A. thaliana* genome (Chen et al., 2010, Chen et al., 2012). Different SWEET genes transport different types of sugar between different types of compartment. For example, SWEET11, SWEET12

and SWEET15 are responsible for transporting sucrose into cells (Chen et al., 2015b, Chen et al., 2010). On the other hand, SWEET1, SWEET2, SWEET4 and SWEET8 are glucose transporters (Chen et al., 2015b, Chen et al., 2010).

SWEET2 is localised on the tonoplast that surrounds the vacuole, which is a major sugar storage compartment (Chen et al., 2015a). Some SWEET genes have redundant functions and inactivation of pairs is required to see a phenotype. For example, Chen et al., (2012) demonstrated that SWEET 11 contains 88% amino acid similarity with SWEET 12. Both of these sucrose transporter proteins are localised in the plasma membrane of phloem parenchyma cells of mature leaves and function in sucrose efflux to sieve element- companion cell (SE-CC) complexes (Chen et al., 2012).

During plant-pathogen interactions, the pathogen often alters sugar efflux at the site of infection for its benefit by regulating different *SWEET* genes, depending on the type of pathogen (Chen et al., 2010). For example, in *A. thaliana* plants, *SWEET 4*, *SWEET 5*, *SWEET 7*, *SWEET 8*, *SWEET 10*, *SWEET 12* and *SWEET 15* are highly induced upon infection with the pathogen *Pseudomonas syringae* pv. tomato, strain DC3000 (Chen et al., 2010). In addition, the *SWEET12* gene is also induced in *A. thaliana* plants infected with the fungal powdery mildew pathogen *Golovinomyces cichoracearum*, whilst *SWEET 4*, *SWEET 15* and *SWEET 17* are differentially regulated in *A. thaliana* inoculated with the necrotroph *Botrytis cinerea* (Chen et al., 2010). In *Vitis vinifera* plants, *VvSWEET4* is induced after inoculating with the necrotroph *B. cinerea*, but this gene is not expressed after inoculating with biotrophic pathogens *Erysiphe necator* or *Plasmopara ulmicola* (Chong et al., 2014). It has been reported that the expression of *SWEET* genes is induced by pathogenic pathogen transcription activator-like (TAL) effectors, which bind to specific promoters of *SWEET* genes (Antony et al., 2010, Chen et al., 2010, Chong et al., 2014, Cohn et al., 2014, Hu et al., 2014, Yang et al., 2006). For instance, expression of the sucrose transporter *MeSWEET10a* in *Manihot esculenta* (the dicot cassava) is induced by

TAL20<sub>xam668</sub> from the causal agent of bacterial blight of cassava, *Xanthomonas axonopodis* pv. *manihotis* (Cohn et al., 2014). In *Oryza sativa* plants infected with rice blight, *OsSWEET 11* is induced by AvrXa7, PthXo2 and PthXo3, while the former and latter effectors are induced by *OsSWEET14* gene expression in leaves upon infection (Antony et al., 2010, Chen et al., 2010, Yang et al., 2006). In addition, *Xanthomonas citri* pv *citri* strain Xcc306 releases the PthA4 effector to induce the expression of the glucose and sucrose transporter *CsSWEET1* in citrus plants (Hu et al., 2014). Recently it has been predicted that *P. brassicae* expresses effectors which are different to the TAL effectors that are specifically expressed by bacteria. The plasmodia effectors show similarities to effector candidates of biotrophic smut fungi in the *Ustilaginomycetes* (Schwelm et al., 2015). However, the target host genes of this effector and its function in inducing or repressing the host metabolism, development or defence remains unknown.

Furthermore, the sugar transporter genes are also differently regulated depending upon the source of carbon required by different types of pathogen. Wheat powdery mildew, *Blumeria graminis* sp *tritici* takes up glucose as a main carbon source from wheat (*Triticum aestivum* L.) leaves (Sutton et al., 2007, Sutton et al., 1999). In *A. thaliana* plants, a high concentration of glucose, which is linked to powdery mildew fungus infection, induces the expression of the glucose transporter STP4 and cell wall invertase activity in infected mature leaves (Fotopoulos et al., 2003, Sutton et al., 2007). In contrast, the corn smut fungus *Ustilago maydis* directly takes up sucrose from its host *Zea mays* through the plasma membrane-localized active sucrose transporter SRT1, an energy dependent H<sup>+</sup>-symporter (Wahl et al., 2010). However, there is a lack of knowledge on the source of carbon required by plasmodia.

#### **4.1.4 Aims and Objectives**

The work presented in this chapter was carried out to understand carbohydrate metabolism in *P. brassicae*-infected plants, using *A. thaliana* as a host. First, we

analysed the expression of host genes involved in sucrose hydrolysis and sucrose transporters, using transcriptomic data obtained from a previous study. The transcriptomic data were used to create specific hypotheses. The hypotheses were then tested using mutants and transgenic *A. thaliana* plants. The response of mutant and transgenic plant development, specifically in hypocotyl cellular structure was then examined and compared with Col-0 plants and their respective uninfected plants. Further to this, it was investigated whether carbohydrate metabolism in leaves and galls was changed in selected mutants during *P. brassicae* infection.

**Aims:**

1. To examine the impact of alterations in host genes associated with sucrolytic activity on disease development and carbohydrate metabolism.
2. To examine the role of selected host SWEET sugar transporters in disease development and carbohydrate metabolism.

**Objectives:**

1. To examine host transcriptome data to identify the sucrolytic and sucrose transporter genes that are expressed in infected tissues.
2. To examine the impact of mutations in host cytosolic invertase (*cinv1*, 2) genes and sucrose synthase (*sus1*, 2, 3, 4) genes on disease development.
3. To examine the spatial pattern of gene expression associated with sugar permeases (SWEETs) during disease development.
4. To examine the impact of mutations in sugar permeases (*sweet11*, *sweet12* and *sweet11,12*) on disease development.
5. To examine the impact on the carbohydrate metabolism of the leaves and galls in selected mutants.

## **4.2 Materials and Methods**

### **4.2.1 Plant Material and Growth Condition**

Seeds of *sus1,2,3,4* and *cinv1,2* mutants were acquired from Alison M. Smith (John Innes Centre, Norwich NR4 7UH, United Kingdom), and AtSWEET11:AtSWEET11-GUS, AtSWEET12:AtSWEET12-GUS, *atsweet11* (*Salk\_073269*), *atsweet12* (*Salk\_031696*) and *atsweet11,12* seeds were acquired from Li-Qing Chen (Carnegie Institution for Science, CA94305, USA) (Bieniawska et al., 2007, Barratt et al., 2009, Chen et al., 2010). All plants were grown and infected as described previously in Section 2.2.3.

Photographs were taken of the shoot and root/hypocotyl of wild type, *sus1,2,3,4* and *cinv1,2* plants with a Canon EOS 300D digital camera (Canon, Japan) at 16 and 26 DPI.

### **4.2.2 Technovit Sectioning of Hypocotyl Samples and Measurement of *A. thaliana* Hypocotyl Width**

Hypocotyl tissues of Col-0, *sus1,2,3,4*, *cinv1,2*, *sweet11*, *sweet12* and *sweet11,12* were harvested from plants at 16 and 26 DPI. These tissues were sectioned as described in Section 2.2.4, except the microscope slides used in this section were stained with a drop of 0.1 % (w/v) methylene blue (3:10, 2g methylene blue in 100ml of 95% alcohol: deionized water), with 2 drops of 10% potassium hydroxide (KOH). Hypocotyl widths from three sections of each biological replicate were measured by using Image J (<http://imagej.nih.gov/ij/>).

### **4.2.3 GUS Histochemical Analysis**

Mature leaf, developing leaf, a 3 mm section of hypocotyl and root tissue samples at 16 and 26 DPI of three biological replicates (plants) per treatment were pre-treated with 90% (v/v) ice-cold acetone for 5 minutes. The solution was replaced with 1x GUS assay buffer (100mM Na-phosphate buffer pH7, 5 mM potassium ferricyanide, 5 mM potassium ferrocyanide and 10 mM EDTA). Then, 1x GUS assay buffer was

replaced with 1x GUS assay buffer containing 1 mg/ml 5-Bromo-4-chloro-3-indolyl  $\beta$ -D-glucuronide), infiltrated for 20 minutes and incubated overnight at room temperature in the dark. The sample was rinsed in distilled water when the signal had fully developed. The water was then replaced with 70% ethanol. Then the samples were incubated for 1-2 hours in the dark. After 1-2 hours, 70% ethanol was replaced with 100% ethanol for microscopic observations and images taken using a Leica epifluorescence stereomicroscope.

Hypocotyl tissues of *A. thaliana* SWEET11:SWEET11-GUS and SWEET12:SWEET12 - GUS were sectioned as described previously in Section 2.2.4, except the microscope slides in this section were stained with a drop of 0.05% (w/v) Safranin O solution.

#### **4.2.4 Measurement of Carbohydrate**

##### *Extraction of soluble carbohydrate*

Root/hypocotyl, developing leaf and mature leaf samples from four plants were excised and weighed for the measurement of soluble carbohydrate. Weighed samples were placed in 2 ml grinder tubes (Eppendorf), immediately frozen in liquid nitrogen, and stored at -80°C. Soluble carbohydrates were extracted by heating the plant tissue samples at 70°C in 500  $\mu$ L 80% (v/v) ethanol. After 20 minutes, the ethanol was pipetted into a new tube and another extraction performed. The extracts were pooled and dried with a SpeedVac (Sc110) for four to six hours. Dried extracts were re-suspended in 200  $\mu$ L dH<sub>2</sub>O and vortexed. Leaf samples were then treated with a saturated suspension of charcoal (MERCK) decolourizing powder and centrifuged at 12 000 *g* for ten minutes to remove any residual colour.

##### *Enzyme-linked assay of soluble carbohydrates*

The amounts of glucose, fructose and sucrose of four biological and two technical replicates were quantified using an enzyme-linked assay that detects the reduction of NAD<sup>+</sup> or NADH<sup>+</sup> to NADH or NADPH by glucose-6-phosphate dehydrogenase.

The enzyme-linked assay was performed on the extracted samples and standards utilising four enzymes that in a stepwise manner convert the different carbohydrates into 6-phosphogluconate and NADH or NADPH. The reduction of NAD<sup>+</sup> or NADP<sup>+</sup> to NADH or NADPH by G6PDH was measured by monitoring the increase of the following reactions:

(i) Glucose-6-Phosphate Dehydrogenase (G6PDH)

Glucose-6-phosphate + NAD<sup>+</sup> or NADP<sup>+</sup> → 6-phosphogluconate + NADH or NADPH

(ii) Hexokinase (HXK)

Glucose + ATP → glucose-6-phosphate

Fructose + ATP → fructose-6-phosphate

(iii) Phosphoglucose-Isomerase (PGI)

Fructose-6-phosphate → glucose-6-phosphate

(iv) Invertase

Sucrose + H<sub>2</sub>O → glucose + fructose

Ten µL of the samples or ten µL of the mixture of glucose, fructose, and sucrose as a standard in the total volume of 125µL of G6PDH-buffer (100mM HEPES, 5mM MgCl<sub>2</sub>, 1 mM ATP and 0.4 mM NADP<sup>+</sup>) and 2 U G6PDH from yeast (Roche) in a black 96-well microtitre plate (Corning) were used in the enzyme-linked assay. Alternatively, the assay can be performed in a modified G6PDH-buffer (100mM HEPES, 5mM MgCl<sub>2</sub>, 1 mM ATP and 1 mM NAD<sup>+</sup>) and 2 U G6PDH from *Leuconostoc mesenteroides* (Roche). An initial reading was taken of fluorescence at 440 nm using an excitation wavelength of 340 nm in a Fluostar Optima plate reader fluorimeter (BMG LABTECH GmbH, Offenburg, Germany). This allowed any residual glucose-6-phosphate to be catalysed thus providing a 'blank reading'. When the excitation reading had stabilised, 3 U Hexokinase (Roche) was added to each reaction, mixed and incubated for 10 minutes, and the reading was recorded when no further change in absorbance and excitation occurred. This procedure was

followed by the addition of 2 U PGI (Roche) and 85 U Invertase (Sigma). The amount of glucose, fructose, or sucrose equivalents produced by each reaction was calculated relative to the standard curve (this was then subtracted from the following reaction).

#### **4.2.5 Statistical Analysis**

All statistical analysis was carried out using GraphPad Prism software version 6 (GraphPad software, Inc.). Graphs were also produced using GraphPad.

## 4.3 Results

### 4.3.1 Transcriptomic Analysis of Host Carbohydrate Metabolism

Microarray data obtained from Malinowski et al., (2012) (*unpublished data*) was used to examine host gene expression during clubroot infection, specifically in carbohydrate metabolism. This microarray data is from two stages of clubroot gall formation, at the onset (16 DPI) and late (26 DPI), and two types of clubroot-infected plant tissues, hypocotyls and upper roots. The alteration of carbohydrate metabolism following *P. brassicae* infection occurred through changes in the expression of sucrolytic enzymes including sucrose synthase and invertase. In addition, the expression of passive sugar transporters including *SWEET* genes was also altered in response to *P. brassicae* infection.

The expression of sucrose synthase genes involved in the hydrolysis of sucrose into UDP-glucose and fructose was examined (Table 4.1). There are six sucrose synthase genes in *A. thaliana*. Generally, most of the sucrose synthase genes expressed in hypocotyl and upper root tissues were up-regulated in response to *P. brassicae* infection, especially *SUS3* at 16 and 26 DPI. In addition, the average expression levels of *SUS1* and *SUS4* were high when compared with other *SUS* genes. In contrast, the expression of *SUS5* and *SUS6* genes were either slightly repressed or not significantly different between uninfected and infected root and hypocotyl tissues at 16 and 26 DPI (Table 4.1).

There are three types of invertase genes in *A. thaliana*, which are distinguished based on subcellular location and pH optimum. Both vacuolar and cell wall invertase are acidic invertases, whilst cytosolic invertase is a neutral to alkaline invertase. In contrast to sucrose synthase genes, the expression of cytosolic invertase genes was repressed in hypocotyl and upper root tissues of *P. brassicae*-infected at 16 and 26 DPI (Table 4.1). Among the invertase genes of *A. thaliana* plants, only *CWINV1* was up-regulated in hypocotyl and root tissues in response to clubroot infection.

**Table 4.1.** Expression of sucrose synthase (*SUS*), Invertase (*INV*) and *SWEET* genes in clubroot – infected plants at 16 and 26 dpi in hypocotyl and root tissues. Expression values are log<sub>2</sub>-fold-change in infected plants relative to uninfected plants (p value ≤0.05).

		Hypocotyl		Root		Average Expression
		16 dpi	26 dpi	16 dpi	26 dpi	
<b>Sucrose synthase</b>						
<i>SUS1</i>	AT5G20830	0.84	n.s	0.81	0.481	10.24
<i>SUS2</i>	AT5G49190	1.38	0.93	0.89	1.2	4.35
<i>SUS3</i>	AT4G02280	2.29	3.84	2.59	3.56	5.98
<i>SUS4</i>	AT3G43190	0.76	-0.63	1.45	0.601	10.5
<i>SUS5</i>	AT5G37180	-0.66	n.s	-0.87	n.s	5.83
<i>SUS6</i>	AT1G73370	-0.7	-0.6	n.s	n.s	7.41
<b>Cytosolic invertase</b>						
<i>CINV1</i>	AT1G35580	-0.55	-0.68	n.s	-0.91	9.25
<i>CINV2</i>	AT4G09510	-0.89	-1.12	-0.43	-0.79	5.27
<b>Vacuole invertase</b>						
<i>VAC-INV1</i>	AT1G62660	-0.79	-0.69	n.s	-1.62	7.41
<i>VAC-INV2</i>	AT1G12240	-1.09	-2.08	-1.17	-1.98	7.79
<b>Cell wall invertase</b>						
<i>CWINV1</i>	AT3G13790	1.92	n.s	1.41	1.72	8.04
<i>CWINV5</i>	AT3G13784	-3.46	-2.22	-1.53	-1.31	3.75
<b>SWEET transporters</b>						
<b>SWEET gene</b>						
<i>SWEET1</i>	AT1G21460	-2.42	-2.23	-1.43	-2.033	5.02
<i>SWEET2</i>	AT3G14770	n.s	0.827	-0.971	-0.819	6.57
<i>SWEET4</i>	AT3G28007	-1.17	n.s	n.s	n.s	3.47
<i>SWEET11</i>	AT3G48740	n.s	3.81	n.s	3.95	4.55
<i>SWEET12</i>	AT5G23660	n.s	1.02	n.s	0.85	3.18
<i>SWEET13</i>	AT5G50800	-2.17	-1.34	-0.84	-0.71	4.27
<i>SWEET16</i>	AT3G16690	-3.33	-2.88	-1.88	-4.58	6.72
<i>SWEET17</i>	AT4G15920	-1.53	-1.6	-1.48	-1.58	7.68

n.s.=not significant.

Average expression value= total average of log-intensities value of uninfected and infected samples.

Expression of genes with average values ≤3 are not shown in this table.

Biological replicates= three plants in each treatment.

Expression value scale:



As shown in Table 4.1, *SWEET11* and *12* genes were strongly expressed at late gall formation (26 DPI) in the hypocotyl and roots of *P. brassicae*-infected *A. thaliana* plants. The expression of other *SWEET* genes was either repressed or not significantly different between uninfected and infected tissues.

#### **4.3.2. Analysis of the Impact of *P. brassicae* Infection on the Morphology of *A. thaliana* Col-0, *cinv1,2* and *sus1,2,3,4***

It is hypothesised that *SUS* rather than *CINV* is important in infected tissue. To better understand the role of *CINV* and *SUS* following *P. brassicae* infection, *cinv1,2* and *sus1,2,3,4* mutants were used and compared to Col-0 plants. To achieve this, 14 days old Col-0, *cinv1,2* and *sus1,2,3,4* plants were inoculated with *P. brassicae* spores or water. The impact of clubroot infection on the shoot and root/hypocotyl morphologies of wild type Col-0 and two sucrolytic mutants, *cinv1,2* and *sus1,2,3,4*, at 16 and 26 DPI was recorded (Figures 4.2).

Col-0 rosette size was not affected at 16 DPI, but by 26 DPI infected rosettes were smaller than uninfected rosettes (Figure 4.2 A,B). Similar results were seen in *cinv1,2* plants (Figure 4.2 A, B). Uninfected *sus1,2,3,4* plants had smaller rosettes than Col-0 at 16 DPI, but this difference disappeared when infected with *P. brassicae* (Figure 4.2 A). Infected *sus1,2,3,4* plants were bigger than uninfected *sus1,2,3,4* plants and bigger than Col-0 at 26 DPI (Figure 4.2B). The root/hypocotyl morphology at 16 DPI did not differ between uninfected and infected plants with wild type, *cinv1,2* or *sus1,2,3,4* genotypes (data not shown). At 26 DPI a similar degree of gall formation was visible on hypocotyl tissues of infected Col-0, *cinv1,2* and *sus1,2,3,4* plants (Figure 4.2 C).

#### **4.3.3. Microscopic Analysis of the Impact of *P. brassicae* Infection on *A. thaliana* Col-0, *cinv1,2* and *sus1,2,3,4***

To better visualize the impact of clubroot infection at the cellular level, cross sections of hypocotyls from uninfected Col-0, *cinv1,2* and *sus1,2,3,4* plants were taken at 16 and 26 DPI (Figure 4.3). Methylene blue was used to stain the cross sections, with xylem cells staining a light blue, in contrast with other cell types, which stained dark blue. The aim of this work was to understand the developmental changes that occurred following *P. brassicae* infection in Col-0 plants and to compare these changes with those observed in *cinv1,2* and *sus1,2,3,4* plants.

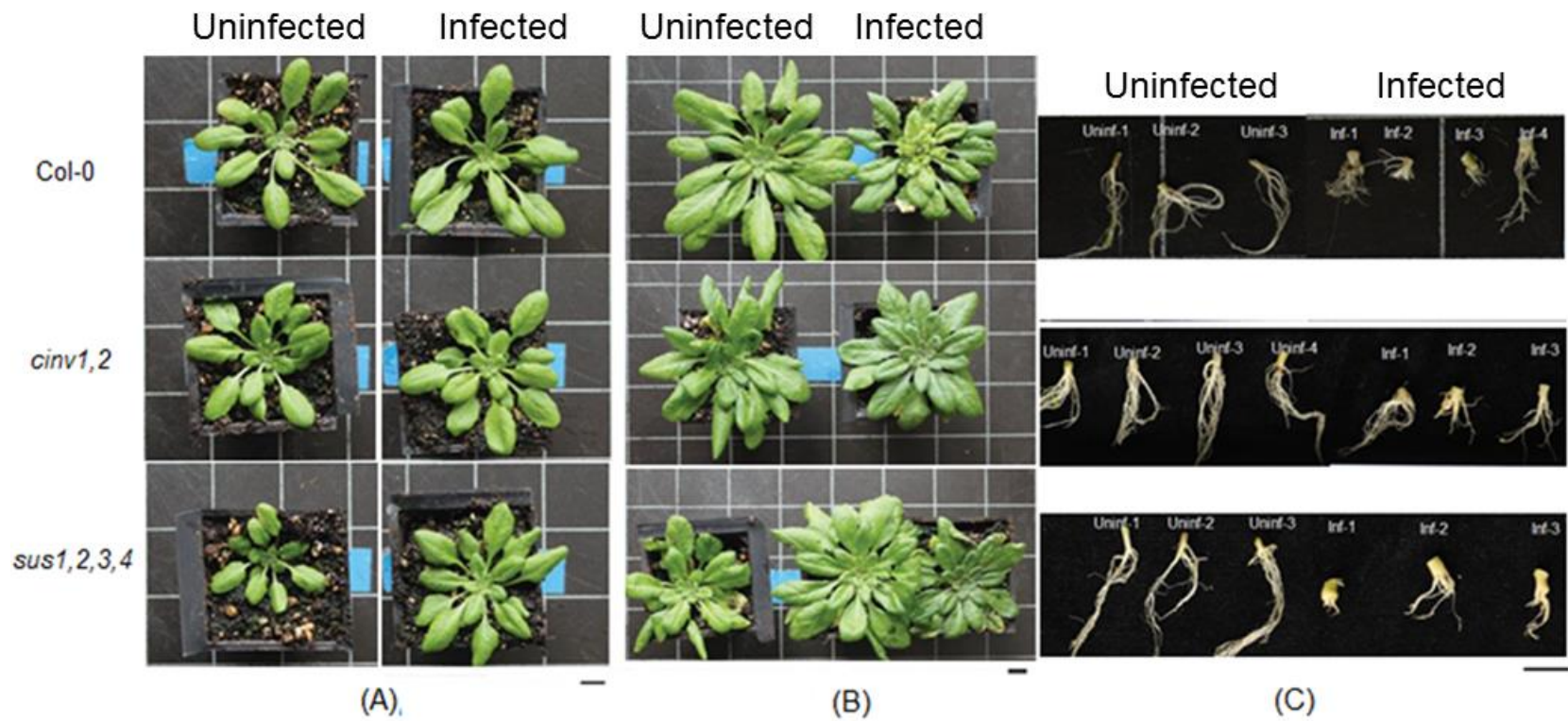


**Figure 4.2** Plant morphology of (A) shoot of 20 day old plants, 16 DPI, (B) shoot of 30 day old plants, 26 DPI and (C) root/hypocotyl of 30 day old plants (26 DPI) grown at  $100 \mu\text{mol m}^{-2} \text{sec}^{-1}$ . Scalebar = 1 cm.

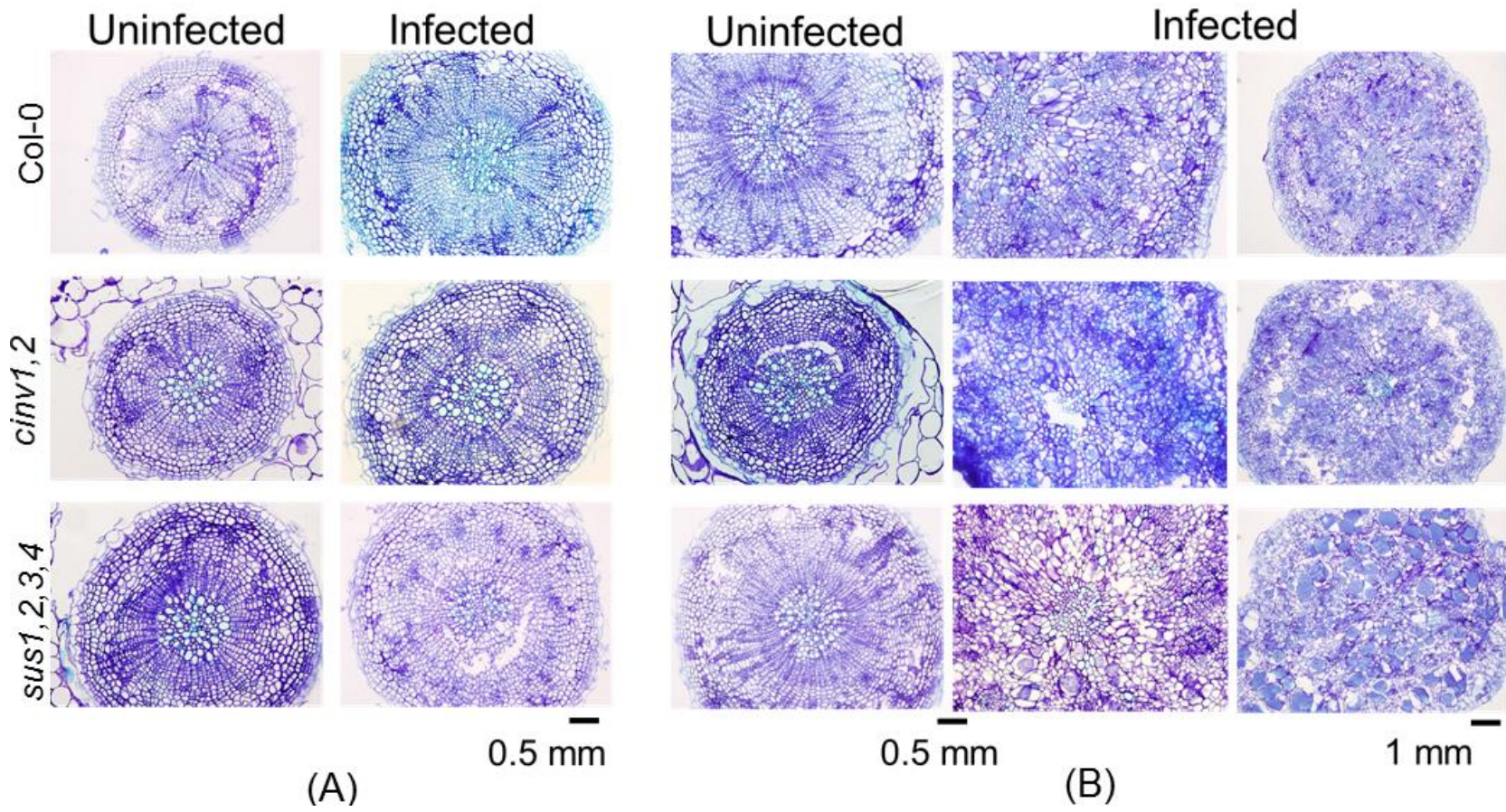


**Figure 4.3.** The effects of deletions in sucrose synthase (*SUS1-4*) genes and cytosolic invertase (*CINV1-2*) genes were visualized in sections of uninfected and *P. brassicae*-infected plants at (A) 16 DPI and (B) 26 DPI.

Secondary hypocotyl thickening of Col-0 plants was not affected at 16 DPI, but by 26 DPI infected hypocotyls were enlarged compared to uninfected tissue (Figure 4.3 A, B). Infected tissues showed the presence of swollen host cells that contained plasmodia (Figure 4.3 B). A similar result was seen in *sus1,2,3,4* plants (Figure 4.3 B). Secondary hypocotyl thickening of *cinv1,2* plants was slower in uninfected tissues than in Col-0 with the presence of epidermis and endodermis cell layers but this difference was not evident when infected (Figure 4.3 A, B). Infected tissues of *cinv1,2* show the presence of swollen host cells containing plasmodia, similar to Col-0 and *sus1,2,3,4*.

To better determine the differences in root/hypocotyl morphologies between Col-0, *cinv1,2* and *sus1,2,3,4* plants, the width of the hypocotyl was measured at 16 and 26 DPI (Figure 4.4).

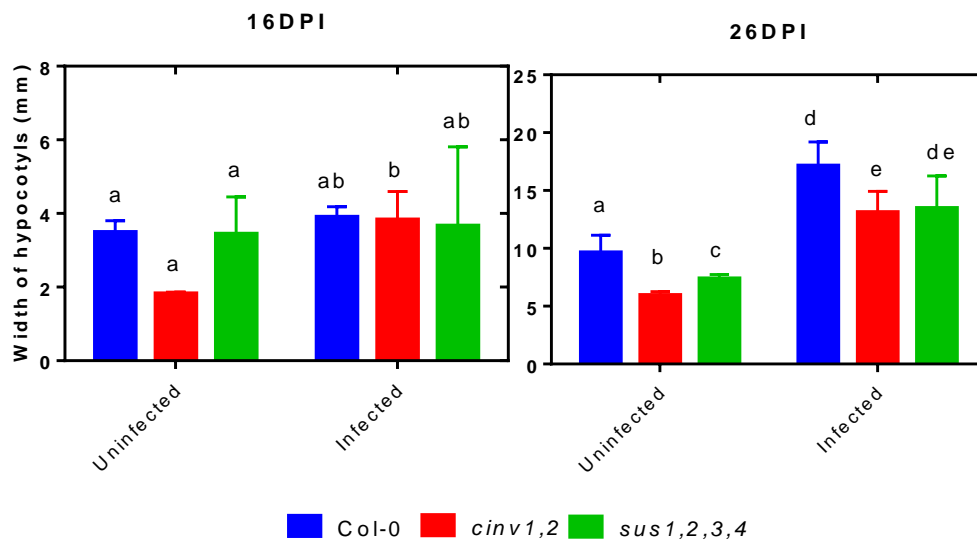


**Figure 4.4.** The width of hypocotyl sections in uninfected and *P. brassicae*-infected Col-0, *cinv1,2* and *sus1,2,3,4* plants at 16 and 26 DPI. Results are the average of four width measurements per replicate plant+ standard deviation (except uninfected, *cinv1, 2* at 16 DPI only two plants were used in the width measurement). Means that do not share a letter differ significantly (Log<sub>10</sub> and two-way ANOVA, p-value≤0.05). The significant test between uninfected and infected plants was based on Sidak's multiple comparison test while between Col-0 and mutants plants was based on Turkey's multiple comparison test.

The Col-0 hypocotyl width was not affected at 16 DPI, but by 26 DPI infected hypocotyls were bigger than uninfected hypocotyls. Similar results were seen in *cinv1,2* and *sus1,2,3,4* plants at 16 DPI. Only two uninfected *cinv1,2* plants at 16

DPI were used in the measurement. By 26 DPI, *cinv1,2* and *sus1,2,3,4* plants showed a smaller hypocotyl width than Col-0 plants when uninfected, but this difference was not evident in *sus1,2,3,4* plants when infected. Infected *cinv1,2* plants were smaller than Col-0 plants at 26 DPI (Figure 4.4).

#### **4.3.4. Analysis of the Impact of *P. brassicae* Infection on the Carbohydrates in the Root/hypocotyl, Developing Leaf and Mature Leaf of *A. thaliana* Col-0, *cinv1,2* and *sus1,2,3,4***

To determine local and systemic effects on carbohydrate metabolism following *P. brassicae* infection, root/hypocotyl, developing leaf and mature leaf samples from Col-0, *cinv1,2* and *sus1,2,3,4* plants were used. The root/hypocotyl and the developing leaf are sink tissues, while the mature leaf is a source which supplies carbohydrate to the whole plant. The root/hypocotyl and the developing leaf may compete with each other to gain carbohydrates from source tissues.

The carbohydrate content of uninfected and infected root/hypocotyl tissue of Col-0, *cinv1,2* and *sus1,2,3,4* plants were compared at 16 and 26 DPI (Figure 4.5). At 16 DPI the glucose and fructose content of infected Col-0 plants increased, but sucrose was not affected. At 26 DPI fructose and sucrose were higher than in uninfected tissue (Figure 4.5). A similar result was seen in *sus1,2,3,4* plants at 16 DPI, but at 26 DPI glucose and fructose were increased, while sucrose was not affected in infected *sus1,2,3,4* plants. Infected *cinv1,2* plants showed an increase in glucose, fructose and sucrose compared with uninfected plants at 16 DPI. By 26 DPI, infected *cinv1,2* plants showed an increase in fructose similar to Col-0, but the sucrose concentration was similar in uninfected and infected *cinv1,2* plants (Figure 4.5).

The carbohydrate content of uninfected and infected developing leaves of Col-0, *cinv1,2* and *sus1,2,3,4* plants was compared at 16 and 26 DPI (Figure 4.6). Glucose, fructose and sucrose in infected Col-0 were not affected at 16 DPI, but by 26 DPI those sugars were higher than in uninfected plants. Similar results were observed with *cinv1,2* and *sus1,2,3,4* plants. At 16 DPI there was little

difference between uninfected and infected plants but at 26 DPI all sugars were higher, although the hexose content tended to be lower than that of infected Col-0 plants (Figure 4.6).

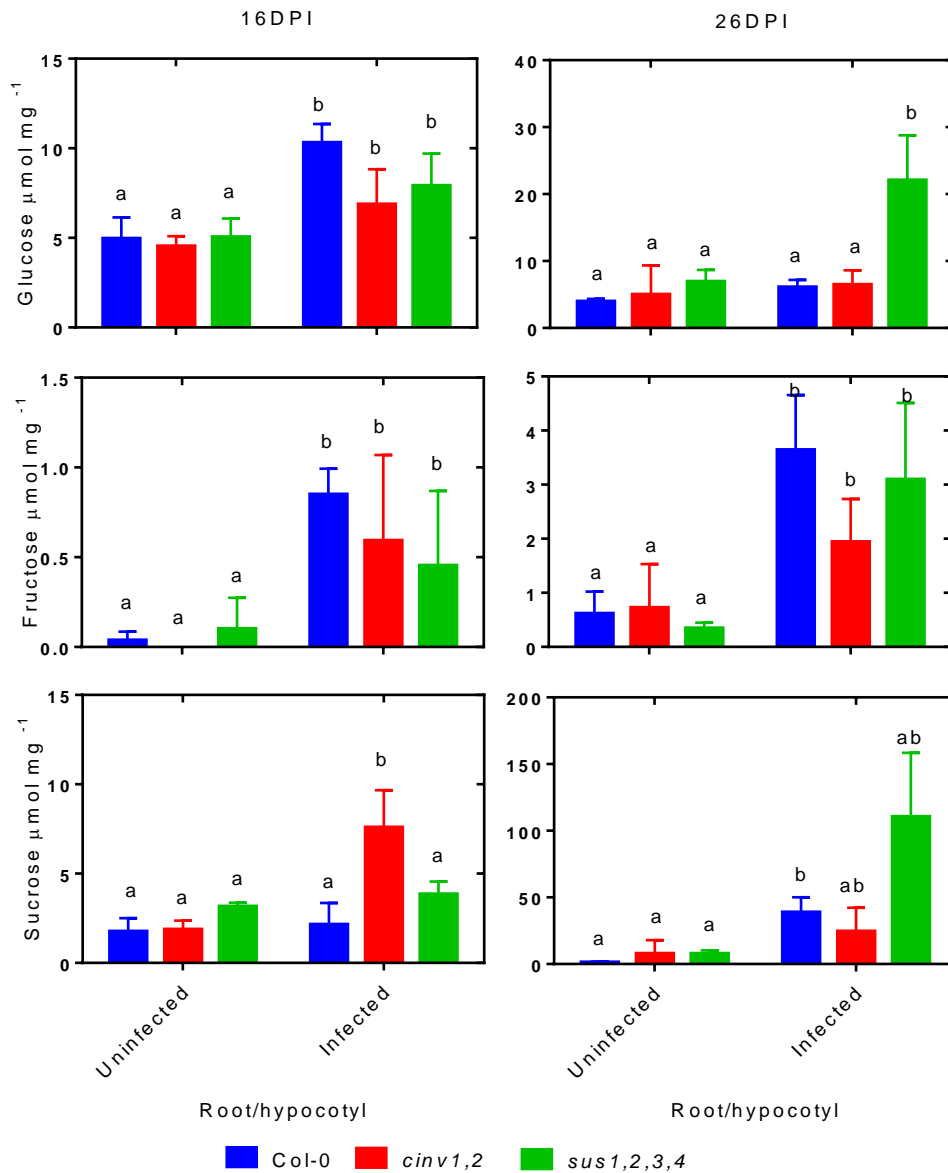


**Figure 4.5.** Amount of sugar in root/hypocotyl of uninfected and infected Col-0, *cinv1,2* and *sus1,2,3,4* plants at 16 and 26 DPI. Results are the average amount of sugar per four replicate plant + standard deviation. Means that do not share a letter differ significantly (Log<sub>10</sub> and two-way ANOVA, p-value ≤ 0.05). The significant test between uninfected and infected plants was based on Sidak's multiple comparison test while between Col-0 and mutants plants was based on Turkey's multiple comparison test.

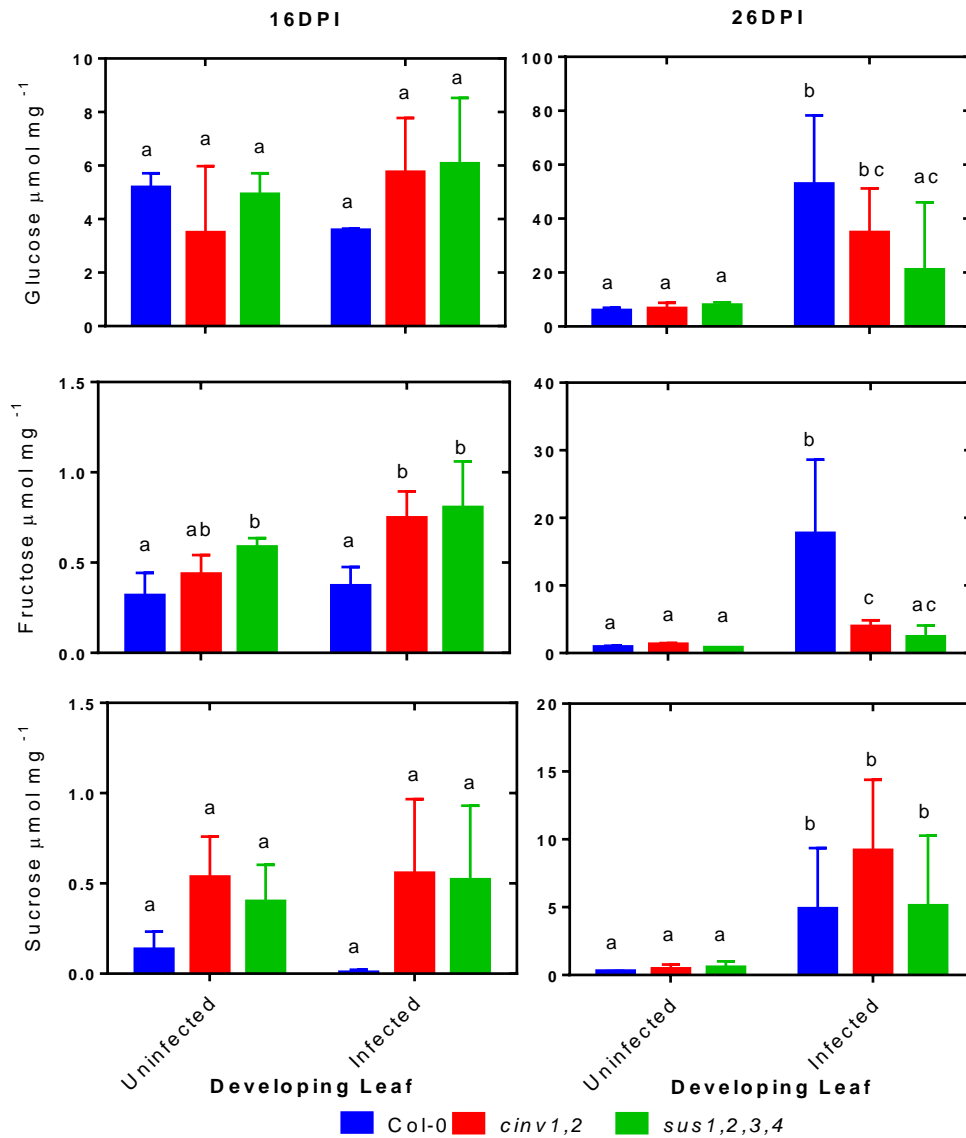


**Figure 4.6.** Amount of sugar in developing leaf of uninfected and infected Col-0, *cinv1,2* and *sus1,2,3,4* plants at 16 and 26 DPI. Results are the average amount of sugar per four replicate plant + standard deviation. Means that do not share a letter differ significantly (Log<sub>10</sub> and two-way ANOVA, p-value ≤ 0.05). The significant test between uninfected and infected plants was based on Sidak's multiple comparison test while between Col-0 and mutants plants was based on Turkey's multiple comparison test.

The carbohydrate content in mature leaves of uninfected and infected Col-0, *cinv1,2* and *sus1,2,3,4* plants was compared at 16 and 26 DPI (Figure 4.7). Again, there was little difference between uninfected and infected Col-0 plants at 16 DPI, but all sugars were higher at 26 DPI. Similar results were seen with *cinv1,2* and *sus1,2,3,4* plants. There was little difference at 16 DPI with elevated sugars at 26 DPI, but somewhat ≤ that seen in Col-0.

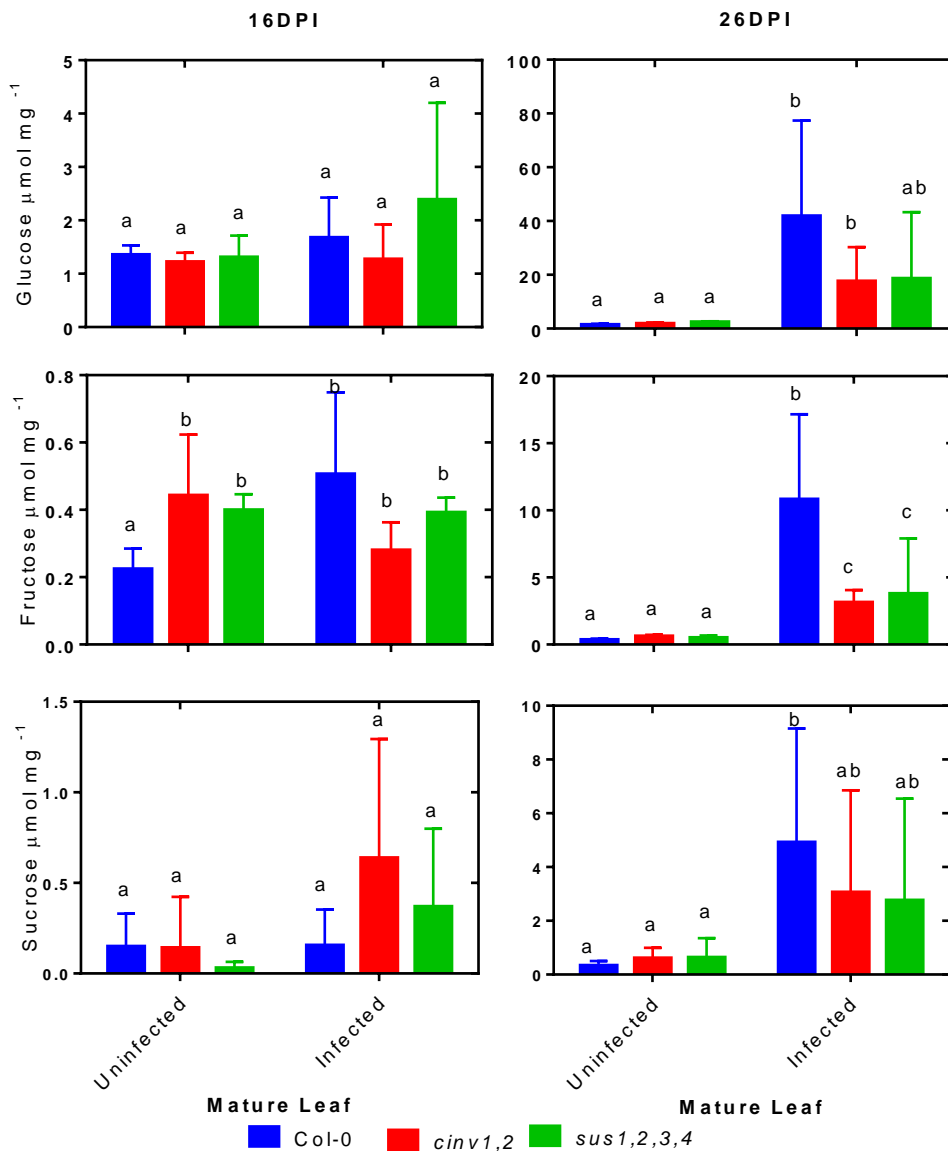


**Figure 4.7.** Amount of sugar in the mature leaf of uninfected and infected Col-0, *cinv1,2* and *sus1,2,3,4* plants at 16 and 26 DPI. Results are the average amount of sugar per four replicate plant + standard deviation. Means that do not share a letter differ significantly (Log<sub>10</sub> and two-way ANOVA, p-value≤0.05). The significant test between uninfected and infected plants was based on Sidak's multiple comparison test while between Col-0 and mutants plants was based on Turkey's multiple comparison test.

#### 4.3.5. Microscopic Analysis of Impact of *P. brassicae* Infection on SWEET11:SWEET11-GUS and SWEET12:SWEET12-GUS

It is hypothesised that *P. brassicae* acts as an effective metabolic sink by altering host carbohydrate metabolism through a localised increase in sugar transporter expression and a modification of carbon partitioning. I also hypothesised that the expression of SWEET11 and SWEET12 are induced by *P. brassicae* effectors to

obtain sugar from the host. *P. brassicae* generates sink strength through gall formation in root/hypocotyl tissues. To better understand how sucrose transporters were altered in response to *P. brassicae* infection, 14-day-old plants that contained SWEET11:SWEET11-GUS and SWEET12:SWEET12-GUS constructs were inoculated with *P. brassicae* spores or water and stained for  $\beta$ -glucuronidase activity at 16 and 26 DPI. SWEET11:SWEET11-GUS and SWEET12:SWEET12-GUS were actively expressed in root, hypocotyl and developing leaf tissues at 16 and 26 DPI in both uninfected and infected plants (Figure 4.8-4.11). However, no expression was observed in mature leaves.

Cross sections of hypocotyls from uninfected and infected *SWEET11:SWEET11-GUS* and *SWEET12:SWEET12-GUS* transgenic plants were taken at 16 and 26 DPI. Safranin-O was used to stain the cross sections, with cells expressing SWEET11:SWEET11-GUS and SWEET12:SWEET12-GUS appearing blue, in contrast with other cells types which stained red (Figure 4.12 - 4.14).

In uninfected plants, at 16 DPI, SWEET11:SWEET11-GUS and SWEET12:SWEET12-GUS were predominantly expressed in continuous rings of vascular parenchyma, phloem bundles, and xylem parenchyma cells in transverse sections of uninfected and infected tissue (Figure 4.12, 4.13). A similar pattern was seen in uninfected plants at 26 DPI.

In infected hypocotyls 26 DPI, the expression pattern of SWEET11:SWEET11-GUS and SWEET12:SWEET12-GUS became unclear because the vascular parenchyma became distorted and discontinuous with the presence of swollen host cells that contained plasmodia (Figure 4.13).

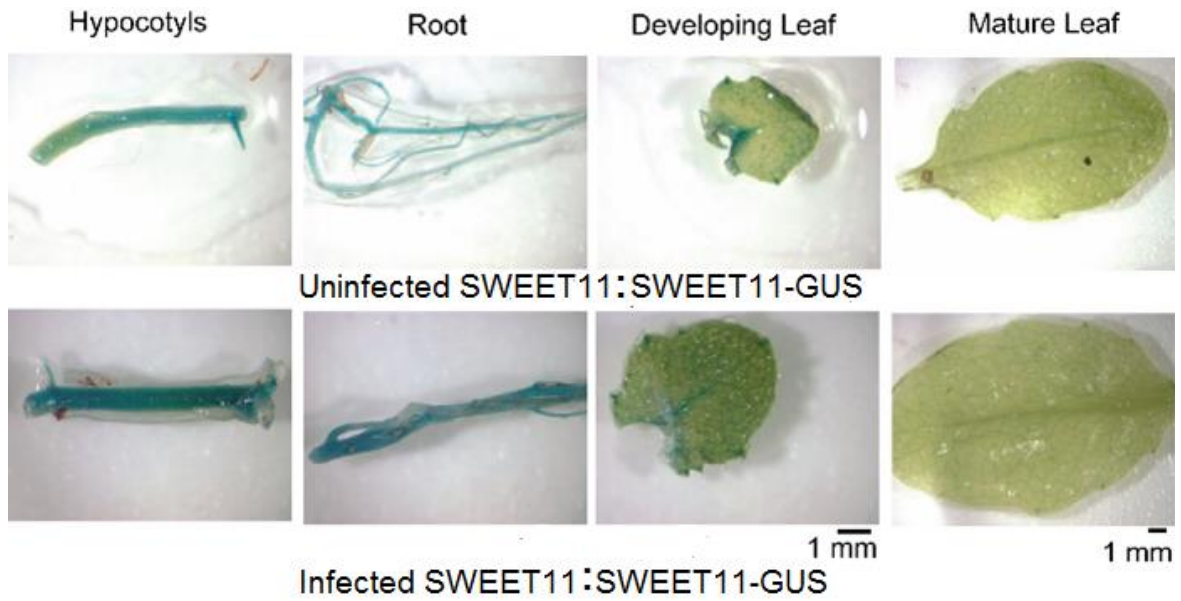


**Figure 4.8** Expression of SWEET11:SWEET11-GUS in hypocotyl, root, developing leaf and mature leaf tissues of uninfected and infected *A. thaliana* transgenic SWEET11:SWEET11-GUS plants at 16 DPI.

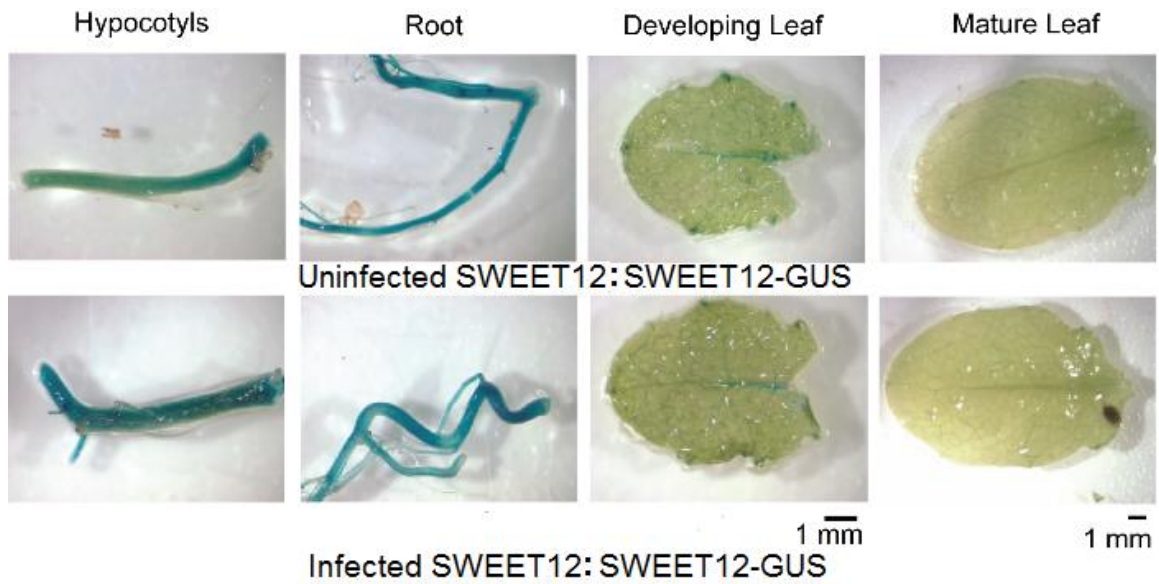


**Figure 4.9** Expression of SWEET12:SWEET12-GUS in hypocotyl, root, developing leaf and mature leaf tissues of uninfected and infected *A. thaliana* transgenic SWEET12:SWEET12-GUS plants at 16 DPI.

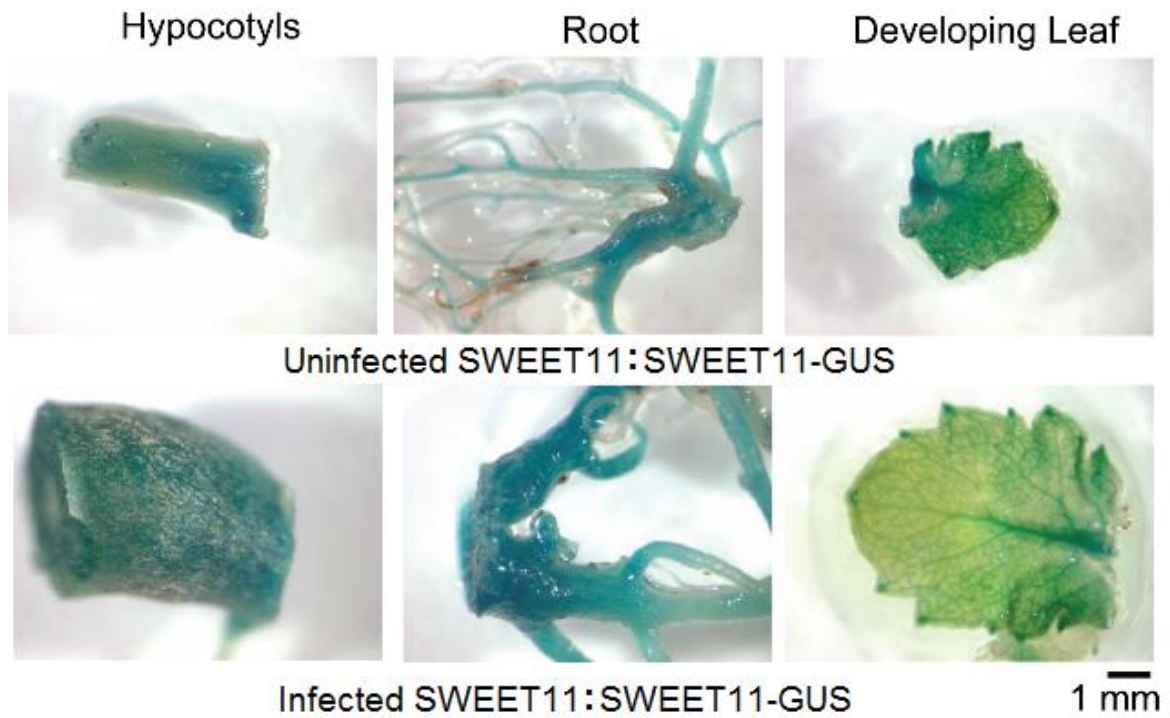


**Figure 4.10.** Expression of SWEET11:SWEET11-GUS in hypocotyl, root and developing leaf tissues of uninfected and infected *A. thaliana* transgenic SWEET11:SWEET11-GUS plants at 26 DPI.

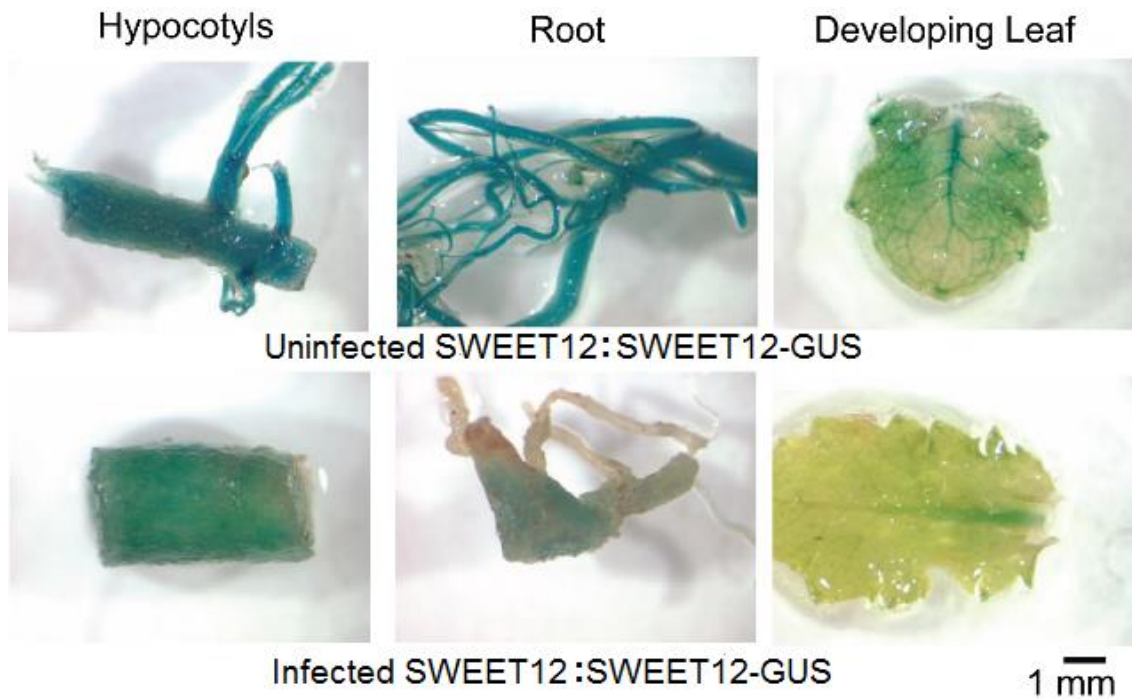


**Figure 4.11.** Expression of SWEET12:SWEET12-GUS in hypocotyl, root and developing leaf tissues of uninfected and infected *A. thaliana* transgenic SWEET12:SWEET12-GUS plants at 26 DPI.

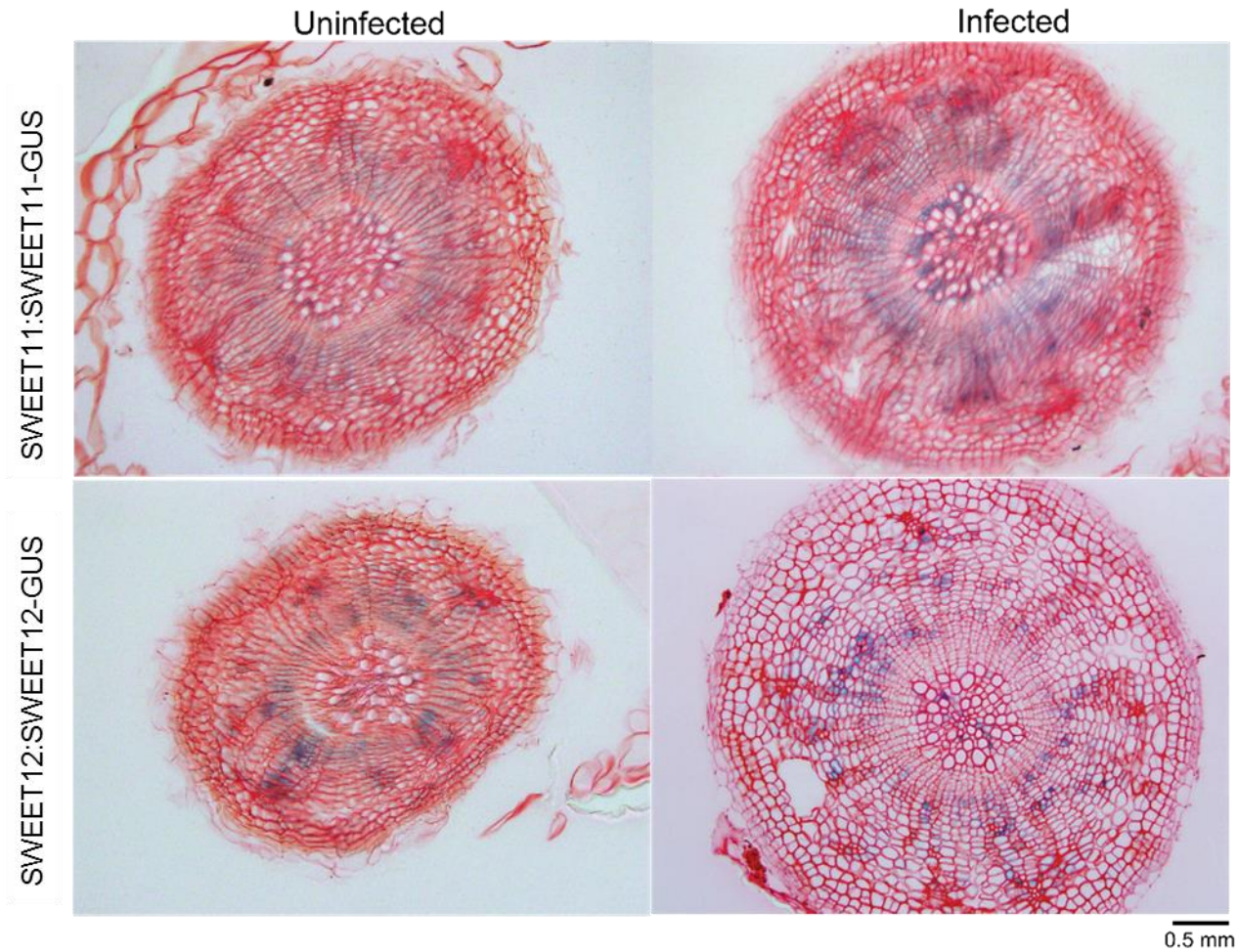


**Figure 4.12.** SWEET11::GUS and SWEET12::GUS activity were visualized in sections of uninfected and infected hypocotyls at 16 DPI. SWEET11::GUS and SWEET12::GUS were expressed in a continuous ring of vascular parenchyma, xylem parenchyma and phloem bundle.

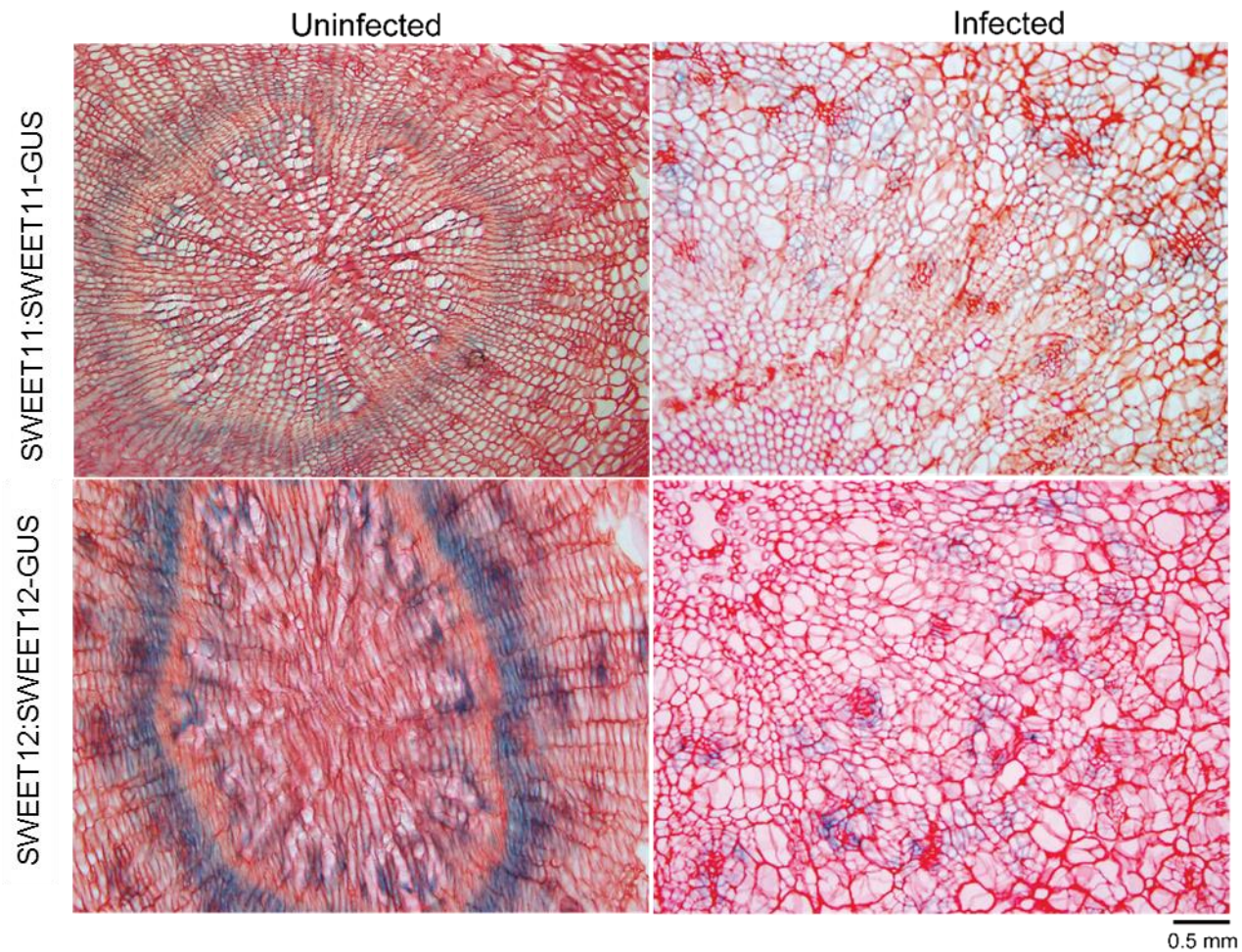


**Figure 4.13.** SWEET11::GUS and SWEET12::GUS activity were visualized in sections of uninfected and infected hypocotyls at 26 DPI. SWEET11: GUS and SWEET12:GUS were expressed in a continuous ring of vascular parenchyma, xylem parenchyma and phloem bundle in uninfected plants. We also observed disruption of the continuous ring of vascular parenchyma cells in infected plants with the presence of swollen cells containing *P. brassicae*.

In higher magnification images, cells containing plasmodia were located near the sites of expression of SWEET11:SWEET11-GUS in a discontinuous ring of vascular parenchyma (Figure 4.14 A). A high magnification image of infected SWEET12:SWEET12-GUS transgenic plants showed that SWEET12:SWEET12-GUS was expressed in phloem parenchyma (Figure 4.14 B). Staining was lost from the xylem parenchyma.

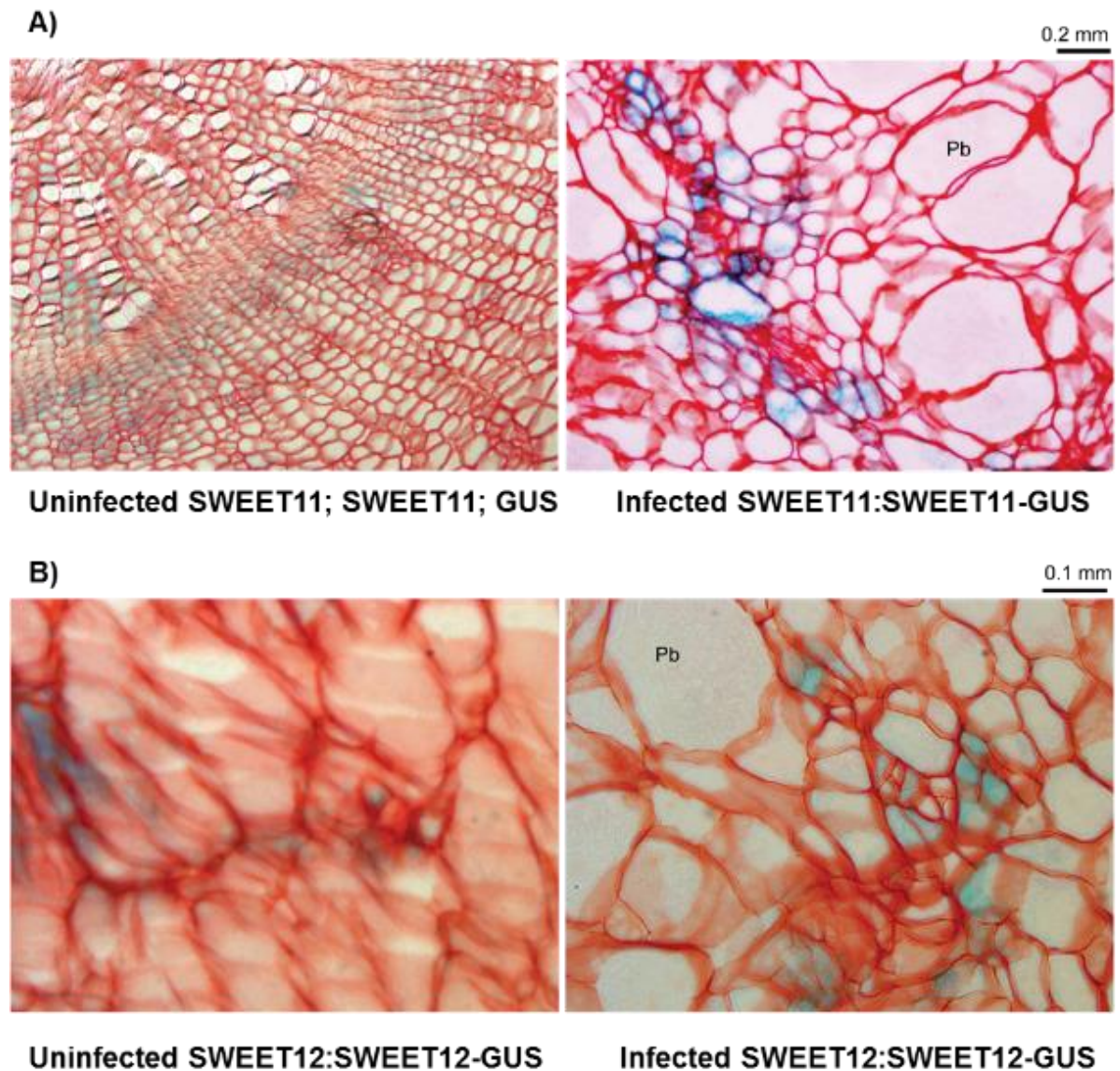


**Figure 4.14.** A close-up of (A) SWEET11: GUS activity in a discontinuous ring of vascular parenchyma. (B) SWEET12: GUS activity in phloem parenchyma cells. Pb: Cell contains *P. brassicae*.

#### **4.3.6. Microscopic Analysis of the Impact of *P. brassicae* Infection on *A. thaliana* Col-0, *sweet11*, *sweet12* and *sweet11,12***

As *P. brassicae* infection led to an accumulation of sucrose associated with phloem unloading, we investigated the impact of disrupting this process on gall formation. We used *sweet11* and *sweet12* single mutants and *sweet11,12* double mutants to disturb sucrose transport via passive sucrose transporters. Secondary thickening of the infected hypocotyl of Col-0 plants was enlarged compared to uninfected tissues at 16 and 26 DPI (Figure 4.15, 4.16). By 26 DPI, infected tissues showed the presence of swollen host cells that contained plasmodia (Figure 4.16). A similar result was seen in *sweet11*, *sweet12* and *sweet11,12* plants (Figure 4.15, 4.16).

Secondary hypocotyl thickening of *sweet11*, *sweet12* and *sweet11,12* plants was slower in uninfected tissue than in Col-0 with the presence of epidermis and endodermis cell layers but this difference was not evident in infected tissue (Figure 4.15). By 26 DPI, infected tissues of *sweet11* and *sweet12* plants showed the presence of swollen host cells that contained plasmodia, which were similar to those observed in Col-0 plants (Figure 4.16). Swollen host cells in infected *sweet11,12* plants were smaller than in infected Col-0 plants indicating the development of plasmodia was slowed, with a reduction of gall size (Figure 4.17).

Figure 4.18 shows the hypocotyl widths of uninfected and infected Col-0, *sweet11*, *sweet12* and *sweet11,12* plants at 16 and 26 DPI. Infected Col-0 plants exhibited a significant increase in hypocotyl width, with infected plants having a hypocotyl width two times bigger than their uninfected control plants at 16 and 26 DPI (Figure 4.18). Similar responses were seen in *sweet11*, *sweet12* and *sweet11,12* plants. However, uninfected *sweet11*, *sweet12* and *sweet11,12* plants had thinner hypocotyls than Col-0 plants at 16 DPI, but this difference was evident at 26 DPI. When infected, the hypocotyl widths of all three mutants were similar to that of Col-0 at 16 DPI. However, at 26 DPI the *sweet11,12* hypocotyl width was smaller than that of Col-0 (Figure 4.18).

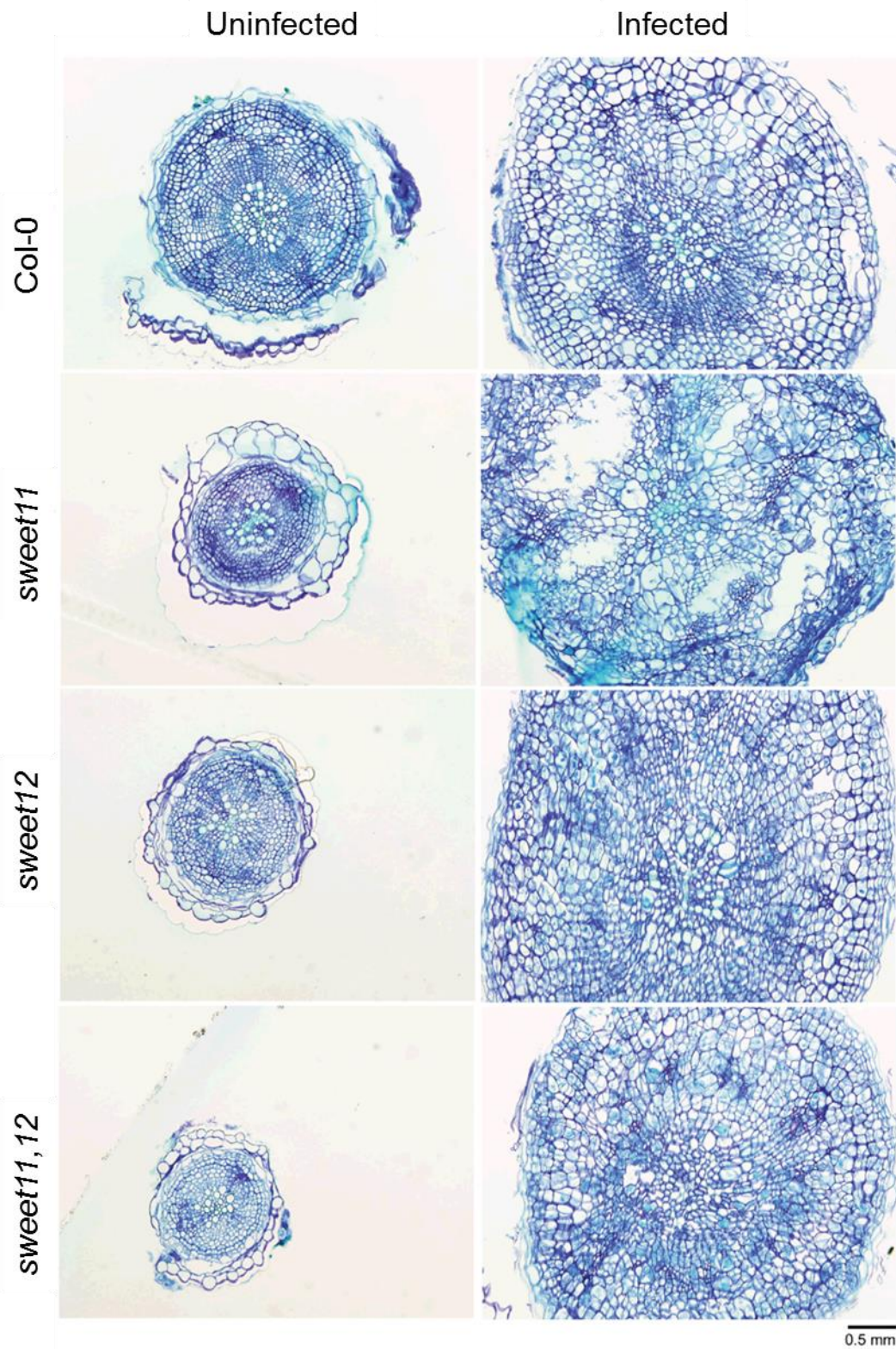


**Figure 4.15.** The effects of deletions in *sweet11*, *sweet12* and *sweet11,12* genes were visualized in sections of uninfected and *P. brassicae*-infected plants at 16 DPI.

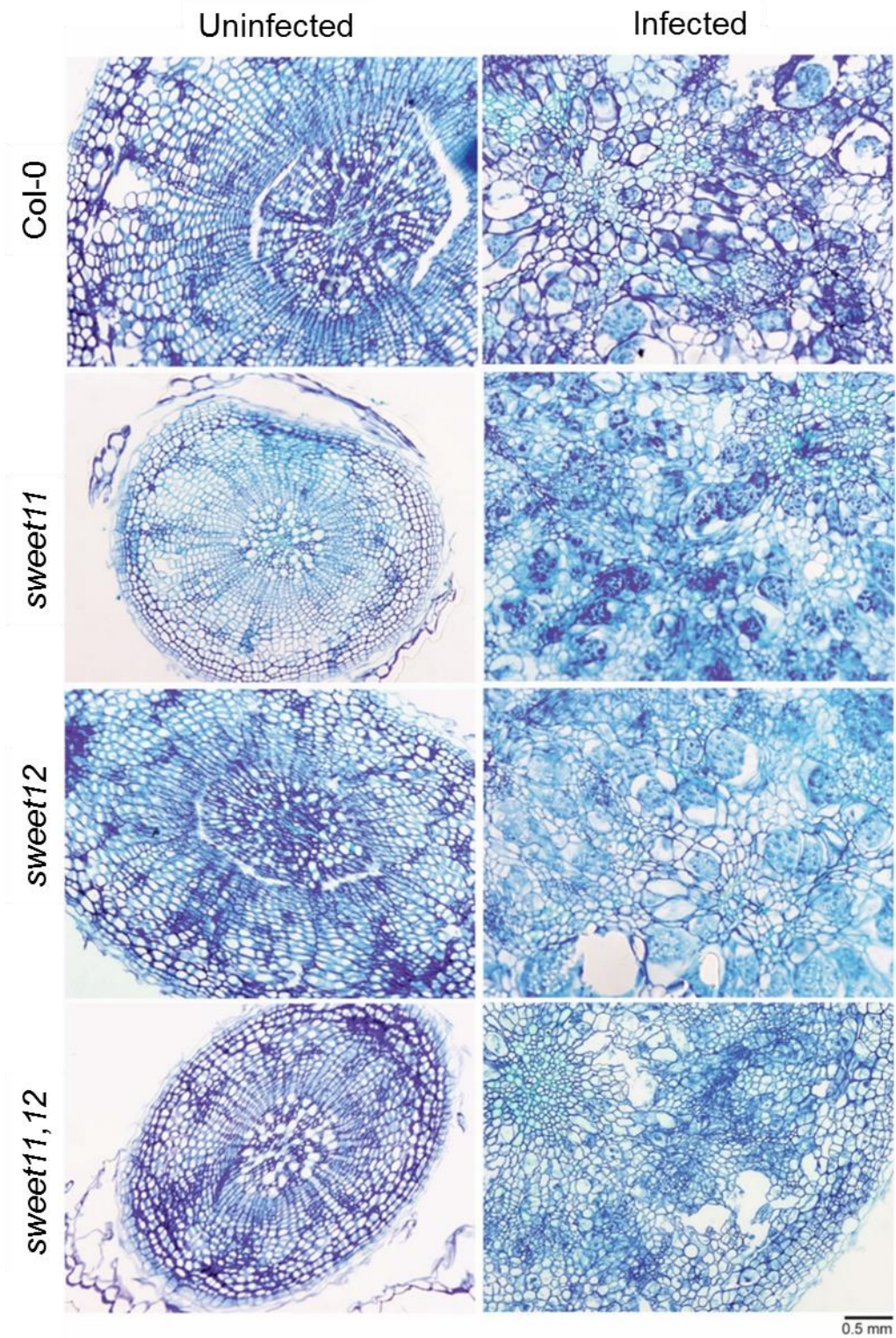


**Figure 4.16.** The effects of deletions in *sweet11*, *sweet12* and *sweet11,12* genes were visualized in sections of uninfected and *P. brassicae*-infected plants at 26 DPI.

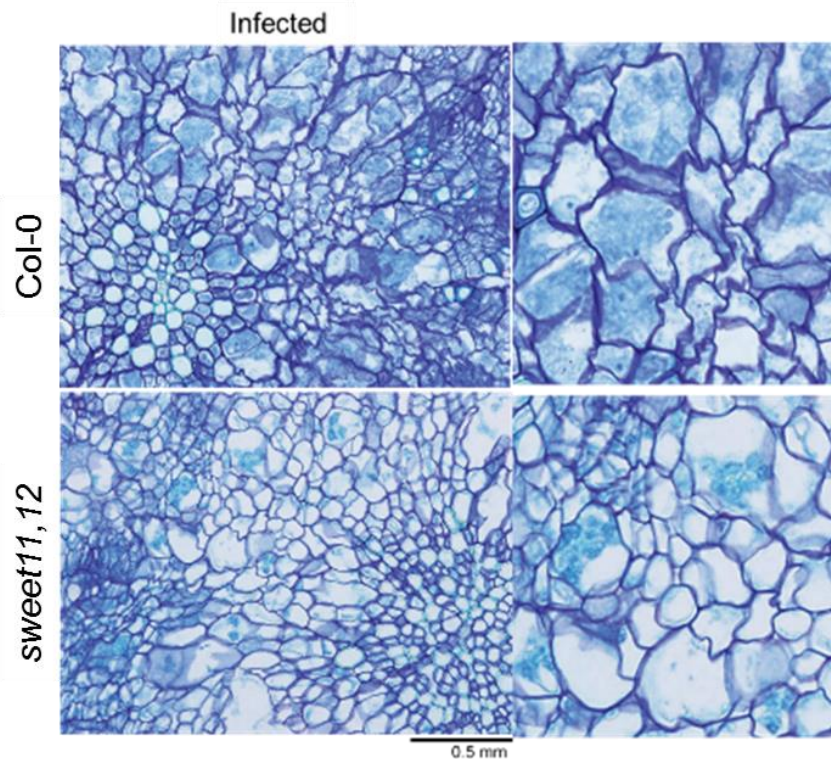


**Figure 4.17.** The effects of deletions in *SWEET11* and *SWEET12* genes when compared with Col-0 were visualized in sections of infected plants at 26 DPI.

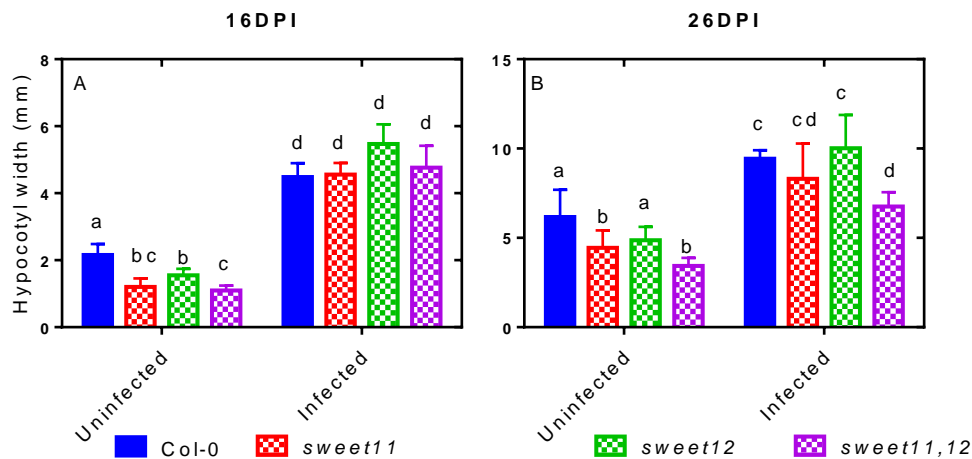


**Figure 4.18.** The width of hypocotyl sections in uninfected and *P. brassicae*-infected Col-0, *sweet11*, *sweet12* and *sweet11,12* plants at (A) 16 and (B) 26 DPI. Results are the average of width measurements per four replicate plant + standard deviation. Means that do not share a letter differ significantly ( $\text{Log}_{10}$  and two-way ANOVA,  $p\text{-value} \leq 0.05$ ). The significant test between uninfected and infected plants was based on Sidak's multiple comparison test while between Col-0 and mutant plants was based on Turkey's multiple comparison test.

#### **4.3.7. Analysis of the Impact of *P. brassicae* Infection on the Carbohydrates in the Root/hypocotyl, Developing Leaf and Mature Leaf of *A. thaliana* Col-0, *sweet11*, *sweet12* and *sweet11,12* plants**

Col-0, *sweet11*, *sweet12* and *sweet11,12* plants displayed characteristic symptoms of clubroot disease, with gall formation occurring in the hypocotyl and upper root system. However, galls of infected *sweet11,12* plants were smaller than those of Col-0 plants. Root/hypocotyl, developing leaves and mature leaves from Col-0, *sweet11*, *sweet12* and *sweet11,12* plants were used to determine local and systemic effects of *P. brassicae* on carbohydrate metabolism.

The carbohydrate content of uninfected and infected root/hypocotyl tissues of Col-0, *sweet11*, *sweet12* and *sweet11,12* plants were compared at 16 and 26 DPI (Figure 4.19). Col-0 glucose and sucrose were not affected at 16 DPI, but by 26 DPI these sugars were higher than in uninfected Col-0 plants (Figure 4.19). Similar results were seen with *sweet11*, *sweet12* and *sweet11,12* at 16 DPI. By 26 DPI, glucose in uninfected *sweet11,12* was higher and sucrose was lower than uninfected Col-0. This pattern was also observed in infected *sweet11,12* compared to infected Col-0 (Figure 4.19).

The carbohydrate content in developing leaves of uninfected and infected Col-0, *sweet11*, *sweet12* and *sweet11,12* were compared at 16 and 26 DPI (Figure 4.20). In Col-0 plants glucose, fructose and sucrose were not affected at 16 DPI, glucose was higher at 26 DPI (Figure 4.20). There was little difference at 16 DPI with elevated sucrose in infected *sweet11* plant, but somewhat higher than that seen in Col-0. By 26 DPI, glucose, fructose and sucrose in infected *sweet12* and *sweet11,12* were higher than in uninfected plants of the same lines (Figure 4.20).

The carbohydrate content of mature leaves of uninfected and infected Col-0, *sweet11*, *sweet12* and *sweet11,12* plants was compared at 16 and 26 DPI (Figure 4.21). In Col-0 plants, glucose, fructose and sucrose were not affected by infection

at 16 and 26 DPI. There was little difference in infected *sweet 11,12* with elevated sugars than that seen in Col-0 at 16 DPI. Similar results were seen at 26 DPI (Figure 4.21).

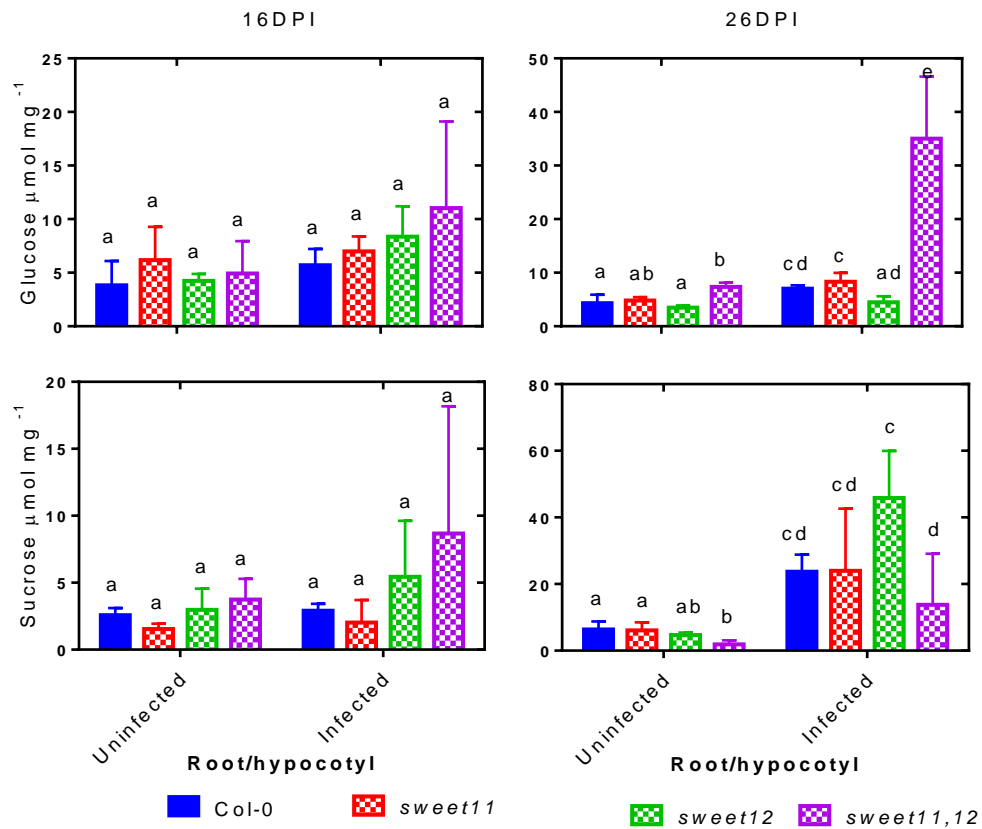


**Figure 4.19.** Amount of glucose and sucrose in root/hypocotyl of uninfected and infected Col-0, *sweet11*, *sweet12* and *sweet11,12* plants at (A) 16 and (B) 26 DPI. Results are the average amount of sugar per replicate plant + standard deviation. Means that do not share a letter differ significantly (Log<sub>10</sub> and two-way ANOVA, p-value ≤ 0.05). The significant test between uninfected and infected plants was based on Sidak's multiple comparison test while between Col-0 and mutants plants was based on Turkey's multiple comparison test.

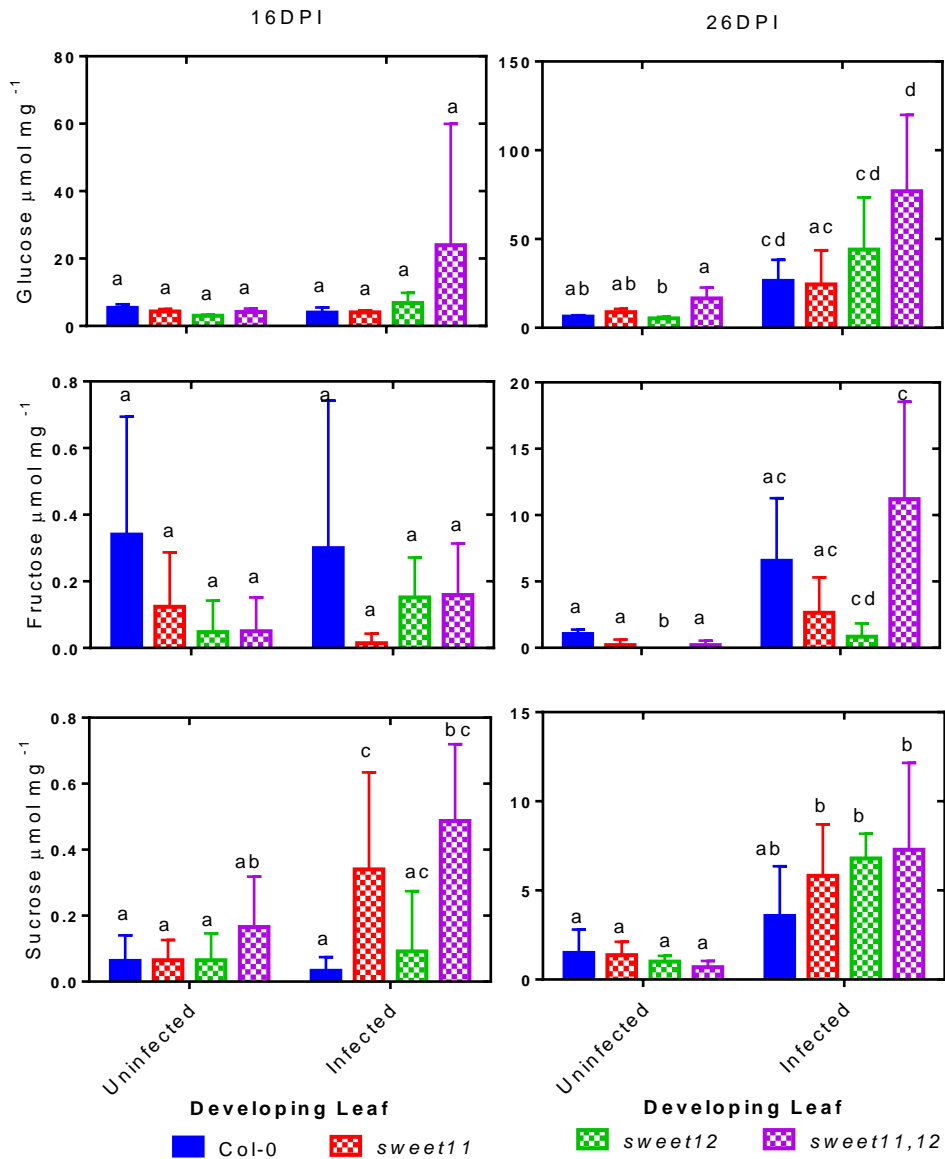


**Figure 4.20.** Amount of glucose, fructose and sucrose in developing leaf of uninfected and infected Col-0, *sweet11*, *sweet12* and *sweet11,12* plants at (A) 16 and (B) 26 DPI. Results are the average amount of sugar per replicate plant + standard deviation. Means that do not share a letter differ significantly ( $\text{Log}_{10}$  and two-way ANOVA,  $p\text{-value} \leq 0.05$ ). The significant test between uninfected and infected plants was based on Sidak's multiple comparison test while between Col-0 and mutants plants was based on Turkey's multiple comparison test.

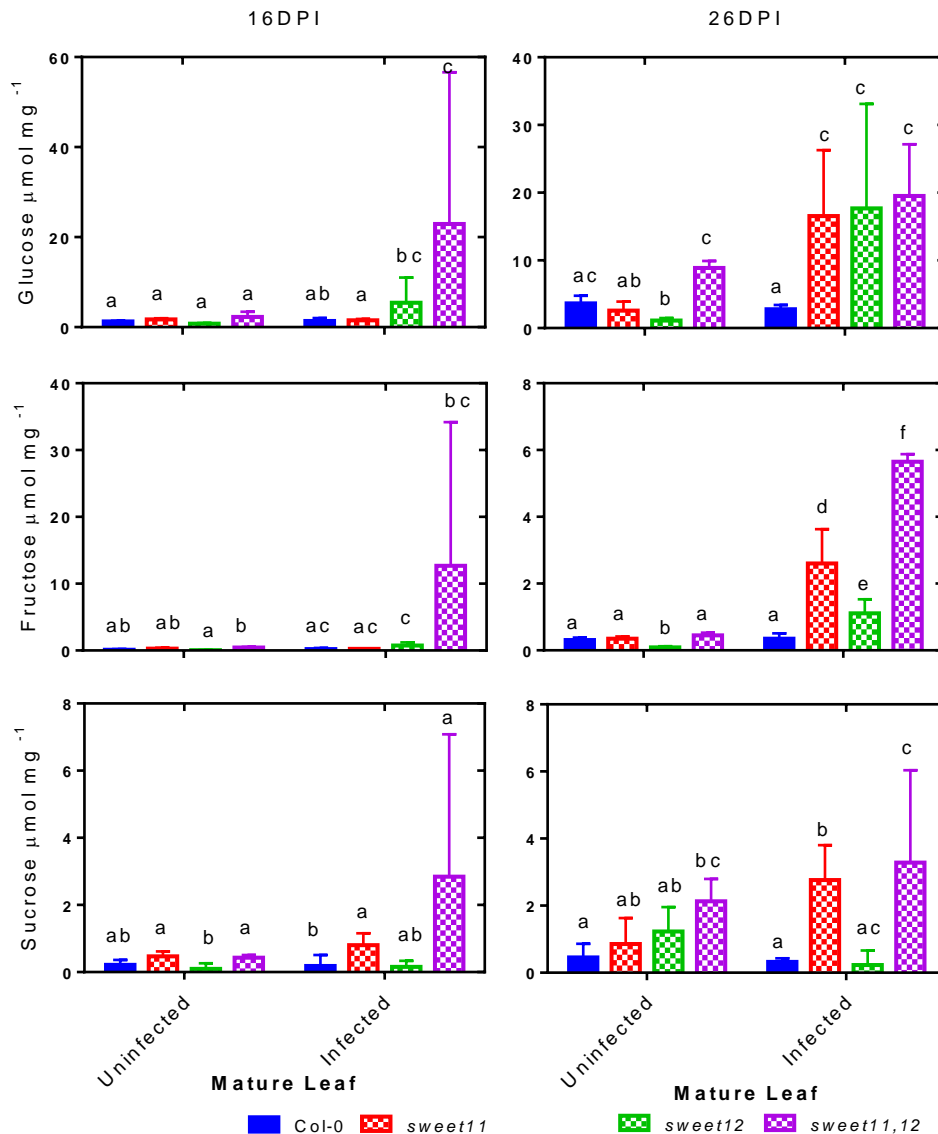


**Figure 4.21.** Amount of glucose, fructose and sucrose in mature leaf of uninfected and infected Col-0, *sweet11*, *sweet12* and *sweet11,12* plants at (A) 16 and (B) 26 DPI. Results are the average of sugar amount per replicate plant + standard deviation. Means that do not share a letter differ significantly ( $\text{Log}_{10}$  and twoway ANOVA,  $p\text{-value} \leq 0.05$ ). The significant test between uninfected and infected plants was based on Sidak's multiple comparison test while between Col-0 and mutants plants was based on Turkey's multiple comparison test.

## 4.4 Discussion

Galls formed in the hypocotyl and upper main root of *P. brassicae*-infected *A. thaliana* plants after inoculation with *P. brassicae*. Galls became a sink for metabolites, including carbohydrates. This chapter has shown host carbohydrate metabolism changed upon *P. brassicae* infection. The altered carbohydrate metabolism of tissues of infected plants occurred through sucrose hydrolysis and sucrose transporter activities, which resulted in increased sink strength. The source-sink status of the plant was altered through the increase of metabolic activity in root/hypocotyl tissues in response to *P. brassicae* infection.

### 4.4.1 The Local Effects of *P. brassicae* Infection on Carbohydrate Metabolism

The first aim of this chapter was to examine the role of sucrolytic genes in *P. brassicae* development and host carbohydrate metabolism. It was hypothesised that *P. brassicae* acts as an effective metabolic sink by altering host carbohydrate metabolism through a localised increase in sucrolytic gene expression in the cytoplasm and a modification of carbon partitioning.

Following *P. brassicae* infection, *SUS 1-4* were up-regulated in infected tissue at 16 and 26 DPI (Table 4.1). The expression of *SUS* genes is correlated to hypoxia in infected tissues, which subsequently induces anaerobic respiration (Bieniawska et al., 2007, Baud et al., 2004, Cabello et al., 2014, Martin et al., 1993). The hypoxia is also a common effect in tissues infected with other plant pathogens including cyst and root knot nematodes (Cabello et al., 2014). *SUS1* and *SUS4* are up-regulated in *A. thaliana* plants infected with the sugar beet cyst nematode *Herarodera schachtii* or the tropical root knot nematode *Meloidogyne javanica* (Cabello et al., 2014). A lack of *SUS1-4* genes caused an accumulation of glucose and fructose in infected tissues at 26 DPI, but did not reduce gall formation (Figure 4.4, 4.5). This indicates that *P. brassicae* induces development of a sink in *sus1,2,3,4*. Besides, I suggest that the accumulation of glucose and fructose in *sus 1,2,3,4* mutants were caused by the activity of CINV when the *SUS* activity was low.

A lack of *CINV* genes reduced the size of galls at 26 DPI. However, examination of infected tissues of *cinv1,2* plants showed that plasmodia colonized host cells and the pathogen developed in a similar manner to Col-0 (Figure 4.3). This suggests that the lack of *CINV1* and *CINV2* activity reduced plant growth but that this did not affect *P. brassicae* development. Besides, Bieniawska et al., (2007) suggested that *CINV* activity alone is sufficient to support the growth of non-photosynthetic tissues under aerobic conditions. Therefore, in gall formation where the oxygen supply was limited, *SUS* genes were predominantly expressed to hydrolyse sucrose into reducing sugars in the cytoplasm. This could explain the down-regulation of *CINV* genes in infected tissues at 16 and 26 DPI (Table 4.1). Similarly, *CINV1* is down-regulated in *A. thaliana* plants following *H. schachtii* and *M. javanica* infection (Cabello et al., 2014).

I hypothesised that *SUS* rather than *CINV* is important in infected plants. However, results demonstrated in this chapter did not support the hypothesis. Gall formation and plasmodia development were unaffected in *sus1,2,3,4* and *cinv1,2* mutants. This indicates that *P. brassicae* was made the gall a sink. It might induced host activity. For instance, in *cinv1,2*, *P. brassicae* might induced *SUS* activity of the host or it might induced its own sucrolytic genes.

The second aim of this chapter was to examine the role of *SWEET* sugar transporters in *P. brassicae* development and host carbohydrate metabolism. It was hypothesised that *P. brassicae* acts as an effective metabolic sink by altering host carbohydrate metabolism through a localised increase in sugar transporter expression and a modification of carbon partitioning. Following *P. brassicae* infection, *SWEET11* and *SWEET12* gene expression was not affected at 16 DPI, but by 26 DPI *SWEET11* and *SWEET12* genes were up regulated in infected tissues (Table 4.1). Besides, by 26 DPI, *SWEET11:SWEET11-GUS* and *SWEET12:SWEET12-GUS* were expressed in phloem parenchyma cells which were located close to swollen host cells that contained plasmodia. I recorded that

gall formation was reduced in *sweet11,12* plants and that the swollen cells that contained plasmodia were smaller than in infected Col-0 plants (Figure 4.17). This suggests that secondary plasmodia were less developed in plants that lack *SWEET11* and *SWEET12* genes. In addition, the lack of *SWEET11* and *SWEET12* genes caused an increase in glucose concentration in infected tissues. It has been suggested that the accumulation of glucose in sink tissue is related to inefficient use of glucose or rapid hydrolysis of sucrose in storage sinks (Hajirezaei et al., 2000). This suggests that sucrose in the apoplastic space was hydrolysed by CWINV after sucrose transport was compromised.

In Col-0 plants, *CWINV1* was also up-regulated in infected tissue at 16 and 26 DPI (Table 4.1). CWINV has been reported to induce a sugar-mediated defence signal in infected leaves against the apoplastic pathogen *Xanthomonas campestris* (*Xcv*) (e.g. (Sonnewald et al., 2012). This indicates that CWINV activity is required for inducing plant defence in infected leaves. However, the role of CWINV in inducing plant defence in infected leaves is not evident in *P. brassicae*-infected roots. Siemens et al., (2011) reported that expression of a CWINV inhibitor reduces gall formation in root tissues. This indicates that CWINV activity is required for pathogen development. CWINV hydrolyses sucrose in the apoplastic space into hexose sugars. This suggests that hexose sugars in the apoplastic space need to be transported into the host cytoplasm before being taken up by plasmodia. Besides, following *P. brassicae* infection, transcriptomic analysis of *A. thaliana* plants showed that *SUS5* and *SUS6* were either slightly repressed or not significantly different at 16 and 26 DPI in root and hypocotyl tissues. It has been reported that these genes are involved in callose synthesis (Barratt et al., 2009). Callose is involved in plant defence, providing an effective barrier against pathogens (Luna et al., 2011). It has been reported that callose deposition is suppressed by a high concentration of sucrose and induced in the presence of the polysaccharide chitosan and Reactive Oxygen Species (ROS) (Luna et al., 2011). This suggests that following *P. brassicae* infection the plant defence response was suppressed, with down regulation of genes

associated with callose synthesis. This could result in successful colonization by *P. brassicae*.

Moreover, transcriptomic analysis of *A. thaliana* plants showed that other *SWEET* genes including *SWEET1*, *4*, *13*, *16* and *17* were down regulated at 16 and 26 DPI in root and hypocotyl tissues in response to *P. brassicae* infection (Table 4.1). *SWEET2* expression was slightly increased at 26 DPI in hypocotyl tissue and decreased at both time points in root tissue in response to *P. brassicae* infection. *SWEET1*, *SWEET2*, and *SWEET4* function as glucose transporters (Chen et al., 2015a, Chen et al., 2010). Recently, *SWEET2* has been reported to be expressed in epidermal cells of the root apex and is localized to the tonoplast, a major sugar storage compartment (Chen et al., 2015a). The expression of *SWEET2* in the root apex is correlated with the supply of glucose to soil microbes (Chen et al., 2015a). However, following *P. brassicae* infection, this gene was down regulated in root tissues. This suggests that, during *P. brassicae* infection, glucose was not stored in the tonoplast, but it could be localized in the host cytoplasm before being taken up by plasmodia.

*SWEET16* and *17* function as fructose transporters (Chen et al., 2010, Guo et al., 2014) and these genes were strongly repressed in root and hypocotyl tissues at 16 and 26 DPI in response to *P. brassicae* infection. *SWEET17* functions as a bidirectional fructose transporter across the tonoplast of roots to maintain cytosolic fructose (Chen et al., 2010, Guo et al., 2014). In the event of a high concentration of fructose in the cytosol, *SWEET17* transports fructose into the vacuole, while during sugar starvation or in actively growing cells especially in the root elongation region, *SWEET17* transports fructose from the vacuole for catabolism in the cytosol (Chen et al., 2010, Guo et al., 2014). Following *P. brassicae* infection, the amount of fructose increased in root/hypocotyl tissues of Col-0 plants and sucrolytic mutants (Figure 4.5). However, the *SWEET17* gene was down regulated in root and hypocotyl tissues. This suggests that, during *P. brassicae* infection, the accumulation

of fructose in infected tissues could be localized in the host cytoplasm before it is taken up by plasmodia.

#### **4.4.2 The Systemic Effects of *P. brassicae* Infection on Host Carbohydrate Metabolism**

Photosynthesis takes place in the mature source leaves of plants. Mature leaves supply carbohydrate to developing leaves and the root/hypocotyl tissues. Following *P. brassicae* infection, the rates of photosynthesis in uninfected and infected leaves are similar, but the carbohydrate content decreases in infected leaves as a result of increases export of carbohydrate (Evans and Scholes, 1996). We recorded that the amount of glucose, fructose, and sucrose increased in mature leaves of *P. brassicae*-infected Col-0 plants, when galls formed. This indicates that the sink strength was altered in response to *P. brassicae* infection.

Furthermore, the expression of SWEET:SWEET11-GUS and SWEET12:SWEET12-GUS were observed in developing leaves, but not in mature leaves of *A. thaliana* transgenic plants (Figure 4.8-4.11). This contrasts with the results reported by Chen et al., (2012). SWEET11: SWEET11-GUS and SWEET12:SWEET12-GUS expression in mature source leaves might be lost during plant development. Besides, in developing leaves, SWEET:SWEET11-GUS and SWEET12:SWEET12-GUS were expressed in major and minor veins (Figure 4.8-4.11). It has been reported that *SWEET11* and *SWEET12* are highly expressed in leaves and the expression of these genes is accompanied by the genes involved in sucrose biosynthesis and phloem loading (Chen et al., 2012). This indicates that *SWEET11* and *SWEET12* are involved in phloem loading in leaves tissues. A study using GFP and GUS protein fusion to SWEET11 and SWEET12 revealed that, both of these proteins localize in the plasma membrane of parenchyma cells (Chen et al., 2012). This indicates that both SWEET11 and SWEET12 are involved in exporting sucrose into the cell wall either in the mesophyll cell or cell closer to the site of loading (Chen et al., 2012). The role of SWEET 11 and SWEET12 is coupled with SUT, which transports sucrose

from the cell wall into the cytoplasm (Chen et al., 2012). SUT which is localized to the phloem of leaves minor veins, is suggested to be involved in phloem loading (Riesmeier et al., 1994). The amount of sucrose increased in mature leaves of plants lacking *SWEET11* and *SWEET12* genes (Figure 4.21, 26 DPI). This is consistent with reported literature where plants which phloem loading has been blocked, accumulate soluble sugar and starch in the leaf tissues (Chen et al., 2012, Riesmeier et al., 1994, Srivastava et al., 2008). From this evidence, I suggest that sucrose transport was reduced in mature leaves of *sweet11,12* plants.

#### **4.5 Conclusion**

This chapter has shown that galls develop normally without *CINV1-2* or *SUS1-4* genes. However, *P. brassicae* induces a sink in *sus1,2,3,4* plants as evidenced by carbohydrate accumulation. Moreover, *sweet11,12* mutants displayed slower *P. brassicae* development due to the change in carbohydrate partitioning. Besides, *SWEET11:SWEET11-GUS* and *SWEET12:SWEET12-GUS* expression showed that sucrose was transported to plasmodia through these sucrose transporters, especially at late stages. Furthermore, the plant defence in infected tissues might be compromised by the down regulation of genes associated with callose synthesis. On the other hand, the up regulation of *CWINV* in response to *P. brassicae* infection has been suggested to be required for pathogen development. The expression of *CWINV1* was not evident for activating plant defence when infected with *P. brassicae*. Lastly, accumulation of carbohydrates in mature source leaves was evidence of increasing sink strength in infected plants.

## Chapter 5: General Discussion

### 5.1. Aims of the Thesis

The aim of this thesis was to investigate the metabolic interaction between *P. brassicae* and *A. thaliana*, by testing the following hypotheses:

- *P. brassicae* hijacks plant development and causes alterations in metabolite concentrations involved in both metabolism and signaling;
- The metabolome is an interface between the plant and pathogen which is influenced by their transcriptomes. Therefore, the metabolites of specific pathways that change in response to *P. brassicae* infection will correlate with changes in the plant transcriptome.
- Clubroot galls act as an effective metabolic sink by altering host carbohydrate metabolism; if host genes involved in carbohydrate metabolism are important for gall formation, deletion of those genes will result in altered carbohydrate partitioning and will affect gall formation.

### 5.2. How Do Changes in Plant Cellular Structure Correlate with Changes in the Metabolome during *P. brassicae* Infection?

An alteration of metabolites in response to *P. brassicae* infection occurred at the very beginning of cortical infection, although plant primary growth did not show clear differences between uninfected and infected hypocotyl tissue at this stage. This suggests that this change in metabolites resulted from responses of the plant to *P. brassicae* infection, rather than from an alteration of plant development.

Work presented in Chapter 2 includes hierarchical clustering heat maps, PCA and PLS-DA of metabolomics data, categorising the uninfected and infected samples into two groups between 7 and 28 DPI. An alteration in metabolite pattern between uninfected and infected plants was seen in response to infection. Most of the putative metabolites that increased in infected tissue at early infection stages are associated

with amino acid metabolism. This includes L-serine, homocarnosine, metabolites involved in purine metabolism such as 5-aminoimidazole, and adenosine 5'-monophosphate which is involved in zeatin biosynthesis (Table 2.3). However, when a precursor of metabolite synthesis such as adenosine 5'-monophosphate is increased, it does not indicate that the product also increases – alternatively precursors in a biosynthetic pathway may accumulate if downstream steps are reduced.

Some secondary metabolites increased in infected tissue during early infection, including glutathionyl spermidine which is part of glutathione metabolism, 6,7-dimethoxycoumarin which is part of coumarin biosynthesis, and 3-benzoyloxypropyl-glucosinolate. Coumarin, which originates from the phenylpropanoid pathway, is involved in plant defences against phytopathogens (Bourgaud et al. 2006). Indole glucosinolates are also involved in plant defence. It has been suggested that cruciferous plants are suitable hosts to *P. brassicae* due to the presence of large quantities of indole glucosinolates in their vacuoles (Ludwig-Muller et al., 1999a). Chinese cabbage and *A. thaliana* plants that are susceptible to *P. brassicae* infection contain high concentrations of indole glucosinolates in infected tissue (Ludwig-Muller et al. 1993, 1999b). *P. brassicae* infection causes cell damage and subsequently triggers the release of indole glucosinolates from the vacuole into the cytoplasm (Ludwig-Muller et al. 1999a). Initially, it has been suggested that the degradation product of indole glucosinolate could contribute to an additional precursor for auxin biosynthesis which leads to an accumulation of auxin in infected tissue of Chinese cabbage plants (Ludwig-Muller et al., 1993). However, it has been reported that indole glucosinolate is not a source for an accumulation of auxin upon *P. brassicae* infection as it does not influence the development of clubroot disease in *A. thaliana* plants. Camalexin, a compound which shares a similar precursor with indole glucosinolate also does not contribute to development of gall formation, although it is accumulated following *P. brassicae* infection (Siemens et al., 2008).

At the onset of gall formation, metabolites that are involved in glucosinolate and phenylpropanoid biosynthesis decreased in infected tissue. This suggests that metabolites involved in plant defence could potentially be suppressed by plasmodia. Finally, at late gall formation, the cellular structure of infected tissue contained swollen and distorted cells. The cytoplasm of infected cells contained secondary plasmodia and a new generation of spores. At this stage, it has been suggested that large plasmodia that colonize infected cells have acquired a high metabolic activity compared with small plasmodia (Schuller et al., 2014), which are mostly present during onset gall formation. This suggests that most of the metabolites that change at late gall formation are potentially important to the pathogen. Results from Chapter 2 showed that putative metabolites associated with pyrimidine metabolism, gibberellin inactivation, and the biosynthesis of alkaloids and piperidine increased at 28 DPI, when a large gall was visible.

### **5.3. How Does Host Gene Expression in Response to *P. brassicae* Infection Alter Plant Metabolism?**

In chapter 3, the metabolites identified as changing during *P. brassicae* infection were grouped according to carbohydrate, energy, nucleotides, amino acid, vitamins, cofactor and secondary metabolism pathways. Figure 5.1 summarises the metabolites that are altered during gall development. The alterations in metabolite concentration found in Figure 5.1 were integrated with transcriptomic data at 16 and 26 DPI obtained from a previous study (Malinowski et al., *unpublished*).

Amino sugar and nucleotide sugar metabolism, which was categorised in carbohydrate metabolism, was altered during *P. brassicae* infection. The biosynthesis of pectin is part of amino sugar and nucleotide sugar metabolism. At 26 DPI, genes associated with pectin synthesis were down regulated in infected tissues, which subsequently resulted in an abundance of free Beta-L-arabinose 1-phosphate (L-Ara-1P), glucuronate-1P (GlcA-1P) and galacturonate (GalA-1P). The

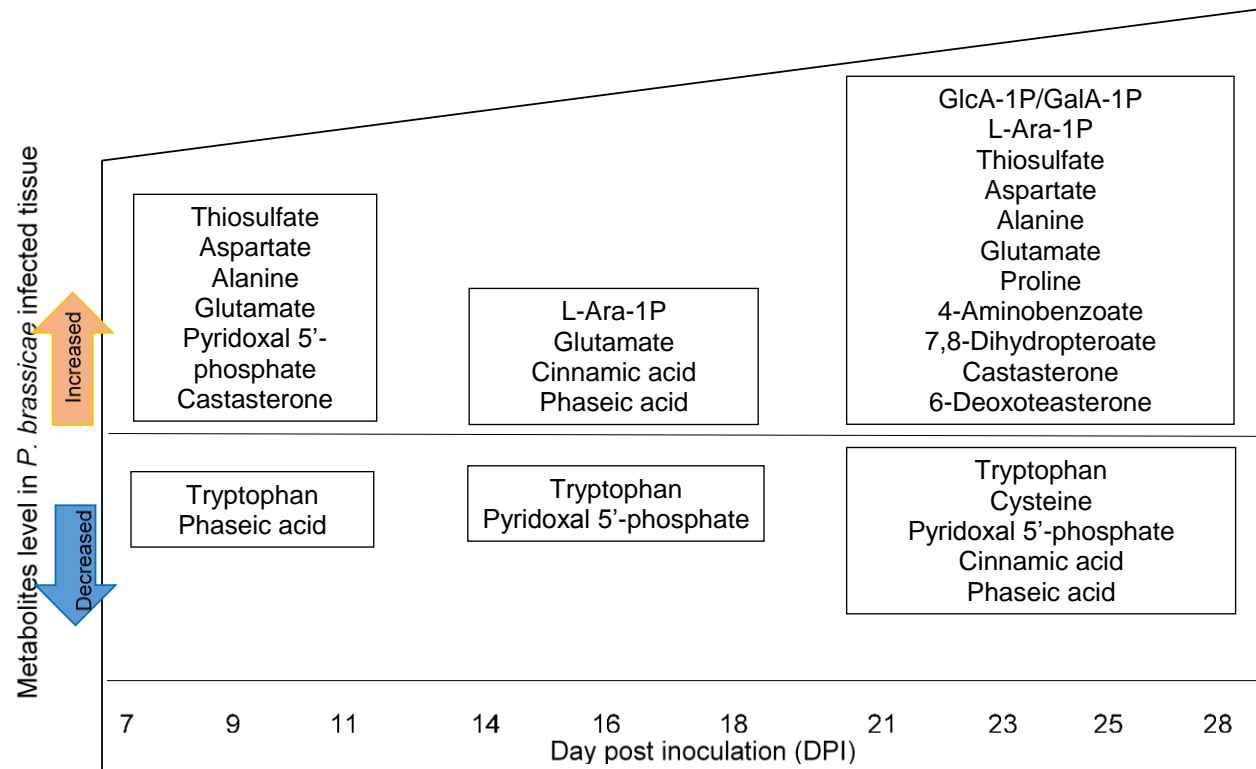


**Figure 5.1.** Putative metabolite alterations in response to *P. brassicae* infection between 7 and 28 DPI.

manipulation of host pectin synthesis by *P. brassicae* is an example of the contrasting infection mechanisms between biotrophic and necrotrophic pathogens.

During infection, necrotrophic fungi such as *Botrytis cinerea* enter the host cell by secreting enzymes such as polygalacturonase to depolymerize pectin structure in order to decrease the strength of plant cell walls (Ferrari et al., 2003). As a result of this depolymerisation, oligogalacturonides are released from pectin and act as a carbon source for the pathogen (Ridley et al., 2001, D'Ovidio et al., 2004). *P. brassicae* on the other hand lacks the plant cell wall degrading carbohydrate-active enzymes (CAZymes) that are involved in pectin degradation (Schwelm et al., 2015). This indicates that *P. brassicae* does not enter host cells via degradation of pectin localized in the plant primary cell walls. Besides, pectin polysaccharide which is a large polymer in the middle lamella, plays a role in cell adhesion. While the plant mother cell is divided into two daughter cells, adhesion between two daughter plant cells is maintained. As plant cells expand, adherent walls between two daughter cells remain fused along the line of the middle lamella. However, abnormal cell adhesion in reinforcing zones could cause cell separation (Jarvis et al., 2003) letting a single cell expand. This may leads to disorganisation of cell structure in *P. brassicae*-infected tissues.

In the sulfur metabolism pathway, thiosulfate accumulated in *A. thaliana* hypocotyl tissue during *P. brassicae* infection. The sulfur metabolism pathway involves thiosulfate as the electron donor and sulfate as the electron acceptor. The transcriptomic data at 16 and 26 DPI obtained from a previous study (Malinowski et al., *unpublished*) showed that the expression of the *A. thaliana* 3-mercaptopyruvate sulfurtransferase gene, which is involved in the synthesis of thiosulfate and pyruvate from 3-mercaptopyruvate, appeared not to be significantly different between infected and uninfected tissue. Electron transfer from thiosulfate to sulfate is regulated by a sulfur-oxidation reaction through the cytochrome C-1 (SOX) gene. The down-regulation of the host's SOX gene in infected tissue at 16 and 26 DPI might caused

the accumulation of thiosulfate. It is possible that *P. brassicae* regulates the sulfur cycle to increase the production of thiosulfate as its sulfur source. The *P. brassicae* genome contains the SOX gene, which could oxidize thiosulfate and is also the gene encoding thiosulfate sulfur transferase (Schwelm et al., 2015), which converts thiosulfate to sulfite. Probably, *P. brassicae* regulates the sulfur cycle to increase the production of thiosulfate as its sulfur source and suppress the host's sulfur metabolism genes.

In the amino acid metabolism pathway, amino acids such as glutamate, aspartate, alanine and proline accumulated in *P. brassicae* infected tissue. Wagner et al. (2012) reported that glutamate and alanine accumulated in a genotype of *B. napus* that was susceptible to *P. brassicae* and exhibited extensive disease symptoms. This shows that glutamate and alanine maybe required for the development of *P. brassicae* inside a susceptible host. In fact, glutamate and aspartate can be catabolized for the production of energy. The expression of the host genes associated with the metabolism of those amino acids was altered at 16 and 26 DPI. However, the *P. brassicae* genome contains several genes associated with amino acid metabolism including glutamate synthase, aspartate kinase, homoserine O-succinyltransferase. These genes are associated with synthesis of glutamate and degradation of aspartate (Schwelm et al., 2015). It is possible that *P. brassicae* manipulates the expression of host genes involved in aspartate and alanine metabolism. *P. brassicae* might potentially take up and catabolize aspartate using its aspartate kinase and homoserine O-succinyltransferase genes to release energy. Besides, the *P. brassicae* genome lacks genes associated with tryptophan, cysteine, alanine and proline metabolism. Tryptophan and cysteine are decreased while alanine and proline are increased in infected tissue.

Amino acids that are associated with plant defence such as cysteine decreased in infected tissue. Possibly, the synthesis of this amino acid was shifted in favour of plasmodia leading to the accumulation of thiosulfate. Proline accumulated in infected

tissue at 25 and 28 DPI and genes associated with the synthesis of this amino acid were up-regulated at 26 DPI. It has been reported that proline accumulates only at the later stages of infection in *P. brassicae*-infected *B. napus* plants, when the concentration of *P. brassicae* DNA is relatively high compared to the early stage of infection (Wagner et al., 2012). Proline is a compatible solute, associated with host stresses including drought stress (Takagi 2008). The reduction of xylem formation in infected plants could limit water transport to the whole plant, mimicking a drought stress condition. The accumulation of proline in tissue infected with *P. brassicae* may protect plants from osmotic stress.

Pyridoxal 5'-phosphate which is required for vitamin B6 metabolism, was increased at 7 DPI and decreased at 18 and 25 DPI in response to *P. brassicae* infection. In addition, following *P. brassicae* infection, D-Ribulose 5-phosphate, a precursor of pyridoxal 5'-phosphate, was found to have increased in infected tissue at 25 DPI and the *A. thaliana* gene encoding pyridoxal 5'-phosphate synthase, synthesising pyridoxal 5'-phosphate, was up-regulated in response to *P. brassicae* infection at 26 DPI. This indicates that *de novo* biosynthesis of vitamin B6 was increased in infected tissue. Meanwhile, 4-aminobenzoate and 7, 8-dihydropteroate, which are required for folate biosynthesis, also increased at 25 DPI. This indicated that the production of these metabolites associated with tetrahydrofolate (THF), a cofactor for several cellular processes, was increased. The expression of the *A. thaliana* gene encoding folylpolyglutamate synthase (6.3.2.17) to synthesis THF, was up-regulated at 16 and 26 DPI. The *P. brassicae* genome lacks genes associated with thiamine biosynthesis. It has been suggested that *P. brassicae* depends on the host for this vitamin (Schwelm et al., 2015). The loss of genes associated with cofactor biosynthetic pathways in plant pathogens is a signature of biotrophy (Kemen et al., 2011, Schwelm et al., 2015). It has been suggested that biotrophic pathogens have evolved to synthesise less energy consuming sources of metabolites, such as nitrogen and sulfate, rather than vitamins, which are more energy consuming (Kemen et al., 2011). This may suggest that *P. brassicae* obtains vitamin B6 and

folates as essential cofactors for cellular biological processes from the host by inducing host biosynthetic pathways.

In secondary metabolism, secondary metabolites such as cinnamic acid, a compound involved in the biosynthesis of phenylpropanoids, increased at 16 DPI and decreased at 25 DPI. Cinnamic acid is derived from the amino acid phenylalanine by the activity of phenylalanine ammonia-lyase (*PAL*), which was up-regulated at 16 DPI and down-regulated at 26 DPI. Cinnamic acid has antimicrobial activity, which suggests that *A. thaliana* plants activate their defence response at 16 DPI, when this compound accumulates in infected tissue. Phaseic acid for carotenoid biosynthesis, which was derived from the degradation of abscisic acid (ABA), increased at 16 DPI and decreased during late gall formation. As phaseic acid increased, the *A. thaliana* gene that encodes ABA-beta-D-glucosidase, which hydrolyses abscisic acid glucose ester to form ABA, was up-regulated at 16 DPI. As phaseic acid decreased, however, this gene was down-regulated at 25 DPI. It has been reported that ABA plays a major role in the susceptibility of tomato against *Botrytis cinerea* through repression of *PAL* activity, which subsequently reduced SA-defence pathways (Audenaert et al., 2002). From this result, firstly I assume that accumulation of phaseic acid at 16 DPI is correlated with the inactivation of ABA in *P. brassicae*-infected plants to increase the expression of the *PAL* gene, which subsequently triggers SA-dependent pathways. Maybe this was achieved by ABA being actively converted to unstable 8'-hydroxy-ABA, which subsequently rearranges to phaseic acid. In the meantime, SA could be suppressed by *P. brassicae* effector PbBSMT to inactivate the role of SA in plant defence (Ludwig-Muller et al., 2015). However, it has been reported that ABA content was four times higher in *P. brassicae*-infected root of Chinese cabbage plants than uninfected plants at 21 DPI (Devos et al., 2005). The accumulation of ABA at late gall formation is maybe correlated to severe stress upon pathogen infection. It was not correlated with the down-regulation of the *PAL* gene at 26 DPI which was found in the transcriptomic

data of this study. Details on the role of ABA during *P. brassicae* infection requires further investigation.

Furthermore, castasterone and 6-deoxoteasterone, which are precursors for brassinosteroid biosynthesis, increased in infected tissue at 25 DPI. Generally, most of the genes associated with brassinosteroid biosynthesis leading to the synthesis of brassinolide, the most biologically active brassinosteroid, were up-regulated in infected tissue at 26 DPI. This result agrees with the previous finding of a cell type-specific transcriptomic analysis that gene expression associated with brassinosteroid synthesis was up-regulated in hypertrophied cells containing large plasmodia (Schuller et al., 2014). This was supported by the fact that the application of propiconazole, an inhibitor of brassinolide synthesis, resulted in a reduction of gall size, indicating that this compound is involved in cell division and cell expansion in gall development (Schuller et al., 2014).

The precise identification of metabolites and their regulation are critical to the understanding of the role of important metabolites in *P. brassicae*-infected tissue. Although metabolomic data were integrated with host transcriptomic data to gain an understanding of the interaction between *P. brassicae* and its host, validation of this approach is required. Besides, the sample extraction method used in this thesis only measured polar metabolites, the quantification of which strongly depends on the positive ionization conditions and only gives a snapshot of selected metabolites in hypocotyl tissue between 7 and 28 DPI. Unfortunately, this reveals nothing about non-polar metabolites such as lipids and metabolites that are only potentially ionized in negative condition. Future work would include validation of putative metabolites that were identified in Chapter 3, for example by using specific inhibitors to inhibit specific pathways. Furthermore, plant mutants in specific metabolic pathways and targeted metabolomics such as liquid/gas chromatography MS or MS-MS also can be potential approaches to validate the metabolomic data obtained in this study. Meanwhile, establishing the exact location of metabolites would allow an

assessment of whether the pathogen itself is a competing sink or whether sink metabolism is induced in the host infected cells or uninfected cells of infected tissue. This could be achieved using the MALDI-imaging technique (Kaspar et al., 2011).

#### **5.4. Is Sugar Permease a Key Facilitator of Carbohydrate Metabolism in Infected Sink Tissues?**

Chapter 4 demonstrated that host carbohydrate metabolism changed upon *P. brassicae* infection. The altered carbohydrate metabolism of tissues of infected plants occurred through sucrose hydrolysis and sucrose transporter activities, which resulted in increased sink strength. The source-sink status of the plant was altered through the increase of metabolic activity in root/hypocotyl tissues in response to *P. brassicae* infection.

Transcriptomic data showed that *SUS 1-4* were up-regulated in infected tissue at 16 and 26 DPI, but the expression of *CINV1* and *CINV2* were down-regulated. Expression of *SUS1-4* during *P. brassicae* infection was likely related to hypoxia in gall tissue, as suggested by other studies about *SUS* genes which relate to anaerobic respiration (Bieniawska et al. 2007; Baud et al. 2004; Martin et al. 1993). In addition, the expression of the *SUS1* and *SUS4* genes in tissue infected with *P. brassicae* was similar to their expression in response to the sugar beet cyst nematode *Heterodera schachtii* or the tropical root knot nematode *Meloidogyne javanica* (Cabello et al. 2014). However, a lack of *SUS1-4* did not reduce gall formation. The lack of *CINV1* and *CINV2* on the other hand reduced the size of galls at 26 DPI, although plasmodia colonized host cells and pathogen development was similar to that in Col-0 plants. This suggests that the lack of *CINV1* and *CINV2* activity reduced plant growth but still resulted in normal gall development.

Throughout the work presented in Chapter 4, the initial hypothesis was that *SUS* rather than *CINV* was important in infected plants. However, the results did not support the hypothesis. Gall formation and plasmodia development were unaffected

in *sus1,2,3,4* and *cinv1,2* mutants, although lack of *SUS1-4* genes caused an accumulation of glucose and fructose in infected tissues at 26 DPI and a lack of *CINV1,2* genes reduced plant growth. This indicates that *P. brassicae* itself makes the gall a sink. This might be due to induced host activity. For instance, in *cinv1,2*, *P. brassicae* might induce SUS activity of the host or it might express its own sucrolytic genes. However, there is no evidence of the presence of invertase genes in the *P. brassicae* genome (Rolfe et al., *unpublished*).

Gall formation was reduced in *sweet11,12* plants and the swollen cells contained plasmodia that were smaller than in infected Col-0 plants. By 26 DPI, SWEET11:SWEET11-GUS and SWEET12:SWEET12-GUS were expressed in phloem parenchyma cells which were located close to swollen host cells that contained plasmodia. Figure 5.2 shows a model of how sucrose from the host might be supplied to plasmodia. As shown on this schematic, genes encoding SWEET sugar transporters are transcriptionally induced after infection with *P. brassicae*. *SWEET11* and *SWEET12* are suggested to unload sucrose from the companion cells into the apoplast, concurrent with symplastic unloading via plasmodesmata. Active sucrose transporters could also potentially unload sucrose from the companion cells to the apoplast. Infected cells containing multinucleate plasmodia take up sucrose via plasmodesmata, and sucrose in the apoplast is hydrolysed by extracellular invertase before being transported into the cytoplasm of infected cells through hexose transporters (Figure 5.2a). Sucrose in the cytoplasm is hydrolysed by sucrose synthase. A lack of *SWEET11* and *SWEET12* reduces the efficiency of this sucrose transport into infected cells, which subsequently reduces the development of plasmodia (Figure 5.2b).

The induction of SWEET11 and SWEET12 expression and their location in response to *P. brassicae* infection has been demonstrated in this thesis. The work presented here suggests that SWEET11 and SWEET12 play an important role in supplying carbohydrate to *P. brassicae* development. Future work would include assessment

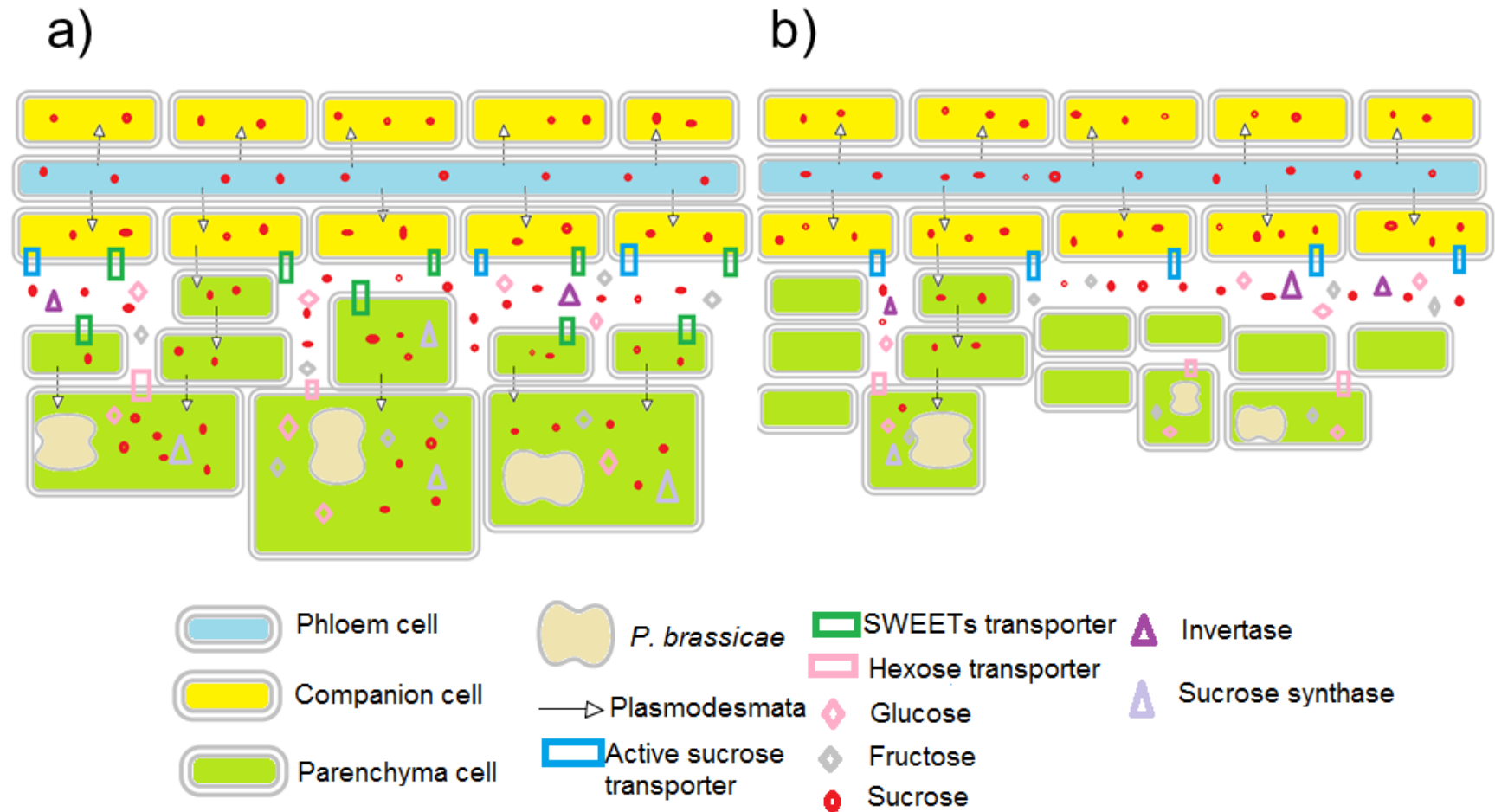


**Figure 5.2.** Model of sucrose transport in a) Col-0 wild type plant and b) *sweet11/12* plant. Sucrose is unloaded from the companion cells into the apoplast via SWEET transporters or active sucrose transporters and symplastic unloading via plasmodesmata. Sucrose in the apoplast is hydrolysed into hexose sugars by invertase, and hydrolysed by sucrose synthase in cytoplasm. Hexose sugars in the apoplast could potentially be taken up by infected cells through hexose transporters. A lack of SWEET transporters reduces the size of galls in *P. brassicae*-infected plants.

of the plasmodesmata of cells in infected tissue to quantify the capacity for the sucrose to pass the cell wall interface of infected cells containing plasmodia. This could be achieved using electron microscopy which could assess the frequency of occurrence and diameter of plasmodesmata on fixed material. Alternatively, the function and capacity of plasmodesmata can be determined using three-dimensional photoactivation microscopy on live material (Liescha and Schulz, 2012). This approach uses fluorescent tracers with diffusion properties similar to cytosolic materials and provides an image of the complex shape of the cells. Furthermore, the movement of sucrose in infected tissue through the existence of functional plasmodesmata between large cells containing plasmodia and parenchyma cells close to the phloem could be assessed using carboxyfluorescein (CF). Previously, this approach was used to observe the unloading process of CF from the phloem to the syncytium, and take up by a nematode (Hofmann et al., 2007).

## **5.5. Conclusion**

An undirected metabolomic approach in this study gives clues to metabolic changes during *P. brassicae* infection. A direct approach is required to have confidence in the identity of metabolites and their concentrations. Coupling metabolomic and transcriptomic methods provides greater insight into metabolic changes. However, translating these findings from the model system of *A. thaliana* plants to crops is more challenging as molecular tools are limited, but would be beneficial to address issues associated with increased food security.

In the future, plant metabolic characteristics might be used for diagnostic purpose during clubroot infection facilitating the development of agrochemical and new resistant lines of plant (whether by conventional breeding or genetic engineering). In addition the mechanistic insight provided by metabolomics may lead to new strategies to limit disease development. For example, the analysis of carbohydrate metabolism in infected plants and the slowed disease development in *SWEET* mutants identifies sugar transport as a potential mechanism to limit disease

development, whether by inhibiting host or pathogen transporters or altering other aspects of sink development. Another avenue might explore the biotrophic nature of the disease. *P. brassicae* requires vitamins such as B6 from the host and impeding the synthesis, transport or uptake of this would likely limit disease development. Although this work has been done in the model *A. thaliana*, the elucidation of fundamental mechanisms underpinning disease development will be applicable in Brassica crop plants.

## References

- Agarwal, A., Kaul, V., Faggian, R., Rookes, J. E., Ludwig-Mueller, J. & Cahill, D. M. (2011) Analysis of global host gene expression during the primary phase of the *Arabidopsis thaliana*-*Plasmodiophora brassicae* interaction. *Functional Plant Biology*, 38, 462-478.
- Ahmad, A., Shafique, S. & Shafique, S. (2014) Intracellular interactions involved in induced systemic resistance in tomato. *Scientia Horticulturae*, 176, 127-133.
- Akhtar, S. A. (2014) The molecular mechanisms underlying gall formation in *Plasmodiophora brassicae* infected *Arabidopsis thaliana*. *Department of Animal and Plant Sciences*. Sheffield, The University of Sheffield.
- Antony, G., Zhou, J., Huang, S., Li, T., Liu, B., White, F. & Yang, B. (2010) Rice xa13 Recessive Resistance to Bacterial Blight Is Defeated by Induction of the Disease Susceptibility Gene *Os-11N3*. *The Plant Cell*, 22, 3864-3876.
- Audenaert, K., De Meyer, G. B. & HaFte, M. M. (2002) Abscisic acid determines basal susceptibility of tomato to *Botrytis cinerea* and suppresses Salicylic acid-dependent signaling mechanisms. *Plant Physiology*, 128, 491-501.
- Barau, J., Grandis, A., De Andrade Carvalho, V. M., Teixeira, G. S., Alcala Zaparoli, G. H., Scatolin Do Rio, M. C., Rincones, J., Buckeridge, M. S. & Guimaraes Pereira, G. A. (2015) Apoplastic and intracellular plant sugars regulate developmental transitions in witches' broom disease of cacao. *Journal of Experimental Botany*, 66, 1325-1337.
- Barratt, D. H. P., Derbyshire, P., Findlay, K., Pike, M., Wellner, N., Lunn, J., Feil, R., Simpson, C., Maule, A. J. & Smith, A. M. (2009) Normal growth of *Arabidopsis* requires cytosolic invertase but not sucrose synthase. *Proceedings of the National Academy of Sciences*, 106, 13124-13129.
- Bartlem, D. G., Jones, M. G. K. & Hammes, U. Z. (2013) Vascularization and nutrient delivery at root-knot nematode feeding sites in host roots. *Journal of Experimental Botany*.
- Basset, G. J. C., Quinlivan, E. P., Gregory, J. F. & Hanson, A. D. (2005) Folate synthesis and metabolism in plants and prospects for biofortification. *Crop Science*, 45, 449-453.
- Baud, S., Vaultier, M. N. & Rochat, C. (2004) Structure and expression profile of the sucrose synthase multigene family in *Arabidopsis*. *Journal of Experimental Botany*, 55, 397-409.

- Bieniawska, Z., Paul Barratt, D. H., Garlick, A. P., Thole, V., Kruger, N. J., Martin, C., Zrenner, R. & Smith, A. M. (2007) Analysis of the sucrose synthase gene family in *Arabidopsis*. *The Plant Journal*, 49, 810-828.
- Bloem, E., Haneklaus, S. & Schung, E. (2015) Milestones in plant sulfur research on sulfur-induced-resistance (SIR) in Europe. *Frontiers in Plant Science*, 5.
- Bowen, J. K., Mesarich, C. H., Bus, V. G. M., Beresford, R. M., Plummer, K. M. & Templeton, M. D. (2011) *Venturia inaequalis*: the causal agent of apple scab. *Molecular Plant Pathology*, 12, 105-122.
- Bourgaud, F., Hehn, A., Larbat, R., Doerper, S., Gontier, E., Kellner, S. & Matern, U. (2006) Biosynthesis of coumarins in plants: a major pathway still to be unravelled for cytochrome P450 enzymes. *Phytochemistry Reviews*, 5, 293-308.
- Brodmann, D., Schuller, A., Ludwig-Muller, J., Aeschbacher, R. A., Wiemken, A., Boller, T. & Wingler, A. (2002) Induction of trehalase in *Arabidopsis* plants infected with the trehalose-producing pathogen *Plasmodiophora brassicae*. *Molecular Plant-Microbe Interactions*, 15, 693-700.
- Burki, F., Kudryavtsev, A., Matz, M., Aglyamova, G., Bulman, S., Fiers, M., Keeling, P. & Pawlowski, J. (2010) Evolution of Rhizaria: new insights from phylogenomic analysis of uncultivated protists. *BMC Evolutionary Biology*, 10, 377.
- Cabello, S., Lorenz, C., Crespo, S., Cabrera, J., Ludwig, R., Escobar, C. & Hofmann, J. (2014) Altered sucrose synthase and invertase expression affects the local and systemic sugar metabolism of nematode-infected *Arabidopsis thaliana* plants. *Journal of Experimental Botany*, 65, 201-212.
- Cao, T., Srivastava, S., Rahman, M. H., Kav, N. N. V., Hotte, N., Deyholos, M. K. & Strelkov, S. E. (2008) Proteome-level changes in the roots of *Brassica napus* as a result of *Plasmodiophora brassicae* infection. *Plant Science*, 174, 97-115.
- Carvalho, B. S. & Irizarry, R. A. (2010) A framework for oligonucleotide microarray preprocessing. *Bioinformatics*, 26, 2363-2367.
- Castanheira, S., Mielnichuk, N. & Perez-Martin, J. (2014) Programmed cell cycle arrest is required for infection of corn plants by the fungus *Ustilago maydis*. *Development*, 141, 4817-4826.
- Chang, Q., Liu, J., Wang, Q., Han, L., Liu, J., Li, M., Huang, L., Yang, J. & Kang, Z. (2013) The effect of *Puccinia striiformis* f. sp. *tritici* on the levels of water-

soluble carbohydrates and the photosynthetic rate in wheat leaves. *Physiological and Molecular Plant Pathology*, 84, 131-137.

- Chen, H.-Y., Huh, J.-H., Yu, Y.-C., Ho, L.-H., Chen, L.-Q., Tholl, D., Frommer, W. B. & Guo, W.-J. (2015a) The *Arabidopsis* vacuolar sugar transporter SWEET2 limits carbon sequestration from roots and restricts *Pythium* infection. *Plant Journal*, 83, 1046-1058.
- Chen, L.-Q., Cheung, L. S., Feng, L., Tanner, W. & Frommer, W. B. (2015b) Transport of Sugars. *Annual Review of Biochemistry*, Vol 84, 84, 865-894.
- Chen, L.-Q., Hou, B.-H., Lalonde, S., Takanaga, H., Hartung, M. L., Qu, X.-Q., Guo, W.-J., Kim, J.-G., Underwood, W., Chaudhuri, B., Chermak, D., Antony, G., White, F. F., Somerville, S. C., Mudgett, M. B. & Frommer, W. B. (2010) Sugar transporters for intercellular exchange and nutrition of pathogens. *Nature*, 468, 527-U199.
- Chen, L.-Q., Qu, X.-Q., Hou, B.-H., Sosso, D., Osorio, S., Fernie, A. R. & Frommer, W. B. (2012) Sucrose Efflux Mediated by SWEET Proteins as a Key Step for Phloem Transport. *Science*, 335, 207-211.
- Chilton, M.-D., Drummond, M. H., Merlo, D. J., Sciaky, D., Montoya, A. L., Gordon, M. P. & Nester, E. W. (1977) Stable incorporation of plasmid DNA into higher plant cells: the molecular basis of crown gall tumorigenesis. *Cell*, 11, 263-271.
- Choi, J., Choi, D., Lee, S., Ryu, C.-M. & Hwang, I. (2011) Cytokinins and plant immunity: old foes or new friends? *Trends in Plant Science*, 16, 388-394.
- Chong, J., Piron, M.-C., Meyer, S., Merdinoglu, D., Bertsch, C. & Mestre, P. (2014) The SWEET family of sugar transporters in grapevine: VvSWEET4 is involved in the interaction with *Botrytis cinerea*. *Journal of Experimental Botany*, 65, 6589-6601.
- Chou, H.-M., Bundock, N., Rolfe, S. A. & Scholes, J. D. (2000) Infection of *Arabidopsis thaliana* leaves with *Albugo candida* (white blister rust) causes a reprogramming of host metabolism. *Molecular Plant Pathology*, 1, 99-113.
- Cohn, M., Bart, R. S., Shybut, M., Dahlbeck, D., Gomez, M., Morbitzer, R., Hou, B.-H., Frommer, W. B., Lahaye, T. & Staskawicz, B. J. (2014) *Xanthomonas axonopodis* Virulence Is Promoted by a Transcription Activator-Like Effector Mediated Induction of a SWEET Sugar Transporter in Cassava. *Molecular Plant-Microbe Interactions*, 27, 1186-1198.

- De Ascensao, A. R. F. D. C. & Dubery, I. A. (2003) Soluble and wall-bound phenolics and phenolic polymers in *Musa acuminata* roots exposed to elicitors from *Fusarium oxysporum f.sp. cubense*. *Phytochemistry*, 63, 679-686.
- Dekhuijzen, H. M. & Overeem, J. C. (1971) The role of cytokinins in clubroot formation. *Physiological Plant Pathology*, 1, 151-161.
- Dekhuijzen, H. M. (1981) The occurrence of free and bound cytokinins in plasmodia of *Plasmodiophora brassicae* isolated from tissue cultures of clubroots. *Plant cell reports*, 1, 18-20.
- Denslow, S. A., Walls, A. A. & Daub, M. E. (2005) Regulation of biosynthetic genes and antioxidant properties of vitamin B-6 vitamers during plant defense responses. *Physiological and Molecular Plant Pathology*, 66, 244-255.
- Dessaux, Y., Petit, A. & Tempe, J. (1993) Chemistry and biochemistry of opines, chemical mediators of parasitism. *Phytochemistry*, 34, 31-38.
- Devos, S., Laukens, K., Deckers, P., Van Der Straeten, D., Beeckman, T., Inze, D., Van Onckelen, H., Witters, E. & Prinsen, E. (2006) A hormone and proteome approach to picturing the initial metabolic events during *Plasmodiophora brassicae* infection on *Arabidopsis*. *Molecular Plant-Microbe Interactions*, 19, 1431-1443.
- Devos, S., Vissenberg, K., Verbelen, J. P. & Prinsen, E. (2005) Infection of Chinese cabbage by *Plasmodiophora brassicae* leads to a stimulation of plant growth: impacts on cell wall metabolism and hormone balance. *New Phytologist*, 166, 241-250.
- Divon, H. H. & Fluhr, R. (2007) Nutrition acquisition strategies during fungal infection of plants. *FEMS Microbiology Letters*, 266, 65-74.
- Dixon, G. R. (2009) The occurrence and economic impact of *Plasmodiophora brassicae* and clubroot Disease. *Journal of Plant Growth Regulation*, 28, 194-202.
- Dixon, R. A. & Paiva, N. L. (1995) Stress-induced phenylpropanoid metabolism. *The Plant Cell*, 7, 1085-1097.
- Djamei, A. & Kahmann, R. (2012) *Ustilago maydis*: Dissecting the molecular interface between pathogen and plant. *Plos Pathogens*, 8.
- Doidy, J., Grace, E., Kuehn, C., Simon-Plas, F., Casieri, L. & Wipf, D. (2012) Sugar transporters in plants and in their interactions with fungi. *Trends in Plant Science*, 17, 413-422.

- Donald, E. C., Lawrence, J. M. & Porter, I. J. (2002) Evaluation of a fluorescent staining technique as an indicator of pathogenicity of resting spores of *Plasmodiophora brassicae*. *Australasian Plant Pathology*, 31, 373-379.
- D'ovidio, R., Mattei, B., Roberti, S. & Bellincampi, D. (2004) Polygalacturonases, polygalacturonase-inhibiting proteins and pectic oligomers in plant pathogen interactions. *Biochimica et Biophysica Acta (BBA) - Proteins and Proteomics*, 1696, 237-244.
- Emery, R. J. N., Leport, L., Barton, J. E., Turner, N. C. & Atkins, C. A. (1998) cis - Isomers of cytokinins predominate in chickpea seeds throughout their development. *Plant Physiology*, 117, 1515-1523.
- Etchells, J. P., Provost, C. M. & Turner, S. R. (2012) Plant vascular cell division Is maintained by an interaction between PXY and ethylene signalling. *Plos Genetics*, 8.
- Evans, J. L. & Scholes, J. D. (1996) The effect of clubroot upon the carbon metabolism of its host? *Journal of Experimental Botany*, 47, 72-72.
- Faggian, R. & Strelkov, S. E. (2009) Detection and measurement of *Plasmodiophora brassicae*. *Journal of Plant Growth Regulation*, 28, 282-288.
- Feng, J., Hwang, R., Hwang, S.-F., Strelkov, S. E., Gossen, B. D., Zhou, Q.-X. & Peng, G. (2010) Molecular characterization of a serine protease Pro1 from *Plasmodiophora brassicae* that stimulates resting spore germination. *Molecular Plant Pathology*, 11, 503-512.
- Fernandez, O., Bã©thencourt, L., Quero, A., Sangwan, R. S. & Clã©ment, C. (2010) Trehalose and plant stress responses: friend or foe? *Trends in Plant Science*, 15, 409-417.
- Ferrari, S., Vairo, D., Ausubel, F. M., Cervone, F. & De Lorenzo, G. (2003) Tandemly duplicated *Arabidopsis* genes that encode polygalacturonase-inhibiting proteins are regulated coordinately by different signal transduction pathways in response to fungal infection. *The Plant Cell*, 15, 93-106.
- Fester, T., Berg, R. H. & Taylor, C. G. (2008) An easy method using glutaraldehyde-introduced fluorescence for the microscopic analysis of plant biotrophic interactions. *Journal of Microscopy*, 231, 342-348.
- Flores-Mireles, A. L., Eberhard, A. & Winans, S. C. (2012) *Agrobacterium tumefaciens* can Obtain Sulfur from an Opine that is Synthesized by Octopine

- Synthase Using S-methylmethionine as a Substrate. *Molecular Microbiology*, 84, 845-856.
- Fotopoulos, V., Gilbert, M. J., Pittman, J. K., Marvier, A. C., Buchanan, A. J., Sauer, N., Hall, J. L. & Williams, L. E. (2003) The monosaccharide transporter gene, AtSTP4, and the cell-wall invertase, At beta fruct1, are induced in *Arabidopsis* during infection with the fungal biotroph *Erysiphe cichoracearum*. *Plant Physiology*, 132, 821-829.
- Gao, L., Kelliher, T., Nguyen, L. & Walbot, V. (2013) *Ustilago maydis* reprograms cell proliferation in maize anthers. *Plant Journal*, 75, 903-914.
- Garavito, M. F., Narváez-Ortiz, H. Y. & Zimmermann, B. H. (2015) Pyrimidine metabolism: Dynamic and versatile pathways in pathogens and cellular development. *Journal of Genetics and Genomics*, 42, 195-205.
- Garnica, D. P., Upadhyaya, N. M., Dodds, P. N. & Rathjen, J. P. (2013) Strategies for wheat stripe rust pathogenicity identified by transcriptome sequencing. *Plos One*, 8, e67150.
- Gelvin, S. B. (2010) Plant proteins involved in *Agrobacterium*-mediated genetic transformation. *Annual Review of Phytopathology*, Vol 48.
- Gelvin, S. B. (2012) Traversing the cell: *Agrobacterium* T-DNA's journey to the host genome. *Frontiers in plant science*, 3, 52.
- Gendreau, E., Traas, J., Desnos, T., Grandjean, O., Caboche, M. & Hofte, H. (1997) Cellular basis of hypocotyl growth in *Arabidopsis thaliana*. *Plant Physiology*, 114, 295-305.
- Gibb, S. & Strimmer, K. (2012) MALDIquant: a versatile R package for the analysis of mass spectrometry data. *Bioinformatics*, 28, 2270-2271.
- Goethals, K., Vereecke, D., Jaziri, M., Van Montagu, M. & Holsters, M. (2001) Leafy gall formation by *Rhodococcus fascians*. *Annual Review of Phytopathology*, 39, 27-52.
- Gohlke, J. & Deeken, R. (2014) Plant responses to *Agrobacterium tumefaciens* and crown gall development. *Frontiers in plant science*, 5.
- Graveland, R., Dale, P. & Mithen, R. (1992) Gall development in hairy root cultures infected with *Plasmodiophora brassicae*. *Mycological Research*, 96, 225-228.

- Grsic-Rausch, S., Kobelt, P., Siemens, J. M., Bischoff, M. & Ludwig-Muller, J. (2000) Expression and localization of nitrilase during symptom development of the clubroot disease in *Arabidopsis*. *Plant Physiology*, 122, 369-378.
- Gruner, K., Griebel, T., Navarova, H., Attaran, E. & Zeier, J. (2013) Reprogramming of plants during systemic acquired resistance. *Frontiers in plant science*, 4.
- Guo, W.-J., Nagy, R., Chen, H.-Y., Pfrunder, S., Yu, Y.-C., Santelia, D., Frommer, W. B. & Martinoia, E. (2014) SWEET17, a Facilitative Transporter, Mediates Fructose Transport across the Tonoplast of *Arabidopsis* Roots and Leaves. *Plant Physiology*, 164, 777-789.
- Hackstadt, A. J. & Hess, A. M. (2009) Filtering for increased power for microarray data analysis. *BMC Bioinformatics*, 10, 11-11.
- Hajirezaei, M. R., Takahata, Y., Trethewey, R. N., Willmitzer, L. & Sonnewald, U. (2000) Impact of elevated cytosolic and apoplastic invertase activity on carbon metabolism during potato tuber development. *Journal of Experimental Botany*, 51, 439-445.
- Hamann, T., Bennett, M., Mansfield, J. & Somerville, C. (2009) Identification of cell-wall stress as a hexose-dependent and osmosensitive regulator of plant responses. *Plant Journal*, 57, 1015-1026.
- Hammes, U. Z., Schachtman, D. P., Berg, R. H., Nielsen, E., Koch, W., McIntyre, L. M. & Taylor, C. G. (2005) Nematode-Induced Changes of Transporter Gene Expression in *Arabidopsis* Roots. *Molecular Plant-Microbe Interactions*, 18, 1247-1257.
- Harholt, J., Suttangkakul, A. & Vibe Scheller, H. (2010) Biosynthesis of pectin. *Plant Physiology*, 153, 384-395.
- Heller, A. & Thines, M. (2009) Evidence for the importance of enzymatic digestion of epidermal walls during subepidermal sporulation and pustule opening in white blister rusts (*Albuginaceae*). *Mycological Research*, 113, 657-667.
- Heuberger, A. L., Robison, F. M., Lyons, S. M. A., Broeckling, C. D. & Prenni, J. E. (2014) Evaluating plant immunity using mass spectrometry-based metabolomics workflows. *Frontiers in Plant Science*, 5.
- Heyl, A. & Schmulling, T. (2003) Cytokinin signal perception and transduction. *Current Opinion in Plant Biology*, 6, 480-488.
- Hietala, A. M., Kvaalen, H., Schmidt, A., Johnk, N., Solheim, H. & Fossdal, C. G. (2004) Temporal and spatial profiles of chitinase expression by Norway

spruce in response to bark colonization by *Heterobasidion annosum*. *Applied and Environmental Microbiology*, 70, 3948-3953.

- Hofmann, J. & Grundler, F. M. (2008) Starch as a sugar reservoir for nematode-induced syncytia. *Plant signaling & behavior*, 3, 961-2.
- Hofmann, J., Szakasits, D., Bloechl, A., Sobczak, M., Daxboeck-Horvath, S., Golinowski, W., Bohlmann, H. & Grundler, F. M. W. (2008) Starch serves as carbohydrate storage in nematode-induced syncytia. *Plant Physiology*, 146, 228-235.
- Hofmann, J., Wieczorek, K., Bloechl, A. & Grundler, F. M. W. (2007) Sucrose supply to nematode-induced syncytia depends on the apoplasmic and symplasmic pathways. *Journal of Experimental Botany*, 58, 1591-1601.
- Hong, J. K. & Hwang, B. K. (2002) Induction by pathogen, salt and drought of a basic class II chitinase mRNA and its in situ localization in pepper (*Capsicum annuum*). *Physiologia Plantarum*, 114, 549-558.
- Hoth, S., Schneidereit, A., Lauterbach, C., Scholz-Starke, J. & Sauer, N. (2005) Nematode infection triggers the *de novo* formation of unloading phloem that allows macromolecular trafficking of green fluorescent protein into syncytia. *Plant Physiology*, 138, 383-392.
- Howard, R. J., Strelkov, S. E. & Harding, M. W. (2010) Clubroot of cruciferous crops - new perspectives on an old disease. *Canadian Journal of Plant Pathology- Revue Canadienne De Phytopathologie*, 32, 43-57.
- Hu, Y., Zhang, J., Jia, H., Sosso, D., Li, T., Frommer, W. B., Yang, B., White, F. F., Wang, N. & Jones, J. B. (2014) Lateral organ boundaries 1 is a disease susceptibility gene for citrus bacterial canker disease. *Proceedings of the National Academy of Sciences*, 111, E521-E529.
- Irizarry, R. A., Hobbs, B., Collin, F., Beazer-Barclay, Y. D., Antonellis, K. J., Scherf, U. & Speed, T. P. (2003) Exploration, normalization, and summaries of high density oligonucleotide array probe level data. *Biostatistics*, 4, 249-264.
- Jain, A., Singh, A., Singh, S. & Singh, H. B. (2015) Phenols enhancement effect of microbial consortium in pea plants restrains *Sclerotinia sclerotiorum*. *Biological Control*, 89, 23-32.
- Jain, A., Singh, S., Kumar Sarma, B. & Bahadur Singh, H. (2012) Microbial consortium-mediated reprogramming of defence network in pea to enhance tolerance against *Sclerotinia sclerotiorum*. *Journal of Applied Microbiology*, 112, 537-550.

- Jarvis, M. C., Briggs, S. P. H. & Knox, J. P. (2003) Intercellular adhesion and cell separation in plants. *Plant Cell and Environment*, 26, 977-989.
- Jones, J. D. G. & Dangl, J. L. (2006) The plant immune system. *Nature*, 444, 323-329.
- Jubault, M., Hamon, C., Gravot, A., Lariagon, C., Delourme, R., Bouchereau, A. & Manzanares-Dauleux, M. J. (2008) Differential regulation of root arginine catabolism and polyamine metabolism in clubroot-susceptible and partially resistant *Arabidopsis* genotypes. *Plant Physiology*, 146, 2008-2019.
- Jubault, M., Lariagon, C., Taconnat, L., Renou, J.-P., Gravot, A., Delourme, R. & Manzanares-Dauleux, M. J. (2013) Partial resistance to clubroot in *Arabidopsis* is based on changes in the host primary metabolism and targeted cell division and expansion capacity. *Functional and Integrative Genomics*, 13, 191-205.
- Juergensen, K., Scholz-Starke, J., Sauer, N., Hess, P., Van Bel, A. J. E. & Grundler, F. M. W. (2003) The companion cell-specific *Arabidopsis* disaccharide carrier AtSUC2 is expressed in nematode-induced syncytia. *Plant Physiology*, 131, 61-69.
- Kaever, A., Landesfeind, M., Possienke, M., Feussner, K., Feussner, I. & Meinicke, P. (2012) MarVis-Filter: Ranking, Filtering, Adduct and Isotope Correction of Mass Spectrometry Data. *Journal of Biomedicine and Biotechnology*, 2012, 7.
- Kageyama, K. & Asano, T. (2009) Life Cycle of *Plasmodiophora brassicae*. *Journal of Plant Growth Regulation*, 28, 203-211.
- Kakimoto, T. (2001) Identification of plant cytokinin biosynthetic enzymes as dimethylallyl diphosphate:ATP/ADP isopentenyltransferases. *Plant and Cell Physiology*, 42, 677-685.
- Katahira, R. & Ashihara, H. (2006) Dual function of pyrimidine metabolism in potato (*Solanum tuberosum*) plants: pyrimidine salvage and supply of [beta]-alanine to pantothenic acid synthesis. *Physiologia Plantarum*, 127, 38-43.
- Kaspar, S., Peukert, M., Svatos, A., Matros, A. & Mock, H.-P. (2011) MALDI-imaging mass spectrometry - An emerging technique in plant biology. *Proteomics*, 11, 1840-1850.
- Keen, N. T. & Williams, P. H. (1969) Synthesis and degradation of starch and lipids following infection of cabbage by *Plasmodiophora brassicae* *Phytopathology*, 59, 778.

- Kemen, E., Gardiner, A., Schultz-Larsen, T., Kemen, A. C., Balmuth, A. L., Robert-Seilaniantz, A., Bailey, K., Holub, E., Studholme, D. J., Maclean, D. & Jones, J. D. G. (2011) Gene gain and loss during evolution of obligate parasitism in the white rust pathogen of *Arabidopsis thaliana*. *PLoS Biology*, 9, e1001094.
- Kim, Y. J. & Hwang, B. K. (1994) Differential accumulation of beta-1,3-glucanase and chitinase isoforms in pepper stems infected by compatible and incompatible isolates of *Phytophthora capsici*. *Physiological and Molecular Plant Pathology*, 45, 195-209.
- Kim, D. S., Kim, N. H. & Hwang, B. K. (2015) The *Capsicum annuum* class IV chitinase ChitIV interacts with receptor-like cytoplasmic protein kinase PIK1 to accelerate PIK1-triggered cell death and defence responses. *Journal of Experimental Botany*, 66, 1987-1999.
- Knaus, A. & Ludwig-Mueller, J. (2013) The ethylene signalling pathway is needed to restrict root gall growth in *Arabidopsis* after infection with the obligate biotrophic protist *Plasmodiophora brassicae*. *Journal of Plant Growth Regulation*, 32, 9-21.
- Kobelt, P., Siemens, J. & Sacristan, M. D. (2000) Histological characterisation of the incompatible interaction between *Arabidopsis thaliana* and the obligate biotrophic pathogen *Plasmodiophora brassicae*. *Mycological Research*, 104, 220-225.
- Koch, E., Cox, R. & Williams, P. H. (1991) Infection of *Arabidopsis thaliana* by *Plasmodiophora brassicae*. *Journal of Phytopathology-Phytopathologische Zeitschrift*, 132, 99-104.
- Lang, J., Vigouroux, A., Planamente, S., El Sahili, A., Blin, P., Aumont-Nicaise, M., Dessaux, Y., Morera, S. & Faure, D. (2014) *Agrobacterium* uses a unique ligand-binding mode for trapping opines and acquiring a competitive advantage in the niche construction on plant host. *Plos Pathogens*, 10.
- Lanver, D., Berndt, P., Tollot, M., Naik, V., Vranes, M., Warmann, T., Muench, K., Roessel, N. & Kahmann, R. (2014) Plant Surface Cues Prime *Ustilago maydis* for Biotrophic Development. *Plos Pathogens*, 10.
- Lee, Y. K., Hippe-Sanwald, S., Jung, H. W., Hong, J. K., Hause, B. & Hwang, B. K. (2000) In situ localization of chitinase mRNA and protein in compatible and incompatible interactions of pepper stems with *Phytophthora capsici*. *Physiological and Molecular Plant Pathology*, 57, 111-121.
- Lemarie, S., Robert-Seilaniantz, A., Lariagon, C., Lemoine, J., Marnet, N., Levrel, A., Jubault, M., Manzanares-Dauleux, M. J. & Gravot, A. (2015) Camalexin

- contributes to the partial resistance of *Arabidopsis thaliana* to the biotrophic soilborne protist *Plasmodiophora brassicae*. *Frontiers in plant science*, 6.
- Li, B., Liu, H., Zhang, Y., Kang, T., Zhang, L., Tong, J., Xiao, L. & Zhang, H. (2013) Constitutive expression of cell wall invertase genes increases grain yield and starch content in maize. *Plant Biotechnology Journal*, 11, 1080-1091.
- Liesche, J. & Schulz, A. (2012) Quantification of plant cell coupling with three-dimensional photoactivation microscopy. *Journal of Microscopy*, 247, 2-9.
- Links, M. G., Holub, E., Jiang, R. H. Y., Sharpe, A. G., Hegedus, D., Beynon, E., Sillito, D., Clarke, W. E., Uzuhashi, S. & Borhan, M. H. (2011) *De novo* sequence assembly of *Albugo candida* reveals a small genome relative to other biotrophic oomycetes. *Bmc Genomics*, 12.
- Loewus, F. A. & Loewus, M. W. (1983) Myoinositol- its biosynthesis and metabolism. *Annual Review of Plant Physiology and Plant Molecular Biology*, 34, 137-161.
- Lovelock, D. A., Donald, C. E., Conlan, X. A. & Cahill, D. M. (2013) Salicylic acid suppression of clubroot in broccoli (*Brassica oleracea* var. *italica*) caused by the obligate biotroph *Plasmodiophora brassicae*. *Australasian Plant Pathology*, 42, 141-153.
- Ludwig-Muller, J. & Schuller, A. (2008) What can we learn from clubroots: alterations in host roots and hormone homeostasis caused by *Plasmodiophora brassicae*. *European Journal of Plant Pathology*, 121, 291-302.
- Ludwig-Muller, J., Juelke, S., Geiss, K., Richter, F., Mithoefer, A., Sola, I., Rusak, G., Keenan, S. & Bulman, S. (2015) A novel methyltransferase from the intracellular pathogen *Plasmodiophora brassicae* methylates salicylic acid. *Molecular Plant Pathology*, 16, 349-364.
- Ludwig-Muller, J., Prinsen, E., Rolfe, S. A. & Scholes, J. D. (2009) Metabolism and Plant Hormone Action During Clubroot Disease. *Journal of Plant Growth Regulation*, 28, 229-244.
- Ludwig-Muller, J., Bendel, U., Thermann, P., Ruppel, M., Epstein, E. & Hilgenberg, W. (1993) Concentration of indole-3-acetic acid in plants of tolerant and susceptible varieties of Chinese cabbage infected with *Plasmodiophora brassicae* var. *woron*. *New Phytologist*, 125, 763-769.
- Ludwig-Muller, J., Bennett, R. N., Kiddle, G., Ihmig, S., Ruppel, M. & Hilgenberg, W. (1999b) The host range of *Plasmodiophora brassicae* and its relationship to endogenous glucosinolate content. *New Phytologist*, 141, 443-458.

- Ludwig-Muller, J., Pieper, K., Ruppel, M., Cohen, J. D., Epstein, E., Kiddle, G. & Bennett, R. (1999a) Indole glucosinolate and auxin biosynthesis in *Arabidopsis thaliana* (L.) Heynh. glucosinolate mutants and the development of clubroot disease. *Planta*, 208, 409-419.
- Luna, E., Pastor, V., Robert, J. R. M., Flors, V., Mauch-Mani, B. & Ton, J. (2011) Callose Deposition: A Multifaceted Plant Defense Response. *Molecular Plant-Microbe Interactions*, 24, 183-193.
- Maag, D., Erb, M. & Glauser, G. (2015) Metabolomics in plant-herbivore interactions: challenges and applications. *Entomologia Experimentalis Et Applicata*, 157, 18-29.
- Macfalane, I. & Last, F. T. (1959) Some effects of *Plasmodiophora brassicae* Woron. on the growth of the young cabbage plant. *Annals of Botany*, 23, 547-570.
- Malinowski, R., Smith, J. A., Fleming, A. J., Scholes, J. D. & Rolfe, S. A. (2012) Gall formation in clubroot-infected *Arabidopsis* results from an increase in existing meristematic activities of the host but is not essential for the completion of the pathogen life cycle. *Plant Journal*, 71, 226-238.
- Malinowski, R., Novák, O., Borhan, M. H., Spíchal, L., Strnad, M. & Rolfe, S. A. (2016) The role of cytokinins in clubroot disease. *European Journal of Plant Pathology*, 1-15.
- Martin, T., Frommer, W. B., Salanoubat, M. & Willmitzer, L. (1993) Expression of an *Arabidopsis* sucrose synthase gene indicates a role in metabolization of sucrose both during phloem loading and in sink organs. *The Plant Journal*, 4, 367-377.
- Mcdonald, M. R., Sharma, K., Gossen, B. D., Deora, A., Feng, J. & Hwang, S.-F. (2014) The role of primary and secondary infection in host response to *Plasmodiophora brassicae*. *Phytopathology*, 104, 1078-1087.
- Micali, C. O., Neumann, U., Grunewald, D., Panstruga, R. & O'connell, R. (2011) Biogenesis of a specialized plant-fungal interface during host cell internalization of *Golovinomyces orontii* haustoria. *Cellular Microbiology*, 13, 210-226.
- Mithen, R. & Magrath, R. (1992) A contribution to the life history of *Plasmodiophora brassicae*: secondary plasmodia development in root galls of *Arabidopsis thaliana*. *Mycological Research*, 96, 877-885.

- Mithen, R. & Magrath, R. (1992) A contribution to the life history of *Plasmodiophora brassicae*: secondary plasmodia development in root galls of *Arabidopsis thaliana*. *Mycological Research*, 96, 877-885.
- Miyawaki, K., Tarkowski, P., Matsumoto-Kitano, M., Kato, T., Sato, S., Tarkowska, D., Tabata, S., Sandberg, G. & Kakimoto, T. (2006) Roles of *Arabidopsis* ATP/ADP isopentenyltransferases and tRNA isopentenyltransferases in cytokinin biosynthesis. *Proceedings of the National Academy of Sciences of the United States of America*, 103, 16598-16603.
- Mok, D. W. S. & Mok, M. C. (2001) Cytokinin metabolism and action. *Annual Review of Plant Physiology and Plant Molecular Biology*, 52, 89-118.
- Muenha, S., Lingner, U., Floss, D. S., Ludwig, N., Sauer, N. & Deising, H. B. (2008) The hemibiotrophic lifestyle of *Colletotrichum* species. *Journal of Plant Physiology*, 165, 41-51.
- Muller P. & Hilgenberg, W. (1986) Isomers of zeatin and zeatin riboside in clubroot tissue-evidence for trans-zeatin biosynthesis by *Plasmodiophora brassicae* *Physiologia Plantarum*, 66, 245-250.
- Naiki, T., Kawaguchi, C. & Ikegami, H. (1984) Root hair reinfection in Chinese cabbage seedlings by the secondary zoospores of *Plasmodiophora brassicae* *Annals of the Phytopathological Society of Japan*, 50, 216-220.
- Neueschwander, U., Suter, M. & Brunold, C. (1991) Regulation of sulfate assimilation by light and O-Acetyl-L-Serine in *Lemna minor* L. *Plant Physiology*, 97, 253-258.
- Neuhuser, S. & Kirchmair, M. (2011) *Sorosphaerula* nom. n. for the Plasmodiophorid Genus *Sorosphaera* J. Schroter 1886 (Rhizaria: Endomyxa: Phytomyxea: Plasmodiophorida). *Journal of Eukaryotic Microbiology*, 58, 469-470.
- Oliver R. P. & Ipcho, S. V. S. (2004) *Arabidopsis* pathology breathes new life into the necrotrophs-vs.-biotrophs classification of fungal pathogens. *Molecular Plant Pathology*, 5, 347-352.
- Ott, P. G., Varga, G. J., Szatmari, A., Bozso, Z., Klement, E., Medzihradzsky, K. F., Besenyi, E., Czalleng, A. & Klement, Z. (2006) Novel extracellular chitinases rapidly and specifically induced by general bacterial elicitors and suppressed by virulent bacteria as a marker of early basal resistance in tobacco. *Molecular Plant-Microbe Interactions*, 19, 161-172.
- Paesold, S. & Ludwig-Mueller, J. (2013) Reduction of clubroot (*Plasmodiophora brassicae*) formation in *Arabidopsis thaliana* after treatment with

- prohexadione-calcium, an inhibitor of oxoglutaric acid-dependent dioxygenases. *Plant Pathology*, 62, 1357-1365.
- Paesod, S., Siegel, I., Seidel, C. & Ludwig-Mueller, J. (2010) Flavonoid accumulation in *Arabidopsis thaliana* root galls caused by the obligate biotrophic pathogen *Plasmodiophora brassicae*. *Molecular Plant Pathology*, 11, 545-562.
- Parker, D., Beckmann, M., Zubair, H., Enot, D. P., Caracuel-Rios, Z., Overy, D. P., Snowdon, S., Talbot, N. J. & Draper, J. (2009) Metabolomic analysis reveals a common pattern of metabolic re-programming during invasion of three host plant species by *Magnaporthe grisea*. *Plant Journal*, 59, 723-737.
- Pedras, M. S. C., Zheng, Q.-A. & Strelkov, S. (2008) Metabolic changes in roots of the oilseed canola infected with the biotroph *Plasmodiophora brassicae*: phytoalexins and phytoanticipins. *Journal of Agricultural and Food Chemistry*, 56, 9949-9961.
- Perez-Martin, J., Castillo-Lluva, S., Sgarlata, C., Flor-Parra, I., Mielnichuk, N., Torreblanca, J. & Carbo, N. (2006) Pathocycles: *Ustilago maydis* as a model to study the relationships between cell cycle and virulence in pathogenic fungi. *Molecular Genetics and Genomics*, 276, 211-229.
- Perez-Nadales, E., Nogueira, M. F. A., Baldin, C., Castanheira, S., El Ghalid, M., Grund, E., Lengeler, K., Marchegiani, E., Mehrotra, P. V., Moretti, M., Naik, V., Oses-Ruiz, M., Oskarsson, T., Schaefer, K., Wasserstrom, L., Brakhage, A. A., Gow, N. A. R., Kahmann, R., Lebrun, M.-H., Perez-Martin, J., Di Pietro, A., Talbot, N. J., Toquin, V., Walther, A. & Wendland, J. (2014) Fungal model systems and the elucidation of pathogenicity determinants. *Fungal Genetics and Biology*, 70, 42-67.
- Pertry I., Vaclavikova, K., Depuydt, S., Galuszka, P., Spichal, L., Temmerman, W., Stes, E., Schmuelling, T., Kakimoto, T., Van Montagu, M. C. E., Strnad, M., Holsters, M., Tarkowski, P. & Vereecke, D. (2009) Identification of *Rhodococcus fascians* cytokinins and their modus operandi to reshape the plant. *Proceedings of the National Academy of Sciences of the United States of America*, 106, 929-934.
- Quilliam, R. S. (2006) The role of cell wall invertase activity in source-sink relations in vegetative tissues of *Arabidopsis thaliana* and in response to wounding and pathogen infection. *Department of Animal and Plant Sciences*. Sheffield, The University of Sheffield.
- Raa, A. N. (1971) Indole-3-acetic acid levels and the role of indole-3-acetic acid oxidase in the normal root and club-root of cabbage. *Physiologia Plantarum*, 25, 130-134.

- Redkar, A., Hoser, R., Schilling, L., Zechmann, B., Krzymowska, M., Walbot, V. & Doehlemann, G. (2015) A secreted effector protein of *Ustilago maydis* guides maize leaf cells to form tumors. *Plant Cell*, 27, 1332-1351.
- Ridley B. L., O'Neill, M. A. & Mohnen, D. (2001) Pectins: structure, biosynthesis, and oligogalacturonide-related signaling. *Phytochemistry*, 57, 929-967.
- Riemenschneider, A., Nikiforova, V., Hoefgen, R., De Kok, L. J. & Papenbrock, J. (2005a) Impact of elevated H<sub>2</sub>S on metabolite levels, activity of enzymes and expression of genes involved in cysteine metabolism. *Plant Physiology and Biochemistry*, 43, 473-483.
- Riemenschneider, A., Riedel, K., Hoefgen, R., Papenbrock, J. & Hesse, H. (2005b) Impact of reduced O-acetylserine(thiol)lyase isoform contents on potato plant metabolism. *Plant Physiology*, 137, 892-900.
- Rieseier, J. W., Willmitzer, L. & Frommer, W. B. (1994) Evidence for an essential role of the sucrose transporter in phloem loading and assimilate partitioning. *Embo Journal*, 13, 1-7.
- Roberts, L. D., Souza, A. L., Gerszten, R. E. & Clish, C. B. (2012) Targeted Metabolomics. *Current Protocols in Molecular Biology*, CHAPTER, Unit30.2-Unit30.2.
- Roitsch, T. & Ehness, R. (2000) Regulation of source/sink relations by cytokinins. *Plant Growth Regulation*, 32, 359-367.
- Roitsch, T. (1999) Source-sink regulation by sugar and stress. *Current Opinion in Plant Biology*, 2, 198-206.
- Ryder L. S. & Talbot, N. J. (2015) Regulation of appressorium development in pathogenic fungi. *Current Opinion in Plant Biology*, 26, 8-13.
- Sakakibara, H. (2006) Cytokinins: Activity, biosynthesis, and translocation. *Annual Review of Plant Biology*.
- Schluepmann, H., Pellny, T., Van Dijken, A., Smeekens, S. & Paul, M. (2003) Trehalose 6-phosphate is indispensable for carbohydrate utilization and growth in *Arabidopsis thaliana*. *Proceedings of the National Academy of Sciences of the United States of America*, 100, 6849-6854.
- Schluepmann, H., Van Dijken, A., Aghdasi, M., Wobbes, B., Paul, M. & Smeekens, S. (2004) Trehalose mediated growth inhibition of *Arabidopsis* seedlings is due to trehalose-6-phosphate accumulation. *Plant Physiology*, 135, 879-890.

- Schuller, A., Kehr, J. & Ludwig-Mueller, J. (2014) Laser Microdissection Coupled to Transcriptional Profiling of *Arabidopsis* Roots Inoculated by *Plasmodiophora brassicae* Indicates a Role for Brassinosteroids in Clubroot Formation. *Plant and Cell Physiology*, 55, 392-411.
- Schwelm, A., Fogelqvist, J., Knaust, A., Juelke, S., Lilja, T., Bonilla-Rosso, G., Karlsson, M., Shevchenko, A., Dhandapani, V., Choi, S. R., Kim, H. G., Park, J. Y., Lim, Y. P., Ludwig-Mueller, J. & Dixelius, C. (2015) The *Plasmodiophora brassicae* genome reveals insights in its life cycle and ancestry of chitin synthases. *Scientific Reports*, 5.
- Shulaev, V. (2006) Metabolomics technology and bioinformatics. *Briefings in Bioinformatics*, 7, 128-139.
- Shulaev, V., Cortes, D., Miller, G. & Mittler, R. (2008) Metabolomics for plant stress response. *Physiologia Plantarum*, 132, 199-208.
- Siemens, J., Glawischnig, E. & Ludwig-Mueller, J. (2008) Indole glucosinolates and camalexin do not influence the development of the clubroot disease in *Arabidopsis thaliana*. *Journal of Phytopathology*, 156, 332-337.
- Siemens, J., Gonzalez, M.-C., Wolf, S., Hofmann, C., Greiner, S., Du, Y., Rausch, T., Roitsch, T. & Ludwig-Mueller, J. (2011) Extracellular invertase is involved in the regulation of clubroot disease in *Arabidopsis thaliana*. *Molecular Plant Pathology*, 12, 247-262.
- Siemens, J., Keller, I., Sarx, J., Kunz, S., Schuller, A., Nagel, W., Schmulling, T., Parniske, M. & Ludwig-Mueller, J. (2006) Transcriptome analysis of *Arabidopsis* clubroots indicate a key role for cytokinins in disease development. *Molecular Plant-Microbe Interactions*, 19, 480-494.
- Smith, F. W., Hawkesford, M. J., Ealing, P. M., Clarkson, D. T., Vandenberg, P. J., Belcher, A. R. & Warrilow, G. S. (1997) Regulation of expression of a cDNA from barley roots encoding a high affinity sulphate transporter. *Plant Journal*, 12, 875-884.
- Song, G. C., Choi, H. K. & Ryu, C.-M. (2013) The folate precursor para-aminobenzoic acid elicits induced resistance against Cucumber mosaic virus and *Xanthomonas axonopodis*. *Annals of Botany*, 111, 925-934.
- Sonnewald, S., Priller, J. P. R., Schuster, J., Glickmann, E., Hajirezaei, M.-R., Siebig, S., Mudgett, M. B. & Sonnewald, U. (2012) Regulation of Cell Wall-Bound

- Invertase in Pepper Leaves by *Xanthomonas campestris* pv. *vesicatoria* Type Three Effectors. *Plos One*, 7.
- Spichal, L. (2012) Cytokinins - recent news and views of evolutionally old molecules. *Functional Plant Biology*, 39, 267-284.
- Srivastava, A. C., Ganesan, S., Ismail, I. O. & Ayre, B. G. (2008) Functional Characterization of the *Arabidopsis* AtSUC2 Sucrose/H<sup>+</sup> Symporter by Tissue-Specific Complementation Reveals an Essential Role in Phloem Loading But Not in Long-Distance Transport. *Plant Physiology*, 148, 200-211.
- Stasolla, C., Katahira, R., Thorpe, T. A. & Ashihara, H. (2003) Purine and pyrimidine nucleotide metabolism in higher plants. *Journal of Plant Physiology*, 160, 1271-1295.
- Stes, E., Francis, I., Pertry, I., Dolzblasz, A., Depuydt, S. & Vereecke, D. (2013) The leafy gall syndrome induced by *Rhodococcus fascians*. *FEMS Microbiology Letters*, 342, 187-195.
- Stes, E., Prinsen, E., Holsters, M. & Vereecke, D. (2012) Plant-derived auxin plays an accessory role in symptom development upon *Rhodococcus fascians* infection. *Plant Journal*, 70, 513-527.
- Sumner, L. W., Mendes, P. & Dixon, R. A. (2003) Plant metabolomics: large-scale phytochemistry in the functional genomics era. *Phytochemistry*, 62, 817-836.
- Sutton, P. N., Gilbert, M. J., Williams, L. E. & Hall, J. L. (2007) Powdery mildew infection of wheat leaves changes host solute transport and invertase activity. *Physiologia Plantarum*, 129, 787-795.
- Sutton, P. N., Henry, M. J. & Hall, J. L. (1999) Glucose, and not sucrose, is transported from wheat to wheat powdery mildew. *Planta*, 208, 426-430.
- Suzuki, K., Matsumiya, E., Ueno, Y. & Mizutani, J. (1992) Some properties of germination-stimulating factor from plants for resting spores of *Plasmodiophora brassicae*. *Annals of the Phytopathological Society of Japan*, 58, 699-705.
- Takagi, H. (2008) Proline as a stress protectant in yeast: physiological functions, metabolic regulations, and biotechnological applications. *Applied Microbiology and Biotechnology*, 81, 211-223.
- Takahashi, K. & Yamaguchi, T. (1988) A method for assessing the pathogenic activity of resting spores of *Plasmodiophora brassicae* by fluorescence microscopy. *Annals of the Phytopathological Society of Japan*, 54, 466-475.

- Takahashi, K. (1994) Influences of some environmental factors on the viability of resting spores of *Plasmodiophora brassicae* Wor. incubated in sterile soil. *Annals of the Phytopathological Society of Japan*, 60, 658-666.
- Tambasco-Studart, M., Titiz, O., Raschle, T., Forster, G., Amrhein, N. & Fitzpatrick, T. B. (2005) Vitamin B6 biosynthesis in higher plants. *Proceedings of the National Academy of Sciences of the United States of America*, 102, 13687-13692.
- Thompson, D. V., Melchers, L. S., Idler, K. B., Schilperoort, R. A. & Hooykaas, P. J. J. (1988) Analysis of the complete nucleotide sequence of the *Agrobacterium tumefaciens* VirB operon *Nucleic Acids Research*, 16, 4621-4636.
- Thornton, C. R., Jarvis, B. C. & Cooke, R. C. (1991) A chitin assay for the enumeration of *Plasmodiophora brassicae* resting spores in clubroot tissue. *Mycological Research*, 95, 879-882.
- Tommerup, I. C. & Ingram, D. S. (1971) Life-cycle of *Plasmodiophora brassicae* woron in brassica clutres and in intact roots *New Phytologist*, 70, 327-332.
- Van Kan, J. A. L. (2006) Licensed to kill: the lifestyle of a necrotrophic plant pathogen. *Trends in Plant Science*, 11, 247-253.
- Verma, P. R. & Petrie, G. A. (1980) Effect of seed infestation and flower bud inoculation on systemic infection of turnip rape by *Albugo candida*. *Canadian Journal of Plant Science*, 60, 266-271.
- Vladimirov, I. A., Matveeva, T. V. & Lutova, L. A. (2015) Opine biosynthesis and catabolism genes of *Agrobacterium tumefaciens* and *Agrobacterium rhizogenes*. *Russian Journal of Genetics*, 51, 121-129.
- Voegelé, R. T., Hahn, M., Lohaus, G., Link, T., Heiser, I. & Mendgen, K. (2005) Possible Roles for Mannitol and Mannitol Dehydrogenase in the Biotrophic Plant Pathogen *Uromyces fabae*. *Plant Physiology*, 137, 190-198.
- Voegelé, R. T., Struck, C., Hahn, M. & Mendgen, K. (2001) The role of haustoria in sugar supply during infection of broad bean by the rust fungus *Uromyces fabae*. *Proceedings of the National Academy of Sciences of the United States of America*, 98, 8133-8138.
- Wagner, G., Charton, S., Lariagon, C., Laperche, A., Lugan, R., Hopkins, J., Frendo, P., Bouchereau, A., Delourme, R., Gravot, A. & Manzanares-Dauleux, M. J. (2012) Metabotyping: A New Approach to Investigate Rapeseed (*Brassica napus* L.) Genetic Diversity in the Metabolic Response to Clubroot Infection. *Molecular Plant-Microbe Interactions*, 25, 1478-1491.

- Wahl, R., Wippel, K., Goos, S., Kaemper, J. & Sauer, N. (2010) A Novel High-Affinity Sucrose Transporter Is Required for Virulence of the Plant Pathogen *Ustilago maydis*. *Plos Biology*, 8.
- Walters, D. R. & Shuttleton, M. A. (1985) Polyamines in the roots of turnip infected with *Plasmodiophora brassicae* Wor *New Phytologist*, 100, 209-214.
- Ward, J. E., Akiyoshi, D. E., Regier, D., Datta, A., Gordon, M. P. & Nester, E. W. (1988) Characterization of the virB operon from an *Agrobacterium tumefaciens* Ti plasmid. *Journal of Biological Chemistry*, 263, 5804-5814.
- Webster, M. A. & Dixon, G. R. (1991) Calcium, pH and inoculum concentration influencing colonization by *Plasmodiophora brassicae* *Mycological Research*, 95, 64-73.
- Williams, P. H., Keen, N. T., Strandbe.Jo & Mcnabola, S. S. (1968) Metabolite synthesis and degradation during clubroot development in cabbage hypocotyls *Phytopathology*, 58, 921-928.
- Wittek, F., Kanawati, B., Wenig, M., Hoffmann, T., Franz-Oberdorf, K., Schwab, W., Schmitt-Kopplin, P. & Vlot, A. C. (2015) Folic acid induces salicylic acid-dependent immunity in *Arabidopsis* and enhances susceptibility to *Alternaria brassicicola*. *Molecular Plant Pathology*, 16, 616-622.
- Xia, J., Mandal, R., SineInikov, I. V., Broadhurst, D. & Wishart, D. S. (2012) MetaboAnalyst 2.0-a comprehensive server for metabolomic data analysis. *Nucleic Acids Research*, 40, W127-W133.
- Xia, J., SineInikov, I. V., Han, B. & Wishart, D. S. (2015) MetaboAnalyst 3.0-making metabolomics more meaningful. *Nucleic Acids Research*, 43, W251-W257.
- Yang, B., Sugio, A. & White, F. F. (2006) Os8N3 is a host disease-susceptibility gene for bacterial blight of rice. *Proceedings of the National Academy of Sciences*, 103, 10503-10508.
- Yogendra, K. N., Kushalappa, A. C., Sarmiento, F., Rodriguez, E. & Mosquera, T. (2015) Metabolomics deciphers quantitative resistance mechanisms in diploid potato clones against late blight. *Functional Plant Biology*, 42, 284-298.
- Yokotani, N., Tsuchida-Mayama, T., Ichikawa, H., Mitsuda, N., Ohme-Takagi, M., Kaku, H., Minami, E. & Nishizawa, Y. (2014) OsNAC111, a blast disease-responsive transcription factor in rice, positively regulates the expression of defense-related genes. *Molecular Plant-Microbe Interactions*, 27, 1027-1034.

- Yonekura-Sakakibara, K., Kojima, M., Yamaya, T. & Sakakibara, H. (2004) Molecular characterization of cytokinin-responsive histidine kinases in maize. Differential ligand preferences and response to cis-zeatin. *Plant Physiology*, 134, 1654-1661.
- Zhang, Y., Liu, B., Li, X., Ouyang, Z., Huang, L., Hong, Y., Zhang, H., Li, D. & Song, F. (2014) The *de novo* biosynthesis of vitamin B6 is required for disease resistance against *Botrytis cinerea* in tomato. *Molecular Plant-Microbe Interactions*, 27, 688-699.
- Zrenner, R., Riegler, H., Marquard, C. R., Lange, P. R., Geserick, C., Bartosz, C. E., Chen, C. T. & Slocum, R. D. (2009) A functional analysis of the pyrimidine catabolic pathway in *Arabidopsis*. *The New Phytologist*, 183, 117-132.



**Table S1.** Putative metabolites with corrected mass (Mz) and m+H adducts, detected mass per charge by mass analyser (FormerY), exact mass according to KEGG and pathways associated with carbohydrate metabolism. Blue line refer to low level metabolite and brown line refers to high level of metabolites in *P. brassicae*-infected tissues at 7, 16 and 25 DPI.

Mz	Former Y	Exact mass	Pathway	Putative compound
Carbohydrate metabolism at 7 DPI				
68.06	69.06	68.03	Butanoate metabolism	3-Butyn-1-al
180.06	181.07	180.06	Ascorbate and aldarate metabolism	myo-Inositol,L-Galactose,L-Gulose
182.06	183.07	182.08	Galactose metabolism	Sorbitol
194.08	195.09	194.04	Pentose and glucuronate interconversions	D-Glucuronate, D-Galacturonate, D-Tagaturonate,3-Dehydro-L-gulonate, D-Fructuronate
		194.079	Inositol phosphate metabolism	D-Glucuronate, 1-O-Methyl-myo-inositol, 3-O-Methyl-myo-inositol
196.08	197.08	196.06	Pentose and glucuronate interconversions	D-Mannonate, L-Gulonate,D-Altronate
			Ascorbate and aldarate metabolism	L-Gulonate. L-Galactonate
103.09	104.10	103.06	Butanoate metabolism	4-Aminobutanoate
501.24	502.25	501.48	Amino sugar and nucleotide sugar metabolism	Chitosan, D-Glucosaminide
534.02	535.02	534.03	Amino sugar and nucleotide sugar metabolism	UDP-4-keto-D-xylose
580.08	581.09	580.03	Amino sugar and nucleotide sugar metabolism	UDP-D-galacturonate
58.07	59.08	58.04	Propanoate metabolism	Acetone
113.97	114.97	114.00	Pyruvate metabolism	Acetylenedicarboxylate
Carbohydrate metabolism at 16 DPI				
68.06	69.06	68.03	Butanoate metabolism	3-Butyn-1-al
72.05	73.06	72.06	Butanoate metabolism	Butanal

178.08	179.09	178.05	Ascorbate and aldarate metabolism	L-Gulono, L-Galactono-1,4-lactone
180.06	181.07	180.06	Ascorbate and aldarate metabolism	myo-Inositol,L-Galactose,L-Gulose
344.15	345.16	344.13	Galactose metabolism	6-O-alpha-D-Galactosyl-D-glucitol
607.07	608.07	607.08	Amino sugar and nucleotide sugar metabolism	UDP-GlcNac, UDP-ManNac, UDP-GalNac
148	149.01	148.04	Propanoate metabolism	(S)-2-Methylmalate
348.05	349.06	348.05	Fructose and mannose metabolism	2-(alpha-D-Mannosyl)-3-phosphoglycerate
Carbohydrate metabolism at 25 DPI				
389.1	390.11	389.07	Amino sugar and nucleotide sugar metabolism	N-Acetylneuraminate 9-phosphate
164.06	165.08	164.07	Amino sugar and nucleotide sugar metabolism	6-Deoxy-L-galactose
563.04	564.04	563.06	Amino sugar and nucleotide sugar metabolism	UDP-4-deoxy-4-formamido-beta-L-arabinopyranose
166.07	167.09	166.05	Ascorbate and aldarate metabolism	L-Arabinonate, L-Xylonate, L-Lyxonate
			Pentose and glucuronate interconversions	D-Xylonate, L-Xylonate, L-Lyxonate
196.08	197.08	196.06	Ascorbate and aldarate metabolism	L-Gulonate, L-Galactonate
535.02	536.03	535.06	Amino sugar and nucleotide sugar metabolism	UDP-4-amino-4-deoxy-L-arabinose
325.14	326.15	325.10	Amino sugar and nucleotide sugar metabolism	N-Glycoloyl-neuraminate
587.01	588.02	587.07	Amino sugar and nucleotide sugar metabolism	GDP-4-dehydro-6-deoxy-D-mannose
255.96	256.98	256.00	Ascorbate and aldarate metabolism	L-Ascorbate 6-phosphate
546.12	547.13	546.10	Pentose and glucuronate interconversions	Pectate
276.07	277.08	276.02	Pentose phosphate pathway	6-Phospho-D-gluconate
125.92	126.93	125.97	Glyoxylate and dicarboxylate metabolism	Formyl phosphate
821.1	822.11	821.13	Propanoate metabolism	Propenoyl-CoA

160.07	161.08	160.04	Inositol phosphate metabolism	3D-3,5/4-Trihydroxycyclohexane-1,2-dione
419.95	420.96	419.96	Inositol phosphate metabolism	D-myo-Inositol, 1D-myo-Inositol
273.97	274.98	274.01	Amino sugar and nucleotide sugar metabolism	1-Phospho-alpha-D-galacturonate, D-Glucuronate 1-phosphate
229.97	230.98	230.02	Amino sugar and nucleotide sugar metabolism	alpha-D-Xylose 1-phosphate,beta-L-Arabinose 1-phosphate
84.02	85.02	84.02	Butanoate metabolism	3-Butynoate
103.09	104.10	103.06	Butanoate metabolism	4-Aminobutanoate
258.03	259.03	258.01	Pentose and glucuronate interconversions	D-Glucono-1,5-lactone 6-phosphate
339.96	340.97	340.00	Pentose phosphate pathways	beta-D-Fructose 1;6-bisphosphate
173.97	174.98	174.02	Glyoxylate and dicarboxylate metabolism	cis-Aconitate
155.98	156.99	155.98	Glyoxylate and dicarboxylate metabolism	2-Phosphoglycolate
342.08	343.09	342.12	Galactose metabolism	Sucrose, Lactose, alpha-D-Galactosyl-(1->3)-1D-myo-inositol
101.99	103.00	102.03	Propanoate metabolism	2-Oxobutanoate, Acetoacetate, (S)-Methylmalonate semialdehyde
118	119.01	118.03	Propanoate metabolism	Succinate
659.84	660.86	659.86	Inositol phosphate metabolism	Phytic acid
113.97	114.97	114.00	Pyruvate metabolism	Acetylenedicarboxylate
66.08	367.09	366.07	Glycolysis / Gluconeogenesis	Salicin 6-phosphate

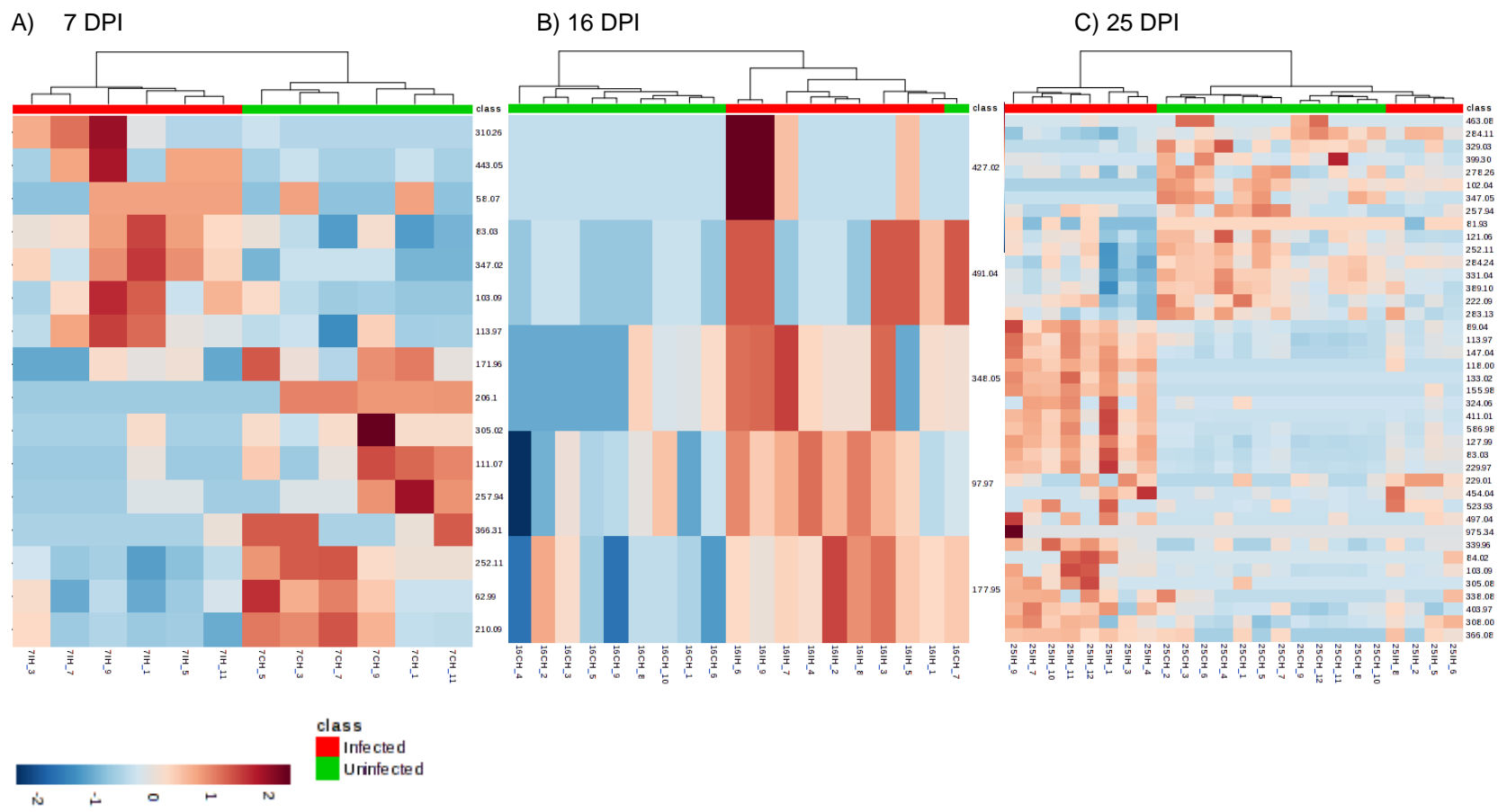


**Figure S2.** Intensity signal of potential metabolites involved in energy and nucleotide in *P. brassicae*-infected and uninfected plants at A) 7, B) 16 and C) 25 DPI. M/z variables were colour coded by a gradient depending on their Log<sub>10</sub> of the intensity value at a significance of p-value  $\leq 0.05$ . Results are clustered between uninfected (green) and infected (red) biological replicates. The m/z value of each metabolite is shown (See Table S2 for possible identification).

**Table S2.** Putative metabolites with corrected mass (Mz) and m+H adducts, detected mass per charge by mass analyser (FormerY), exact mass according to KEGG and pathways associated with energy and nucleotide metabolism. Blue line refer to low level metabolite and brown line refers to high level of metabolites in *P. brassicae*-infected tissues at 7, 16 and 25 DPI.

Mz	Former Y	Exact mass	Pathway	Putative compound
Energy metabolism at 7 DPI				
210.09	211.10	210.07	Carbon fixation in photosynthetic organism	Sedoheptulose
206.1	207.11	206.13	Photosynthesis	Plastoquinol-1
62.98	63.99	63.00	Nitrogen metabolism	Nitrate
257.94	258.95	257.91	Oxidative phosphorylation	Triphosphate
113.97	114.97	112.94	Sulfur metabolism	Thiosulfate
Energy metabolism at 16 DPI				
427.01	428.02	427.02	Photosynthesis	Adenosine 5'-diphosphate
97.96	98.98	97.98	Photosynthesis	Phosphoric acid
		97.97	Sulfur metabolism	Sulfuric acid
Energy metabolism at 25 DPI				
81.93	82.94	81.97	Sulfur metabolism	Sulfite
121.06	122.07	121.02	Sulfur metabolism	L-Cysteine
222.09	223.09	222.07	Sulfur metabolism	Cystathionine
257.94	258.95	257.91	Oxidative phosphorylation	Triphosphate
339.96	340.97	340.00	Carbon fixation in photosynthetic organisms	D-Fructose 1;6-bisphosphate
113.97	114.97	112.94	Sulfur metabolism	Thiosulfate

147.04	148.05	147.05	Sulfur metabolism	O-acetyl-L-Serine
Mz	Former Y	Exact mass	Pathway	Putative compound
Nucleotides metabolism at 7 DPI				
252.1	253.11	252.09	Purine metabolism	Deoxyinosine
305.01	306.03	305.04	Pyrimidine metabolism	2',3'-Cyclic CMP
111.07	112.08	111.04	Pyrimidine metabolism	Cytosine
443.05	444.06	443.02	Purine metabolism	Guanosine 5'-diphosphate
83.03	84.04	83.05	Purine metabolism	5-Aminoimidazole
347.02	348.02	347.06	Purine metabolism	Adenosine 5'-monophosphate, 2'-Deoxyguanosine 5'-monophosphate, 3'-Adenosine monophosphate
103.09	104.10	103.06	Pyrimidine metabolism	3-Aminoisobutyric acid
Nucleotides metabolism at 16 DPI				
491.03	492.04	491.00	Purine metabolism	2'-Deoxyadenosine 5'-triphosphate
427.01	428.02	427.03	Purine metabolism	Adenosine 5'-diphosphate, Adenosine 5'-phosphosulfate
348.05	349.06	348.05	Purine metabolism	Inosine monophosphate
Nucleotides metabolism at 25 DPI				
102.04	103.05	102.04	Purine metabolism	N-Formiminoglycine
252.1	253.11	252.09	Purine metabolism	Deoxyinosine
463.08	464.08	463.07	Purine metabolism	N6-(1;2-Dicarboxyethyl)-AMP
284.11	285.11	284.08	Purine metabolism	Xanthosine
329.03	330.03	329.05	Purine metabolism	Cyclic adenylic acid

347.05	348.06	347.06	Purine metabolism	Adenosine 5'-monophosphate, 2'-Deoxyguanosine 5'-monophosphate, 3'-Adenosine monophosphate
331.04	332.05	331.07	Purine metabolism	2'-Deoxyadenosine 5'-phosphate
389.1	390.11	389.07	Purine metabolism	5'-Acetylphosphoadenosine
283.13	284.14	283.09	Purine metabolism	Guanosine
229.97	230.98	230.02	Purine metabolism	D-Ribose 5-phosphate, alpha-D-Ribose 1-phosphate
83.03	84.04	83.05	Purine metabolism	5-Aminoimidazole
133.02	134.02	133.05	Purine metabolism	Ureidoglycine
411.01	412.02	411.03	Purine metabolism	2'-Deoxyadenosine 5'-diphosphate
586.98	587.98	586.96	Purine metabolism	Adenosine tetraphosphate
229.01	230.01	229.04	Purine metabolism	5-Phosphoribosylamine
454.04	455.04	454.07	Purine metabolism	1-(5'-Phosphoribosyl)-5-amino-4-(N-succinocarboxam)(SICAR)
523.93	524.94	523.97	Purine metabolism	Xanthosine 5'-triphosphate
84.02	85.02	84.03	Purine metabolism	Imidazolone
338.08	339.09	338.06	Purine metabolism	1-(5'-Phosphoribosyl)-5-amino-4-imidazolecarboxami (AICAR)
103.09	104.10	103.06	Pyrimidine metabolism	3-Aminoisobutyric acid
118	119.01	118.03	Pyrimidine metabolism	Methylmalonate
305.01	306.03	305.04	Pyrimidine metabolism	2',3'-Cyclic CMP
89.04	90.05	89.05	Pyrimidine metabolism	3-Aminopropionic acid
155.98	156.99	156.02	Pyrimidine metabolism	Orotate
324.06	325.07	324.04	Pyrimidine metabolism	Uridine monophosphate, Uridine 3'-monophosphate
89.04	90.05	89.05	Pyrimidine metabolism	beta-Alanine
497.04	498.05	497.00	Pyrimidine metabolism	2'-Deoxy-5-hydroxymethylcytidine-5'-triphosphate
403.97	404.98	404.00	Pyrimidine metabolism	Uridine 5'-diphosphate

308	309.00	308.04	Pyrimidine metabolism	Deoxyuridine monophosphate
-----	--------	--------	-----------------------	----------------------------

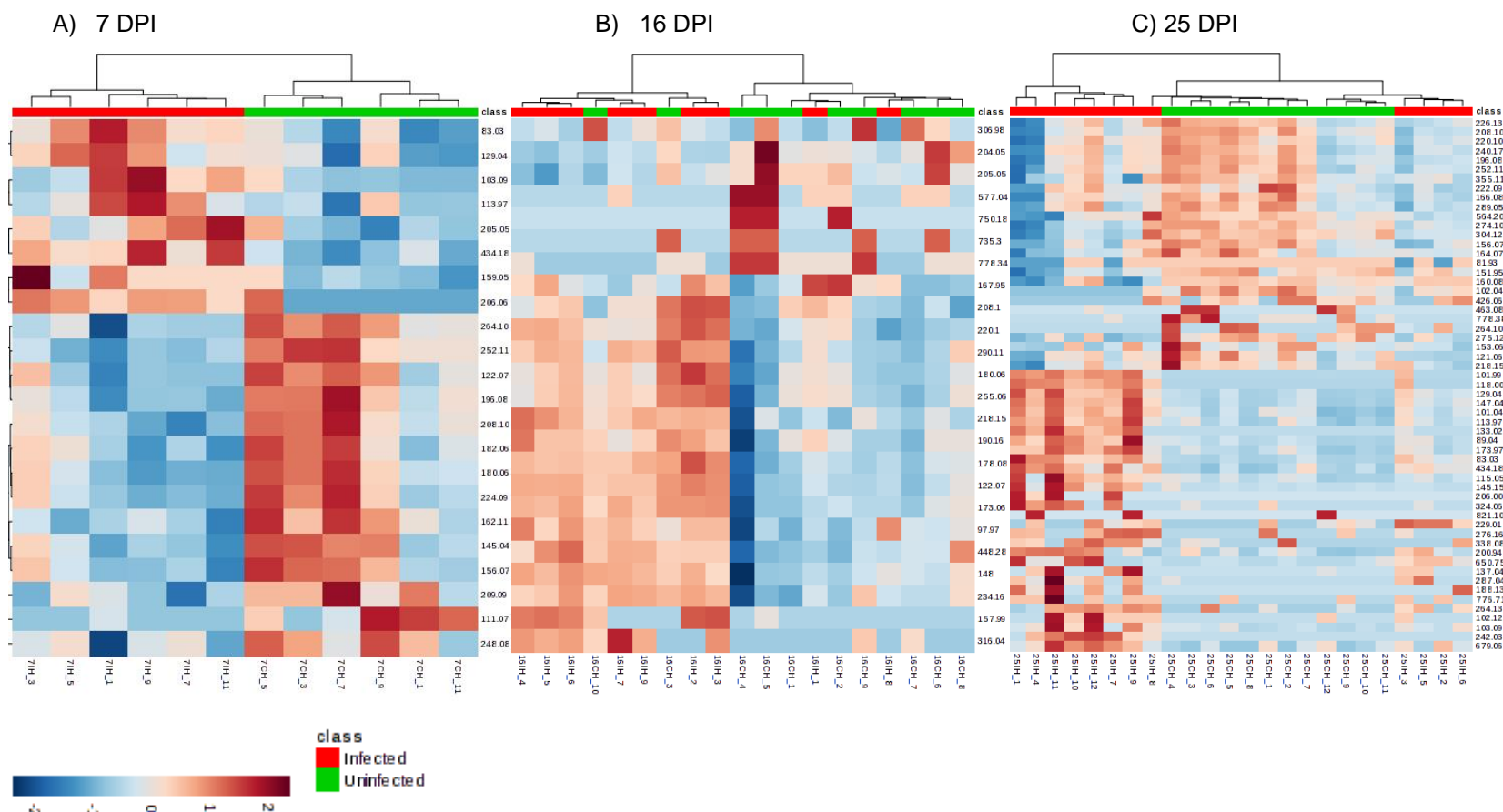


**Figure S3.** Signal intensities of metabolites potentially involved in amino acid metabolism in *P. brassicae*-infected and uninfected plants at A) 7, B) 16 and C) 25 DPI. M/z variables were colour coded by a gradient depending on their Log10 of the intensity value at a significance of p-value  $\leq 0.05$ . Results are clustered between uninfected (green) and infected (red) biological replicates. The m/z value of each metabolite is shown (See Table S3 for possible identification).

**Table S3.** Putative metabolites with corrected mass (Mz) and m+H adducts, detected mass per charge by mass analyser (FormerY), exact mass according to KEGG and pathways associated with amino acid metabolism. Blue line refer to low level metabolite and brown line refers to high level of metabolites in *P. brassicae*-infected tissues at 7, 16 and 25 DPI.

Mz	Former Y	Exact mass	Pathway	Putative compound
Amino acid metabolism at 7DPI				
264.1	265.11	264.11	Tryptophan metabolism	Formyl-N-acetyl-5-methoxykynurenamine
252.1	253.11	252.07	Tryptophan metabolism	5-Hydroxy-N-formylkynurenine
208.1	209.11	208.08	Tryptophan metabolism	L-Kynurenine, Formyl-5-hydroxykynurenamine
224.08	225.10	224.08	Tryptophan metabolism	3-Hydroxy-L-kynurenine, 5-Hydroxykynurenine
248.08	249.09	248.12	Tryptophan metabolism	6-Hydroxymelatonin, 5-Hydroxyindoleacetyl glycine
145.04	146.05	145.09	Arginine and proline metabolism	4-Guanidinobutanoate, 4-Acetamidobutanoate
111.07	112.08	111.03	Arginine and proline metabolism	Pyrrole-2-carboxylate
162.11	163.11	162.10	Lysine degradation	N6-Hydroxy-L-lysine
196.08	197.08	196.04	Tyrosine metabolism	3-(3;4-Dihydroxyphenyl)pyruvate
182.06	183.07	182.06	Tyrosine metabolism	3-(4-Hydroxyphenyl)lactate, Homovanillate, 3-Methoxy-4-hydroxyphenylglycolaldehyde, 3;4-Dihydroxyphenylpropanoate;
180.06	181.07	180.09	Tyrosine metabolism	3-Hydroxykynurenamine, 5-Hydroxykynurenamine
209.08	210.09	209.07	Tyrosine metabolism	p-Hydroxyphenylacetyl glycine
122.07	123.07	122.04	Phenylalanine metabolism	Benzoate
156.07	157.08	156.05	Histidine metabolism	4-Imidazolone-5-propanoate, Imidazole lactate
159.05	160.06	159.07	Tryptophan metabolism	Indole-3-acetaldehyde
206.06	207.07	206.05	Tryptophan metabolism	Indolylmethylthiohydroximate
205.05	206.06	205.07	Tryptophan metabolism	Indolelactate, Xanthurenic acid, 5-Methoxyindoleacetate, 6-Hydroxykynurenate

129.03	130.04	129.04	Arginine and proline metabolism	4-Oxoproline, L-1-Pyrroline-3-hydroxy-5-carboxylate, 1-Pyrroline-4-hydroxy-2-carboxylate, N4-Acetylaminobutanal
103.09	104.10	103.06	Arginine and proline metabolism	4-Aminobutanoate
83.03	84.04	83.07	Lysine degradation	Piperidine
434.18	435.19	434.23	Glutathione metabolism	Glutathionylspermidine
Amino acid metabolism at 16 DPI				
204.05	205.06	204.09	Tryptophan metabolism	L-Tryptophan
205.05	206.06	205.07	Tryptophan metabolism	Indolelactate, Xanthurenic acid, 5-Methoxyindoleacetate, 6-Hydroxykynurenate
306.97	307.99	306.97	Tyrosine metabolism	3-Iodo-L-tyrosine
577.04	578.05	577.08	Histidine metabolism	Phosphoribosyl-formimino-AICAR-phosphate
735.3	736.31	735.30	Glutathione metabolism	Homotrypanothione disulfide
778.34	779.35	778.35	Glutathione metabolism	Bis(glutathionyl)spermine disulfide
750.18	751.19	750.14	D-Glutamine and D-glutamate metabolism	UDP-N-acetylmuramoyl-L-alanine
208.1	209.11	208.08	Tryptophan metabolism	3-Anthraniloyl-L-alanine, Formyl-5-hydroxykynurenamine
220.1	221.10	220.08	Tryptophan metabolism	5-Hydroxy-L-tryptophan
255.06	256.07	255.04	Tryptophan metabolism	5-(3'-Carboxy-3'-oxopropyl)-4,6-dihydroxypicolinate
218.15	219.16	218.11	Tryptophan metabolism	N-Acetylserotonin
190.16	191.16	190.11	Tryptophan metabolism	5-Methoxytryptamine, N-Methylserotonin
157.99	159.00	158.02	Tryptophan metabolism	gamma-Oxalocrotonate
173.06	174.06	173.07	Arginine and proline metabolism	N-Acetyl-L-glutamate 5-semialdehyde
234.16	235.16	234.14	Arginine and proline metabolism	p-Coumaroylputrescine
290.11	291.12	290.12	Arginine and proline metabolism, Alanine; aspartate and glutamate metabolism	N-(L-Arginino)succinate

		290.11	Lysine biosynthesis	N-Succinyl-LL-2,6-diaminoheptanedioate
316.04	317.05	316.07	Tyrosine metabolism	Cysteinyl-dopa
180.06	181.07	180.09	Tryptophan metabolism	3-Hydroxykynurenine, 5-Hydroxykynurenine
122.07	123.07	122.04	Phenylalanine metabolism	Benzoate
167.94	168.95	167.97	Cysteine and methionine metabolism	3-Sulfopyruvate
148	149.01	148.02	Cysteine and methionine metabolism	4-Methylthio-2-oxobutanoic acid
448.27	449.29	448.25	Glutathione metabolism	Glutathionylaminopropylcadaverine
Amino acid metabolism at 25 DPI				
264.1	265.11	264.11	Tryptophan metabolism	Formyl-N-acetyl-5-methoxykynurenine
252.1	253.11	252.07	Tryptophan metabolism	5-Hydroxy-N-formylkynurenine
208.1	209.11	208.08	Tryptophan metabolism	L-Kynurenine, Formyl-5-hydroxykynurenine
220.1	221.10	220.08	Tryptophan metabolism	5-Hydroxy-L-tryptophan
160.08	161.08	160.04	Tryptophan metabolism	2-Oxadipate, Tryptamine,
218.15	219.16	218.11	Tryptophan metabolism	N-Acetylserotonin
355.11	356.12	355.16	Arginine and proline metabolism	S-Adenosylmethioninamine
274.1	275.11	274.13	Arginine and proline metabolism	N <sup>2</sup> -Succinyl-L-arginine
304.12	305.13	304.14	Arginine and proline metabolism	Nopaline
275.12	276.13	275.11	Arginine and proline metabolism	N-Succinyl-L-citrulline
196.08	197.08	196.04	Tyrosine metabolism	3,4-Dihydroxyphenylpyruvate
166.08	167.09	166.06	Tyrosine metabolism	3-Methoxy-4-hydroxyphenylacetaldehyde
102.04	103.05	102.03	Cysteine and methionine metabolism	2-Oxobutanoate
153.06	154.06	153.08	Tyrosine metabolism	Dopamine
164.07	165.08	164.05	Phenylalanine metabolism	Phenylpyruvate, 4-Coumarate, trans-2-Hydroxycinnamate, 2-Hydroxy-3-phenylpropenoate, 3-Coumaric acid
156.07	157.08	156.05	Histidine metabolism	4-Imidazolone-5-propanoate, Imidazole lactate
426.06	427.06	426.09	Cysteine and methionine metabolism	S-Glutathionyl-L-cysteine

81.93	82.94	81.97	Cysteine and methionine metabolism	Sulfite, Hydrogen sulfite
222.09	223.09	222.07	Cysteine and methionine metabolism	L-Cystathionine
151.94	152.96	151.98	Cysteine and methionine metabolism	3-Sulfinylpyruvate
289.05	290.06	289.08	Lysine biosynthesis	N-Succinyl-2-L-amino-6-oxoheptanedioate
463.08	464.08	463.07	Alanine; aspartate and glutamate metabolism	N6-(1;2-Dicarboxyethyl)-AMP
121.06	122.07	121.02	Glycine; serine and threonine metabolism	L-Cysteine, D-Cysteine
778.34	779.35	778.35	Glutathione metabolism	Bis(glutathionyl)spermine disulfide
206.06	207.07	206.05	Tryptophan metabolism	Indolylmethylthiohydroximate
		206.04	Lysine biosynthesis	Homocitrate, Homoisocitrate
137.04	138.04	137.05	Tryptophan metabolism	Anthranilate
147.04	148.05	147.05	Arginine and proline metabolism	L-Glutamate, L-4-Hydroxyglutamate semialdehyde, 2-Oxo-4-hydroxy-5-aminovalerate
89.04	90.05	89.05	Cysteine and methionine metabolism	L-Alanine
133.02	134.02	133.04	Arginine and proline metabolism	L-Aspartate
129.03	130.04	129.04	Arginine and proline metabolism	4-Oxoproline, L-1-Pyrroline-3-hydroxy-5-carboxylate, 1-Pyrroline-4-hydroxy-2-carboxylate, N4-Acetylamino butanal
103.09	104.10	103.06	Arginine and proline metabolism	4-Aminobutanoate
145.04	146.05	145.09	Arginine and proline metabolism	4-Guanidinobutanoate, 4-Acetamidobutanoate
173.06	174.06	173.07	Arginine and proline metabolism	N-Acetyl-L-glutamate 5-semialdehyde
115.05	116.06	115.06	Arginine and proline metabolism	L-Proline, D-Proline
276.16	277.16	276.16	Arginine and proline metabolism	p-Coumaroylagmatine
264.13	265.14	264.15	Arginine and proline metabolism	Feruloylputrescine
188.13	189.14	188.15	Lysine degradation	N6,N6,N6-Trimethyl-L-lysine, N6-Acetyl-L-lysine
83.03	84.04	83.07	Lysine degradation	Piperidine
242.03	243.04	242.00	Lysine degradation	5-Phosphonoxy-L-lysine

118	119.01	118.03	Tyrosine metabolism	Succinate
650.75	651.76	650.79	Tyrosine metabolism	Triiodothyronine
776.71	777.72	776.69	Tyrosine metabolism	Thyroxine
101.99	103.00	102.03	Tyrosine metabolism	Acetoacetate
338.08	339.09	338.05	Histidine metabolism	1-(5-Phosphoribosyl)imidazole-4-acetate, 1-(5'-Phosphoribosyl)-5-amino-4-imidazolecarboxami
101.04	102.05	101.05	Cysteine and methionine metabolism	1-Aminocyclopropane-1-carboxylate
200.94	201.95	200.98	Cysteine and methionine metabolism	S-Sulfo-L-cysteine
229.01	230.01	229.04	Alanine; aspartate and glutamate metabolism	5-Phosphoribosylamine
324.06	325.07	324.02	Phenylalanine, tyrosine and tryptophan biosynthesis	5-O-(1-Carboxyvinyl)-3-phosphoshikimate
287.04	288.05	287.06	Phenylalanine, tyrosine and tryptophan biosynthesis	Indoleglycerol phosphate
434.18	435.19	434.23	Glutathione metabolism	Glutathionylspermidine
821.1	822.11	821.13	Beta-Alanine metabolism	Propenoyl-CoA
679.06	680.07	679.10	D-Glutamine and D-glutamate metabolism	UDP-N-acetylmuramic acid

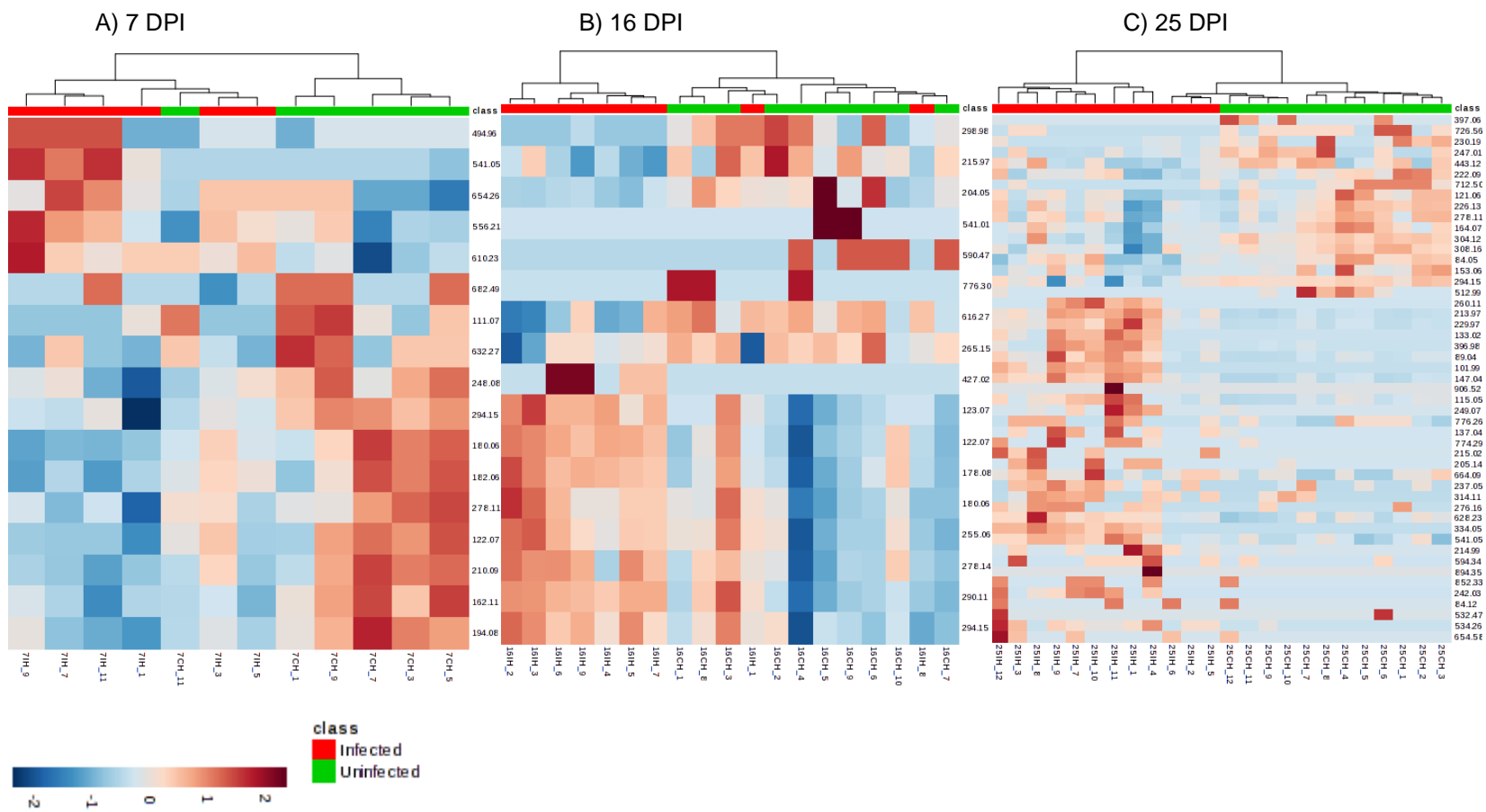


**Figure S4.** Signal intensities of potential metabolites involved in cofactor and vitamin metabolism in *P. brassicae*-infected and uninfected plants at A) 7, B) 16 and C) 25 DPI. M/z variables were colour coded by a gradient depending on their Log10 of the intensity value at a significance of p-value  $\leq 0.05$ . Results are clustered between uninfected (green) and infected (red) biological replicates. The m/z value of each metabolite is shown (See Table S4 for possible identification).

**Table S4.** Putative metabolites with corrected mass (Mz) and m+H adducts, detected mass per charge by mass analyser (FormerY), exact mass according to KEGG and pathways associated with cofactor and vitamin metabolism. Blue line refer to low level metabolite and brown line refers to high level of metabolites in *P. brassicae*-infected tissues at 7, 16 and 25 DPI.

Mz	Former Y	Exact mass	Pathway	Putative compound
Cofactors and vitamins metabolism at 7 DPI				
682.48	683.50	682.53	Ubiquinone and other terpenoid-quinone biosynthesis	3-Octaprenyl-4-hydroxybenzoate, 2-Octaprenyl-6-methoxy-1,4-benzoquinone
294.15	295.16	294.39	Ubiquinone and other terpenoid-quinone biosynthesis	2-Demethylmenaquinone
180.06	181.07	180.04	Ubiquinone and other terpenoid-quinone biosynthesis	3-(4-Hydroxyphenyl)pyruvate
		180.05	Nicotinate and nicotinamide metabolism	Nicotinurate
182.06	181.07	182.06	Ubiquinone and other terpenoid-quinone biosynthesis	3-(4-Hydroxyphenyl)lactate
278.11	279.11	278.13	Ubiquinone and other terpenoid-quinone biosynthesis	alpha-Ribazole
		278.13	Riboflavin metabolism	alpha-Ribazole
111.07	112.08	111.03	Nicotinate and nicotinamide metabolism	2;5-Dihydroxypyridine, 2;6-Dihydroxypyridine
122.07	123.07	122.05	Nicotinate and nicotinamide metabolism	Nicotinamide
210.09	211.10	210.10	Nicotinate and nicotinamide metabolism	2;6-Dihydroxypseudooxynicotine
162.11	163.11	162.12	Nicotinate and nicotinamide metabolism	(R;S)-Nicotine
194.08	195.09	194.11	Nicotinate and nicotinamide metabolism	6-Hydroxypseudooxynicotine
248.08	249.09	248.06	Vitamin B6 metabolism	Pyridoxamine phosphate
494.95	495.97	495.00	Folate biosynthesis	2-Amino-4-hydroxy-6-(erythro-1;2;3-trihydroxypropy
541.05	542.06	541.00	Folate biosynthesis	Formamidopyrimidine nucleoside triphosphate
Cofactors and vitamins metabolism at 16 DPI				

204.05	205.06	204.04	Ubiquinone and other terpenoid-quinone biosynthesis	Spirodilactone, 1,4-Dihydroxy-6-naphthoate
590.47	591.48	590.43	Ubiquinone and other terpenoid-quinone biosynthesis	Ubiquinone-6
541.05	542.06	541.00	Folate biosynthesis	Formamidopyrimidine nucleoside triphosphate
776.3	777.31	776.26	Folate biosynthesis	5;6;7;8-Tetrahydromethanopterin
215.97	216.97	216.00	Vitamine B6 metabolism	4-Phosphoerythronate
298.98	299.99	299.01	Thiamine metabolism	4-Amino-2-methyl-5-diphosphomethylpyrimidine
294.15	295.16	294.39	Ubiquinone and other terpenoid-quinone biosynthesis	2-Demethylmenaquinone
180.06	181.07	180.04	Ubiquinone and other terpenoid-quinone biosynthesis	3-(4-Hydroxyphenyl)pyruvate
		180.05	Nicotinate and nicotinamide metabolism	Nicotinurate
123.06	124.08	123.03	Nicotinate and nicotinamide metabolism	Nicotinate
122.07	123.07	122.05	Nicotinate and nicotinamide metabolism	Nicotinamide
178.08	179.09	178.11	Nicotinate and nicotinamide metabolism	(S)-6-Hydroxynicotine
255.06	256.07	256.08	Nicotinate and nicotinamide metabolism	Nicotinate D-ribonucleoside
427.02	428.02	427.03	Pantothenate and CoA biosynthesis	Adenosine 3',5'-bisphosphate
Cofactors and vitamins metabolism at 25 DPI				
222.09	223.09	222.05	Ubiquinone and other terpenoid-quinone biosynthesis	2-Succinylbenzoate
164.07	165.08	164.05	Ubiquinone and other terpenoid-quinone biosynthesis	4-Coumarate
294.15	295.16	294.39	Ubiquinone and other terpenoid-quinone biosynthesis	2-Demethylmenaquinone
278.11	279.11	278.13	Ubiquinone and other terpenoid-quinone biosynthesis	alpha-Ribazole
712.5	713.51	712.54	Ubiquinone and other terpenoid-quinone biosynthesis	2-Octaprenyl-3-methyl-5-hydroxy-6-methoxy-1,4-benzoquinone

726.56	727.57	726.56	Ubiquinone and other terpenoid-quinone biosynthesis	Ubiquinone-8
160.08	161.08	160.04	Nicotinate and nicotinamide metabolism	2-Formylglutarate
443.12	444.13	443.16	Folate biosynthesis	Dihydrofolate
512.99	513.99	513.01	Folate biosynthesis	2,5-Diamino-6-(5'-triphosphoryl-3',4'-trihydroxy-2'-oxopentyl)-amino-4-oxopyrimidine
102.04	103.05	102.03	Vitamin B6 metabolism	Succinate semialdehyde
247.01	248.01	247.02	Vitamin B6 metabolism	Pyridoxal 5'-phosphate
314.11	315.12	314.07	Ubiquinone and other terpenoid-quinone biosynthesis	Geranyl diphosphate
532.47	533.48	532.43	Ubiquinone and other terpenoid-quinone biosynthesis	2-Hexaprenyl-6-methoxyphenol
334.04	335.06	334.06	Nicotinate and nicotinamide metabolism	Nicotinamide D-ribonucleotide
664.09	665.10	665.10	Nicotinate and nicotinamide metabolism	Deamino-NAD <sup>+</sup>
89.04	90.05	89.05	Pantothenate and CoA biosynthesis	3-Aminopropionic acid
205.14	206.15	205.13	Pantothenate and CoA biosynthesis	Pantothenol
541.05	542.06	541.00	Folate biosynthesis	Formamidopyrimidine nucleoside triphosphate
237.05	238.05	237.09	Folate biosynthesis	6-Pyruvoyltetrahydropterin
396.98	397.99	395.01	Folate biosynthesis	Molybdopterin
774.29	775.30	774.25	Folate biosynthesis	7,8-Dihydromethanopterin
137.04	138.04	137.05	Folate biosynthesis	4-Aminobenzoate
249.07	250.07	249.04	Vitamin B6 metabolism	Pyridoxine phosphate
213.97	214.97	213.99	Vitamin B6 metabolism	2-Oxo-3-hydroxy-4-phosphobutanoate
214.99	216.00	215.02	Vitamin B6 metabolism	O-Phospho-4-hydroxy-L-threonine
101.99	103.00	102.03	Vitamin B6 metabolism	Succinate semialdehyde
229.97	230.98	230.02	Vitamin B6 metabolism	D-Ribulose 5-phosphate
242.03	243.04	242.08	Riboflavin metabolism	7,8-Dimethylalloxazine
276.16	277.16	276.11	Riboflavin metabolism	5-Amino-6-(1-D-ribitylamino)uracil

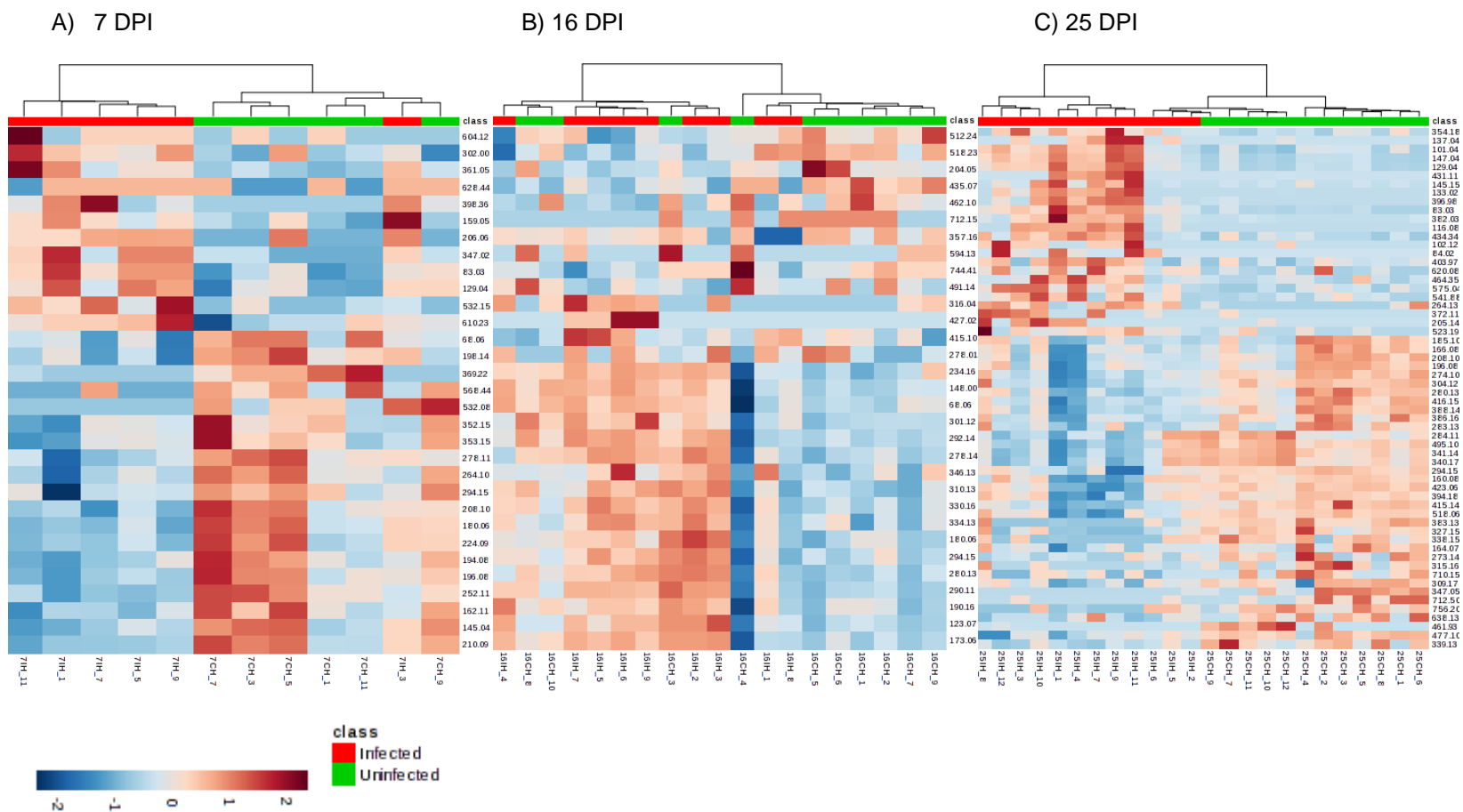


**Figure S5.** Signal intensities of potential terpenoids, polyketides, and other secondary metabolites in *P. brassicae*-infected and uninfected plants at A) 7, B) 16, and C) 25 DPI. *m/z* variables were colour coded by a gradient depending on their Log<sub>10</sub> of the intensity value at a significance of *p*-value  $\leq 0.05$ . Results are clustered between uninfected (green) and infected (red) biological replicates. The *m/z* value of each metabolite is shown (See Table S5 for possible identification).

**Table S5.** Putative metabolites with corrected mass (Mz) and m+H adducts, detected mass per charge by mass analyser (FormerY), exact mass according to KEGG and pathways associate with terpenoids, polyketides, and other secondary metabolites. Blue line refer to low level metabolite and brown line refers to high level of metabolites in *P. brassicae*-infected tissues at 7, 16 and 25 DPI.

Mz	Former Y	Exact mass	Pathway	Putative compound
Terpenoids, polyketides and other secondary metabolites at 7 DPI				
568.44	569.45	568.43	Carotenoid biosynthesis	Zeaxanthin, Lutein, 3;4-Dihydroanhydrorhodovibrin, Spheroidene, Rhodopinal
264.1	265.11	264.14	Carotenoid biosynthesis	Abscisic acid
353.15	354.16	353.17	Zeatin biosynthesis	Dihydrozeatin riboside
68.06	69.06	68.06	Brassinosteroids biosynthesis	Isoprene
224.09	225.10	224.07	Phenylpropanoid biosynthesis	Sinapate
194.08	195.09	194.06	Phenylpropanoid biosynthesis	Ferulate, 5-Hydroxyconiferaldehyde
196.08	197.08	196.07	Phenylpropanoid biosynthesis	5-Hydroxyconiferyl alcohol
208.1	209.11	208.07	Phenylpropanoid biosynthesis	Sinapoyl aldehyde
180.06	181.07	180.08	Phenylpropanoid biosynthesis	Coniferyl alcohol, Caffeic acid
210.09	211.10	210.09	Phenylpropanoid biosynthesis	Sinapyl alcohol, 5-Hydroxyferulate, Sinapate
278.1	279.11	278.12	Glucosinolate biosynthesis	2-(7'-Methylthio)heptylmalate
252.11	253.11	252.06	Glucosinolate biosynthesis	S-(4-Methylthiobutylthiohydroximoyl)-L-cysteine
369.22	370.23	369.19	Isoquinoline alkaloid biosynthesis	Corydaline
352.15	353.16	352.15	Isoquinoline alkaloid biosynthesis	Palmatine
294.15	295.16	180.04	Isoquinoline alkaloid biosynthesis	3-(4-Hydroxyphenyl)pyruvate
532.08	533.08	532.12	Isoflavonoid biosynthesis	Biochanin A 7-O-(6-O-malonyl-beta-D-glucoside), Malonylglycitin, (-)-Maackiain-3-O-glucosyl-6"-O-malonate
628.43	629.45	628.45	Carotenoid biosynthesis	R.g.-Keto III
347.02	348.02	347.06	Zeatin biosynthesis	Adenosine 5'-monophosphate
398.35	399.37	398.35	Brassinosteroid biosynthesis	Campest-4-en-3-one

361.05	362.05	361.05	Glucosinolate biosynthesis	Glucoputranjivin
206.06	207.07	206.05	Glucosinolate biosynthesis	Indolylmethylthiohydroximate
604.12	605.13	605.11	Anthocyanin biosynthesis	Pelargonidin 3-O-3",6"-O-dimalonylglucoside
302	303.01	303.05	Anthocyanin biosynthesis	Delphinidin
610.22	611.24	610.19	Flavonoid biosynthesis	Neohesperidin
532.15	533.16	532.12	Isoflavonoid biosynthesis	Biochanin A 7-O-(6-O-malonyl-beta-D-glucoside), Malonylglycitin, (-)-Maackiain-3-O-glucosyl-6"-O-malonate
Terpenoids, polyketides and other secondary metabolites at 16 DPI				
744.41	745.42	744.46	Carotenoid biosynthesis	(3S;2'S)-4-Ketomyxol 2'-alpha-L-fucoside
435.07	436.08	435.07	Glucosinolate biosynthesis	Glucoberteroin
204.05	205.06	204.0899, 204.082	Glucosinolate biosynthesis	L-Tryptophan, 2-Oxo-8-methylthiooctanoic acid
594.13	595.13	595.17	Anthocyanin biosynthesis	Cyanidin 3-O-rutinoside, Pelargonin, Cyanidin 3-O-(6-O-p-coumaroyl)glucoside, Pelargonidin 3-O-(6-caffeoyl-beta-D-glucoside), Pelargonidin 3-O-sophoroside
462.1	463.11	463.12	Anthocyanin biosynthesis	Peonidin 3-O-glucoside
712.15	713.15	713.16	Anthocyanin biosynthesis	Delphinidin 3-O-(6"-O-malonyl)-beta-glucoside-3'-O-beta-glucoside
357.16	358.17	357.16	Isoquinoline alkaloid biosynthesis	Deacetylcolchicine
491.14	492.15	491.18	Isoquinoline alkaloid biosynthesis	Demethylalangiside, Demethylisoalangiside
512.24	513.25	512.22	Indole alkaloid biosynthesis	Raucaffricine
234.15	235.16	234.13	Carotenoid biosynthesis	Strigolactone ABC-rings
346.13	347.14	346.14	Carotenoid biosynthesis	Strigol
330.16	331.16	330.15	Carotenoid biosynthesis	5-Deoxystrigol
280.13	281.14	280.13	Carotenoid biosynthesis	Phaseic acid, 8'-Hydroxyabscisate
427.02	428.02	427.03	Zeatin biosynthesis	Adenosine 5'-diphosphate
415.14	416.11	415.13	Zeatin biosynthesis	N6-(delta2-Isopentenyl)-adenosine 5'-monophosphate

68.06	69.06	68.06	Brassinosteroids biosynthesis	Isoprene
180.06	181.07	180.08	Phenylpropanoid biosynthesis	Coniferyl alcohol, Caffeic acid
148	149.01	148.02	Phenylpropanoid biosynthesis	Cinnamic acid
148	149.01	148.02	Glucosinolate biosynthesis	4-Methylthio-2-oxobutanoic acid
278.14	279.15	278.12	Glucosinolate biosynthesis	2-(7'-Methylthio)heptylmalic acid, 3-(7'-Methylthio)heptylmalic acid
301.12	302.12	301.13	Isoquinoline alkaloid biosynthesis	(S)-6-O-Methylnorlaudanosoline
294.15	295.16	294.17	Indole alkaloid biosynthesis	10-Deoxysarpagine
292.14	293.15	292.16	Indole alkaloid biosynthesis	16-Epivellosimine, Vellosoimine
310.13	311.14	310.17	Indole alkaloid biosynthesis	Sarpagine
334.13	335.14	334.17	Indole alkaloid biosynthesis	Vinorine
290.11	291.12	290.08	Flavonoid biosynthesis	cis-3,4-Leucopelargonidin, Luteoforol; 3-Deoxy-leucocyanidin, D-Catechin, (-)-Epicatechin, Fisetinidol-4beta-ol
316.04	317.05	316.06	Flavone and flavonol biosynthesis	3-O-Methylquercetin
Terpenoids, polyketides and other secondary metabolites at 25 DPI				
280.13	281.14	280.13	Carotenoid biosynthesis	Phaseic acid, 8'-Hydroxyabscisate
712.5	713.51	712.47	Carotenoid biosynthesis	Hydroxychlorobactene glucoside
304.12	305.13	304.16	Zeatin biosynthesis	3-(3-Amino-3-carboxypropyl)-N6-(delta2-isopentenyl)-adenine
495.1	496.11	495.09	Zeatin biosynthesis	Isopentenyladenosine-5'-diphosphate
415.14	416.11	415.13	Zeatin biosynthesis	N6-(delta2-Isopentenyl)-adenosine 5'-monophosphate
347.05	348.06	347.06	Zeatin biosynthesis	Adenosine 5'-monophosphate
383.13	384.14	383.18	Zeatin biosynthesis	Dihydrozeatin-O-glucoside
196.08	197.08	196.04	Phenylpropanoid biosynthesis	3,4-Dihydroxyphenylpyruvate
166.08	167.09	166.06	Phenylpropanoid biosynthesis	Caffeyl alcohol
164.07	165.08	164.05	Phenylpropanoid biosynthesis	4-Coumarate, trans-2-Hydroxycinnamate, cis-2-Hydroxycinnamate, Caffeic aldehyde

309.17	310.18	310.17	Phenylpropanoid biosynthesis	Sinapine
386.16	387.17	386.12	Phenylpropanoid biosynthesis	1-O-Sinapoyl-beta-D-glucose
208.1	209.11	208.07	Phenylpropanoid biosynthesis	Sinapoyl aldehyde
		208.12	Biosynthesis of alkaloids derived from histidine and purine	Pilocarpine
463.08	464.08	463.10	Glucosinolate biosynthesis	7-Methylthioheptyl glucosinolate
222.09	223.09	222.06	Glucosinolate biosynthesis	2-(3'-Methylthio)propylmalic acid, 3-(3'-Methylthio)propylmalic acid
423.06	424.07	423.07	Glucosinolate biosynthesis	Gluconasturtiin
477.1	478.11	477.12	Glucosinolate biosynthesis	8-Methylthiooctyl glucosinolate
756.2	757.21	757.20	Anthocyanin biosynthesis	Cyanidin 3-O-(6-O-p-coumaroyl)glucoside-5-O-glucoside
518.06	519.07	519.11	Anthocyanin biosynthesis	Pelargonidin 3-O-(6-O-malonyl-beta-D-glucoside)
710.15	711.16	711.14	Anthocyanin biosynthesis	Cyanidin-3-O-(6''-O-malonyl-2''-O-glucuronyl)glucoside
283.13	284.14	283.12	Isoquinoline alkaloid biosynthesis	Morphinone
327.15	328.16	327.15	Isoquinoline alkaloid biosynthesis	(S)-Scoulerine
339.13	340.14	339.15	Isoquinoline alkaloid biosynthesis	(S)-Canadine
315.16	316.17	315.15	Isoquinoline alkaloid biosynthesis	3'-Hydroxy-N-methyl-(S)-coclaurine
341.14	342.15	341.16	Isoquinoline alkaloid biosynthesis	Isocorypalmine
273.14	274.15	273.14	Isoquinoline alkaloid biosynthesis	4'-O-Methylnorbelladine
388.14	389.15	388.14	Isoquinoline alkaloid biosynthesis	Secologanin
294.15	295.16	294.17	Indole alkaloid biosynthesis	10-Deoxysarpagine
274.1	275.11	274.08	Flavonoid biosynthesis	Afzelechin, Apiforol, epi-Afzelechin , 5-Deoxyleucopelargonidin,
284.11	285.11	284.07	Isoflavonoid biosynthesis	Biochanin A, Calycosin, 2'-Hydroxyformononetin, (-)-Maackiain, Prunetin, Glycitein, (+)-Maackiain
394.18	395.18	394.14	Isoflavonoid biosynthesis	Rotenone
340.17	341.17	340.13	Isoflavonoid biosynthesis	Glyceocarpin
461.93	462.93	461.96	Flavone and flavonol biosynthesis	Quercetin 3,3'-bissulfate
638.13	639.13	638.11	Flavone and flavonol biosynthesis	Luteolin 7-O-beta-D-diglucuronide

372.11	373.11	372.14	Phenylpropanoid biosynthesis	Syringin
264.13	265.14	264.15	Carotenoid biosynthesis	Feruloylputrescine
		264.10	Glucosinolate biosynthesis	2-(6'-Methylthio)hexylmalic acid
84.02	85.02	84.06	Zeatin biosynthesis	3-Methyl-2-butenal
575.04	576.05	575.06	Zeatin biosynthesis	Isopentenyladenosine-5'-triphosphate
431.11	432.12	431.12	Zeatin biosynthesis	trans-Zeatin riboside monophosphate
403.97	404.98	404.00	Zeatin biosynthesis	Uridine 5'-diphosphate
464.35	465.35	464.35	Brassinosteroids biosynthesis	Castasterone
434.34	435.34	434.38	Brassinosteroids biosynthesis	6-Deoxoteasterone
308	309.00	308.01	Terpenoid backbone biosynthesis	(R)-5-Diphosphomevalonate
338.08	339.09	338.10	Phenylpropanoid biosynthesis	p-Coumaroyl quinic acid, Sinapoyl-CoA
147.04	148.05	147.07	Glucosinolate biosynthesis	5-Methylthiopentanaloxime
133.02	134.02	133.06	Glucosinolate biosynthesis	4-Methylthiobutanaloxime
205.14	206.15	205.11	Glucosinolate biosynthesis	Tetrahomomethionine
620.08	621.09	621.11	Anthocyanin biosynthesis	Cyanidin 3-O-3'',6''-O-dimalonylglucoside
137.04	138.04	137.08	Isoquinoline alkaloid biosynthesis	Tyramine
354.18	355.19	354.17	Isoquinoline alkaloid biosynthesis	(S)-cis-N-Methylcanadine
523.19	524.20	523.21	Isoquinoline alkaloid biosynthesis	Deacetylisoipecoside, Deacetylpecoside
382.03	383.04	382.00	Flavone and flavonol biosynthesis	Quercetin 3-sulfate
541.88	542.88	541.91	Flavone and flavonol biosynthesis	Quercetin 3,3',7-trissulfate, Quercetin 3,4',7-trissulfate





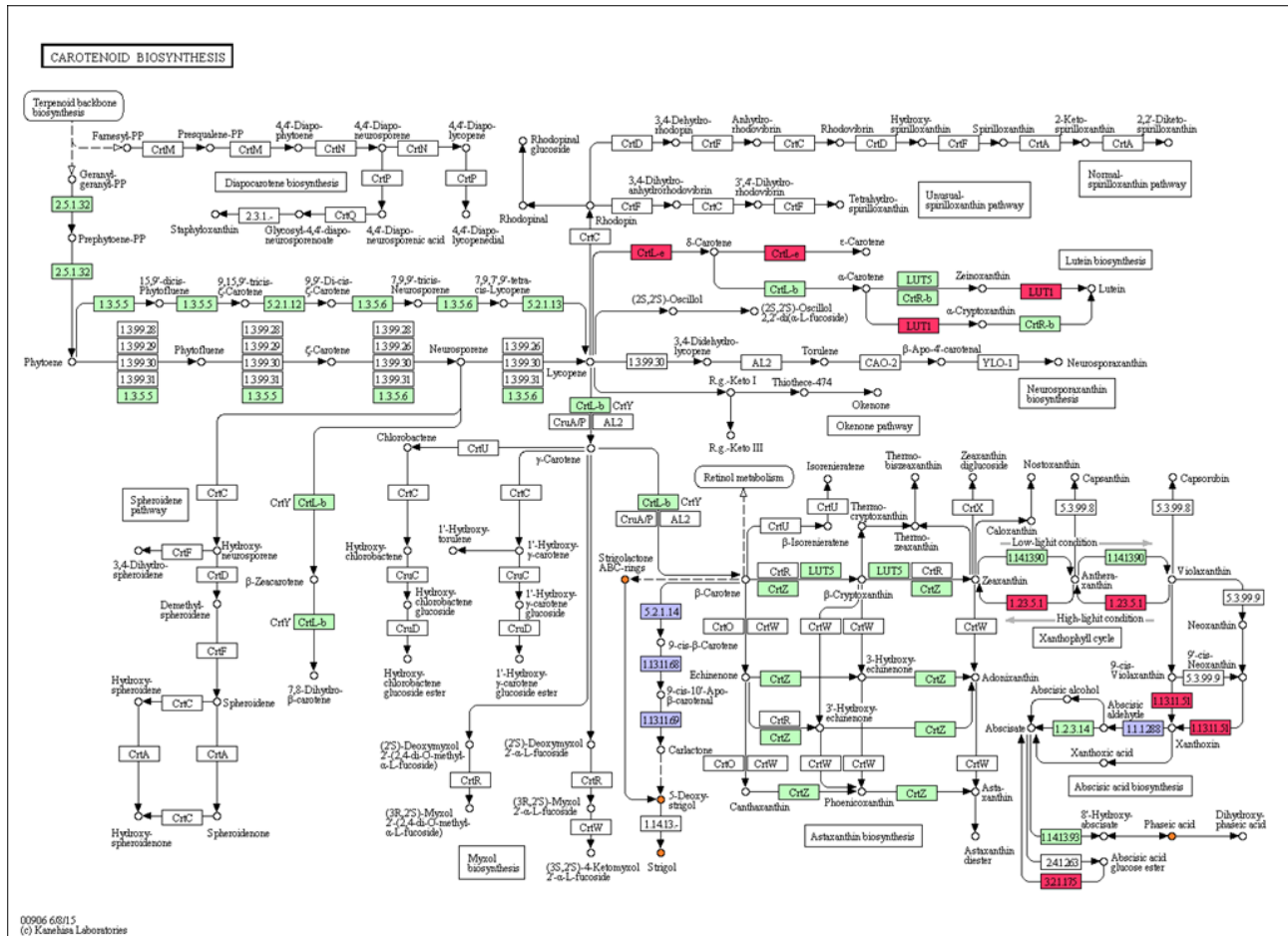


**Figure S8.** The expression of genes involved in carotenoid biosynthesis in *P. brassicae*-infected tissue at 16 DPI. Light blue boxes show down-regulated gene expression ( $\log_2$  fold-change  $\leq -1$ ,  $p \leq 0.05$ ), red boxes show up-regulated gene expression ( $\log_2$  FC  $\geq 1$ ,  $p \leq 0.05$ ), green boxes show genes that do not show a significant change in expression between uninfected and infected tissue. White boxes show genes that have not been identified in *A. thaliana*. Blue circles show potentially decreased metabolites and orange circles show potentially increased metabolites in *P. brassicae*-infected tissue ( $p$ -value  $\leq 0.05$ ).

